INHERITANCE AND IMPROVEMENT OF DISEASE RESISTANCE OR STRESS TOLERANCE FOR TRITICEAE CROPS

EDITED BY: Pengtao Ma, Huagang He, Cheng Liu, Yi Wang, Yunfeng Xu and Dale Zhang

PUBLISHED IN: Frontiers in Genetics

frontiers Research Topics

frontiers

ISSN 1664-8714
ISBN 978-2-88974-815-0
DOI 10.3389/978-2-88974-815-0

About Frontiers

Frontiers is more than just an open-access publisher of scholarly articles: it is a pioneering approach to the world of academia, radically improving the way scholarly research is managed. The grand vision of Frontiers is a world where all people have an equal opportunity to seek, share and generate knowledge. Frontiers provides immediate and permanent online open access to all its publications, but this alone is not enough to realize our grand goals.

Frontiers Journal Series

The Frontiers Journal Series is a multi-tier and interdisciplinary set of open-access, online journals, promising a paradigm shift from the current review, selection and dissemination processes in academic publishing. All Frontiers journals are driven by researchers for researchers; therefore, they constitute a service to the scholarly community. At the same time, the Frontiers Journal Series operates on a revolutionary invention, the tiered publishing system, initially addressing specific communities of scholars, and gradually climbing up to broader public understanding, thus serving the interests of the lay society, too.

Dedication to Quality

Each Frontiers article is a landmark of the highest quality, thanks to genuinely collaborative interactions between authors and review editors, who include some of the world's best academicians. Research must be certified by peers before entering a stream of knowledge that may eventually reach the public - and shape society; therefore, Frontiers only applies the most rigorous and unbiased reviews.
Frontiers revolutionizes research publishing by freely delivering the most outstanding research, evaluated with no bias from both the academic and social point of view. By applying the most advanced information technologies, Frontiers is catapulting scholarly publishing into a new generation.

What are Frontiers Research Topics?

Frontiers Research Topics are very popular trademarks of the Frontiers Journals Series: they are collections of at least ten articles, all centered on a particular subject. With their unique mix of varied contributions from Original Research to Review Articles, Frontiers Research Topics unify the most influential researchers, the latest key findings and historical advances in a hot research area! Find out more on how to host your own Frontiers Research Topic or contribute to one as an author by contacting the Frontiers Editorial Office: frontiersin.org/about/contact

INHERITANCE AND IMPROVEMENT OF DISEASE RESISTANCE OR STRESS TOLERANCE FOR TRITICEAE CROPS

Topic Editors:
Pengtao Ma, Yantai University, China
Huagang He, Jiangsu University, China
Cheng Liu, Shandong Academy of Agricultural Sciences, China
Yi Wang, Sichuan Agricultural University, China
Yunfeng Xu, Kansas State University, United States
Dale Zhang, Henan University, China

Citation: Ma, P., He, H., Liu, C., Wang, Y., Xu, Y., Zhang, D., eds. (2022). Inheritance and Improvement of Disease Resistance or Stress Tolerance for Triticeae Crops. Lausanne: Frontiers Media SA. doi: 10.3389/978-2-88974-815-0

Table of Contents

frontiers in Genetics

EDITORIAL
published: 10 March 2022
doi: 10.3389/fgene.2022.877926

Editorial: Inheritance and Improvement of Disease Resistance or Stress Tolerance for *Triticeae* Crops

Pengtao Ma[1], *Huagang He*[2], *Yi Wang*[3], *Yunfeng Xu*[4], *Dale Zhang*[5] *and Cheng Liu*[6]*

[1]School of Life Sciences, Yantai University, Yantai, China, [2]School of Life Sciences, Jiangsu University, Zhenjiang, China, [3]Triticeae Research Institute, Sichuan Agricultural University, Chengdu, China, [4]Department of Agronomy, Kansas State University, Manhattan, KS, United States, [5]State Key Laboratory of Crop Stress Adaptation and Improvement, College of Agriculture, Henan University, Kaifeng, China, [6]Crop Research Institute, Shandong Academy of Agriculture Sciences, Jinan, China

Keywords: ***Triticeae*** **crops, stress tolerance, disease resistance, genetic improvement, molecular mechanism editorial on the research topic**

Editorial on the Research Topic

Inheritance and Improvement of Disease Resistance or Stress Tolerance for *Triticeae* Crops

INTRODUCTION

Triticeae crops are the most important grain crops worldwide. However, they are consistently challenged by biotic and/or abiotic stresses, including pathogens, pests, salt, drought, low and high temperature and heavy metals (Li H. et al., 2019). To combat these threats, the *Triticeae* crops have naturally evolved complex response system to these challenges during their evolutionary history (Langridge and Reynolds, 2021; Tosa 2021). Artificial mutation in the modern period also increased the genetic variation available to cope with these challenges (Krasileva et al., 2017; Chen et al., 2020). In *Triticeae* breeding history, some excellent variations have been selected and used to improve agronomic performance (Li W. et al., 2019). With the development of modern biotechnology and genome/transcriptome sequencing technology, it is expected that many more novel variations will emerge rapidly, and how to identify and use them efficiently in breeding is an important present and future topic. In this topic, recent advances in disease resistance or stress tolerance studies for *Triticeae* crops are presented, in 10 publications including one review and nine research articles, contributed by 72 authors.

DISEASE RESISTANCE IN *TRITICEAE* CROPS

Powdery mildew is a devastating wheat disease that affect yield and quality. One study identified a broad spectrum powdery mildew resistance gene *PmH4568* in a Chinese wheat cultivar Heng 4,568, which can be used in resistance breeding (Gao et al.). Septoria nodorum blotch (SNB) is a necrotrophic disease of wheat. Francki et al. evaluated the SNB resistance in the glumes of wheat and analyzed its genetic relationship with foliar disease response, and found that glume and foliar response to SNB in wheat is regulated by multiple environment-specific loci which function independently. Wheat root and stem diseases related to soil change have become severe

OPEN ACCESS

Edited and reviewed by:
Andrew H. Paterson, University of Georgia, United States

Correspondence:
Cheng Liu
lch6688407@163.com

Specialty section:
This article was submitted to Plant Genomics, a section of the journal Frontiers in Genetics

Received: *17 February 2022*
Accepted: *22 February 2022*
Published: *10 March 2022*

Citation:
Ma P, He H, Wang Y, Xu Y, Zhang D and Liu C (2022) Editorial: Inheritance and Improvement of Disease Resistance or Stress Tolerance for Triticeae Crops. Front. Genet. 13:877926. doi: 10.3389/fgene.2022.877926

threats to global wheat production. Su et al. summarized the genetics of resistance to three related diseases, including common root rot, fusarium crown rot and sharp eyespot.

ABIOTIC STRESSES IN *TRITICEAE* CROPS

Soil salinization is one of the major abiotic stresses that affect the wheat yield and quality. He et al. identified eight salt-tolerance-related miRNAs and their corresponding 11 target mRNAs that are useful to develop genetically improved salt-tolerant wheat varieties. Tong et al. screened salt-tolerant *Thinopyrum ponticum* under two coastal region salinity stress levels which can be used as excellent germplasm to develop salt-tolerant cultivars. In wheat drought stress, chlorophyll content of the flag leaf is an important trait for drought tolerance. Yang et al. identified several genetic loci affecting flag leaf chlorophyll under different water regimes. In wheat, autophagy is involved in the regulation of variousbiotic and abiotic stresses. Li et al. analyzed the programmed degradation of pericarp cells in wheat grains depends on autophagy.

EVOLUTION OF GENE FAMILIES RELATED TO BIOTIC AND ABIOTIC STRESSES IN *TRITICEAE* CROPS

Nucleotide binding site (NBS)-leucinerich repeat (LRR) receptor (NBS-LRR, also termed as NLR) is a large and one of the most important gene family against wheat disease. Li et al. and Qian et al. identifiedand characterized the NBS-LRR genes in genome of barely and *Secale cereale*, respectively, which are both important material for the molecular breeding of other *Triticeae* crops. Plant heat shock factor (HSF) is another important gene family against external biotic and abiotic stresses. Li et al. compared the HSF genes from *Secale cereale* and its *Triticeae* relatives, and the results revealed ancient and recent gene expansions of this gene family.

AUTHOR CONTRIBUTIONS

PM, HH, YW, YX, DZ, and CL organized the Research Topic as guest editors and supervised the reviewing of the submitted manuscripts. PM wrote the draft of the the Editorial paper and HH, YW, YX, DZ, and CL revised and approved the submitted version.

FUNDING

This work was supported financially supported by National Natural Science Foundation of China (32072053) and Taishan Scholars Project (tsqn201812123).

ACKNOWLEDGMENTS

We are greatly appreciated for the contributions from all the authors and reviewers as well as the support of the editorial office of Frontiers in Genetics.

REFERENCES

Chen, L., Zhao, J., Song, J., and Jameson, P. E. (2020). Cytokinin Dehydrogenase: a Genetic Target for Yield Improvement in Wheat. *Plant Biotechnol. J.* 18, 614–630. doi:10.1111/pbi.13305

Krasileva, K. V., Vasquez-Gross, H. A., Howell, T., Bailey, P., Paraiso, F., Clissold, L., et al. (2017). Uncovering Hidden Variation in Polyploid Wheat. *Proc. Natl. Acad. Sci. USA* 114, E913–E921. doi:10.1073/pnas.1619268114

Langridge, P., and Reynolds, M. (2021). Breeding for Drought and Heat Tolerance in Wheat. *Theor. Appl. Genet.* 134, 1753–1769. doi:10.1007/s00122-021-03795-1

Li, H., Murray, T. D., McIntosh, R. A., and Zhou, Y. (2019a). Breeding New Cultivars for Sustainable Wheat Production. *Crop J.* 7, 715–717. doi:10.1016/j.cj.2019.11.001

Li, W., Zhang, Q., Wang, S., Langham, M. A., Singh, D., Bowden, R. L., et al. (2019b). Development and Characterization of Wheat-Sea Wheatgrass (*Thinopyrum Junceiforme*) Amphiploids for Biotic Stress Resistance and Abiotic Stress Tolerance. *Theor. Appl. Genet.* 132, 163–175. doi:10.1007/s00122-018-3205-4

Tosa, Y. (2021). Toward Development of Resistant Lines against a Transboundary Plant Disease: Wheat Blast. *J. Gen. Plant Pathol.* 87, 394–397. doi:10.1007/s10327-021-01021-w

Conflict of Interest: The authors declare that the research was conducted in the absence of any commercial or financial relationships that could be construed as a potential conflict of interest.

Publisher's Note: All claims expressed in this article are solely those of the authors and do not necessarily represent those of their affiliated organizations, or those of the publisher, the editors and the reviewers. Any product that may be evaluated in this article, or claim that may be made by its manufacturer, is not guaranteed or endorsed by the publisher.

frontiers in Genetics

BRIEF RESEARCH REPORT
published: 24 May 2021
doi: 10.3389/fgene.2021.694682

Genome-Wide Analysis of *NLR* Disease Resistance Genes in an Updated Reference Genome of Barley

*Qian Li†, Xing-Mei Jiang† and Zhu-Qing Shao**

School of Life Sciences, Nanjing University, Nanjing, China

Barley is one of the top 10 crop plants in the world. During its whole lifespan, barley is frequently infected by various pathogens. In this study, we performed genome-wide analysis of the largest group of plant disease resistance (*R*) genes, the nucleotide binding site–leucine-rich repeat receptor (*NLR*) gene, in an updated barley genome. A total of 468 *NLR* genes were identified from the improved barley genome, including one RNL subclass and 467 CNL subclass genes. Proteins of 43 barley *CNL* genes were shown to contain 25 different integrated domains, including WRKY and BED. The *NLR* gene number identified in this study is much larger than previously reported results in earlier versions of barley genomes, and only slightly fewer than that in the diploid wheat *Triticum urartu*. Barley Chromosome 7 contains the largest number of 112 *NLR* genes, which equals to seven times of the number of *NLR* genes on Chromosome 4. The majority of *NLR* genes (68%) are located in multigene clusters. Phylogenetic analysis revealed that at least 18 ancestral *CNL* lineages were presented in the common ancestor of barley, *T. urartu* and *Arabidopsis thaliana*. Among them fifteen lineages expanded to 533 sub-lineages prior to the divergence of barley and *T. urartu*. The barley genome inherited 356 of these sub-lineages and duplicated to the 467 *CNL* genes detected in this study. Overall, our study provides an updated profile of barley *NLR* genes, which should serve as a fundamental resource for functional gene mining and molecular breeding of barley.

Keywords: barley, *NLR* gene, disease resistance, gene family, evolutionary analysis

OPEN ACCESS

Edited by:
Pengtao Ma,
Yantai University, China

Reviewed by:
Xiaoqin Sun,
Institute of Botany (CAS), China
Xu Hongxing,
Henan University, China

****Correspondence:***
Zhu-Qing Shao
zhuqingshao@nju.edu.cn

† These authors have contributed equally to this work

Specialty section:
This article was submitted to Plant Genomics, a section of the journal Frontiers in Genetics

Received: *13 April 2021*
Accepted: *26 April 2021*
Published: *24 May 2021*

Citation:
Li Q, Jiang X-M and Shao Z-Q (2021) Genome-Wide Analysis of NLR Disease Resistance Genes in an Updated Reference Genome of Barley. Front. Genet. 12:694682. doi: 10.3389/fgene.2021.694682

INTRODUCTION

Plants are consistently challenged by various pathogens during its whole lifespan. A two-layered immune system has been developed along the plant long-term evolution to defense infectious pathogens from environments (Wang et al., 2020; Zhang J. et al., 2020). The first layer immune system can recognize pathogen-associated molecular patterns (PAMPs) through plant cell surface-localized receptors, which induce PAMP-triggered immunity (PTI) (Wang et al., 2020; Zhang J. et al., 2020). Some pathogens can release effector proteins into plant cells to dampen signal transduction of PTI (Wang et al., 2020; Zhang J. et al., 2020). In response, the second layer immune system is required to detect those effectors, through proteins encoded by intracellular disease resistance genes (*R* genes), which induce effector-triggered immunity (ETI) (Wang et al., 2020; Zhang J. et al., 2020). Several types of *R* genes have been identified in the past twenty

years. Among them, the nucleotide binding site (NBS)-leucine-rich repeat (LRR) receptor (*NBS-LRR*, also termed as *NLR*) gene family comprise the majority of *R* genes identified to date (Kourelis and van der Hoorn, 2018).

NLR genes are specifically discovered in the plant lineage, and their origin could be traced back to the common ancestor of all green plants (Shao et al., 2019). Phylogenetic analysis suggested that *NLR* genes had diverged into different subclasses prior to the divergence of green plants (Shao et al., 2019). Distinct N-terminal protein domains, including Toll/Interleukin-1 receptor (TIR) domain, Coiled-coil (CC) domain and Resistance to powdery mildew8 (RPW8) domain, have been found from different *NLR* subclasses. Accordingly, the three *NLR* subclasses were named as *TIR-NLR* (*TNL*), *CC-NLR* (*CNL*), and *RPW8-NLR* (*RNL*), respectively (Meyers et al., 2003; Shao et al., 2016). Genome-wide analysis revealed that angiosperm genomes contain abundant and variable number of *NLR* genes. For example, the *NLR* gene number in Poaceae species ranges from 145 in *Zea mays* to 2298 in *Triticum aestivum* (Liu et al., 2021). *NLR* subclasses composition is also different among angiosperm species. Generally, all monocots and most sequenced magnoliids lack the *TNL* subclasses, whereas the majority of dicot species genomes have all three *NLR* subclasses (Liu et al., 2021).

Defining the *NLR* gene composition in a species is not only helpful for exploring the evolutionary pattern of *NLR* gene family, but also important for mining and utilization of functional *NLR* genes. Genome-wide *NLR* gene analysis have greatly promoted functional *NLR* gene cloning in several crops. For example, dozens of *NLR* genes against rice blast have been identified from rice and other Poaceae species by genome-wide identification and comparative genomic analysis (Yang et al., 2013; Wang et al., 2019). Recently, analysis of multiple wheat genomes contributed to the successful cloning of *Sm1*, a *R* gene resistant to the orange wheat blossom midge (OWBM, *Sitodiplosis mosellana* Géhin) (Walkowiak et al., 2020).

Cultivated barley, *Hordeum vulgar*e L. ssp. *vulgare*, is one of the top ten crop plants in the world[1]. The product is not only used for animal feeding and malt production, but also serves as a major food staple in many contraries and regions of the world. In 2018, the world-wide production of barley ranks the fourth among all cereal crops (FAOSTAT, 2018). However, like other cereals, barley is also frequently infected by a variety of pathogens. Dozens of different diseases caused by fungi, bacteria, viruses and nematodes have been reported in barley, which result in significant yield reduction and poor grain quality (Murray and Brennan, 2009). However, only a few *R* genes have been identified from barley, including the *Rph1*, *Rph15* and some *MLA* alleles (Seeholzer et al., 2010; Chen et al., 2021).

Two previous studies performed genome-wide analyses of *NLR* genes, using earlier versions of the barley genome assemblies by short-read sequence strategy, and only 100 or so *NLR* genes were identified (Andersen et al., 2016; Habachi-Houimli et al., 2018). These numbers are much smaller than those in diploid wheat genomes, which have more than 500 *NLR* genes (Liu et al., 2021). A recent study reported a newly assembly of barley genome of the cultivar Morex by long-read sequencing technology (Mascher et al., 2021). Investigation of the gene composition in the *MLA* locus revealed that three tandem *CNL* genes at this locus were missed in the earlier assemblies but present in the new assembly (Mascher et al., 2021). The quality of genome assembly and annotation is critical to genome-wide analysis to gene families, especially to *R* genes with resembled repeats and duplicates. The above comparison indicated that the *NLR* genes in barley genome might be greatly underestimated. In this study, we performed a genome-wide *NLR* gene analysis based on the newly released barley genome, which should provide full and more comprehensive information of *NLR* genes in this important crop.

MATERIALS AND METHODS

Data Used in This Study

The protein coding DNA sequences, amino acid sequences and gff3 annotation files of the reference genome sequence assembly of barley cv. Morex V3. were downloaded from the electronic data archive library (e!DAL)[2] (Mascher et al., 2021). The *Arabidopsis thaliana NLR* genes were retrieved from our previous study (Zhang et al., 2016). The *T. urartu NLR* genes were downloaded from the angiosperm *NLR* atlas ANNA[3] (Liu et al., 2021).

Identification and Classification of Barley *NLR* Genes

NLR gene identification in the barley genome was performed using BLAST and hidden Markov models search (HMMsearch) methods as described previously (Shao et al., 2014). Briefly, the amino acid sequence of the NBS (also named as NB-ARC) domain was downloaded from the Pfam database (accession number: PF00931) and used as a query to search for NLR proteins using the BLASTp program of the NCBI BLAST software, with expectation value (*E*-value) setting to 1.0. Simultaneously, the HMM profile of the NBS domain was used as a query to perform a HMMsearch against protein sequences of barley with an *E*-value setting of 1.0. Then, the results from the two methods were merged together. A round of HMMscan was performed for all the obtained hits against the Pfam-A database (*E*-value set to 0.0001) to confirm the presence of the NBS domain. Genes do not encode a conserved NBS domain were removed from the datasets. The non-redundant candidate sequences were subjected to the online NCBI Conserved Domains Database (CDD) to identify the CC, RPW8, LRR and other integrated domains. MEME analysis (Bailey et al., 2009) was performed to discover conserved motifs in the NBS domain of the identified *NLR* genes. The number of displayed motifs was set to 20 with all other parameters default settings as described by Nepal and Benson (2015).

[1]https://www.croptrust.org/crop/barley/

[2]http://doi.org/10.5447/ipk/2021/3

[3]http://compbio.nju.edu.cn/app/ANNA/

Chromosomal Distribution of Barley *NLR* Genes

Chromosomal distribution of barley *NLR* genes was analyzed as described previously (Ameline-Torregrosa et al., 2008). The barley gff3 annotation file was parsed to extract the genomic locations of identified *NLR* genes. A sliding window analysis was performed with a window size of 250 kb. If two successive annotated *NLR* genes were located within 250 kb on a chromosome, they were considered as clustered.

Phylogenetic Analysis

Sequence alignment and phylogenetic analysis were performed as described by Shao et al. (2014); Zhang Y. M. et al. (2020). Briefly, amino acid sequences of the conserved NBS domain encoded by barley *NLR* genes were retrieved and aligned using ClustalW with default options, and then manually corrected in MEGA 7.0 (Kumar et al., 2016). Too short or extremely divergent sequences were excluded from the analysis. Phylogenetic analysis was carried out by IQ-TREE using the maximum likelihood method (Nguyen et al., 2015) after selecting the best-fit model by ModelFinder (Kalyaanamoorthy et al., 2017). Branch support values were estimated using SH-aLRT and UFBoot2 tests (Minh et al., 2013). The phylogeny was reconciled as previously described (Shao et al., 2014) to reconstruction the ancestral state of the *NLR* genes.

Synteny and Gene Duplication Analysis

Pair-wise all-against-all BLAST was performed for the barley protein sequences. The obtained results and the gff3 annotation file were then subjected to MCScanX for determination of the gene duplication type (Wang et al., 2012). Microsynteny relationships were analyzed and displayed using Tbtools (Chen et al., 2020).

RESULTS

Barley Genome Contains Over 400 *NLR* Genes

By surveying the annotated protein coding genes of the improved barley genome, a total of 468 *NLR* genes were identified (**Supplementary Table 1**), accounting for approximately 0.7% of the more than 62,648 annotated protein coding genes. The number of *NLR* genes identified from the improved barley genome is three to fourfold larger than those reported in the previous studies (Andersen et al., 2016; Habachi-Houimli et al., 2018). To assign the identified *NLR* genes into different subclasses, a BLASTp analysis was performed for all obtained *NLR* genes against the well-defined *A. thaliana NLR* proteins (Zhang et al., 2016). The results showed that the 468 barley *NLR* genes comprise one *RNL* and 467 *CNL* genes. *TNL* genes were not detected in the barley genome, which is consistent with the notion that *TNL* genes are lost in the common ancestor of monocots (Collier et al., 2011; Shao et al., 2016; Liu et al., 2021).

Domain structure analysis revealed high structure diversity of barley NLR proteins. Proteins encoded by the 467 *CNL* genes could be classified into 14 groups according to their domain composition and arrangement (**Figure 1A**). Among them, only 119 *CNL* genes encode intact CNL proteins that contain both the N-terminal CC domain and the C-terminal LRR domain, in addition to the central NBS domain (**Figure 1A**). Seven of these intact *CNL* genes encode additional integrated domains (IDs) at the C-terminal, forming a CNL-ID structure; and one has both N-terminal and C-terminal IDs, forming a ID-CNL-ID structure (**Figure 1A**). There are 32 *CNL* genes encoding proteins without the N-terminal CC domain. The presence/absence of additional IDs at N-terminal and/or C-terminal further separated these genes into NL (29 genes), NL-ID (1), ID-NL (1), and N-ID-NL (1) groups (**Figure 1A**). There are 229 *CNL* genes encoding proteins without the C-terminal LRR domain, including 206 CN, 19 CN-ID, three ID-CN and one ID-CN-ID protein (**Figure 1A**). 87 *CNL* genes lost both the N-terminal CC domain and the C-terminal LRR domain (**Figure 1A**). Five and three of them fused IDs at N-terminal and C-terminal, respectively (**Figure 1A**). A total of 25 different IDs were detected from 43 barley NLR proteins, accounting for 9% of all NLR proteins. Several of them have been shown to have important function in NLR protein function, e.g., WRKY and BED family domains.

We detected the presence of five key motifs in the amino acid sequence of NBS domain by MEME analysis (Bailey et al., 2009). The result showed that the five motifs P-loop, Kinase- 2, RNBS-B, GLPL, and RNBS-D are readily detected and highly conserved in barley *NLR* proteins as reported in other angiosperms (Shao et al., 2016). Likewise, frequent losses of motifs were detected in many barley *NLR* proteins. Among the 468 NLR proteins, only 283 preserve all five motifs, accounting for 60% of all NLR proteins (**Figure 1B**). In contrast, nearly 40% NLR proteins lost at least one key motif in the NBS domain (**Figure 1B**).

A Majority of Barley *NLR* Genes Are Presented in Cluster on Chromosomes

All 468 barley *NLR* genes were mapped to specific chromosomes except one. Calculation of the *NLR* gene numbers on the seven chromosomes suggested an uneven gene distribution among different chromosomes (**Figure 2A**). Chromosome 4 has only 16 *NLR* genes; in contrast, Chromosome 7 contains the maximal of 112 *NLR* genes, which equals to seven times of *NLR* gene number on Chromosome 4. Chromosomes 1, 2, 3, 5, and 6 each has 77, 59, 67, 66, and 69 *NLR* genes, respectively.

The distribution of *NLR* genes on barley chromosomes were further deciphered by retrieve their physical locations from the genomic gff3 file. Within each chromosome, most *NLR* genes are enriched near the telomeric region, whereas very few *NLR* genes are located at the centromere region. A total of 252 *NLR* loci were defined on the seven chromosomes, including 150 singletons and 102 multigene clusters (**Figure 2B** and **Supplementary Table 1**). The result revealed that 318 *NLR* genes are present in the 102 clusters, occupying 68% of the total *NLR* genes. This ratio is slightly lower than that in *A. thaliana* (Meyers et al., 2003). There are three *NLR* genes per cluster on average. Among the 102 defined clusters, 54 of them contains only two *NLR* genes,

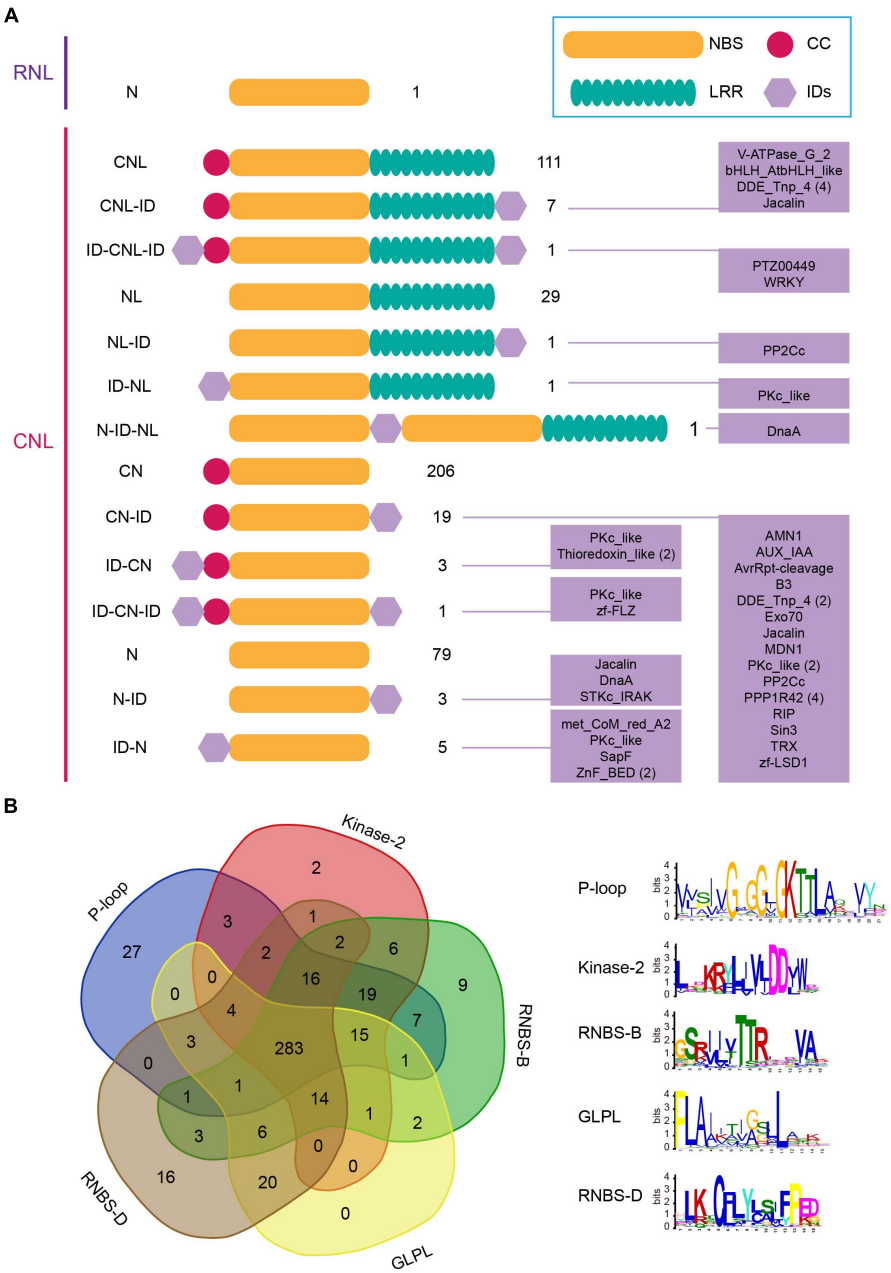

FIGURE 1 | Identification and classification of barley *NLR* genes. **(A)** Domain compositions and arrangements of proteins encoded by 468 barley *NLR* genes. **(B)** Presence of five key motifs in the amino acid sequence of the NBS domain of 468 barley *NLR* genes.

including 9, 8, 11, 1, 9, 8, and 8 such loci on Chromosome 1–7, respectively. The largest cluster is on chromosome 7, which has 11 *NLR* genes (**Figure 2B**). Over 15 clusters have more than 5 *NLR* genes.

NLR gene may duplicate through different mechanisms. We determined the duplication types of barley *NLR* genes using the MCScanX (Wang et al., 2012). The result shows that 74 *NLR* genes show tandem arrays, 146 are proximal duplicates (with no more than 8 interval *non-NLR* genes), 240 dispersed duplicates and eight are segmental duplicates (**Figure 2C**).

Species-Specific Preservation and Amplification of Ancestral *NLR* Lineages During the Speciation of Barley and Wheat

To trace the evolutionary history of barley *NLR* genes, phylogenetic analysis was conducted by incorporating *NLR* genes from a diploid wheat *T. urartu* genome and a dicot species *A. thaliana* genome. Only *CNL* and *RNL* genes of *A. thaliana* were included in the analysis, because the two monocot species

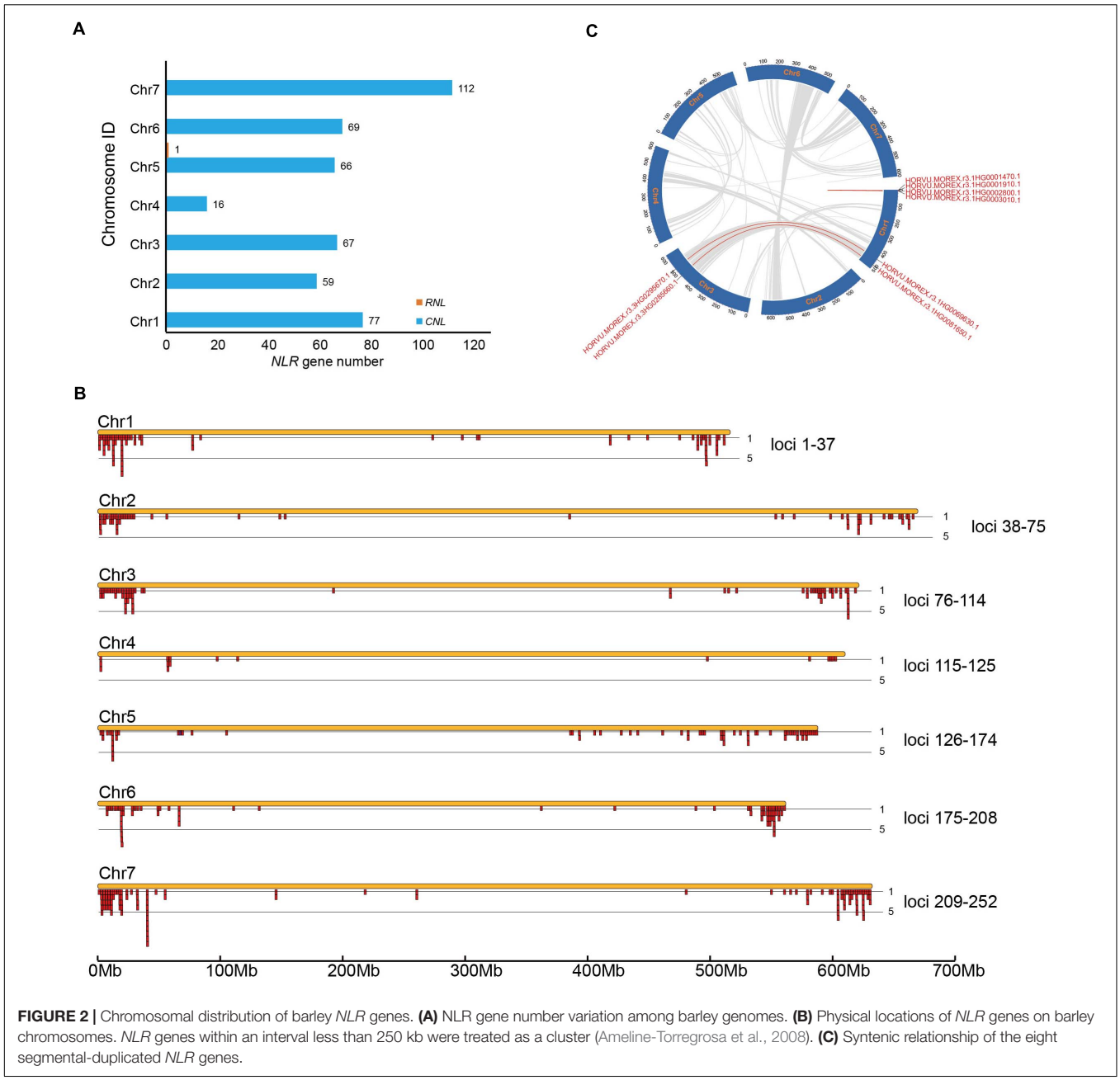

FIGURE 2 | Chromosomal distribution of barley *NLR* genes. **(A)** NLR gene number variation among barley genomes. **(B)** Physical locations of *NLR* genes on barley chromosomes. *NLR* genes within an interval less than 250 kb were treated as a cluster (Ameline-Torregrosa et al., 2008). **(C)** Syntenic relationship of the eight segmental-duplicated *NLR* genes.

do not contain *TNL* genes. The phylogenetic analysis result revealed that *NLR* genes from the three species form two deeply separated clades with a high support value, representing the ancient divergence of *RNL* and *CNL* subclasses (**Figure 3** and **Supplementary Figure 1**). *RNL* genes from the three species further separated into two lineages, namely *ADR1* and *NRG1*. The only *RNL* gene in barley (HORVU.MOREX.r3.5HG0438750) together with one *T. urartu RNL* gene (TRIUR3_09219) form a highly supported lineage with four *A. thaliana ADR1* genes (**Supplementary Figure 1**). The remaining two *A. thaliana RNL* genes form a sister lineage to *ADR1*, corresponding to the *NRG1* lineage. This topology is in accordance with the previous finding that the *RNL-NRG1* lineage was lost in the common ancestor of monocots (Collier et al., 2011; Shao et al., 2016; Liu et al., 2021).

CNL genes from the three species form two deep and well-supported clades (**Figure 3A** and **Supplementary Figure 1**). One contains the previously defined *A. thaliana CNL-B* clade genes, whereas the other one contains *A. thaliana CNL-C* and *D* clades genes (Meyers et al., 2003). Notably, only eight barley *CNL* gene and 12 *T. urartu CNL* genes are presented in the *CNL-B* clade, whereas the remaining over 400 *CNL* genes in each species are presented in the *CNL-C/D* clade. This phenomenon is quite different to that observed in *A. thaliana*, which has equal number of *CNL* genes in the two clades (Meyers et al., 2003).

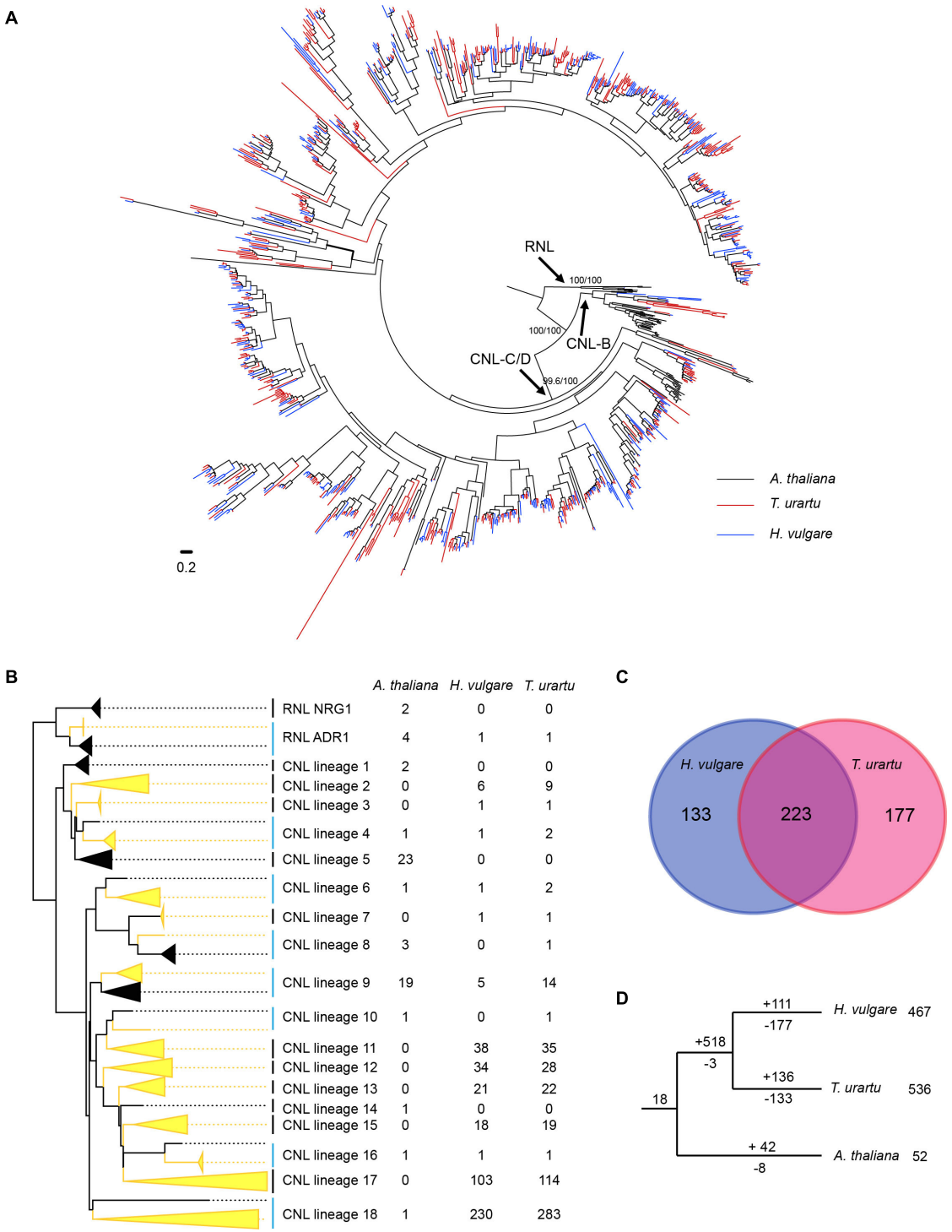

FIGURE 3 | Phylogenetic and evolutionary analysis of *RNL* and *CNL* genes from barley, *T. urartu* and *A. thaliana*. **(A)** The phylogeny was constructed based on the conserved NBS domain of *CNL* and *RNL* genes from the three species. Branch support values obtained from SH-aLRT (%) and UFBoot2 (%) are labeled on basal nodes. The *CNL*-B, and *CNL*-C/D lineages are labeled according to Meyers et al. (2003). **(B)** Predicted ancestral lineages in the common ancestor of the three species. Gene number of each species on these lineages are indicated at the right of the phylogeny. **(C)** Shared and species-specific inherited of the 533 *CNL* sub-lineages that presented in the common ancestor of barley and *T. urartu*. **(D)** Duplication/loss events of the *CNL* genes during the speciation of barley, *T. urartu* and *A. thaliana*. Gene duplication/loss events are indicated by numbers with "+" or "-" on each branch, respectively.

The results suggested that lineage-specific expansion of *CNL-C/D* genes occurred in the two monocot species.

Further reconciling the *NLR* phylogeny with species relationship revealed that at least 18 ancestral *CNL* lineages were presented in the progenitor of the three species before the divergence of monocots and eudicots (**Figure 3B** and **Supplementary Figure 1**). Among the 18 ancestral *CNL* lineages, seven (Lineage 4, 6, 8, 9, 10, 16, and 18) were inherited by *A. thaliana* and at least one of the Poaceae species. Among them, the lineages 4, 6, and 16 seem to have conservatively evolved in all three species, with no more than four genes per species (**Figure 3B**). In contrast, lineage 18 has expanded greatly to 230 and 283 genes in barley and *T. urartu*, respectively, whereas only maintained one copy in *A. thaliana*. The *NLR* genes in this single lineage occupies about half of all *NLR* genes in barley and *T. urartu*, providing a good example of differential expansion among different lineages. Lineage 9 experienced moderate expansion in *A. thaliana* and the two Poaceae species, with 5–19 *NLR* genes in each species.

There are three lineages only inherited by *A. thaliana* and eight lineages only inherited by barley and/or *T. urartu*, indicating that the two monocot species inherited more ancestral *CNL* lineages than *A. thaliana*. In total, the ancestor of barley and *T. urartu* inherited 15 of the 18 ancestral *CNL* lineages that emerged in the common ancestor of *A. thaliana* and the two Poaceae species. These ancestral *CNL* lineages further diverged into 533 sub-lineages before separation of barley and *T. urartu* (**Figure 3C**). Among them, 223 sub-lineages were maintained in both species after speciation, whereas 133 and 177 sub-lineages were only inherited by barley and *T. urartu*, respectively (**Figure 3C**). This means a considerable of *CNL* sub-lineages have been independently lost in the two species. Besides the gene loss events, species-specific gene duplication also occurred frequently. For example, some sub-lineages duplicated to up to ten copies in barley since it separated from *T. urartu* (**Supplementary Figure 1**). The species-specific gene duplication occurred more than loss of ancestral sub-lineages in *T. urartu*, which resulted in the fact that the *NLR* gene number in its current genome is larger than that in the ancestor of barley and *T. urartu*. However, in barley the *NLR* sub-lineage loss has not compensated by species-specific gene duplications, suggesting an "expansion to contraction" shift of the evolutionary pattern.

DISCUSSION

Plant *R* genes play vital roles in its defense against various pathogens (Xue et al., 2020). The *NLR* gene family composes the largest group of plant *R* genes (Kourelis and van der Hoorn, 2018). With the development of DNA sequencing technology, hundreds of plant genomes have been sequenced in the past 20 years, which have greatly benefitted the evolutionary analysis and functional mining of *R* genes in economically important plants (Wang et al., 2019; Liu et al., 2021). Genome-wide identification and evolutionary analysis has been performed in over 300 angiosperms since the studies in rice and *A. thaliana* genomes 20 years ago (Bai et al., 2002; Meyers et al., 2003; Liu et al., 2021). Previous studies identified less than 200 *NLR* genes from barley assemblies generated from short-read sequence sequencing strategy (Andersen et al., 2016; Habachi-Houimli et al., 2018). The number was much smaller than that in wheat, a close relative of barley that separated 11.6 million years ago (Chalupska et al., 2008). The hexaploid wheat *T. aestivum* has over 2000 *NLR* genes due to recently occurred polyploidization, whereas the diploid wheat *T. urartu* has 537 *NLR* genes. However, by improving the barley genome with long-read sequence strategy, a recently study revealed that the *NLR* gene number in barley might have been underestimated (Mascher et al., 2021).

In this study, a total of 468 *NLR* genes were identified from the improved barley genome. The abundance of *NLR* genes in barley is only slightly smaller than that in the diploid wheat *T. urartu*. Since similar methodologies were used by our and previous studies (Andersen et al., 2016; Habachi-Houimli et al., 2018), the result suggested that the great difference of *NLR* gene numbers in barley identified in the present study and previous studies should be caused by genome assembling issues of the short-read sequence strategy. This is in accordance with the result of a recent study, which showed that the updated barley genome has more *NLR* genes at the *MLA* locus than the early version genome assembly (Mascher et al., 2021). Furthermore, the wide distribution of barley *NLR* genes on the phylogeny that constructed with *NLR* genes from *T. urartu* and *A. thaliana* suggested that *NLR* gene diversity in barley is also comparable with those in *T. urartu*. Recent studies reported that some functional *NLR* genes can be transformed from wheat or barley to each other for molecular breeding (Halterman et al., 2001; Zhang et al., 2019). The high abundance and diversity of *NLR* genes in barley reported in the present study suggested that barley could be an important resource for exploring *NLR* genes to serve its relatives. Tandem duplication of *NLR* gene can generate *NLR* clusters on chromosomes, which is important for maintaining *NLR* diversity and generating novel functional *R* genes (Innes et al., 2008; Shao et al., 2014). In barley, the *MLA* locus is also a multigene cluster with several functional alleles identified (Seeholzer et al., 2010; Mascher et al., 2021). Our data revealed that 318 of identified *NLR* genes in barley form 102 clusters on its seven chromosomes, accounting for 68% of all *NLR* genes. These *NLR* clusters may serve as important reservoirs for preserving and generating of barley *NLR* diversity. Therefore, deciphering the character of chromosomal distribution and cluster arrangement of barley *NLR* genes would be helpful for map-based cloning of functional *R* genes and molecular breeding in barley.

Plant-microbe interaction is a long-term "arms race," which can drive rapid turnover of *NLR* profiles during species-speciation (Liu et al., 2021). Therefore, *NLR* genes often exhibit rapid losses and duplications of ancestral lineages, resulting in few conserved *NLR* lineages preserved across different species. For example, only seven ancestral lineages were inherited by four legume species and maintained in a conservative manner (Shao et al., 2014). The rare long-term conservatively evolved *NLR* genes must have been constrained by conserved functions. For example, *RNL* genes function as NLR signal transducers in

both *Arabidosis* and tobacco (Castel et al., 2019; Saile et al., 2020). In this study, we identified five lineages, namely lineages 4, 6, 8, 10, and 16, that conservatively evolved in both *A. thaliana* and the two Poaceae species. Interestingly, the *NLR* genes from *A. thaliana* in lineage 4 and lineage 10 are *RPS2* and *RPM1*. Proteins encoded by both genes are responsible for resistance to *Pseudomonas syringae* by monitoring the state changes of the host protein RIN4 (Bent et al., 1994; Mackey et al., 2002). Determining the close relationship of these *NLR* genes in barley to *A. thaliana* functional *R* genes and uncovering their conserved evolutionary pattern may provide clues for exploring their function in barley.

The ancestor of *T. urartu* and barley have expanded its *NLR* sub-lineage to 533 after its separation from *A. thaliana* about 100 million years ago. The majority of these *NLR* sub-lineages are descendants of *CNL* lineage 18. However, the 533 sub-lineages presented in the ancestor of *T. urartu* and barley are differently inherited by the two species. *T. urartu* only preserved 400 of these sub-lineages and duplicated to the 536 *CNL* genes in its current genome, whereas barley preserved 356 of these sub-lineages and duplicated to the 467 *CNL* genes in its current genome. Recently occurred polyploidization caused *NLR* genes in several hexaploid Triticum species expanded to more than 1000, reflecting rapidly changed *NLR* profiles after species-speciation by species-specific gene loss and duplication. Considering the transformable of functional *NLR* genes between the two species (Halterman et al., 2001; Zhang et al., 2019), the shared and species-specific *NLR* genes may further expand the cross-species pan-NLRome.

CONCLUSION

Overall, a total of 468 *NLR* genes were identified from the improved barley genome, including one *RNL* subclass and 467 *CNL* subclass genes. The structure diversity, chromosomal distribution and evolutionary history of barley *NLR* genes were comprehensively analyzed. These results extended the understanding on the abundance and diversity of *NLR* genes in this important crop, which may serve as a fundamental resource for the molecular breeding of barley.

DATA AVAILABILITY STATEMENT

The original contributions presented in the study are included in the article/**Supplementary Material**, further inquiries can be directed to the corresponding author/s.

AUTHOR CONTRIBUTIONS

Z-QS conceived, designed the study, and revised the manuscript. QL and X-MJ obtained, analyzed the data, and wrote the manuscript. All authors read and approved the final manuscript.

FUNDING

This work was supported by the National Natural Science Founding of China (32070243 to Z-QS).

ACKNOWLEDGMENTS

We greatly appreciate the Frontiers editors and reviewers for handling our manuscript and providing critical suggestions.

SUPPLEMENTARY MATERIAL

The Supplementary Material for this article can be found online at: https://www.frontiersin.org/articles/10.3389/fgene.2021.694682/full#supplementary-material

Supplementary Figure 1 | The full phylogeny of *NLR* genes from barley, *T. urartu* and *A. thaliana*.

Supplementary Table 1 | Detailed features of *NLR* genes identified from barley genome.

REFERENCES

Ameline-Torregrosa, C., Wang, B. B., O'Bleness, M. S., Deshpande, S., Zhu, H., Roe, B., et al. (2008). Identification and characterization of nucleotide-binding site-leucine-rich repeat genes in the model plant Medicago truncatula. *Plant Physiol.* 146, 5–21. doi: 10.1104/pp.107.104588

Andersen, E. J., Ali, S., Reese, R. N., Yen, Y., Neupane, S., and Nepal, M. P. (2016). Diversity and evolution of disease resistance genes in barley (*Hordeum vulgare* L.). *Evol. Bioinformatics* 12, 99–108. doi: 10.4137/Ebo.S38085

Bai, J., Pennill, L. A., Ning, J., Lee, S. W., Ramalingam, J., Webb, C. A., et al. (2002). Diversity in nucleotide binding site-leucine-rich repeat genes in cereals. *Genome Res.* 12, 1871–1884. doi: 10.1101/gr.454902

Bailey, T. L., Boden, M., Buske, F. A., Frith, M., Grant, C. E., Clementi, L., et al. (2009). Meme suite: tools for motif discovery and searching. *Nucleic Acids Res.* 37, W202–W208. doi: 10.1093/nar/gkp335

Bent, A. F., Kunkel, B. N., Dahlbeck, D., Brown, K. L., Schmidt, R., Giraudat, J., et al. (1994). RPS2 of *Arabidopsis thaliana*: a leucine-rich repeat class of plant disease resistance genes. *Science* 265, 1856–1860. doi: 10.1126/science.8091210

Castel, B., Ngou, P. M., Cevik, V., Redkar, A., Kim, D. S., Yang, Y., et al. (2019). Diverse NLR immune receptors activate defence via the RPW8-NLR NRG1. *New Phytol.* 222, 966–980. doi: 10.1111/nph.15659

Chalupska, D., Lee, H. Y., Faris, J. D., Evrard, A., Chalhoub, B., Haselkorn, R., et al. (2008). Acc homoeoloci and the evolution of wheat genomes. *Proc. Natl. Acad. Sci.U.S.A.* 105, 9691–9696. doi: 10.1073/pnas.0803981105

Chen, C., Chen, H., Zhang, Y., Thomas, H. R., Frank, M. H., He, Y., et al. (2020). TBtools: an integrative toolkit developed for interactive analyses of big biological data. *Mol. Plant* 13, 1194–1202. doi: 10.1016/j.molp.2020.06.009

Chen, C., Jost, M., Clark, B., Martin, M., Matny, O., Steffenson, B. J., et al. (2021). BED domain-containing NLR from wild barley confers resistance to leaf rust. *Plant Biotechnol. J.* doi: 10.1111/pbi.13542 Online ahead of print,

Collier, S. M., Hamel, L. P., and Moffett, P. (2011). Cell death mediated by the N-terminal domains of a unique and highly conserved class of NB-LRR protein. *Mol. Plant Microbe Interact.* 24, 918–931. doi: 10.1094/MPMI-03-11-0050

FAOSTAT. (2018). Available online at: http://www.fao.org/faostat/en/#home

Habachi-Houimli, Y., Khalfallah, Y., Mezghani-Khemakhem, M., Makni, H., Makni, M., and Bouktila, D. (2018). Genome-wide identification,

characterization, and evolutionary analysis of NBS-encoding resistance genes in barley. *3 Biotech* 8:453. doi: 10.1007/S13205-018-1478-6

Halterman, D., Zhou, F., Wei, F., Wise, R. P., and Schulze-Lefert, P. (2001). The MLA6 coiled-coil, NBS-LRR protein confers AvrMla6-dependent resistance specificity to *Blumeria graminis* f. sp. hordei in barley and wheat. *Plant J.* 25, 335–348. doi: 10.1046/j.1365-313x.2001.00982.x

Innes, R. W., Ameline-Torregrosa, C., Ashfield, T., Cannon, E., Cannon, S. B., Chacko, B., et al. (2008). Differential accumulation of retroelements and diversification of NB-LRR disease resistance genes in duplicated regions following polyploidy in the ancestor of soybean. *Plant Physiol.* 148, 1740–1759. doi: 10.1104/pp.108.127902

Kalyaanamoorthy, S., Minh, B. Q., Wong, T. K. F., von Haeseler, A., and Jermiin, L. S. (2017). ModelFinder: fast model selection for accurate phylogenetic estimates. *Nat. Methods* 14, 587–589. doi: 10.1038/nmeth.4285

Kourelis, J., and van der Hoorn, R. A. L. (2018). Defended to the nines: 25 years of resistance gene cloning identifies nine mechanisms for R protein function. *Plant Cell* 30, 285–299. doi: 10.1105/tpc.17.00579

Kumar, S., Stecher, G., and Tamura, K. (2016). MEGA7: molecular evolutionary genetics analysis version 7.0 for bigger datasets. *Mol. Biol. Evol.* 33, 1870–1874. doi: 10.1093/molbev/msw054

Liu, Y., Zeng, Z., Li, Q., Jiang, X. M., Jiang, Z., Tang, J. H., et al. (2021). An angiosperm NLR atlas reveals that NLR gene reduction is associated with ecological specialization and signal transduction component deletion. *bioRxiv* [Preprint]. doi: 10.1101/2021.02.10.430603

Mackey, D., Holt, B. F., Wiig, A., and Dangl, J. L. (2002). RIN4 interacts with *Pseudomonas syringae* type III effector molecules and is required for RPM1-mediated resistance in *Arabidopsis*. *Cell* 108, 743–754. doi: 10.1016/S0092-8674(02)00661-X

Mascher, M., Wicker, T., Jenkins, J., Plott, C., Lux, T., Koh, C. S., et al. (2021). Long-read sequence assembly: a technical evaluation in barley. *Plant Cell* koab077. doi: 10.1093/plcell/koab077 Online ahead of print,

Meyers, B. C., Kozik, A., Griego, A., Kuang, H., and Michelmore, R. W. (2003). Genome-wide analysis of NBS-LRR-encoding genes in *Arabidopsis*. *Plant Cell* 15, 809–834. doi: 10.1105/tpc.009308

Minh, B. Q., Nguyen, M. A., and von Haeseler, A. (2013). Ultrafast approximation for phylogenetic bootstrap. *Mol. Biol. Evol.* 30, 1188–1195. doi: 10.1093/molbev/mst024

Murray, G. M., and Brennan, J. P. (2009). Estimating disease losses to the Australian wheat industry. *Australas. Plant Pathol.* 38, 558–570. doi: 10.1071/AP09053

Nepal, M. P., and Benson, B. V. (2015). CNL disease resistance genes in soybean and their evolutionary divergence. *Evol. Bioinformatics* 11, 49–63. doi: 10.4137/Ebo.S21782

Nguyen, L. T., Schmidt, H. A., von Haeseler, A., and Minh, B. Q. (2015). IQ-TREE: a fast and effective stochastic algorithm for estimating maximum-likelihood phylogenies. *Mol. Biol. Evol.* 32, 268–274. doi: 10.1093/molbev/msu300

Saile, S. C., Jacob, P., Castel, B., Jubic, L. M., Salas-Gonzales, I., Backer, M., et al. (2020). Two unequally redundant "helper" immune receptor families mediate *Arabidopsis thaliana* intracellular "sensor" immune receptor functions. *PLoS Biol.* 18:e3000783. doi: 10.1371/journal.pbio.3000783

Seeholzer, S., Tsuchimatsu, T., Jordan, T., Bieri, S., Pajonk, S., Yang, W. X., et al. (2010). Diversity at the Mla powdery mildew resistance locus from cultivated barley reveals sites of positive selection. *Mol. Plant Microbe Interact.* 23, 497–509. doi: 10.1094/Mpmi-23-4-0497

Shao, Z. Q., Xue, J. Y., Wang, Q., Wang, B., and Chen, J. Q. (2019). Revisiting the origin of plant NBS-LRR genes. *Trends Plant Sci.* 24, 9–12. doi: 10.1016/j.tplants.2018.10.015

Shao, Z. Q., Xue, J. Y., Wu, P., Zhang, Y. M., Wu, Y., Hang, Y. Y., et al. (2016). Large-scale analyses of angiosperm nucleotide-binding site-leucine-rich repeat genes reveal three anciently diverged classes with distinct evolutionary patterns. *Plant Physiol.* 170, 2095–2109. doi: 10.1104/pp.15.01487

Shao, Z. Q., Zhang, Y. M., Hang, Y. Y., Xue, J. Y., Zhou, G. C., Wu, P., et al. (2014). Long-term evolution of nucleotide-binding site-leucine-rich repeat genes: understanding gained from and beyond the legume family. *Plant Physiol.* 166, 217–234. doi: 10.1104/pp.114.243626

Walkowiak, S., Gao, L., Monat, C., Haberer, G., Kassa, M. T., Brinton, J., et al. (2020). Multiple wheat genomes reveal global variation in modern breeding. *Nature* 588, 277–283. doi: 10.1038/s41586-020-2961-x

Wang, L., Zhao, L., Zhang, X., Zhang, Q., Jia, Y., Wang, G., et al. (2019). Large-scale identification and functional analysis of NLR genes in blast resistance in the Tetep rice genome sequence. *Proc. Natl. Acad. Sci. U.S.A.* 116, 18479–18487. doi: 10.1073/pnas.1910229116

Wang, W., Feng, B., Zhou, J. M., and Tang, D. (2020). Plant immune signaling: advancing on two frontiers. *J. Integr. Plant Biol.* 62, 2–24. doi: 10.1111/jipb.12898

Wang, Y., Tang, H., Debarry, J. D., Tan, X., Li, J., Wang, X., et al. (2012). MCScanX: a toolkit for detection and evolutionary analysis of gene synteny and collinearity. *Nucleic Acids Res.* 40:e49. doi: 10.1093/nar/gkr1293

Xue, J. Y., Takken, F. L. W., Nepal, M. P., Maekawa, T., and Shao, Z. Q. (2020). Editorial: evolution and functional mechanisms of plant disease resistance. *Front. Genet.* 11:593240. doi: 10.3389/fgene.2020.593240

Yang, S., Li, J., Zhang, X., Zhang, Q., Huang, J., Chen, J. Q., et al. (2013). Rapidly evolving R genes in diverse grass species confer resistance to rice blast disease. *Proc. Natl. Acad. Sci. U.S.A.* 110, 18572–18577. doi: 10.1073/pnas.1318211110

Zhang, C., Huang, L., Zhang, H., Hao, Q., Lyu, B., Wang, M., et al. (2019). An ancestral NB-LRR with duplicated 3'UTRs confers stripe rust resistance in wheat and barley. *Nat. Commun.* 10:4023. doi: 10.1038/s41467-019-11872-9

Zhang, J., Coaker, G., Zhou, J. M., and Dong, X. N. (2020). Plant immune mechanisms: from reductionistic to holistic points of view. *Mol. Plant* 13, 1358–1378. doi: 10.1016/j.molp.2020.09.007

Zhang, Y. M., Chen, M., Sun, L., Wang, Y., Yin, J., Liu, J., et al. (2020). Genome-wide identification and evolutionary analysis of NBS-LRR genes from *Dioscorea rotundata*. *Front. Genet.* 11:484. doi: 10.3389/fgene.2020.00484

Zhang, Y. M., Shao, Z. Q., Wang, Q., Hang, Y. Y., Xue, J. Y., Wang, B., et al. (2016). Uncovering the dynamic evolution of nucleotide-binding site-leucine-rich repeat (NBS-LRR) genes in Brassicaceae. *J. Integr. Plant Biol.* 58:13. doi: 10.1111/jipb.12365

Conflict of Interest: The authors declare that the research was conducted in the absence of any commercial or financial relationships that could be construed as a potential conflict of interest.

frontiers in Genetics

REVIEW
published: 23 June 2021
doi: 10.3389/fgene.2021.699342

Genetics of Resistance to Common Root Rot (Spot Blotch), *Fusarium* Crown Rot, and Sharp Eyespot in Wheat

Jun Su[1†], Jiaojie Zhao[1†], Shuqing Zhao[1†], Mengyu Li[1], Shuyong Pang[1], Zhensheng Kang[2], Wenchao Zhen[3*], Shisheng Chen[4], Feng Chen[5] and Xiaodong Wang[1*]*

[1] State Key Laboratory of North China Crop Improvement and Regulation, College of Plant Protection, Hebei Agricultural University, Baoding, China, [2] State Key Laboratory of Crop Stress Biology for Arid Areas, College of Plant Protection, Northwest A&F University, Xianyang, China, [3] College of Agronomy, Hebei Agricultural University, Baoding, China, [4] Institute of Advanced Agricultural Sciences, Peking University, Weifang, China, [5] National Key Laboratory of Wheat and Maize Crop Science, Agronomy College, Henan Agricultural University, Zhengzhou, China

OPEN ACCESS

Edited by:
Pengtao Ma,
Yantai University, China

Reviewed by:
Caixia Lan,
Huazhong Agricultural University, China
Jiajie Wu,
Shandong Agricultural University, China

***Correspondence:**
Xiaodong Wang
zhbwxd@hebau.edu.cn
Zhensheng Kang
kangzs@nwsuaf.edu.cn
Wenchao Zhen
wenchao@hebau.edu.cn

[†] These authors have contributed equally to this work

Specialty section:
This article was submitted to Plant Genomics, a section of the journal Frontiers in Genetics

Received: 23 April 2021
Accepted: 21 May 2021
Published: 23 June 2021

Citation:
Su J, Zhao J, Zhao S, Li M, Pang S, Kang Z, Zhen W, Chen S, Chen F and Wang X (2021) Genetics of Resistance to Common Root Rot (Spot Blotch), Fusarium Crown Rot, and Sharp Eyespot in Wheat. Front. Genet. 12:699342. doi: 10.3389/fgene.2021.699342

Due to soil changes, high density planting, and the use of straw-returning methods, wheat common root rot (spot blotch), *Fusarium* crown rot (FCR), and sharp eyespot (sheath blight) have become severe threats to global wheat production. Only a few wheat genotypes show moderate resistance to these root and crown rot fungal diseases, and the genetic determinants of wheat resistance to these devastating diseases are poorly understood. This review summarizes recent results of genetic studies of wheat resistance to common root rot, *Fusarium* crown rot, and sharp eyespot. Wheat germplasm with relatively higher resistance are highlighted and genetic loci controlling the resistance to each disease are summarized.

Keywords: wheat, resistance, common rot root, spot blotch, *Fusarium* crown rot, sharp eyespot

INTRODUCTION

Long-term environmental changes have greatly affected crop diseases. For example, the higher temperatures associated with global warming may increase the severity of many plant diseases (Cohen and Leach, 2020). Bursts of wheat stem base rot diseases, including common root rot (spot blotch), *Fusarium* crown rot, and sharp eyespot, are highly correlated with crop rotation practices. The large-scale application of wheat-maize rotation in the North China wheat cultivation area has dramatically changed the organic carbon, fertilization state, and nitrogen balance of the soil (Zhao et al., 2006; Wang et al., 2015). The disease suppressive capacity of the soil microbiome is also highly dependent on crop rotational diversity (Peralta et al., 2018).

Pathogenic Profiles

Wheat common root rot is caused by *Bipolaris sorokiniana* infection (**Figure 1A**, teleomorph *Cochliobolus sativus*) in the root and stem base of wheat plants. Severe infections of this fungal pathogen in the root and crown of seedlings may kill plants. *B. sorokiniana* can also induce phenotypes of leaf spot (spot blotch, *Helminthosporium* leaf blight, or foliar blight, **Figure 1B**), seedling wilt, head blight, and black point in *Triticeae* crops (Kumar et al., 2002). The average

yield loss caused by *B. sorokiniana* ranges from 15 to 20%, but under favorable heat and drought conditions this disease can decrease wheat production by 70% and reduce seed quality (Sharma and Duveiller, 2007). This fungal pathogen accumulates several toxins to kill or weaken plant cells, including prehelminthosporol, helminthosporol, helminthosporic acid, sorokinianin, and bipolaroxin (Kumar et al., 2002; Gupta et al., 2018). However, the potential negative effects of *B. sorokiniana*-infected wheat grains (black point) on food safety have not been investigated in detail. *B. sorokiniana* has a very wide host range, as it can infect wheat, barley, maize, rice, and many other grass species (Gupta et al., 2018). Multiple-year *Triticeae* crop rotations of wheat and barley greatly promote the severity of common root rot caused by *B. sorokiniana* (Conner et al., 1996). Maize crops and returned straws may also be infected by this fungus, so common root rot and spot blotch have been more frequently observed in areas of wheat cultivation in North China where methods of large-scale wheat-maize rotation and straw returning have been applied. Wheat resistance to *B. sorokiniana* was largely associated with accumulation of reactive oxygen species (ROS) and transcriptional activation of pathogenesis-related protein (*PR*) genes (Kumar et al., 2001; Wang et al., 2018b).

Fusarium crown rot (FCR) is caused by infection of *Fusarium pseudograminearum* (**Figure 1C**), or other *Fusarium* pathogens including *F. culmorum*, *F. avenaceum*, and *F. graminearum.* These fungal species infect the coleoptile, leaf sheath, and stem base of wheat seedlings, generating browning and decay phenotypes (**Figure 1D**). *Fusarium* pathogens are found globally in arid and semi-arid wheat planting areas (Kazan and Gardiner, 2018). FCR infection caused an estimated 35% yield loss of winter wheat in the Northwest Pacific region of the United States (Smiley et al., 2005). When FCR-infected plants are co-infected with *Fusarium* Head Blight (FHB), wheat seeds are likely to be contaminated by fungal toxins such as deoxynivalenol (DON) and nivalenol (NIV), which greatly threaten the health of human and livestock (Monds et al., 2005; Obanor and Chakraborty, 2014). Maize also can be infected with various *Fusarium* pathogens, and the fungi from infected plants can remain active in returned straw debris for as long as 5 years (Burgess et al., 2001). For these reasons, FCR is a growing threat to wheat cultivation in wheat-maize rotation regions in North China. Based on previous omics studies, wheat resistance to FCR was associated with transcriptional activations of transcription factor, cellular transport and detoxification genes, as well as protein accumulations in photosynthesis, secondary metabolite biosynthesis, phenylpropanoid biosynthesis, and glutathione metabolism (Powell et al., 2017; Qiao et al., 2021).

Wheat sharp eyespot (sheath blight) is caused by infection of *Rhizoctonia cerealis* (**Figure 1E**) in the root and stem base of wheat plants, generating disease symptoms of stem eyespot (**Figure 1F**), crown rot, seedling fatal damage, and head blight. Wheat sharp eyespot is a typical soil-borne fungal disease that is prevalent worldwide (Hamada et al., 2011). *R. cerealis* also has a broad host range, including many cereals. This fungal pathogen can survive in soil or on infected crop residues for a long time. Consequently, practices of wheat-maize rotation and straw-returning have greatly facilitated the burst of this disease in China during the last two decades (Ren et al., 2020). In 2005, approximately 8 million ha of wheat fields in China were infected with sharp eyespot, with an estimated yield loss of about 530,000 tons (McBeath and McBeath, 2010). Sharp eyespot also significantly decreases wheat grain quality (Lemańczyk and Kwaśna, 2013). Wheat resistance to sharp eyespot seemed to be dependent on a complex defense pathway including genes encoding nucleotide binding site-leucine rich repeat (NBS-LRR) protein, ethylene response factor (ERF) transcription factor, and AGC kinase (Zhu et al., 2014a, 2015, 2017).

These three diseases can have similar phenotypes, causing stem base rot and head blight, but there are differences as well. Common root rot caused by *B. sorokiniana* weakens infected wheat plants so they can be easily pulled out. Additionally the stem base and root system feel wet, and black and brown striped spots form on both the stem base and lower leaves (**Figure 1B**). For FCR caused by *F. pseudograminearum*, the stem base of the infected wheat plant becomes dry and fragile, and dark brown rot can be observed in the stem base (**Figure 1D**). For sharp eyespot caused by *R. cerealis*, lesions on the wheat stem are elliptical or have a "eye" shape, with sharply dark brown borders (**Figure 1F**).

Progress in Dissecting the Genetics of Wheat Resistance to Common Root Rot (Spot Blotch)

The use of wheat resistant cultivars remains the most efficient and economical way to control common root rot (spot blotch). However, there are currently insufficient germplasm resources with resistance to common root rot to meet the growing needs for global wheat breeding applications and there have been few studies to identify the genetic loci that control resistance to common root rot (Gupta et al., 2018). Early efforts focused on the introgression of common root rot resistant loci from *Thinopyrum ponticum*, a wheat relative (Li et al., 2004). Wheat breeding programs for common root rot resistance have had limited success because analysis of complex quantitative trait loci (QTL) is required (Joshi et al., 2004). Using bi-parental populations and linkage mapping, four genetic loci with major resistant effect were identified and designated as *Sb* genes. *Sb1* was discovered in the bread wheat line "Saar," was mapped to chromosome 7DS, and is associated with the wheat leaf rust resistance gene *Lr34* (Lillemo et al., 2013). The *Lr34/Yr18/Pm38* gene encodes a ATP-binding cassette (ABC) transporter that confers broad-spectrum resistance to multiple foliar fungal diseases, including leaf rust, stripe rust, and powdery mildew (Krattinger et al., 2009). Another minor QTL linked to *Lr46* on chromosome 1BL was also identified from "Saar." The *Lr46* gene is associated with resistance to leaf rust in adult plants and is also associated with the stripe rust resistance gene *Yr29* (William et al., 2003). The *Sb2* gene was identified in bread wheat cultivar "Yangmai 6," which significantly reduced the spot blotch disease severity on wheat leaves (Kumar et al., 2015). The *Sb2* gene was mapped to chromosome 5BL between simple sequence repeat (SSR) markers of *Xgwm639* and *Xgwm1043*. The *Sb2* gene was later reported to be linked with the *Tsn1* gene, which confers host-selective sensitivity to the fungal toxin ToxA produced by *Pyrenophora tritici-repentis*

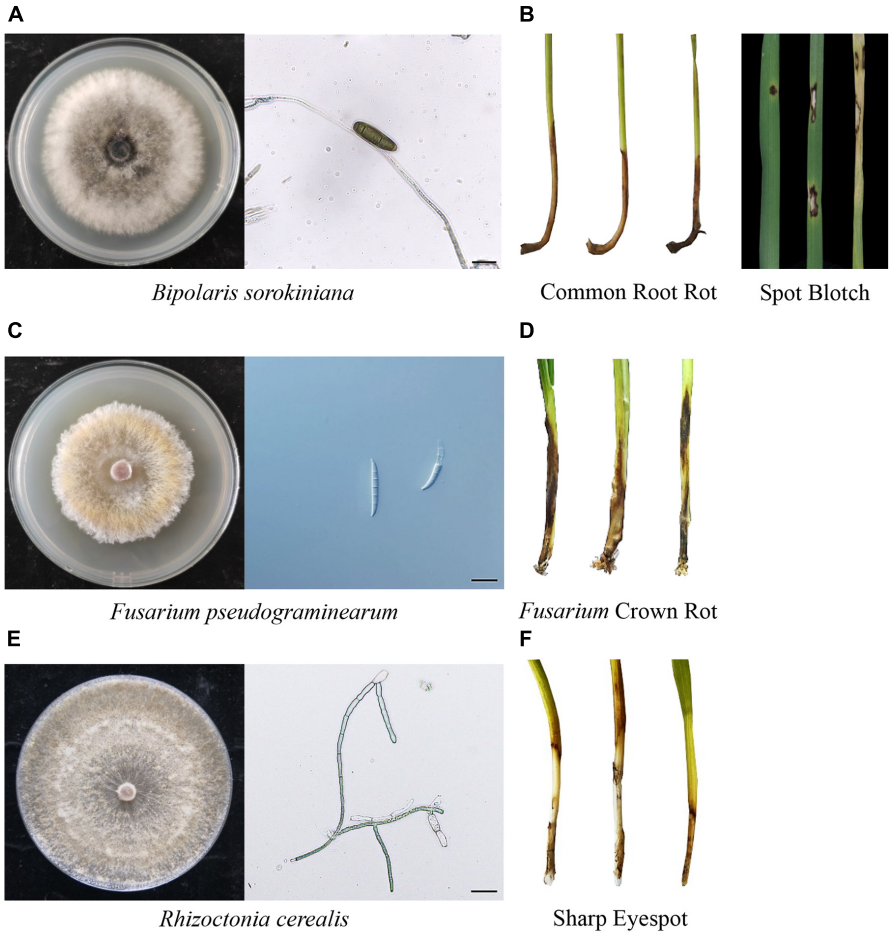

FIGURE 1 | Pathogenic profiles of *Bipolaris sorokiniana*, *Fusarium pseudograminearum*, and *Rhizoctonia cerealis*. **(A)** *B. sorokiniana* was cultivated on potato dextrose agar (PDA) medium and spores were directly collected. **(B)** Common root rot and spot blotch caused by *B. sorokiniana*. Infected wheat plants were easily pulled out, the stem base and root system felt wet, and black and brown striped spots can be observed in both the stem base and lower leaves. **(C)** *F. pseudograminearum* cultivated on PDA medium. Spores of *F. pseudograminearum* can be induced on carboxymethyl cellulose sodium (CMC) medium. **(D)** *Fusarium* crown rot caused by *F. pseudograminearum*. The stem base of infected wheat plants became dry and fragile, and was easily broken apart. Additionally, dark and red brown rot can be observed in the stem base. **(E)** *R. cerealis* was cultivated on PDA medium. **(F)** Sharp eyespot caused by *R. cerealis*. The typical lesions on wheat stem are elliptical or exhibit an "eye" shape with sharply dark brown borders. Scale bar = 20 μm.

(Kumar et al., 2016). The *Sb3* gene was discovered in the winter wheat line "621-7-1" based on its correlation with immune response to *B. sorokiniana* on leaves. Using bulked segregant analysis (BSA), *Sb3* was mapped to chromosome 3BS, flanking SSR markers of *Xbarc133* and *Xbarc147* (Lu et al., 2016). The *Sb4* gene was recently identified from two highly resistant wheat lines, "Zhongyu1211" and "GY17," which prevented the infection of *B. sorokiniana* on both leaves and sheaths of wheat plants. Using RNA-based BSA and single-nucleotide polymorphism (SNP) mapping, *Sb4* was delimitated to a 1.19 cM genetic interval region of chromosome 4BL, which contains 21 predicted genes in the corresponding "Chinese Spring" genome (Zhang et al., 2020). Future work should clone these *Sb* genes to further elucidate the mechanism of wheat resistance toward this devastating fungal pathogen.

Several other major QTLs have been discovered and preliminarily mapped using bi-parental populations. For example, two resistant QTLs derived from "Yangmai 6" were mapped to chromosomes 5B and 7D using microsatellite markers (Kumar et al., 2005). Three QTLs on chromosomes 5B, 6A, and 6D were identified based on analysis of SSR markers from the resistant genotype "G162" (Sharma et al., 2007). Four QTLs controlling resistance of wheat cultivar "Yangmai 6" to *B. sorokiniana* were mapped to chromosomes 2AL, 2BS, 5BL, and 6DL (Kumar et al., 2009). A total of seven QTLs providing resistance to *B. sorokiniana* infections were mapped in the wheat lines "Ning 8201" and "Chirya 3" (Kumar et al., 2010). Three QTLs on chromosomes 1BS, 3BS, and 5AS respectively explained 8.5, 17.6, and 12.3%, of the resistant effect in "SYN1," a CIMMYT (International Maize and Wheat Improvement Center) synthetic-derived bread wheat line (Zhu et al., 2014b). From the Brazilian resistant cultivar "BH 1146," two QTLs on chromosomes 7BL and 7DL were mapped using microsatellite markers (Singh et al., 2016). A prominent resistant QTL near the

TABLE 1 | Genetics of resistance to common root rot (spot blotch) in wheat.

QTL name	Associated markers or SNPs	Resistant wheat germplasms	References
Sb1/Lr34*	7DS: ***Xgwm295***, csLV34		
Qsb	7DS: *wPt-7654*, ***gdm88***	Saar	Lillemo et al., 2013
Qsb/Lr46/Yr29*	1BL: ***wmc719***, *hbe248*, *ncw1-V*		
Sb2/Tsn1*	5BL: ***Xgwm499***, *Xgwm639*, *Xgwm1043*	YS116, CASCABEL	Kumar et al., 2015, 2016; Bainsla et al., 2020; He et al., 2020
Sb3*	3BS: ***Xbarc147***, *XWGGC3957*, *XWGGC4320*	621-7-1	Lu et al., 2016
Sb4*	4B: ***TraesCS4B01G295400.1***	Zhongyu1211, GY17	Zhang et al., 2020
Qsb	5B: ***Xgwm544*** 7D: ***Xgwm437***	Yangmai 6	Kumar et al., 2005
Qsb	5B: ***Xgwm67***	G162	Sharma et al., 2007
QSb.bhu-2A	2AL: *Xbarc353*, ***Xgwm445***		
QSb.bhu-2B	2BS: ***Xgwm148***, *Xgwm374*		
QSb.bhu-5B	5BL: *Xgwm067*, ***Xgwm371***	Yangmai 6	Kumar et al., 2009
QSb.bhu-6D	6DL: ***Xbarc175***, *Xgwm732*		
QSb.bhu-2A	2AS: ***Xgwm425***, *Xbarc159*		
QSb.bhu-2B	2BS: ***Xgwm148***, *Xbarc91*	Ning 8201	Kumar et al., 2010
QSb.bhu-5B	5BL: ***Xgwm067***, *Xgwm213*		
QSb.bhu-7D	7DS:***Xgwm111***, *Xgwm1168*		
QSb.bhu-2B	2BS: ***Xgwm148***, *Xgwm129*		
QSb.bhu-2D	2DS: ***Xgwm455***, *Xgwm815*		
QSb.bhu-3B	3BS: *Xgwm533*, *Xgwm1037*	Chirya 3	Kumar et al., 2010
QSb.bhu-7B	7BS: *Xgwm263*, *Xgwm255*		
QSb.bhu-7D	7DS: ***Xgwm111***, *Xswm008*		
QSb.cim-1B	1B: ***Xwmc128***, *Xgwm374*		
QSb.cim-3B	3B: ***990937| F| 0***, *1123330| F| 0*	SYN1, Mayoor, Tksn1081/Ae. squarrosa (222)	Zhu et al., 2014b
QSb.cim-5A	5A: ***1086218| F| 0***, *982608| F| 0*		
QSb.iiwbr-7B	7BL: *wmc758*, ***wmc335***	BH 1146	Singh et al., 2016
QSb.iiwbr-7D	7DL: *wmc653*, ***barc121***		
Qsb/Vrn-A1*	5AL: ***Vrn-A1***	BARTAI, WUYA, CASCABEL, KATH	Singh et al., 2018; Bainsla et al., 2020; He et al., 2020
Qsb	1A: *wPt-730148*, ***wPt-668214*** 3B: ***wPt-1159, wPt-5769*** 7B: *wPt-2838* 7D: *wPt-664459*	Chirya 7, Forma Vinda de Varmland (PI 192569), IWA8600074 (PI 623098), Trigo (PI 477878), Soprimo (PI 479890), CI 10112 (PI 78814), Florentino (PI 565255), AW 6635A/86 (PI 572693), IWA8611737 (PI 625572), NW56A (PI 429667)	Adhikari et al., 2012
Qsb	1B: ***wsnp_Ex_c24700_33953160*** 5A: ***wsnp_Ex_c15342_23592740, wsnp_Ku_c17951_27138894*** 5B: ***wsnp_Ex_rep_c70120_69069789, wsnp_Ku_c20701_30355248*** 6B: ***wsnp_Ex_c15785_24157360*** 7B: ***wsnp_Ex_c52527_56097039***	PI25989, PI384237, PI384239, PI479802, PI479890, PI576639, PI245377, PI366685, PI481715, PI624517, PI481574, PI91235, PI350795, PI565213	Gurung et al., 2014
Qsb	5B: ***Xgwm544*** 6A: ***Xwgm570*** 7D: ***Xgwm437***	19HRWSN6, 30SAWSN5	Tembo et al., 2017
QSb.sdsu-2D.1	2D: ***Kukri_c31121_1460***		
QSb.sdsu-3A.1	3A: ***Excalibur_c46082_440***	Duster, Colt, Custer, Intrada, MT0495, NE99495, OK04525, OK05122, OK05723W, Venango	Ayana et al., 2018
QSb.sdsu-4A.1	4A: *IWA8475*		
QSb.sdsu-4B.1	4B: ***Excalibur_rep_c79414_306***		
QSb.sdsu-5A.1	5A: ***Kukri_rep_c104877_2166***		
QSb.sdsu-7B.1	7B: *TA005844-0160*		
Qsb	1A: ***S1A_582293281*** 2A: ***S2A_16824871*** 3A: ***S3A_378506623*** 4B: ***S4B_554842477*** 5A: ***S5A_50162259*** 5B: ***S5B_513590441, S5B_504309131, S5B_528990456*** 6B: ***S6B_9296088, S6B_673978653*** 7A: ***S7A_483878120*** 7B: ***S7B_749474154***	Chirya.3, Aust-53, Pak-13, SB12-6704, 7HTWSN-4516, 7HTWSN-4513, Aust-8, SB12-6703, Aust-66, SB12-6720, Aust-12, 7HTWSN-4522, 7HTWSN-4526, 7HTWSN-4412, 7HTWSN-4405, 7HTWSN-4517, H.Sat-8, Aust-59, Aust-29, 7HTWSN-4406, 7HTWSN-4510	Jamil et al., 2018
Qsb	1B: ***BobWhite_c17559_105*** 4A: ***BobWhite_c20322_153, BobWhite_c17524_242*** 5B: ***Tdurum_contig25513_123***, *tplb0027f13_1493* 6A: ***wsnp_Ra_c2270_4383252*** 6B: ***BS00092845_51*** 7A: ***Ku_c15750_761***	N. A.	Ahirwar et al., 2018

(Continued)

TABLE 1 | Continued

QTL name	Associated markers or SNPs	Resistant wheat germplasms	References
	1B: ***TraesCS1B01G416200***	0KATIA, DE9, OK82282//BOW/NKT/3/F4105, PSN/BOW//ROEK/3/MILAN,	
Qsb	5A: ***TraesCS5A01G391400, TraesCS5A01G369700***	KAUZ 2*/OPATA//KAUZ, ALTAR84/AE.SQ//2*, CNDO/R143//ENTE/MEXI-2/3/. . ., PAMIR-94 x, NING9415, RENESANSA, VORONA/CUPE	Bainsla et al., 2020
	1A: ***TraesCS1A01G018700*** 1B: ***TraesCS1B01G424000, TraesCS1B01G423900*** 1D: ***TraesCS1D01G012500, TraesCS1D01G012900*** 2B: ***TraesCS2B01G505200, TraesCS2B01G552700, TraesCS2B01G12400, TraesCS2B01G30100*** 3A: ***TraesCS3A01G107400, TraesCS3A01G103000*** 3B: ***TraesCS3B01G520100*** 3D: ***TraesCS3D01G537500***		
Qsb	5A: ***TraesCS5A01G402700, TraesCS5A01G457100*** 5B: ***TraesCS5B01G066200, TraesCS5B01G224500, TraesCS5B01G521500*** 6A: ***TraesCS6A01G061900*** 7A: ***TraesCS7A01G504700, TraesCS7A01G530700*** 7B: ***TraesCS7B01G002400, TraesCS7B01G003000, TraesCS7B01G169400*** 7D: ***TraesCS7D01G067000, TraesCS7D01G081100, TraesCS7D01G221000***	N. A.	Tomar et al., 2020

Genomic distribution of all these summarized resistant loci were drafted using associated markers and SNPs (bold labeled) that can be found in "Chinese Spring" wheat genome database. Stable QTLs with large effect or linked with designated genes were labeled with asterisk (*) and highlighted in ***Figure 2****.*

Vrn-A1 locus on chromosome 5AL was found in "BARTAI" and "WUYA" CIMMYT breeding lines (Singh et al., 2018). QTLs in *Vrn-A1* and *Sb2/Tsn1* loci were detected in two other CIMMYT breeding lines, "CASCABEL" and "KATH" (He et al., 2020).

Genome-wide association studies (GWAS) have been widely used to identify QTLs. Using 832 polymorphic Diversity Arrays Technology (DArT) markers, four QTLs resistant to spot blotch were mapped to chromosomes 1A, 3B, 7B, and 7D after analysis of 566 spring wheat germplasm (Adhikari et al., 2012). A phenotypic screening of 11 parental genotypes and 55 F_2 lines identified "19HRWSN6" as a resistant source. Subsequent simple linear regression analysis revealed SSR markers on chromosomes 5B, 6A, and 7D associated with resistance to *B. sorokiniana* (Tembo et al., 2017). There has been recent progress in drafting the physical genome of hexaploid wheat (Appels et al., 2018), and high-throughput SNP toolkits are now available for GWAS on various complex traits of wheat (Sun et al., 2020). A total of 528 spring wheat genotypes from different geographic regions were tested for spot blotch resistance and eleven associated SNP markers were found by 9K SNP assay (Gurung et al., 2014). Another study evaluated the responses of 294 hard winter wheat genotypes to *B. sorokiniana* and performed GWAS by 15K SNP assay. Ten wheat genotypes with relatively high resistance were identified, and six major resistant QTLs were found to collectively explain 30% of the phenotypic variation (Ayana et al., 2018). A total of 159 spring wheat genotypes were screened for common root rot resistance and 24 QTLs were identified, with a major one on chromosome 7B that explained 14% of the phenotypic variation of spot blotch severity (Jamil et al., 2018). Another study profiled the resistant phenotype of 287 spring wheat germplasm and performed GWAS using 90K SNP array. Eight genetic loci were associated with incubation period, lesion number, and disease score of *B. sorokiniana* infection (Ahirwar et al., 2018). A recent study phenotyped 301 Afghan wheat germplasm and found that approximately 15% exhibited lower disease scores than the resistant control. A subsequent GWAS approach identified 25 marker-trait associations on more than 12 chromosomes, including previously identified *Vrn-A1,* and *Sb2/Tsn1* loci (Bainsla et al., 2020). Another 141 spring wheat lines were collected for GWAS on spot blotch resistance. A total of 23 genomic loci were identified, including several stable QTLs on chromosomes 2B, 5B, and 7D, and a novel QTL on chromosome 3D (Tomar et al., 2020).

We have summarized the previously reported wheat germplasm with relatively higher resistance to *B. sorokiniana* (**Table 1**). These wheat materials may serve as valuable resources for the genetic improvement of wheat resistance to common root rot (spot blotch). We have also summarized detailed information of previously designated resistant QTLs (**Table 1**) and drafted their genomic distributions using the released genome of hexaploid wheat (**Figure 2**).

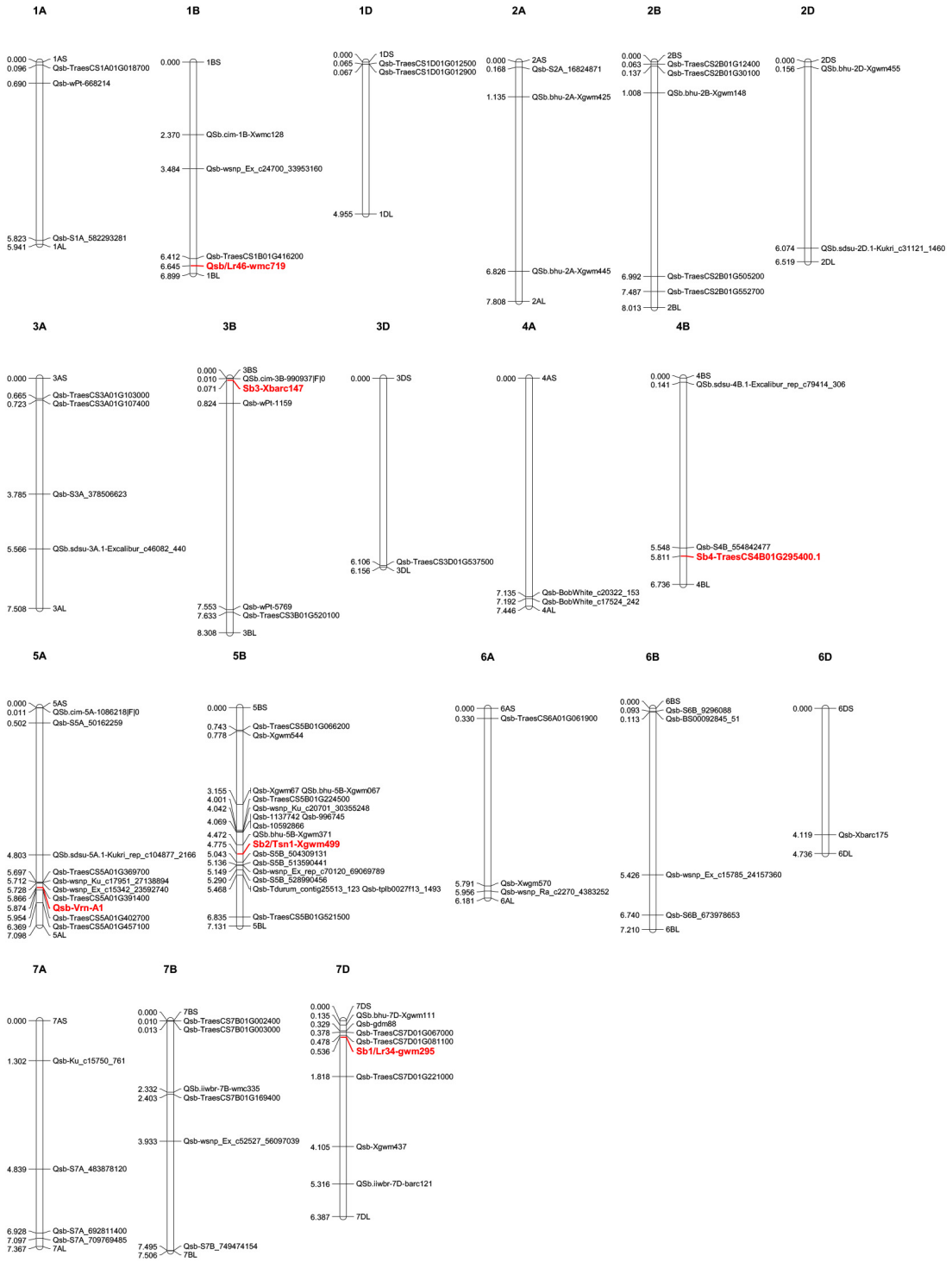

FIGURE 2 | Genetics of resistance to common root rot (spot blotch) in wheat. Molecular markers, SNPs, and genes associated with common root rot or spot blotch resistant QTLs were collected from previous publications and searched against the JBrowse-1.12.3-release of the common wheat "Chinese Spring" genome available from the "*Triticeae* Multi-omics Center (http://202.194.139.32/)." Physical positions (numbers indicated on the left side of each chromosome, in units of 100,000,000 bp) were used to generate a distribution map of all the collected QTLs using Mapchart v2.32 software. Stable QTLs with large effect or linked with designated genes are highlighted in red. Detailed information for these QTLs can be found in **Table 1**.

TABLE 2 | Genetic loci controlling wheat resistance to *Fusarium* crown rot.

QTL name	Associated markers or SNPs	Resistant wheat germplasms	References
Qcrs.cpi-3B*	3BL: ***Xgwm0181***, *wPt-10505, wPt-2277*	CSCR6 (*T. spelta*), Lang, Kennedy	Ma et al., 2010, 2012a,b, 2014; Yang et al., 2010; Zheng et al., 2015
Qcsr.cpi-4B	4BS: ***wPt-5334***, *wPt-4918,* ***Xbarc199***		
Qcr	5A: ***Xwmc110***		
Qcr	6B: ***Xwmc494, Xgwm193, Xwmc397, Xbarc198, Xbarc178***		
	2BS: *Xgdm086,* ***Xbarc200***	W21MMT70, Mendos	Bovill et al., 2006
Qcr	2D: *Xwmc018, Xwmc190*		
	5D: ***Xbarc205***, *barc143*		
Qcr	1AL: ***Xwmc120***, *Xwmc312*	Kukri, 2-49 (Gluyas Early/Gala), Janz	Wallwork et al., 2004; Collard et al., 2005, 2006
QCr.usq-1D.1	1DL: *Xcfd19*, ***Xwmc216***		
QCr.usq-2B.1	2BS: *Xbarc349.1,* ***Xgwm388***		
Qcr/Rht1*	4BL: *Xgwm165*, ***Xgwm251***		
Qcr	7BS: ***Xgwm400***, *Xwmc476*		
QCr.usq-1D.1	1DL: *Xcfd19, wPt-9380*	2-49, W21MMT70, Sunco	Bovill et al., 2010
QCr.usq-2B.2	2B: *wPt-5374,* ***wPt-0434***		
QCr.usq-3B.1	3BL: ***wPt-7301***, *wPt-0365*		
QCr.usq-4B.1	4BS: ***wPt-4535***, *Xgwm251*		
Qcr	7AS: ***wPt-4748***, *wPt-8418*		
Qcr	3B: ***wPt-1834***, *wPt-1151*	2-49, Aso zairai 11, Ernie	Li et al., 2010
Qcrs.wsu-3BL	3BL: *Xgwm247,* ***Xgwm299***	Sunco, Macon, Otis	Poole et al., 2012
Qcr	3BS: ***wPt-5390***, *Xwmc777*		
Qcr	7AS: ***wPt-3702***		
Qcrs.cpi-2D	2DL: ***1131013| F| 0***, *1246993| F| 0*	EGA Wylie	Zheng et al., 2014
Qcrs.cpi-4B.1	4BS: ***100004319| F| 0***, *2324159| F| 0*		
Qcrs.cpi-4B.2	4BS: ***1108472| F| 0***, *1093616| F| 0*		
Qcrs.cpi-5D	5DS: ***1215315| F| 0***, *1237596| F| 0*		
	1AS: ***Xbarc148***, *Xgwm164*	2-49, Sunco, IRN497, CPI133817	Martin et al., 2015
	1BS: *Xcfd65*, ***Xgwm11***		
	1DL: *Xcfd19,* ***Xwmc216***		
	2A: ***Xgwm95,*** *Xcfa2043*		
	2B: ***Xgwm630***, *Xcfa2278*		
	2DS: ***Xgwm484***, *Xgwm102*		
	3AL: ***Xcfa2134,*** *Xcfa2262*		
Qcr	3BL: ***Xgwm299,*** *wPt-0021,* ***Xwmc236***, *wPt-0365*		
	4BS: *Xwmc467, Xgwm165*		
	4BS: ***Xbarc193***, *Xwmc349*		
	6DL: *Xcfd188,* ***Xcfd47***		
	6DL: *Xbarc196,* ***Xbarc273***		
	2DS: ***wPt-669517***	2-49, Sunco, Altay-2000	Erginbasorakci et al., 2018
Qcr	3BS: *wPt-2193, wPt-22988, wPt-732330,* ***wPt-2766***		
QFCR.heau-2A	2AS: *Xwms382, wPt-7462, wPt-3757*	Xunmai 118, Kaimai 26, Yanke 316, Xuke 732, Zhonglemai 9, Jinmai 1, Shenzhou 209, Fannong 1, Jiyanmai 7, UC1110, PI610750	Yang et al., 2019
QFCR.heau-2D	2DS: ***Xcfd53***		
Qcr-6AL*	6AL: ***AX-111106634,*** *AX-94534539*		
QFCR.heau-6A	6AS: ***Xbarc3***, *Xwmc754*		
Qcr-6B	6B: ***SNP position 534,514,143***		
Qcr-6D	6D: ***SNP position 354,819,336***		
TaDIR-B1*	4B: ***TraesCS4B02G385500***	Bainong64	Yang et al., 2021
Qcr	4B: ***AX-111079978, AX-110977572***		
Qcr	1BS: ***Affx-88612017, Affx-109495423***	Henong 982, Shiyou 17, Bao 6818, Quanmai 890, 04 Zhong 36, Junda 129, Xu 10054, Fanmai 5, Lian 0809, Shixin 733, Shi05-6678, Han 06-5170, Luomai 8, Zhongyuanzhixing, Yangao 21, Xumai 33	Jin et al., 2020
Qcr	1DS: ***Affx-92108178, Affx-109205872***		
Qcr	2AL: ***Affx-111557509***		
Qcr	5DS: ***Affx-88597504, Affx-110248324***		
Qcr	5AL: ***Affx-109253960***		
Qcr-5DL*	5DL: ***Affx-110484766***, ***Affx-110079634***		
Qcr	6BS: ***Affx-110282972***		
Qcr	7BL: ***Affx-109846651, Affx-109540847***		
Qcr	2AL: *Kukri_c57491_156*	VICTORYA, Katea, KOLLEGA, DORADE-5/3/BOW"S"/GEN//SHAHI, 2180*K/2163//?/3/W1062A*HVA114/W3416, L 4224 K 12, NE04424, TX69A509.2//BBY/FOX/3/GRK//NO64/PEX/4/CER/5/KAUZ//ALTAR 84/AOS, ID800994.W/MO88	Pariyar et al., 2020
Qcr	3AS: ***wsnp_Ra_c16278_24893033, CAP8_c1393_327***		
Qcr/Fhb1*	3BS: ***CAP12_rep_c3868_270***		
Qcr	3DL: ***wsnp_Ex_c14027_21925404***		
Qcr	4BS: ***wsnp_Ku_c12399_20037334***		
Qcr	4BL: ***RAC875_rep_c72961_977***		
Qcr	5BS: ***wsnp_Ku_c17875_27051169, Excalibur_c23304_353***		
Qcr	5DS: ***RAC875_rep_c111521_246***		
Qcr	5DL: ***Excalibur_c2795_1518***		
Qcr	6BS: *RAC875_c17297_341*		
Qcr	6BL: ***BobWhite_c19298_97***		
Qcr	6DS: *BS00021881_51*		

(Continued)

TABLE 2 | Continued

QTL name	Associated markers or SNPs	Resistant wheat germplasms	References
Qcr	1A: ***BobWhite_c1027_1127, wsnp_Ku_c183_358844*** 1B: ***BS00070139_51, Tdurum_contig13117_1316*** 1D: ***wsnp_Ex_c3372_6195001*** 2D: ***BS00062567_51*** 3B: ***BS00072994_51, BS00079029_51, IACX11310*** 4A: ***BS00035307_51*** 4B: ***Ku_c3385_521*** 5B: ***BS00032003_51, BobWhite_c6094_447*** 6B: ***RAC875_c60007_199*** 7A: ***BobWhite_c33300_159, wsnp_JD_c1219_1766041*** 7B: ***wsnp_be352570B_Ta_2_1***	AUS29529/2/2.49/Cunningham//Kennedy/3/Sunco, CSCR16/2/2.49/Cunningham//Kennedy/3/Sunco/2*Pastor	Rahman et al., 2020
N. A.	N. A.	Cunmai633, LS4607, Pubing01, Hongyun2, Jimai216, Fengyunmai5, Huaihe15076, Luofeng2419, Yanfeng168, Zhengmai22, Zhoumai38, Zhoumai37, Lemai185, Xinmai38, Xinong733, Xinmai45, Guohemai12, Xinong625, Zhengmai162	Shi et al., 2020

Genomic distribution of all these summarized resistant loci were drafted using associated markers and SNPs (bold labeled) that can be found in "Chinese Spring" wheat genome database. Stable QTLs with large effect or linked with designated genes were labeled with asterisk (*) and highlighted in ***Figure 3****.*

Genetic Loci Controlling Wheat Resistance to *Fusarium* Crown Rot

Since the causal agent of *Fusarium* head blight (FHB), *Fusarium graminearum*, can also induce the phenotype of *Fusarium* crown rot (Akinsanmi et al., 2006; Zhou et al., 2019), it is likely that FHB-resistant germplasm and genetic loci can be exploited to improve FCR resistance. For instance, the recently cloned FHB resistance gene *Fhb7* encodes a glutathione S-transferase (GST) and provides broad-spectrum resistance to *Fusarium* diseases, including FCR induced by *F. pseudograminearum*, by detoxifying trichothecenes through de-epoxidation (Wang et al., 2020). However, an earlier investigation of the same wheat genotypes found no significant correlation of resistant phenotype or genetic loci conferring resistance to FHB and FCR (Li et al., 2010). A recent large-scale phenotyping of 205 Chinese wheat cultivars for resistance to both FHB and FCR also found no correlation in resistant phenotypes (Shi et al., 2020). Great efforts have also been made toward identification of FCR-resistant barley germplasm and genetic loci that control FCR resistance in barley (Liu and Ogbonnaya, 2015). Since recent review papers have already summarized QTLs conferring FHB resistance and susceptibility in wheat in detail (Buerstmayr et al., 2020; Fabre et al., 2020), here we have mainly focused on studies reporting wheat resistance to FCR induced by *F. pseudograminearum* and *F. culmorum*.

Genetic studies revealed a major FCR-resistant QTL on chromosome 3BL (*Qcrs.cpi-3B*). This resistant locus, *Qcrs.cpi-3B*, was identified in the wheat genotype "CSCR6" of the taxon *Triticum spelta* (Ma et al., 2010). In a wheat recombinant inbred line population of "Lang/CSCR6," a QTL on chromosome 4B derived from "Lang" explained the soil-free FCR resistance (Yang et al., 2010). Another significant QTL on chromosome 6B was identified as responsible for FCR resistance during an introgression process for durum wheat using "CSCR6" as the donor parent (Ma et al., 2012b). Near-isogenic lines for the *Qcrs.cpi-3B* locus have been developed for both genetic research and breeding practice (Ma et al., 2012a). Subsequent transcriptome and allele specificity analysis revealed differentially expressed genes associated with the *Qcrs.cpi-3B* locus (Ma et al., 2014). Fine mapping of this QTL shortened the genetic interval to 0.7 cM, containing 63 coding genes in the reference wheat genome (Zheng et al., 2015). Future map-based cloning and identification of the functional gene in this large-effect QTL may help elucidate the molecular bases of wheat resistance to FCR.

Other resistant QTLs have been identified using bi-parental populations. Early investigation discovered a resistant locus near the dwarfing gene *Rht1* on chromosome 4B from the wheat cultivar "Kukri" (Wallwork et al., 2004). Inherited from the wheat line "W21MMT70" with partial resistance to FCR, two QTLs were mapped to chromosomes 2D and 5D (Bovill et al., 2006). A major QTL on chromosome 1DL (*QCr.usq-1D1*) and several minor QTLs were identified in wheat line "2-49 (Gluyas Early/Gala)" using SSR markers (Collard et al., 2005, 2006). FCR resistance screening of 32 wheat genotypes identified "2-49," "Aso zairai 11," and "Ernie" as resistant sources. A QTL derived from "Ernie" was mapped to chromosome 3BL near markers *wPt-1151* and *wPt-1834* (Li et al., 2010). An Australian spring wheat cultivar "Sunco" showed partial resistance to FCR induced by *F. pseudograminearum*. Using bi-parental QTL mapping, a major QTL was identified on chromosome 3BL, between SSR markers *Xgwm247* and *Xgwm299* (Poole et al., 2012). These resistant sources of "W21MMT70," "2-49," and "Sunco" were then used for QTL pyramiding (Bovill et al., 2010). Four FCR-resistant QTLs were discovered, and their resistant alleles were derived from the bread wheat commercial variety "EGA Wylie." Major QTLs on chromosomes 5DS and 2DL were consistently detected in all three populations and two minor QTLs were mapped to chromosome 4BS (Zheng et al., 2014). QTL mapping was also performed to find genetic loci controlling partial resistance to FCR in the four wheat germplasm "2-49," "Sunco," "IRN497," and "CPI133817." FCR resistance was evaluated in both seedlings and adult plants. Six QTLs among these resistant

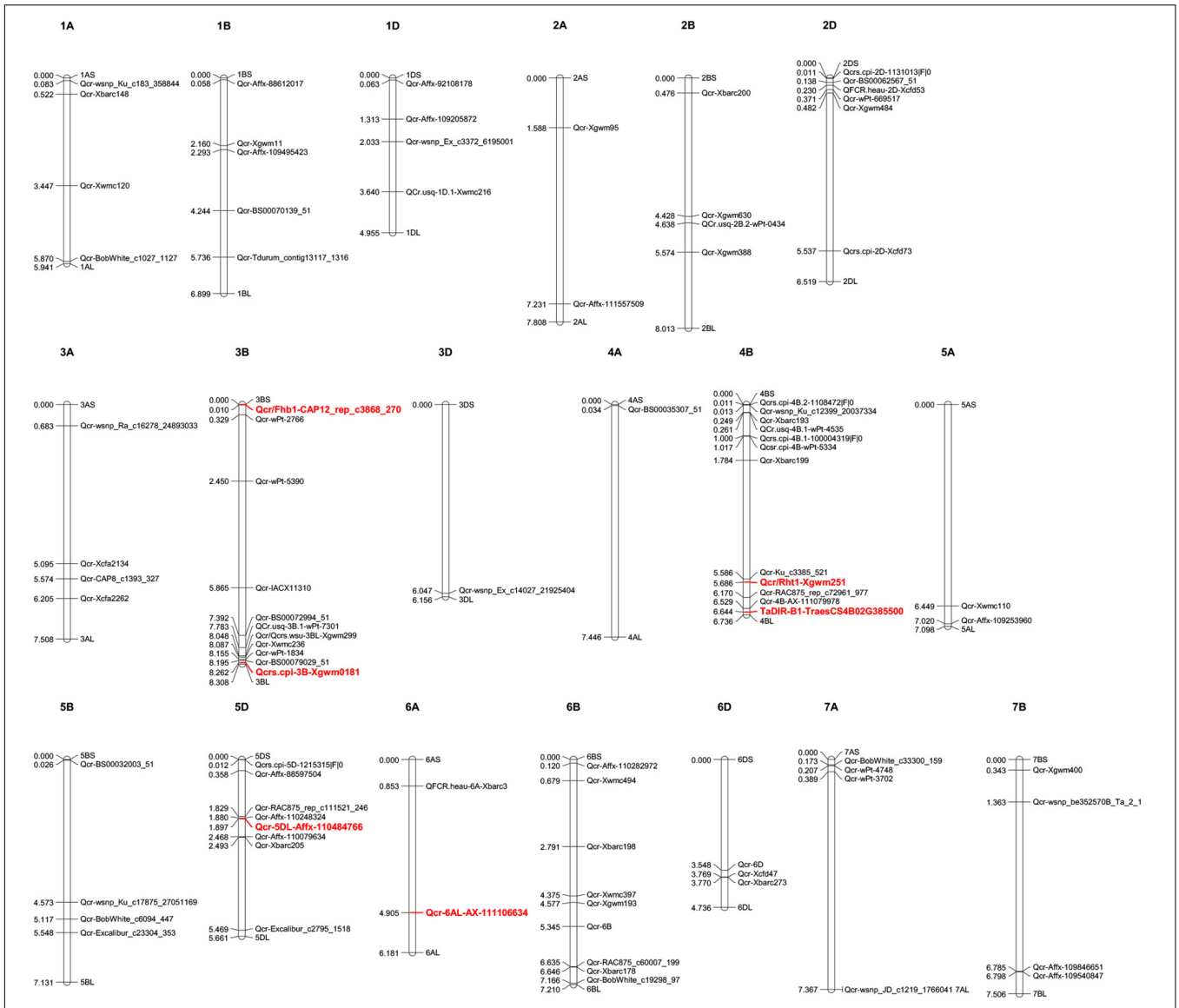

FIGURE 3 | Genetic loci controlling wheat resistance to *Fusarium* crown rot. Molecular markers, SNPs, and genes associated with FCR-resistant QTLs were collected from previous publications and searched against the JBrowse-1.12.3-release of the common wheat "Chinese Spring" genome available from the "*Triticeae* Multi-omics Center (http://202.194.139.32/)." Physical positions (numbers indicated on the left side of each chromosome, in units of 100,000,000 bp) were used to generate a distribution map of all the collected QTLs using Mapchart v2.32 software. Stable QTLs with large effect or linked with designated genes are highlighted in red. Detailed information for these QTLs can be found in **Table 2**.

wheat genotypes were revealed (Martin et al., 2015). Stable QTLs on chromosomes 1DL and 3BL have been identified from wheat germplasm "2-49" and "Sunco," respectively, in several studies.

A GWAS approach was used to screen 2,514 wheat genotypes for FCR resistance, and DArT and SSR markers identified two major QTLs on chromosome 3BL that explained 35 and 49% of the phenotypic variation (Liu et al., 2018). A set of 126 spring bread wheat lines from CIMMYT was phenotyped against FCR induced by *F. culmorum* and further genotyped using DArT markers, which resulted in the identification of three major QTLs on chromosomes 3B and 2D (Erginbasorakci et al., 2018). The use of GWAS for FCR resistance has greatly benefited from advanced high-throughput sequencing techniques and the released hexaploid wheat genome. A total of 234 Chinese wheat cultivars were evaluated for FCR resistance in four greenhouse experiments, with GWAS using a high-density 660K SNP assay. This revealed a major QTL on chromosome 6A, which was subsequently validated using a bi-parental population of "UC1110/PI610750" (Yang et al., 2019). The same team screened the FCR resistance of another 435 wheat introgression lines (generated by crossing of Yanzhan1 with other elite varieties) and performed GWAS using 660K SNP array. Most of the significant SNP associations were distributed on chromosome 4B

TABLE 3 | Genetic determinants of wheat resistance to sharp eyespot.

QTL name	Associated markers or SNPs	Resistant wheat germplasms	References
QSe.cau-1AS	1AS: ***barc148***, *wmc120*	Luke, AQ24788-83	Chen et al., 2013; Guo et al., 2017
QSe.cau-2BS	2BS: *wmc154, barc200*		
QSe.cau-3BS	3BS: *wmc777,* ***barc73***		
QSe.cau-4AL	4AL: ***barc327***, *wmc776*		
QSe.cau-5DL	5DL: ***gwm292***, *cfd29, gwm212*		
QSe.cau-6BL	6BL: *gwm626, barc187,* ***wmc397***		
QSe.cau-7BL	7BL: ***gwm611***, *wmc166,* ***wmc581***		
QSe.jaas-2BS	2BS: *RAC875_c730_234, RAC875_c16697_1502*	CI12633	Wu et al., 2017
QSe.jaas-4BS	4BS: *RAC875_c49792_228, Kukri_c34353_821*		
QSe.jaas-5AL.1	5AL: ***GENE-3601_145***, *Ku_c21002_908*		
QSe.jaas-5AL.2	5AL: ***IAAV3043***, *wsnp_Ex_c55777_58153636*		
QSe.jaas-5BS	5BS: ***wsnp_Ku_c11721_19085513***, *BS00068710_51*		
QSe.jaas-1D*	1D: ***AX-111976732***, *AX-110490771*	Niavt 14, Xuzhou 25	Jiang et al., 2016; Liu et al., 2020
QSe..jaas-2B	2B: ***AX-111049538***		
QSe.jaas-6D	6D: ***AX-111481557, AX-109521374***		
QSe.jaas-7A*	7A: ***AX-109911760***, *AX-110041698*		
QSe.jaas-7D	7D: ***AX-110667549, AX-110559985***		
N. A.	N. A.	Seedling resistance: CI12633, Banmangmai, Banjiemang, Ibis, Hongyouzi, Shaanhe6, Chinese Spring, Hongxingmai, Pingyuan 50, Linfen139, Chuanyu12, Yongfengnong2, Yunong202, Xinmai68, Huabei187, Jinmai50, Neixiang184 Adult plant resistance: Shaanhe6, CI12633, Banmangmai, Chinese Spring, Huomai, Banjiemang, Pingyuan50, Pingyang181, Yumai8, Qingfeng1, Hongyouzi, Hongxingmai, Libellula, Zhengmai8998	Ren et al., 2020

Genomic distribution of all these summarized resistant loci were drafted using associated markers (bold labeled) that can be found in "Chinese Spring" wheat genome database. Stable QTLs with large effect or linked with designated genes were labeled with asterisk (*) and highlighted in ***Figure 4****.*

and a gene encoding a dirigent protein (*TaDIR-B1*) was validated as a negative regulator of FCR resistance (Yang et al., 2021). A recent GWAS approach phenotyped 358 Chinese germplasm for FCR resistance, with less than 10% exhibiting a lower disease index. The wheat 55K SNP assay was applied for association analysis, resulting in detection of significant QTLs on chromosomes 1BS, 1DS, 5DS, 5DL, and 7BL (Jin et al., 2020). GWAS was also performed to evaluate FCR resistance of 161 wheat accessions under growth room and greenhouse conditions using *F. culmorum* as the pathogen. Using a 90K SNP array, a total of 15 QTLs for FCR resistance were detected with one major QTL on chromosome 3BS near the FHB resistance *Fhb1* locus (Pariyar et al., 2020). A marker-assisted recurrent selection approach was next performed on two populations to pyramid minor FCR-resistant QTLs. Using 9K SNP array, a total of 23 marker-trait associations were identified by GWAS (Rahman et al., 2020).

In **Table 2**, we summarize wheat germplasm resistant to FCR induced by either *F. pseudograminearum* or *F. culmorum*. Identified QTLs controlling FCR resistance are also highlighted (**Table 2**), with their genomic distributions annotated using the wheat genome database (**Figure 3**).

Genetic Determinants of Wheat Resistance to Sharp Eyespot

Wheat resistance to sharp eyespot is controlled by QTLs. However, additional efforts should focus on identification of resistant germplasm and genetic loci conferring resistance to this fungal disease. A recent large-scale screening of sharp eyespot resistant germplasm in Chinese wheat cultivars revealed no immune or highly resistant germplasm, and only 4% exhibiting moderate resistance to *R. cerealis* (Ren et al., 2020). Introgression of exogenous chromosome segments from wheat relatives might help generate novel resistant germplasms. For example, a wheat-rye 4R chromosome disomic addition line gained high resistance to sharp eyespot (An et al., 2019). Wheat cultivars "Luke" and "AQ24788-83" showed high resistance to *R. cerealis* and subsequent genetic investigations revealed seven significant sharp eyespot resistant QTLs on chromosomes 1A, 2B, 3B, 4A, 5D, 6B, and 7B (Chen et al., 2013; Guo et al., 2017). Using 90 K SNP and SSR markers, five QTLs on chromosomes 2BS, 4BS, 5AL, and 5BS controlling resistance to *R. cerealis* were identified from the wheat cultivar "CI12633" (Wu et al., 2017). Three QTLs controlling resistance of wheat cultivars "Niavt14" and "Xuzhou25" to *R. cerealis* were mapped to chromosomes

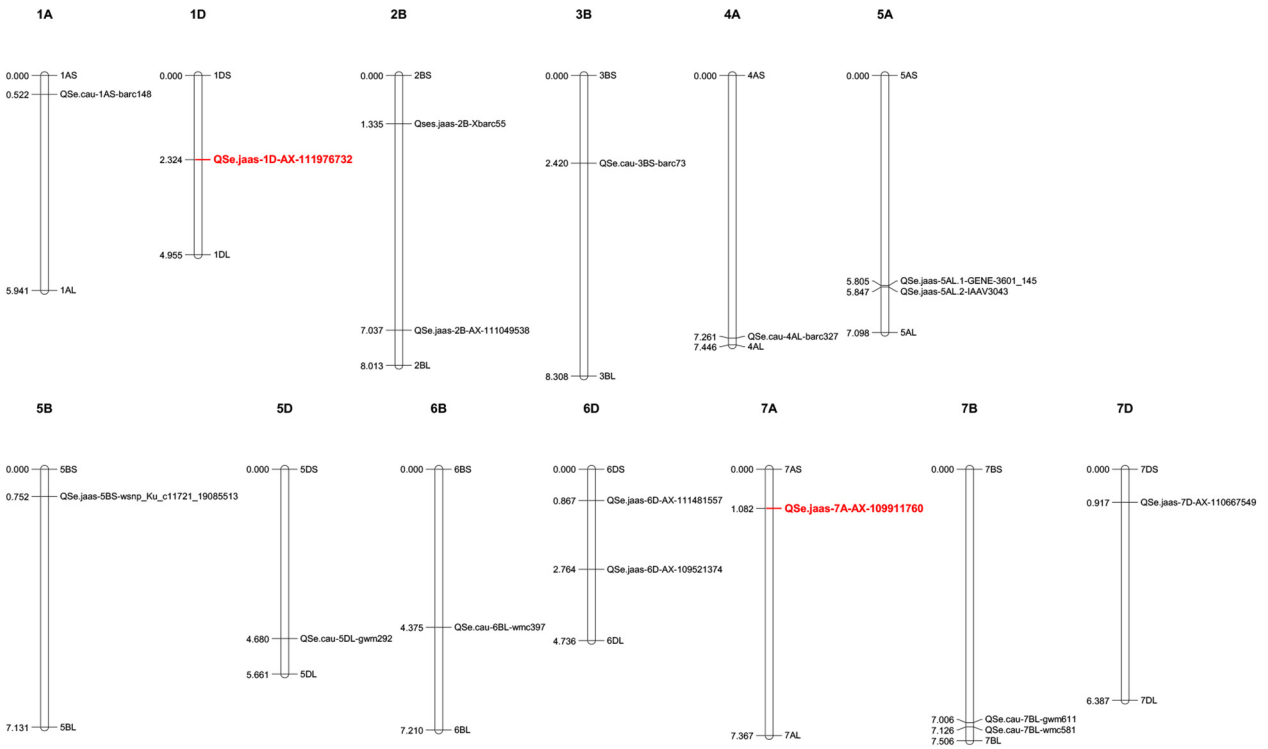

FIGURE 4 | Identified QTLs controlling wheat resistance to sharp eyespot. Molecular markers associated with Rc-resistant QTLs were collected from previous publications and searched against the JBrowse-1.12.3-release of the common wheat "Chinese Spring" genome available from the "Triticeae Multi-omics Center (http://202.194.139.32/)." Physical positions (numbers indicated on the left side of each chromosome, in units of 100,000,000 bp) were used to generate a distribution map of all the collected QTLs using Mapchart v2.32 software. Detailed information for these QTLs can be found in **Table 3**.

2B and 7D (Jiang et al., 2016). A recent study using the same population of "Niavt14/Xuzhou25" and 55K SNPs revealed three novel stable QTLs on chromosomes 1D, 6D, and 7A (Liu et al., 2020).

In **Table 3**, we summarize wheat germplasm resistant to *R. cerealis*. Reported QTLs controlling sharp eyespot resistance are highlighted (**Table 3**), with their genomic distributions annotated using the wheat genome database (**Figure 4**).

DISCUSSION

We have described three rot diseases that commonly infect the stem base of wheat plants (**Figure 1**). These diseases are major threats to wheat productions in wheat-maize rotation areas with large-scale application of straw returning. Wheat breeding is the most efficient way to control these devastating fungal diseases. However, as summarized in this review (**Tables 1–3**), there are few wheat germplasm with relative high resistance to *B. sorokiniana*, *F. pseudograminearum*, or *R. cerealis*. Large-scale screenings of resistant wheat germplasm are still urgently needed for effective wheat breeding applications. New germplasm resources including wheat relatives (e.g., introgression lines using *Thinopyrum ponticum*, *Triticum spelta*, and rye) may have great potential to improve wheat resistance to these root and crown rot fungal diseases.

Genetic improvement of wheat resistance to these diseases requires exploring novel QTLs that control resistance. There are several previously reported resistant QTLs (**Tables 1–3**) and their genomic distributions have been mapped based on the released wheat genome (**Figures 2–4**). Stable QTLs with large effect or linked with designated genes were highlighted. Chromosome location data for all these reported QTLs was provided in **Supplementary Table 1**. Some identified QTLs that confer resistance to *B. sorokiniana* are associated with loci responsible for wheat resistance to other foliar fungal diseases, such as *Lr34/Yr18/Pm38*, *Lr46/Yr29*, and *Tsn1*. Wheat leaves might restrain the infection of different foliar fungal diseases using similar molecular approaches mediated by resistant genes. Wheat germplasm with broad-spectrum resistant loci should be evaluated for potential resistance to spot blotch or common root rot induced by *B. sorokiniana*. Of QTLs that control resistance to *Fusarium* crown rot, ones that also have resistance to FHB may be more valuable, since the major causal agents of these diseases (*F. pseudograminearum*, *F. culmorum*, and *F. graminearum*) are very likely to co-exist in a cultivation environment. For genetic studies on QTLs controlling resistance to sharp eyespot, the large-scale screening of resistant wheat germplasm would greatly accelerate the identification of novel QTLs correlated with resistance to sharp eyespot. There is also an urgent need to employ GWAS technique to screen for more sharp eyespot resistant QTLs at the genome-wide level.

To explore QTLs with potential co-resistance effects to all these three stem base rot diseases, we combined the chromosome distribution maps of all the reported QTLs in **Supplementary Figure 1**. Chromosome regions on 1AS, 3BL, 4BL, 5AL, 5BL, and 7AS are enriched with QTLs conferring resistance to these soil-borne necrotrophic fungal diseases. Constructing near-isogenic lines and using residual heterozygotes allow the use of fine mapping and further positional cloning for key gene/loci that control resistance. With advanced genomic and capture-sequencing techniques such as MutRenSeq, AgRenSeq, and Exome Capture, fast-cloning approaches might accelerate this time-consuming process (Steuernagel et al., 2016; Krasileva et al., 2017; Arora et al., 2019). Gene editing may also increase the rate of genetic improvement of wheat resistance to these fungal diseases (Wang et al., 2018a). Both forward and reverse genetic studies will provide valuable targets for the application of CRISPR-Cas9 in wheat. Nevertheless, the main restraints for fine-mapping and cloning of genes/QTLs conferring resistance to these stem base rot diseases are accurate phenotyping of large-scale segregation populations and functional validation of candidate resistance genes.

Efforts should also be made to convert traditional markers used previously to identify resistant QTLs (microsatellite, SSR, and DrAT) to SNP markers, as SNP markers may serve as valuable tools for high-throughput marker-assisted selection in wheat breeding. Progress in wheat genome research and increased availability of high-density SNP toolkits will facilitate the use of GWAS on collected wheat germplasm to more efficiently identify novel resistant sources and genetic loci.

AUTHOR CONTRIBUTIONS

XW, ZK, and WZ: conceptualization. JS, JZ, SZ, ML, and SP: data collection. XW: original draft preparation. SC and FC: review and editing. XW, ZK, and WZ: supervision. All authors read and agreed to the published version of the manuscript.

FUNDING

This work was supported by Provincial Natural Science Foundation of Hebei (C2021204008), Open Project Program of National Key Laboratory of Wheat and Maize Crop Science, Provincial Supporting Program of Hebei for the Returned Oversea Scholars (C20190180), Open Project Program of State Key Laboratory of North China Crop Improvement and Regulation (NCCIR2020KF-4), National Key R&D Program of China (2017YFD0300906), and Provincial Innovation Program of Hebei for Post-graduate Student (CXZZSS2021070).

ACKNOWLEDGMENTS

The authors would like to thank Prof. Zaifeng Li from Hebei Agricultural University for discussion and input to this work.

SUPPLEMENTARY MATERIAL

The Supplementary Material for this article can be found online at: https://www.frontiersin.org/articles/10.3389/fgene.2021.699342/full#supplementary-material

Supplementary Figure 1 | Combined chromosome distribution map for all the QTLs conferring resistance to common root rot (spot blotch), *Fusarium* crown rot, and sharp eyespot in wheat.

Supplementary Table 1 | Chromosome location data for all the reported QTLs.

REFERENCES

Adhikari, T. B., Gurung, S., Hansen, J. M., Jackson, E. W., and Bonman, J. M. (2012). Association mapping of quantitative trait loci in spring wheat landraces conferring resistance to bacterial leaf streak and spot blotch. *Plant Genome* 5, 1–16.

Ahirwar, R. N., Mishra, V. K., Chand, R., Budhlakoti, N., Mishra, D. C., Kumar, S., et al. (2018). Genome-wide association mapping of spot blotch resistance in wheat association mapping initiative (WAMI) panel of spring wheat (*Triticum aestivum* L.). *PLoS One* 13:e0208196. doi: 10.1371/journal.pone.0208196

Akinsanmi, O. A., Backhouse, D., Simpfendorfer, S., and Chakraborty, S. (2006). Genetic diversity of Australian *Fusarium graminearum* and F. pseudograminearum. *Plant Pathol.* 55, 494–504. doi: 10.1111/j.1365-3059.2006.01398.x

An, D., Ma, P., Zheng, Q., Fu, S., Li, L., Han, F., et al. (2019). Development and molecular cytogenetic identification of a new wheat-rye 4R chromosome disomic addition line with resistances to powdery mildew, stripe rust and sharp eyespot. *Theor. Appl. Genet.* 132, 257–272. doi: 10.1007/s00122-018-3214-3

Appels, R., Eversole, K., Stein, N., Feuillet, C., Keller, B., Rogers, J., et al. (2018). Shifting the limits in wheat research and breeding using a fully annotated reference genome. *Science* 361:eaar7191.

Arora, S., Steuernagel, B., Gaurav, K., Chandramohan, S., Long, Y., Matny, O., et al. (2019). Resistance gene cloning from a wild crop relative by sequence capture and association genetics. *Nat. Biotechnol.* 37, 139–143. doi: 10.1038/s41587-018-0007-9

Ayana, G. T., Ali, S., Sidhu, J. S., Hernandez, J. L. G., Turnipseed, B., and Sehgal, S. K. (2018). Genome-wide association study for spot blotch resistance in hard winter wheat. *Front. Plant Sci.* 9:926. doi: 10.3389/fpls.2018.00926

Bainsla, N. K., Phuke, R. M., He, X., Gupta, V., Bishnoi, S. K., Sharma, R. K., et al. (2020). Genome-wide association study for spot blotch resistance in Afghan wheat germplasm. *Plant Pathol.* 69, 1161–1171. doi: 10.1111/ppa.13191

Bovill, W. D., Horne, M., Herde, D. J., Davis, M., Wildermuth, G. B., and Sutherland, M. W. (2010). Pyramiding QTL increases seedling resistance to crown rot (*Fusarium pseudograminearum*) of wheat (*Triticum aestivum*). *Theor. Appl. Genet.* 121, 127–136. doi: 10.1007/s00122-010-1296-7

Bovill, W. D., Ma, W., Ritter, K., Collard, B. C. Y., Davis, M., Wildermuth, G. B., et al. (2006). Identification of novel QTL for resistance to crown rot in the doubled haploid wheat population 'W21MMT70'×'Mendos'. *Plant Breed.* 125, 538–543. doi: 10.1111/j.1439-0523.2006.01251.x

Buerstmayr, M., Steiner, B., and Buerstmayr, H. (2020). Breeding for Fusarium head blight resistance in wheat—progress and challenges. *Plant Breed.* 139, 429–454. doi: 10.1111/pbr.12797

Burgess, L. W., Backhouse, D., Summerell, B. A., and Swan, L. J. (2001). "Crown rot in wheat—-Chapter 20," in *Fusarium-Paul E Nelson Memorial Symposium*, eds B. A. Summerell, J. F. Leslie, D. Backhouse, W. L. Bryden, and L. W. Burgess (St Paul, MIN: The American Phytopathological Society), 271–294.

Chen, J., Li, G. H., Du, Z. Y., Quan, W., Zhang, H. Y., Che, M. Z., et al. (2013). Mapping of QTL conferring resistance to sharp eyespot (Rhizoctonia cerealis) in bread wheat at the adult plant growth stage. *Theor. Appl. Genet.* 126, 2865–2878. doi: 10.1007/s00122-013-2178-6

Cohen, S. P., and Leach, J. E. (2020). High temperature-induced plant disease susceptibility: more than the sum of its parts. *Curr. Opin. Plant Biol.* 56, 235–241. doi: 10.1016/j.pbi.2020.02.008

Collard, B. C. Y., Grams, R. A., Bovill, W. D., Percy, C. D., Jolley, R., Lehmensiek, A., et al. (2005). Development of molecular markers for crown rot resistance in wheat: mapping of QTLs for seedling resistance in a '2-49'×'Janz' population. *Plant Breed.* 124, 532–537. doi: 10.1111/j.1439-0523.2005.01163.x

Collard, B. C. Y., Jolley, R., Bovill, W. D., Grams, R. A., Wildermuth, G. B., and Sutherland, M. W. (2006). Confirmation of QTL mapping and marker validation for partial seedling resistance to crown rot in wheat line '2-49'. *Crop Pasture Sci.* 57, 967–973. doi: 10.1071/ar05419

Conner, R. L., Duczek, L. J., Kozub, G. C., and Kuzyk, A. D. (1996). Influence of crop rotation on common root rot of wheat and barley. *Can. J. Plant Pathol.* 18, 247–254. doi: 10.1080/07060669609500620

Erginbasorakci, G., Sehgal, D., Sohail, Q., Ogbonnaya, F. C., Dreisigacker, S., Pariyar, S. R., et al. (2018). Identification of novel quantitative trait loci linked to crown rot resistance in spring wheat. *Int. J. Mol. Sci.* 19:2666. doi: 10.3390/ijms19092666

Fabre, F., Rocher, F., Alouane, T., Langin, T., and Bonhomme, L. (2020). Searching for FHB resistances in bread wheat: susceptibility at the crossroad. *Front. Plant Sci.* 11:731. doi: 10.3389/fpls.2020.00731

Guo, Y., Du, Z., Chen, J., and Zhang, Z. (2017). QTL mapping of wheat plant architectural characteristics and their genetic relationship with seven QTLs conferring resistance to sheath blight. *PLoS One* 12:e0174939. doi: 10.1371/journal.pone.0174939

Gupta, P. K., Chand, R., Vasistha, N. K., Pandey, S. P., Kumar, U., Mishra, V. K., et al. (2018). Spot blotch disease of wheat: the current status of research on genetics and breeding. *Plant Pathol.* 67, 508–531. doi: 10.1111/ppa.12781

Gurung, S., Mamidi, S., Bonman, J. M., Xiong, M., Brownguedira, G., and Adhikari, T. B. (2014). Genome-wide association study reveals novel quantitative trait loci associated with resistance to multiple leaf spot diseases of spring wheat. *PLoS One* 9:e108179. doi: 10.1371/journal.pone.0108179

Hamada, M. S., Yin, Y., Chen, H., and Ma, Z. (2011). The escalating threat of Rhizoctonia cerealis, the causal agent of sharp eyespot in wheat. *Pest Manag. Sci.* 67, 1411–1419. doi: 10.1002/ps.2236

He, X., Dreisigacker, S., Sansaloni, C., Duveiller, E., Singh, R. P., and Singh, P. K. (2020). QTL mapping for spot blotch resistance in two bi-parental mapping populations of bread wheat. *Phytopathology* 110, 1980–1987. doi: 10.1094/phyto-05-20-0197-r

Jamil, M., Ali, A., Gul, A., Ghafoor, A., Ibrahim, A. M. H., and Mujeeb-Kazi, A. (2018). Genome-wide association studies for spot blotch (Cochliobolus sativus) resistance in bread wheat using genotyping-by-sequencing. *Phytopathology* 108, 1307–1314. doi: 10.1094/phyto-02-18-0047-r

Jiang, Y., Zhu, F., Cai, S., Wu, J., and Zhang, Q. (2016). Quantitative trait loci for resistance to Sharp Eyespot (*Rhizoctonia cerealis*) in recombinant inbred wheat lines from the cross Niavt 14× Xuzhou 25. *Czech J. Genet. Plant Breed.* 52, 139–144. doi: 10.17221/74/2016-cjgpb

Jin, J., Duan, S., Qi, Y., Yan, S., Li, W., Li, B., et al. (2020). Identification of a novel genomic region associated with resistance to Fusarium crown rot in wheat. *Theor. Appl. Genet.* 133, 2063–2073. doi: 10.1007/s00122-020-03577-1

Joshi, A. K., Kumar, S., Chand, R., and Ortizferrara, G. (2004). Inheritance of resistance to spot blotch caused by Bipolaris sorokiniana in spring wheat. *Plant Breed.* 123, 213–219. doi: 10.1111/j.1439-0523.2004.00954.x

Kazan, K., and Gardiner, D. M. (2018). Fusarium crown rot caused by *Fusarium Psudograminearum* in cereal crops: recent progress and future prospects. *Mol. Plant Pathol.* 19, 1547–1562. doi: 10.1111/mpp.12639

Krasileva, K. V., Vasquez-Gross, H. A., Howell, T., Bailey, P., Paraiso, F., Clissold, L., et al. (2017). Uncovering hidden variation in polyploid wheat. *Proc. Natl. Acad. Sci. U.S.A.* 114, E913–E921.

Krattinger, S. G., Lagudah, E. S., Spielmeyer, W., Singh, R. P., Huerta-Espino, J., Mcfadden, H., et al. (2009). A putative ABC transporter confers durable resistance to multiple fungal pathogens in wheat. *Science* 323, 1360–1363. doi: 10.1126/science.1166453

Kumar, J., Hückelhoven, R., Beckhove, U., Nagarajan, S., and Kogel, K.-H. (2001). A compromised Mlo pathway affects the response of barley to the necrotrophic fungus *Bipolaris sorokiniana* (teleomorph: Cochliobolus sativus) and its toxins. *Phytopathology* 91, 127–133. doi: 10.1094/phyto.2001.91.2.127

Kumar, J., Schafer, P., Huckelhoven, R., Langen, G., Baltruschat, H., Stein, E., et al. (2002). Bipolaris sorokiniana, a cereal pathogen of global concern: cytological and molecular approaches towards better control. *Mol. Plant Pathol.* 3, 185–195. doi: 10.1046/j.1364-3703.2002.00120.x

Kumar, S., Roder, M. S., Singh, R. P., Kumar, S., Chand, R., Joshi, A. K., et al. (2016). Mapping of spot blotch disease resistance using NDVI as a substitute to visual observation in wheat (*Triticum aestivum* L.). *Mol. Breed.* 36:95.

Kumar, S., Roder, M. S., Tripathi, S. B., Kumar, S., Chand, R., Joshi, A. K., et al. (2015). Mendelization and fine mapping of a bread wheat spot blotch disease resistance QTL. *Mol. Breed.* 35:218.

Kumar, U., Joshi, A. K., Kumar, S., Chand, R., and Roder, M. S. (2009). Mapping of resistance to spot blotch disease caused by Bipolaris sorokiniana in spring wheat. *Theor. Appl. Genet.* 118, 783–792. doi: 10.1007/s00122-008-0938-5

Kumar, U., Joshi, A. K., Kumar, S., Chand, R., and Roder, M. S. (2010). Quantitative trait loci for resistance to spot blotch caused by Bipolaris sorokiniana in wheat (*T. aestivum* L.) lines 'Ning 8201' and 'Chirya 3'. *Mol. Breed.* 26, 477–491. doi: 10.1007/s11032-009-9388-2

Kumar, U., Kumar, S., Tyagi, K., Chand, R., and Joshi, A. K. (2005). Microsatellite markers for resistance to spot blotch in spring wheat. *Commun. Agric. Appl. Biol. Sci.* 70:59.

Lemańczyk, G., and Kwaśna, H. (2013). Effects of sharp eyespot (Rhizoctonia cerealis) on yield and grain quality of winter wheat. *Eur. J. Plant Pathol.* 135, 187–200. doi: 10.1007/s10658-012-0077-3

Li, H., Conner, R. L., Chen, Q., Li, H., Laroche, A., Graf, R. J., et al. (2004). The transfer and characterization of resistance to common root rot from Thinopyrum ponticum to wheat. *Genome* 47, 215–223. doi: 10.1139/g03-095

Li, H. B., Xie, G. Q., Ma, J., Liu, G. R., Wen, S. M., Ban, T., et al. (2010). Genetic relationships between resistances to Fusarium head blight and crown rot in bread wheat (*Triticum aestivum* L.). *Theor. Appl. Genet.* 121, 941–950. doi: 10.1007/s00122-010-1363-0

Lillemo, M., Joshi, A. K., Prasad, R., Chand, R., and Singh, R. P. (2013). QTL for spot blotch resistance in bread wheat line Saar co-locate to the biotrophic disease resistance loci Lr34 and Lr46. *Theor. Appl. Genet.* 126, 711–719. doi: 10.1007/s00122-012-2012-6

Liu, C., Guo, W., Zhang, Q., Fu, B., Yang, Z., Sukumaran, S., et al. (2020). Genetic dissection of adult plant resistance to sharp eyespot using an updated genetic map of Niavt14× Xuzhou25 winter wheat recombinant inbred line population. *Plant Dis.* 105, 997–1005. doi: 10.1094/pdis-09-20-1924-re

Liu, C., Ma, J., Li, H. B., Liu, Y. X., Liu, G. R., Wen, S. M., et al. (2018). The homoeologous regions on long arms of group 3 chromosomes in wheat and barley harbour major crown rot resistance loci. *Czech J. Genet. Plant Breed.* 47, 109–114.

Liu, C., and Ogbonnaya, F. C. (2015). Resistance to Fusarium crown rot in wheat and barley: a review. *Plant Breed.* 134, 365–372. doi: 10.1111/pbr.12274

Lu, P., Liang, Y., Li, D. F., Wang, Z., Li, W., Wang, G., et al. (2016). Fine genetic mapping of spot blotch resistance gene Sb3 in wheat (*Triticum aestivum*). *Theor. Appl. Genet.* 129, 577–589. doi: 10.1007/s00122-015-2649-z

Ma, J., Li, H. B., Zhang, C., Yang, X. M., Liu, Y., Yan, G., et al. (2010). Identification and validation of a major QTL conferring crown rot resistance in hexaploid wheat. *Theor. Appl. Genet.* 120, 1119–1128. doi: 10.1007/s00122-009-1239-3

Ma, J., Stiller, J., Zhao, Q., Feng, Q., Cavanagh, C. R., Wang, P., et al. (2014). Transcriptome and allele specificity associated with a 3BL locus for Fusarium crown rot resistance in bread wheat. *PLoS One* 9:e113309. doi: 10.1371/journal.pone.0113309

Ma, J., Yan, G., and Liu, C. (2012a). Development of near-isogenic lines for a major QTL on 3BL conferring Fusarium crown rot resistance in hexaploid wheat. *Euphytica* 183, 147–152. doi: 10.1007/s10681-011-0414-1

Ma, J., Zhang, C. Y., Liu, Y. X., Yan, G. J., and Liu, C. J. (2012b). Enhancing Fusarium crown rot resistance of durum wheat by introgressing chromosome segments from hexaploid wheat. *Euphytica* 186, 67–73. doi: 10.1007/s10681-011-0492-0

Martin, A., Bovill, W. D., Percy, C. D., Herde, D. J., Fletcher, S., Kelly, A., et al. (2015). Markers for seedling and adult plant crown rot resistance

in four partially resistant bread wheat sources. *Theor. Appl. Genet.* 128, 377–385. doi: 10.1007/s00122-014-2437-1

McBeath, J. H., and McBeath, J. (2010). "Plant diseases, pests and food security," in *Environmental Change and Food Security in China*. Advances in Global Change Research (Dordrecht: Springer), 117–156. doi: 10.1007/978-1-4020-9180-3_5

Monds, R. D., Cromey, M. G., Lauren, D. R., Menna, M. E. D., and Marshall, J. W. (2005). *Fusarium graminearum*, F. cortaderiae and F. pseudograminearum in New Zealand: molecular phylogenetic analysis, mycotoxin chemotypes and co-existence of species. *Fungal Biol.* 109, 410–420. doi: 10.1017/s0953756204002217

Obanor, F., and Chakraborty, S. (2014). Aetiology and toxigenicity of Fusarium graminearum and F. pseudograminearum causing crown rot and head blight in Australia under natural and artificial infection. *Plant Pathol.* 63, 1218–1229. doi: 10.1111/ppa.12200

Pariyar, S. R., Erginbasorakci, G., Dadshani, S., Chijioke, O. B., Leon, J., Dababat, A. A., et al. (2020). Dissecting the genetic complexity of Fusarium crown rot resistance in wheat. *Sci. Rep.* 10:3200.

Peralta, A. L., Sun, Y., Mcdaniel, M. D., and Lennon, J. T. (2018). Crop rotational diversity increases disease suppressive capacity of soil microbiomes. *Ecosphere* 9:e02235. doi: 10.1002/ecs2.2235

Poole, G. J., Smiley, R. W., Paulitz, T. C., Walker, C., Carter, A. H., See, D. R., et al. (2012). Identification of quantitative trait loci (QTL) for resistance to Fusarium crown rot (*Fusarium pseudograminearum*) in multiple assay environments in the Pacific Northwestern US. *Theor. Appl. Genet.* 125, 91–107. doi: 10.1007/s00122-012-1818-6

Powell, J. J., Carere, J., Fitzgerald, T. L., Stiller, J., Covarelli, L., Xu, Q., et al. (2017). The Fusarium crown rot pathogen *Fusarium pseudograminearum* triggers a suite of transcriptional and metabolic changes in bread wheat (*Triticum aestivum* L.). *Ann. Bot.* 119, 853–867.

Qiao, F., Yang, X., Xu, F., Huang, Y., Zhang, J., Song, M., et al. (2021). TMT-based quantitative proteomic analysis reveals defense mechanism of wheat against the crown rot pathogen *Fusarium pseudograminearum*. *BMC Plant Biol.* 21:82. doi: 10.1186/s12870-021-02853-6

Rahman, M., Davies, P., Bansal, U., Pasam, R., Hayden, M., and Trethowan, R. (2020). Marker-assisted recurrent selection improves the crown rot resistance of bread wheat. *Mol. Breed.* 40:28.

Ren, Y., Yu, P.-B., Wang, Y., Hou, W.-X., Yang, X., Fan, J.-L., et al. (2020). Development of a rapid approach for detecting sharp eyespot resistance in seedling-stage wheat and its application in Chinese Wheat Cultivars. *Plant Dis.* 104, 1662–1667. doi: 10.1094/pdis-12-19-2718-re

Sharma, R. C., and Duveiller, E. (2007). Advancement toward new spot blotch resistant wheats in South Asia. *Crop Sci.* 47, 961–968. doi: 10.2135/cropsci2006.03.0201

Sharma, R. C., Duveiller, E., and Jacquemin, J. M. (2007). Microsatellite markers associated with spot blotch resistance in spring wheat. *J. Phytopathol.* 155, 316–319. doi: 10.1111/j.1439-0434.2007.01238.x

Shi, S., Zhao, J., Pu, L., Sun, D., Han, D., Li, C., et al. (2020). Identification of new sources of resistance to crown rot and Fusarium head blight in Wheat. *Plant Dis.* 104, 1979–1985. doi: 10.1094/pdis-10-19-2254-re

Singh, P. K., He, X., Sansaloni, C., Juliana, P., Dreisigacker, S., Duveiller, E., et al. (2018). Resistance to spot blotch in two mapping populations of common wheat is controlled by multiple QTL of Minor Effects. *Int. J. Mol. Sci.* 19:4054. doi: 10.3390/ijms19124054

Singh, V., Singh, G., Chaudhury, A., Ojha, A., Tyagi, B. S., Chowdhary, A. K., et al. (2016). Phenotyping at hot spots and tagging of QTLs conferring spot blotch resistance in bread wheat. *Mol. Biol. Rep.* 43, 1293–1303. doi: 10.1007/s11033-016-4066-z

Smiley, R. W., Gourlie, J. A., Easley, S. A., and Patterson, L. (2005). Pathogenicity of fungi associated with the wheat crown rot complex in Oregon and Washington. *Plant Dis.* 89, 949–957. doi: 10.1094/pd-89-0949

Steuernagel, B., Periyannan, S. K., Hernández-Pinzón, I., Witek, K., Rouse, M. N., Yu, G., et al. (2016). Rapid cloning of disease-resistance genes in plants using mutagenesis and sequence capture. *Nat. Biotechnol.* 34, 652–655. doi: 10.1038/nbt.3543

Sun, C., Dong, Z., Zhao, L., Ren, Y., Zhang, N., and Chen, F. (2020). The Wheat 660K SNP array demonstrates great potential for marker−assisted selection in polyploid wheat. *Plant Biotechnol. J.* 18, 1354–1360. doi: 10.1111/pbi.13361

Tembo, B., Sibiya, J., Tongoona, P., and Tembo, L. (2017). Validation of microsatellite molecular markers linked with resistance to Bipolaris sorokiniana in wheat (*Triticum aestivum* L.). *J. Agric. Sci.* 155, 1061–1068. doi: 10.1017/s0021859617000144

Tomar, V., Singh, R. P., Poland, J., Singh, D., Joshi, A. K., Singh, P. K., et al. (2020). Genome-wide association study and genomic prediction of spot blotch disease in wheat (*Triticum aestivum* L.) using genotyping by sequencing. *Res. Square [Preprint].*

Wallwork, H., Butt, M., Cheong, J., and Williams, K. J. (2004). Resistance to crown rot in wheat identified through an improved method for screening adult plants. *Aust. Plant Pathol.* 33, 1–7. doi: 10.1071/ap03073

Wang, H., Sun, S., Ge, W., Zhao, L., Hou, B., Wang, K., et al. (2020). Horizontal gene transfer of Fhb7 from fungus underlies Fusarium head blight resistance in wheat. *Science* 368:eaba5435. doi: 10.1126/science.aba5435

Wang, J., Wang, X., Xu, M., Feng, G., Zhang, W., Yang, X., et al. (2015). Contributions of wheat and maize residues to soil organic carbon under long-term rotation in north China. *Sci. Rep.* 5:11409.

Wang, M., Wang, S., Liang, Z., Shi, W., Gao, C., and Xia, G. (2018a). From genetic stock to genome editing: gene exploitation in wheat. *Trends Biotechnol.* 36, 160–172. doi: 10.1016/j.tibtech.2017.10.002

Wang, X., Bi, W., Gao, J., Yu, X., Wang, H., and Liu, D. (2018b). Systemic acquired resistance, NPR1, and pathogenesis-related genes in wheat and barley. *J. Integr. Agr.* 17, 2468–2477. doi: 10.1016/s2095-3119(17)61852-5

William, M., Singh, R. P., Huertaespino, J., Islas, S. O., and Hoisington, D. A. (2003). Molecular marker mapping of leaf rust resistance gene Lr46 and its association with stripe rust resistance gene Yr29 in wheat. *Phytopathology* 93, 153–159. doi: 10.1094/phyto.2003.93.2.153

Wu, X., Cheng, K., Zhao, R., Zang, S., Bie, T., Jiang, Z., et al. (2017). Quantitative trait loci responsible for sharp eyespot resistance in common wheat CI12633. *Sci. Rep.* 7:11799.

Yang, X., Ma, J., Li, H., Ma, H., Yao, J., and Liu, C. (2010). Different genes can be responsible for crown rot resistance at different developmental stages of wheat and barley. *Eur. J. Plant Pathol.* 128, 495–502. doi: 10.1007/s10658-010-9680-3

Yang, X., Pan, Y., Singh, P. K., He, X., Ren, Y., Zhao, L., et al. (2019). Investigation and genome-wide association study for Fusarium crown rot resistance in Chinese common wheat. *BMC Plant Biol.* 19:153. doi: 10.1186/s12870-019-1758-2

Yang, X., Zhong, S., Zhang, Q., Ren, Y., Sun, C., and Chen, F. (2021). A loss−of−function of the dirigent gene TaDIR−B1 improves resistance to Fusarium crown rot in wheat. *Plant Biotechnol. J.* 19, 866–868. doi: 10.1111/pbi.13554

Zhang, P., Guo, G., Wu, Q., Chen, Y., Xie, J., Lu, P., et al. (2020). Identification and fine mapping of spot blotch (*Bipolaris sorokiniana*) resistance gene Sb4 in wheat. *Theor. Appl. Genet.* 133, 2451–2459. doi: 10.1007/s00122-020-03610-3

Zhao, R., Chen, X., Zhang, F., Zhang, H., Schroder, J. L., and Romheld, V. (2006). Fertilization and Nitrogen Balance in a Wheat–Maize Rotation System in North China. *Agron. J.* 98, 938–945. doi: 10.2134/agronj2005.0157

Zheng, Z., Kilian, A., Yan, G., and Liu, C. (2014). QTL conferring fusarium crown rot resistance in the elite bread wheat variety EGA Wylie. *PLoS One* 9:e96011. doi: 10.1371/journal.pone.0096011 doi: 10.1371/journal.pone.0096011

Zheng, Z., Ma, J., Stiller, J., Zhao, Q., Feng, Q., Choulet, F., et al. (2015). Fine mapping of a large-effect QTL conferring Fusarium crown rot resistance on the long arm of chromosome 3B in hexaploid wheat. *BMC Genomics* 16:850. doi: 10.1186/s12864-015-2105-0

Zhou, H., He, X., Wang, S., Ma, Q., Sun, B., Ding, S., et al. (2019). Diversity of the Fusarium pathogens associated with crown rot in the Huanghuai wheat−growing region of China. *Environ. Microbiol.* 21, 2740–2754. doi: 10.1111/1462-2920.14602

Zhu, X., Lu, C., Du, L., Ye, X., Liu, X., Coules, A., et al. (2017). The wheat NB−LRR gene *Ta RCR 1* is required for host defence response to the necrotrophic fungal pathogen *Rhizoctonia cerealis*. *Plant Biotechnol. J.* 15, 674–687. doi: 10.1111/pbi.12665

Zhu, X., Qi, L., Liu, X., Cai, S., Xu, H., Huang, R., et al. (2014a). The wheat ethylene response factor transcription factor pathogen-induced ERF1 mediates host responses to both the necrotrophic pathogen *Rhizoctonia cerealis* and

freezing stresses. *Plant Physiol.* 164, 1499–1514. doi: 10.1104/pp.113.229575

Zhu, X., Yang, K., Wei, X., Zhang, Q., Rong, W., Du, L., et al. (2015). The wheat AGC kinase TaAGC1 is a positive contributor to host resistance to the necrotrophic pathogen *Rhizoctonia cerealis*. *J. Exp. Bot.* 66, 6591–6603. doi: 10.1093/jxb/erv367

Zhu, Z., Bonnett, D., Ellis, M., Singh, P. K., Heslot, N., Dreisigacker, S., et al. (2014b). Mapping resistance to spot blotch in a CIMMYT synthetic-derived bread wheat. *Mol. Breed.* 34, 1215–1228. doi: 10.1007/s11032-014-0111-6

Conflict of Interest: The authors declare that the research was conducted in the absence of any commercial or financial relationships that could be construed as a potential conflict of interest.

frontiers in Genetics

ORIGINAL RESEARCH
published: 29 June 2021
doi: 10.3389/fgene.2021.681768

Evaluation of Septoria Nodorum Blotch (SNB) Resistance in Glumes of Wheat (*Triticum aestivum* L.) and the Genetic Relationship With Foliar Disease Response

Michael G. Francki[1,2], Esther Walker[1,2], Christopher J. McMullan[1] and W. George Morris[1]*

[1] Department of Primary Industries and Regional Development, South Perth, WA, Australia, [2] State Agricultural Biotechnology Centre, Murdoch University, Murdoch, WA, Australia

OPEN ACCESS

Edited by:
Dale Zhang,
Henan University, China

Reviewed by:
Suraj Sapkota,
Crop Genetics and Breeding Research (USDA-ARS), United States
Frank Maulana,
Noble Research Institute, LLC, United States

***Correspondence:**
Michael G. Francki
M.Francki@murdoch.edu.au

Specialty section:
This article was submitted to Plant Genomics, a section of the journal Frontiers in Genetics

Received: *17 March 2021*
Accepted: *07 June 2021*
Published: *29 June 2021*

Citation:
Francki MG, Walker E, McMullan CJ and Morris WG (2021) Evaluation of Septoria Nodorum Blotch (SNB) Resistance in Glumes of Wheat (Triticum aestivum L.) and the Genetic Relationship With Foliar Disease Response. Front. Genet. 12:681768. doi: 10.3389/fgene.2021.681768

Septoria nodorum blotch (SNB) is a necrotrophic disease of wheat prominent in some parts of the world, including Western Australia (WA) causing significant losses in grain yield. The genetic mechanisms for resistance are complex involving multiple quantitative trait loci. In order to decipher comparable or independent regulation, this study identified the genetic control for glume compared to foliar resistance across four environments in WA against 37 different isolates. High proportion of the phenotypic variation across environments was contributed by genotype (84.0% for glume response and 82.7% for foliar response) with genotype-by-environment interactions accounting for a proportion of the variation for both glume and foliar response (14.7 and 16.2%, respectively). Despite high phenotypic correlation across environments, most of the eight and 14 QTL detected for glume and foliar resistance using genome wide association analysis (GWAS), respectively, were identified as environment-specific. QTL for glume and foliar resistance neither co-located nor were in LD in any particular environment indicating autonomous genetic mechanisms control SNB response in adult plants, regulated by independent biological mechanisms and influenced by significant genotype-by-environment interactions. Known *Snn* and *Tsn* loci and QTL were compared with 22 environment-specific QTL. None of the eight QTL for glume or the 14 for foliar response were co-located or in linkage disequilibrium with *Snn* and only one foliar QTL was in LD with *Tsn* loci on the physical map. Therefore, glume and foliar response to SNB in wheat is regulated by multiple environment-specific loci which function independently, with limited influence of known NE-*Snn* interactions for disease progression in Western Australian environments. Breeding for stable resistance would consequently rely on recurrent phenotypic selection to capture and retain favorable alleles for both glume and foliar resistance relevant to a particular environment.

Keywords: septoria nodorum, parastagonospora nodorum, glume, foliar, wheat, QTL, environment

INTRODUCTION

Parastagonospora (syn. ana, *Stagonospora*; teleo, *Phaeosphaeria*) *nodorum* (Berk.) Quaedvlieg, Verkley & Crous is the causal pathogen of Septoria nodorum blotch (SNB) of wheat that infects the lower leaves of the canopy and is identified by dark brown round or lens shaped spots that coalesce and develop black pycnidia as lesions mature (Eyal et al., 1987). Early foliar symptoms in Western Australia (WA) are seen at tillering (Feekes 5) and is a precursor to glume infection. Rain splash disperses spores whereby foliar disease symptoms proliferate under high humidity and infection continues up the canopy through to stem elongation and ripening. Infected heads will turn dark brown often with a purple tint and black pycnidia evident as typical glume blotch symptoms (Eyal et al., 1987). Yield losses are estimated to be approximately 12% where SNB is considered to be a major necrotrophic disease affecting grain yield in Western Australian production environments (Murray and Brennan, 2009) as well as other regions of the world, particularly as a recurrent disease of wheat in several geographical areas of the United States (Cowger et al., 2020). Fungicide applications provide opportunities for controlling the pathogen, but the use of SNB resistant cultivars can significantly reduce on-farm costs. However, breeding for leaf and glume blotch resistance is challenging due to the inherent genetic complexity controlling SNB response when the disease is most damaging (reviewed in Francki, 2013).

Similar to leaf blotch, glume blotch response is under quantitative control having additive-dominance effects for resistance with some interactions with non-allelic genes (Wicki et al., 1999). Dominance for glume blotch susceptibility is common (Fried and Meister, 1987; Wicki et al., 1999) whereas dominance for resistance also exists in specific crosses (Wicki et al., 1999). Moreover, morphological characteristics can have a profound effect on disease response so it is important to discriminate between pleiotropy and linkage with resistance in genetic analysis (Francki, 2013). There have been at least 20 QTL associated with glume resistance identified across the wheat genome with each accounting for up to 24% of the phenotypic variation indicating varying effects of each QTL contributing to resistance (Schnurbusch et al., 2003; Uphaus et al., 2007; Shankar et al., 2008; Czembor et al., 2019; Lin et al., 2020). Similarly, at least 18 QTL have been identified for foliar resistance (reviewed in Francki, 2013; Ruud and Lillemo, 2018) with subsequent reports of others that may represent existing or, indeed, new QTL (Czembor et al., 2019; Ruud et al., 2019; Francki et al., 2020; Lin et al., 2020). Despite the large number of loci, only few were detected in more than one environment including one QTL on 2D (Uphaus et al., 2007), 3A, 3B (Schnurbusch et al., 2003) and 4B (Schnurbusch et al., 2003; Shankar et al., 2008) for glume resistance and 1B (Francki et al., 2011); 7D (Czembor et al., 2019) and two on 2A (Lin et al., 2020) for foliar response. Many QTL detected for glume and foliar SNB response, therefore, appear to be environment-specific. Quantitative genetic analysis detected QTL for either glume or foliar SNB response in different field environments whereby some shared the same marker interval (Schnurbusch et al., 2003; Lin et al., 2020) indicated similar genes may have an effect on disease resistance or susceptibility in both organs. On the contrary, some studies did not detect the same QTL for glume and foliar resistance (Shankar et al., 2008; Czembor et al., 2019) confirming that alternative genes are seemingly under independent control and in agreement with earlier studies (Fried and Meister, 1987; Wicki et al., 1999). However, comparison between the genetic control of glume and foliar response to SNB in those studies were based on bi- (Shankar et al., 2008; Czembor et al., 2019) or multi-parental (Lin et al., 2020) populations where diversity is limited and the extent of alleles and effects on either resistance, susceptibility or both is not broadly exploited in global germplasm pools. Evaluation of a wider gene pool coupled with high marker density genetic mapping would further extrapolate allelic diversity and gene interactions to expand our knowledge on similar and/or independent genetic mechanisms controlling both glume and foliar SNB response in WA environments.

P. nodorum expresses a range of necrotrophic effectors (NE) that interact with corresponding sensitivity loci (*Snn*) that induce necrosis in wheat (reviewed in McDonald and Solomon, 2018). There were nine NE-*Snn* interactions identified in wheat on chromosomes 1A, 1B, 2A, 4B, 5B, and 6A (Abeysekara et al., 2009; Friesen et al., 2009, 2012; Gao et al., 2015; Shi et al., 2015; Phan et al., 2016; Ruud et al., 2017; Downie et al., 2018). It was shown that some *Snn* loci may play a role in foliar disease progression under SNB infection in multiple field environments (Friesen et al., 2009) while other studies indicated known NE-*Snn* interactions were either inconsistent or not associated with QTL in controlling disease development in different environments when inoculated with single or a mixture of isolates (Ruud and Lillemo, 2018; Czembor et al., 2019; Ruud et al., 2019; Francki et al., 2020; Lin et al., 2020). Interestingly, it has been suggested that known NE-*Snn* interactions are not a significant determinant for foliar response in eastern soft red winter wheat germplasm but the effect of unknown *Snn* loci cannot be excluded (Cowger et al., 2020). Similar observations and conclusions were drawn when an extensive collection of wheat germplasm from different regions of the world were evaluated in multi-environments using mixture of isolates from Western Australia (Francki et al., 2020). Despite the increased knowledge of NE-*Snn* interactions controlling foliar response to SNB, the role of characterized NE-*Snn* interactions for glume susceptibility and resistance is largely unknown in WA environments.

Genome-wide association studies (GWAS) provide an opportunity to simultaneously evaluate wheat accessions and identify the genetic basis of trait variation through marker-trait associations (MTA). GWAS is used increasingly to identify the genetic control of foliar response to SNB using germplasm representing a wider representation of alleles from different regions of the world (Ruud et al., 2019; Francki et al., 2020). High-density single nucleotide polymorphic (SNP) markers using the iSelect Infinium 90K SNP genotyping array (Wang et al., 2014) have provided a finer resolution of QTL and their association with previous known genetic and *Snn* specific loci. In multi-environment analysis, QTL for foliar SNB response were detected as environment specific on chromosomes 1A, 1B, 4B, 5A, 5B, 6A, 7A, 7B, 7D (Francki et al., 2020) whereas

loci on chromosomes 2B, 2D, 4A, 4B, 5A, 5B, 6B, 7A, and 7B were detected in more than one field environment (Ruud et al., 2019) but with no common QTL confirmed between studies. The relationship between NE-*Snn* interactions and foliar disease response in adult plant in GWAS was largely inconsistent across multiple environments (Ruud et al., 2019; Cowger et al., 2020; Francki et al., 2020). To date, GWAS has neither been applied to investigate the genetic control for glume blotch resistance nor its association with known NE-*Snn* loci from a wider representation of alleles in global germplasm. Finer mapping resolution using GWAS and the iSelect Infinium 90K SNP genotyping array (Wang et al., 2014) will provide an in-depth analysis and increase our knowledge on the relationship between glume and foliar response and known NE-*Snn* interactions when adult plants are infected with different isolates across multiple field environments in WA.

Although consistent and high disease pressure enabled a reliable evaluation of foliar resistance to SNB across six WA environments (Francki et al., 2020), the lack of sustained disease progression during the grain filling period at five sites in 2016–2018 precluded reliable analysis for glume response. The aim of this study, therefore, was to evaluate glume response to SNB for 232 wheat lines in successive year field trials in environments where sustained glume blotch disease progression was consistent during the grain fill period in Western Australia. Moreover, the study aimed to identify genotype-by-environment interactions, compare and contrast the genetic control of glume with foliar response using GWAS and ascertain the significance of NE-*Snn* interactions in WA environments. The outcome of the study will provide knowledge on shared or independent genetic determinants regulating glume and foliar resistance to SNB in global wheat germplasm when evaluated in multiple field environments under different isolates.

MATERIALS AND METHODS

Plant Material

The GWAS panel consisted of 232 hexaploid wheat lines including 71 lines from Australia, 72 inbred and commercial lines from Centro Internacional de Mejoramiento de Maiz y Trigo (CIMMYT), 78 inbred lines from International Center for Agricultural Research in the Dry Areas (ICARDA), and 11 landraces from various origins. Description of lines, pedigrees and their origins for the GWAS population used in this study was reported in Francki et al. (2020) and detailed in **Supplementary Table 1**.

Field Trial Design

Trials were sown at Department of Primary Industries and Regional Development (DPIRD) Manjimup Research Station and DPIRD South Perth Nursery (Western Australia) in 2018–2020 and 2020, respectively. All trials were sown as completely randomized designs with three replications for each genotype. Plots in each trial at Manjimup were sown as two-rows of 1.9 m length and 0.2 m row spacing. Each row contained ∼100 seeds. The susceptible cultivar "Amery," a Western Australian variety with consistent SNB susceptibility across environments (Francki et al., 2020), was sown as two-row plots of 1.9 m length adjacent to each treatment plot to maintain consistency in disease progression. In the 2020 South Perth trial, plots were sown as two-rows of 0.5 m length and 0.2 m spacing with a spreader two-row plot ("Amery") of 0.5 m length adjacent to each treatment. Each row contained ∼25 seeds. The susceptible genotypes for glume and leaf blotch (three replications) included "Millewa," "Arrino," "Scout" and the landrace, 040HAT10, were sown in each trial at Manjimup and South Perth and used to monitor disease progression. EGA Blanco, 30ZJN09 and 6HRWSN125 were sown as resistant check genotypes.

Isolates, Culture Preparation and Inoculation of Field Trials

Isolates of *P. nodorum* were sourced from the culture collection at DPIRD and collected from different regions of WA. A total of 19, 17 and 12 isolates were selected and used in equal amounts as mixed inoculum for trials in 2018, 2019, and 2020, respectively (**Supplementary Table 2**). At least 40% of the isolates used in each year were represented in the mixed inoculum in the following year with three common isolates, WAC13077, WAC13206 and WAC13872 used in all trials (**Supplementary Table 2**). Fungal cultures and mixed inoculum consisting of equal amounts of *P. nodorum* isolates (10^6 spores/ml) were prepared and all plots for each trial were inoculated at a rate of 28.5 m^2/L as previously described (Francki et al., 2020). Inoculation in each trial commenced from formed tillers to leaf sheaths lengthening and strongly erect (Feekes 3–5) with three subsequent inoculations at 14-day intervals.

Environment Characterization, SNB Disease and Agronomic Measurements

Trials at DPIRD Manjimup research station and South Perth nursery were in close proximity to weather stations for recording of climatic conditions including air temperature, relative humidity, rainfall, solar exposure and pan evaporation to identify parameters that may affect disease progression within and between environments. Climate data was recorded daily and accessed through DPIRD weather and radar database.[1] Thermal time (°Cd) for the duration of disease progression was calculated using the sum of average daily minimum and maximum air temperature as $\sum(\min temp + \max temp/2)$ from the day of first inoculation to the day of disease measurement.

Susceptible check varieties were monitored weekly for SNB disease progression and visually assessed for necrosis on the glume and flag leaf and recorded on a percent glume area disease (PGAD) and percent flag-leaf area disease (PLAD) scale as described by James (1971). Trials were visually assessed for other necrotrophic diseases weekly, particularly yellow spot, with no symptoms detected in any of the trials. Each plot scored five individual random plants for SNB disease symptoms from the middle of the row closest to the spreader susceptible plot. PLAD on the flag leaf represented foliar disease whereas PGAD

[1] https://weather.agric.wa.gov.au/

on the head represented glume disease for each replicate. All plots in the trial were scored at the same time when at least two check susceptible varieties had PGAD > 50% and PLAD > 70%. Foliar and glume disease scores for each replicate determined mean plot values.

Heading date was measured from the number of days from sowing for each replicate to reach 50% full head emergence. Plant height was measured for three random plants from the middle of the row closest to the spreader susceptible plot. Height (cm) was taken from the soil level to the top of the head (excluding awns) and mean plot values was used for statistical analysis.

Statistical Analysis

All statistical analyses for phenotypic evaluation were done using Genstat, 19th edition.[2] Generalized linear models and linear mixed models were used in phenotypic analysis of trait data. Treatment factors, plant height and heading date used as co-variates were fitted to fixed models to estimate main effects and interactions. Best linear unbiased predictors (BLUP) for PGAD and PLAD were calculated for each environment based on linear mixed models assuming fixed effect for genotypes and used for subsequent QTL analysis using GWAS. Finlay-Wilkinson joint regression analysis was used to compare genotypes for SNB response and agronomic traits across four environments. Broad-sense heritability estimates were calculated using the formula $H^2 = \sigma_g{}^2/\sigma_p{}^2$ where $\sigma_g{}^2$ and $\sigma_e{}^2$ are the genotypic and phenotypic variances, respectively (Wray and Visscher, 2008).

Genome-Wide Association Analysis

As the same wheat lines in this study were used previously, detailed methodology for genotyping, analysis of population structure and genome wide association was previously described by Francki et al. (2020). Briefly, the 232 wheat lines were genotyped using the 90K Infinium SNP chip array (Wang et al., 2014) and SNP markers with <80% call rate and <5% minor allele frequencies were removed resulting in a total of 20,563 SNPs used for analysis. TASSEL v.5.2.52 was used to identify marker-trait associations (MTAs) (Bradbury et al., 2007). A mixed linear model (MLM) was determined to be the most appropriate to account for both structure and cryptic relatedness for this population (Francki et al., 2020). The genotypic kinship matrix (K) was estimated by selecting the "Centered_IBS" method and population structure (Q) was corrected using principal component (PC) analysis. The suitable number of PCs for each trait was determined by testing one through 15 PCs with visual assessment of quantile-quantile plots (Q-Q plots). The option "P3D" was not selected during the MLM analysis with the variance component re-estimated after each marker. The R programs "qqman" and "Rcolorbrewer" were used to draw Manhattan plots (Turner, 2017; R Core Team, 2018). A genome-wide significance threshold for MTAs was set at $p < 2.43 \times 10^{-6}$ ($-\log_{10}(p) > 5.61$) using Bonferroni correction with $\alpha = 0.05$. To estimate the number of independent tests the tagger function in Haploview was implemented as described in Maccaferri et al. (2016) with a r^2 of ≤ 0.1. This returned a genome-wide moderate threshold significance of $p < 7.65 \times 10^{-5}$ ($-\log_{10}(p) > 4.12$). A suggestive threshold of significance of $p < 1 \times 10^{-3}$($-\log_{10}(p) > 3.00$) was also included in Manhattan plots as previously reported (Gao et al., 2016; Alomari et al., 2017; Muqaddasi et al., 2019).

Marker pairwise r^2 values were calculated in PLINK 1.9 (Purcell et al., 2007) with a sliding window of 50 and LD decay curves fitted by non-linear regression for each genome (A, B and D) as described by Marroni et al. (2011) with decay of r^2 against distance. LD decay plots were drawn in R with a critical threshold of $r^2 = 0.2$ (R Core Team, 2018). MTA for QTL were defined to be in LD when their physical distance was within the linkage decay value for their respective sub-genomes.

Assignment of QTL, *Snn* and *Tsn1* to the Physical Map

Physical locations of SNP markers were obtained using Pretzel v2.2.6, an interactive, web-based platform for navigating multi-dimensional wheat datasets, including genetic maps and chromosome-scale physical assemblies (Keeble-Gagnère et al., 2019). *Snn* and *Tsn1* loci were anchored to the physical map using SNP markers, or the closest linked SSR markers, as described in Francki et al. (2020). For markers not available in Pretzel v2.2.6, putative locations were obtained using the IWGSC RefSeq v1.0 and the BLAST tool at URGI INRA.[3]

RESULTS

Environment Characterization

Daily average climate measurements during disease progression at DPIRD Manjimup research station in 2018–2020 were consistent in successive years for air temperature, relative humidity, rainfall, solar exposure and pan evaporation (**Supplementary Table 3**). Similarly, the total rainfall recorded was 500, 411, and 441 mm in 2018, 2019, and 2020, respectively. The climatic conditions at Manjimup WA, therefore, were consistent in 2018–2020. However, the site at South Perth WA was higher in average daily air temperature, solar exposure and pan evaporation but lower for relative humidity and rainfall compared to any year at Manjimup (**Supplementary Table 3**), with considerably less total rainfall of 313 mm in the period from first inoculation to final disease score. The trial at South Perth in 2020, therefore, provided an opportunity to compare the response of 232 wheat lines to glume and foliar SNB infection under different climatic environments.

Assessment of Glume Response to SNB

A total of 232 wheat lines were evaluated for glume and leaf response to SNB in each year at Manjimup (2018–2020) and at South Perth in 2020. Thermal times for disease evaluation when PGAD was >50% for at least two susceptible check varieties at Manjimup was 1117^{o}Cd -1238^{o}Cd in 2018–2020 but higher (1589^{o}Cd) at South Perth (**Supplementary Table 4**) indicating

[2]https://genstat.kb.vsni.co.uk

[3]https://urgi.versailles.inra.fr/

climate differences affected rate of progression of glume blotch symptoms. Nevertheless, glume response showed consistently high heritability across all sites (H^2 = 0.79 to 0.89; **Table 1**) indicating that a significant proportion of phenotypic difference within each environment is controlled by genetic variation. The mean and median of the population for glume response were similar (29.0 to 33.0 and 27.0 to 30.0, respectively; **Table 1**) indicating comparable disease pressure for glume response across environments within and between years and normal distribution of disease response for the 232 wheat lines (**Supplementary Figure 1**) in each environment. There was a high and significant linear relationship for PGAD scores between successive trials at Manjimup (r = 0.76 to 0.82; $P < 0.001$) and between the South Perth and Manjimup trials (r = 0.73 to 0.78; $P < 0.001$) indicating consistent glume response of genotypes across all environments (**Table 2**). There was moderate negative correlation between heading date and PGAD in each trial (r = −0.46 to −0.63; $P < 0.001$) and low to moderate negative correlation between plant height and PGAD (r = −0.34 to −0.64; $P < 0.001$) in each environment (**Table 3**) indicating potential pleiotropic effects between morphological traits and glume response. The genotype, environment and their interactions were fitted as terms in a linear mixed model and the significant proportion of glume response was attributed to genotype (84%) followed by genotype-by-environment interactions (14.7%) with only small proportion of the variation (1.3%) attributed by the environment (**Table 4**).

Assessment of Foliar Response to SNB

Similar to glume response, thermal times (when PLAD was >70% for at least two susceptible check varieties) were comparable between years at Manjimup but lower than at South Perth (**Supplementary Table 4**), indicating climate affected rate of foliar disease progression between geographical locations.

TABLE 1 | Summary of percent glume area disease (PGAD), percent leaf area disease (PLAD), heading date (HD) and plant height (PH) for 232 global wheat lines evaluated in four environments in Western Australia in 2018–2020.

	Manjimup 2018				Manjimup 2019				Manjimup 2020				South Perth 2020			
	PGAD	PLAD[a]	HD[a]	PH[a]	PGAD	PLAD	HD	PH	PGAD	PLAD	HD	PH	PGAD	PLAD	HD	PH
Minimum	4.0	2.0	86.0	73.0	1.0	4.0	89.0	71.0	0.0	4.0	95.0	63.0	3.0	3.0	81.0	68.0
Maximum	78.0	97.0	133.0	123.0	83.0	90.0	126.0	117.0	72.0	95.0	131.0	117.0	75.0	97.0	113.0	107.0
Grand Mean	29.0	38.0	111.0	94.0	29.0	40.0	109.0	94.0	30.0	44.0	113.0	89.0	33.0	43.0	93.0	83.0
Median	27.0	36.0	110.0	94.0	27.0	38.0	108.0	93.0	30.0	43.0	113.0	89.0	30.0	42.0	92.0	82.0
Mode	17.0	53.0	115.0	94.0	45.0	52.0	106.0	94.0	45.0	60.0	117.0	91.0	53.0	50.0	89.0	82.0
ANOVA (P)	$P<0.001$	$P<0.001$	$P<0.001$	$P<0.001$	< 0.001	< 0.001	< 0.001	< 0.001	< 0.001	< 0.001	< 0.001	< 0.001	< 0.001	< 0.001	< 0.001	< 0.001
LSD ($P<0.05$)	15.3	19.6	4.9	6.8	14.8	24.4	4.2	6.2	15.3	21.9	5.7	8.6	17.9	21.8	6.6	6.9
CV (%)	31.7	30.6	2.8	4.5	32.4	15.6	2.4	4.2	31.5	31.3	3.1	6.0	34.1	31.5	4.4	5.2
H^2	0.79	0.88	0.94	0.90	0.89	0.91	0.92	0.96	0.86	0.79	0.88	0.78	0.86	0.89	0.81	0.80

[a]*PLAD and agronomic scores reported in Francki et al. (2020).*

TABLE 2 | Phenotypic correlation between four trials at Manjimup (MJ) and South Perth (SP) Western Australia in 2018–2020 of 232 wheat lines for percent glume and leaf area diseased (PGAD and PLAD, respectively).

	PGAD				PLAD			
	MJ2018	MJ2019	MJ2020	SP2020	MJ2018	MJ2019	MJ2020	SP2020
MJ2018	–	–	–	–	–	–	–	–
MJ2019	0.78**	–	–	–	0.82**	–	–	–
MJ2020	0.76**	0.82**	–	–	0.71**	0.75**	–	–
SP2020	0.73**	0.78**	0.75**	–	0.75**	0.77**	0.68**	–

***P<0.001.*

TABLE 3 | Phenotypic correlations (*r*) between percent glume and leaf area disease (PGAD and PLAD, respectively), heading date (HD) and plant height (PH) at four environments in Western Australia in 2018–2020.

	Manjimup 2018				Manjimup 2019				Manjimup 2020				South Perth 2020			
	PGAD	PLAD	HD	PH	PGAD	PLAD	HD	PH	PGAD	PLAD	HD	PH	PGAD	PLAD	HD	PH
HD	−0.53**	−0.66**			−0.58**	−0.70**	–		−0.46**	−0.54**	–		−0.63**	−0.59**	–	
PH	−0.64**	−0.59**	0.40**		−0.48**	−0.52**	0.33**	–	−0.34**	−0.40**	0.37**	–	−0.45**	−0.37**	0.21*	–

***P < 0.001; *P < 0.01.*

PLAD on flag leaves representing foliar response to SNB showed consistently high broad-sense heritability (H^2 = 0.79–0.91) and comparable population mean, median and mode (**Table 1**) with either normal or edge-peaked distribution for foliar disease response (**Supplementary Figure 1**) between environments. High Pearson's correlation was evident (r = 0.68 to 0.82; $P < 0.001$) indicating comparable foliar response of genotypes across four environments (**Table 2**). As with glume response, a moderate but significant negative correlation was observed between foliar response and morphological traits including heading date (r = −0.54 to −0.70; P < 0.001) and plant height (r = −0.37 to −0.59; $P < 0.001$) (**Table 3**). The phenotypic variation for foliar response contributed by genotype, environment and their interactions was similar to glume response with genotype and genotype-by environment interactions accounting for most of the variation (82.7 and 16.2%, respectively) while environmental effects (1.1%) contributed the smallest proportion of variation across environments (**Table 4**).

Comparison of Glume and Foliar Response to SNB

The moderate to high Pearson's correlation (r = 0.56 to 0.82; $P < 0.001$) observed between PGAD and PLAD (**Table 5**) indicated a higher proportion of wheat lines have similar SNB response for glume and foliar disease when evaluated in a given environment regardless of the same or different isolates used as inoculum. A Finlay and Wilkinson joint regression model identified 35 lines as glume resistant (PGAD < 20%) across four environments in 2018–2020 ranked in ascending order based on sensitivity to SNB response compared to susceptible control lines with similar heading date and plant height (**Table 6**). Furthermore, 21 lines identified as resistant to glume infection also had moderate resistance to foliar disease with PLAD < 30% (**Table 6**). The remaining 14 lines identified as glume resistant were identified as moderately susceptible or susceptible to foliar disease (PLAD > 30%) similar to the susceptible control lines (**Table 6**). Therefore, similarities and differences in glume and foliar SNB response of individual genotypes indicated that either comparable or alternative genetic loci play a role in controlling resistance and susceptibility in different organs of adult plants when evaluated across multiple WA environments.

QTL for Glume and Foliar Response to SNB and Relationship With Known NE-*Snn* Interactions

The genetic relatedness of the GWAS panel was previously reported to have low population structure with 15.6% of the genetic variance accounted for in the first three principal components using the 20,563 filtered SNP markers (Francki et al., 2020). Linkage decay for physical distance was estimated by non-linear regression at 9.6 Mbp, 14.9 Mbp, and 21.0 Mbp for the A, B and D sub-genomes, respectively, for threshold R^2 = 0.2 (**Supplementary Figure 2**). The linkage decay values were used as estimates for markers in LD when multiple significant MTA were identified in similar genomic regions on the physical map.

GWAS was used to identify shared and independent genomic regions that control glume and foliar response to SNB in different environments. Heading date and plant height were fitted as co-variates in a general linear model to reduce confounding

TABLE 4 | Linear mixed model analysis for genotypes, environments and their interactions with respect to percent glume and leaf area diseased (PGAD and PLAD, respectively) for 232 wheat lines evaluated in four environments in Western Australia in 2018–2020.

	PGAD				PLAD			
Source of variation	**Wald statistic**	***F***	***P*[a]**	**%Var[b]**	**Wald statistic**	***F***	***P*[a]**	**%Var[b]**
Genotype (G)	6189.21	19.46	< 0.001	84.0	6245.22	19.04	< 0.001	82.7
Environment (E)	96.83	32.28	< 0.001	1.3	80.37	26.79	< 0.001	1.1
GxE	1079.16	1.77	< 0.001	14.7	1222.59	2.04	< 0.001	16.2

[a] *F-test probability of Wald statistic.*
[b] *Percentage of variation associated with each term or interaction.*

TABLE 5 | Pearson's correlation coefficient between four trials at Manjimup (MJ) and South Perth (SP) Western Australia in 2018–2020 of 232 wheat lines for percent glume and leaf area diseased (PGAD and PLAD, respectively).

	PGAD MJ2018	**PGAD MJ2019**	**PGAD MJ2020**	**PGAD SP2020**	**PLAD MJ2018**	**PLAD MJ2019**	**PLAD MJ2020**	**PLAD SP2020**
PGAD MJ2018	–							
PGAD MJ2019	0.78**	–						
PGAD MJ2020	0.76**	0.82**	–					
PGAD SP2020	0.73**	0.78**	0.75**	–				
PLAD MJ2018	0.81**	0.67**	0.65**	0.62**	–			
PLAD MJ2019	0.73**	0.82**	0.71**	0.66**	0.82**	–		
PLAD MJ2020	0.63**	0.66**	0.76**	0.56**	0.71**	0.76**	–	
PLAD SP2020	0.65**	0.68**	0.63**	0.71**	0.75**	0.77**	0.68**	–

***P < 0.001.*

TABLE 6 | Assessment of wheat lines using Finlay-Wilkinson joint regression for low mean PGAD scores (<20%) and stability across four WA environments with corresponding PLAD scores, heading date and plant height compared with control susceptible lines in 2018–2020.

	PGAD			PLAD			Heading Date	Plant Height
Varieties/Inbreds	**Mean (s.e.)**	**Sensitivity (s.e.)[a]**	**Mean square deviation[b]**	**Mean (s.e.)**	**Sensitivity (s.e.)**	**Mean square deviation**	**Mean (s.e.)**	**Mean (s.e.)**
PGAD resistant								
EGA Bonnie Rock	9.95 (9.7)	−17.33 (7.3)	89.3	35.42 (6.8)	−4.78 (4.1)	68.2	104.3 (2.9)	91.4 (2.5)
ZWW09Qno177	13.11 (9.4)	−12.53 (6.2)	210.0	49.02 (6.8)	−5.07 (2.9)	171.7	103.1 (2.8)	90.7 (2.5)
EGA Blanco	6.01 (9.7)	−3.75 (7.3)	32.8	11.60 (6.8)*	−4.25 (4.0)	43.9	108.6 (2.9)	92.1 (2.5)
53:ZIZ12	15.30 (9.4)	−3.75 (6.2)	212.8	34.83 (6.8)	−1.60 (3.0)	261.6	111.7 (2.8)	96.9 (2.5)
ZEE10Qno133	13.62 (9.4)	−3.68 (6.2)	192.6	41.8 (6.8)	1.96 (2.9)	60.2	107.7 (2.8)	84.8 (2.5)
ZVS07Qno227	7.44 (9.4)	−2.94 (6.2)	19.2	41.44 (6.8)	5.70 (2.9)	208.3	104.5 (2.8)	94.7 (2.5)
ZWW09Qno72	16.22 (9.4)	−2.94 (6.2)	58.0	48.2 (6.8)	0.89 (2.9)	83.5	111.2 (2.8)	91.5 (2.5)
ZWB11Qno95	3.88 (9.4)	−2.15 (6.2)	13.4	26.49 (6.8)	5.27 (2.9)	56.5	110.4 (2.8)	91.3 (2.5)
WAWHT2046	16.67 (3.0)	−1.77 (1.2)	71.1	15.33 (3.8)*	−1.57 (1.1)	85.2	103.6 (1.0)	96.7 (1.4)
ZWW10Qno139	6.91 (9.4)	−1.25 (6.2)	64.8	10.99 (6.8)	−1.26 (2.9)	69.9	110.0 (2.5)	100.5 (2.5)
ZEE10Qno77	9.78 (11.3)	−0.23 (7.2)	24.1	24.49 (8.2)*	5.40 (3.3)	34.4	109.8 (2.9)	100.4 (3.0)
ZWW10Qno60	13.51 (9.4)	−0.19 (6.2)	23.9	40.78 (6.8)	−0.25 (2.9)	262.9	111.4 (2.8)	89.3 (2.5)
Pfau	14.83 (3.0)	−0.09 (1.2)	63.5	22.68 (3.8)	−1.51 (1.1)	69.3	110.4 (1.0)	90.8 (1.4)
Yandanooka	17.5 (3.0)	0.11 (1.2)	52.4	37.00 (3.8)	−2.67 (1.1)	77.8	108.2 (1.0)	95.6 (1.4)
54:ZIZ13	9.00 (3.0)	0.26 (1.2)	38.3	19.50 (3.8)	0.36 (1.1)	151.6	111.2 (1.0)	97.2 (1.4)
159:ZIZ13	19.67 (3.0)	0.30 (1.2)	50.0	36.67 (3.8)	1.27 (1.1)	81.8	111.6 (1.0)	91.7 (1.4)
75:ZIZ13	17.50 (3.0)	0.34 (1.2)	27.1	22.58 (3.8)	1.07 (1.1)	177.5	111.3 (1.0)	85.6 (1.4)
6HRWSN125	5.83 (3.0)	0.38 (1.2)	21.9	13.92 (3.8)*	−0.23 (1.1)	248.2	105.5 (1.0)	97.9 (1.4)
Brookton	14.92 (3.0)	0.47 (1.2)	13.1	27.02 (3.8)	3.59 (1.1)	202.2	109.8 (1.0)	94.2 (1.4)
Bumper	15.83 (3.0)	0.71 (1.2)	33.3	24.67 (3.8)	−2.31 (1.1)	162.5	107.8 (1.0)	94.9 (1.4)
Lang	16.67 (3.0)	0.73 (1.2)	86.0	26.17 (3.8)	1.18 (1.2)	132.8	109.7 (1.0)	90.1 (1.4)
ZJN10Qno12	11.08 (3.0)	0.92 (1.2)	55.1	16.62 (3.8)	1.78 (1.1)	82.7	109.9 (1.0)	99.2 (1.4)
88:ZIZ13	15.17 (3.0)	1.06 (1.2)	111.0	32.17 (3.8)	−0.00 (1.1)	60.0	109.9 (1.0)	89.7 (1.4)
110:ZIZ13	16.83 (3.0)	1.18 (1.2)	17.0	26.08 (3.8)	0.89 (1.1)	243.4	110.0 (1.0)	94.0 (1.4)
Excalibur	16.00 (3.0)	1.21 (1.2)	26.9	33.08 (3.8)	1.50 (1.1)	251.9	108.5 (1.0)	90.6 (1.4)
ZWW10Qno31	12.61 (9.4)	1.23 (6.2)	106.1	29.04 (6.8)	6.34 (3.0)	201.5	112.2 (2.8)	96.3 (2.5)
Sokoll	12.00 (3.0)	1.26 (1.2)	62.1	51.02 (3.8)	3.93 (1.1)	202.8	108.5 (1.0)	91.8 (1.4)
56:ZIZ13	18.33 (3.0)	1.32 (1.2)	38.0	36.08 (3.8)	−0.09 (1.1)	183.8	106.8 (1.0)	93.6 (1.4)
EGA Castle Rock	15.51 (4.5)	1.39 (1.4)	93.7	10.03 (5.5)*	−0.19 (1.3)	9.2	101.8 (1.6)	96.6 (2.0)
Suntop	17.58 (3.0)	1.45 (1.2)	70.5	28.05 (3.8)	3.78 (1.1)	352.1	111.0 (1.0)	91.1 (1.4)
30ZJN09	8.17 (3.0)	1.81 (1.2)	8.2	22.30 (3.8)*	−1.01 (1.1)	98.2	106.8 (1.0)	94.7 (1.4)
Tammin	13.33 (3.0)	2.88 (1.2)	48.3	12.85 (3.8)*	−0.544 (1.1)	61.9	112.2 (1.0)	89.9 (1.4)
Ajana	17.92 (3.0)	3.20 (1.2)	100.9	42.63 (3.8)*	4.77 (1.1)	219.9	106.3 (1.0)	90.4 (1.4)
ZWW09Qno157	19.93 (9.4)	4.79 (6.2)	13.5	27.81 (6.8)	3.22 (2.9)	29.3	110.4 (2.8)	102.6 (2.5)
ZVS09Qno133	18.64 (9.4)	5.85 (6.2)	19.1	16.38 (6.8)*	0.47 (2.9)	19.7	110.1 (2.8)	93.7 (2.5)
PGAD susceptible								
Millewa	60.83 (3.0)	1.88 (1.2)	113.1	81.25 (3.8)	−1.44 (1.1)	73.0	105.1 (1.0)	84.2 (1.4)
Arrino	36.92 (3.0)	2.69 (1.2)	86.8	52.08 (3.8)	1.70 (1.1)	88.6	101.8 (1.0)	86.5 (1.4)
Scout	31.08 (3.0)	2.95 (1.2)	157.2	47.92 (3.8)	3.31 (1.1)	116.4	111.6 (1.0)	86.4 (1.4)
040HAT10	47.52 (3.2)	3.30 (1.4)	84.0	59.86 (4.0)	1.21 (1.3)	294.0	107.7 (1.1)	91.0 (1.4)

Wheat lines are ordered according to decreased sensitivity for glume SNB response. Standard error is denoted by s.e. Wheat lines with low PLAD scores evaluated in 2016–2018 (Francki et al., 2020) are shown with an asterisk.

[a] *Genotypes ranked in ascending order from the most stable assessed by sensitivity of PLAD response to environmental effects.*

[b] *Predictability of response to SNB assessed by mean square deviation.*

pleiotropic effects of plant morphology on disease scores in each environment. BLUP for PGAD and PLAD were subsequently used for MTA in GWAS analysis. Q-Q plots showed deviations of the observed associations compared to the null hypothesis indicating SNP markers are associated with glume and foliar SNB response with QTL detected for at least a moderate level of significance of $p < 7.65 \times 10^{-5}$ ($-\log_{10}(p) > 4.12$) in Manhattan plots for each environment (**Supplementary Figures 3, 4**). There were eight QTL detected on chromosomes 1D, 2A, 3A and 7B having at least moderate threshold significance

of $-\log_{10}(p) \geq 4.12$ for glume response to SNB from four environments (**Table 7**). The estimated allelic effects ranged from 7.72 to 20.93% (**Table 7**) indicating the difference in average phenotypic values for each MTA between contrasting homozygous genotypes. Interestingly, only one region at 423.20 Mbp on chromosome 2A was associated with QTL in more than one environment (*QSng.MJ18.daw-2A.2* and QSng.MJ19.daw-2A) possibly representing a similar gene at this locus controlling glume response to SNB in two environments. The remaining were environment-specific as they neither co-located nor in LD with QTL for glume response detected from other sites (**Table 7**). QTL for heading date and plant height with small allelic effects (4.61–12.35% and 4.67–10.75%, respectively) were detected in some environments in 2018–2020 (**Supplementary Table 5**) but none were co-located or in LD with QTL for glume resistance (**Table 7**). Therefore, QTL for glume resistance was unlikely to be associated with morphological characteristics.

At total of 14 QTL were detected for foliar response in trials at Manjimup and South Perth in 2018–2020 (**Table 7**). There were SNP markers 1445 bp apart that detected QTL at Manjimup in 2018 and 2019, *QSnl.MJ18.daw-5A* and *QSnl.MJ19.daw-5A* (**Table 7**), indicating QTL are co-located on chromosome 5A. The remaining QTL for foliar response were detected in only one environment and, therefore, were determined as environment-specific (**Table 7**). The estimated allelic effects ranged from 8.39 to 24.50% (**Table 7**). The physical position of SNP markers associated with heading date and plant height (**Supplementary Table 5**) were not co-located or in LD and, therefore, were not considered to be associated with foliar response.

To ascertain a genetic relationship with glume response, it was necessary to detect genomic regions for foliar response and compare the position of markers associated with respective QTL on the wheat physical map. A genetic relationship between glume and foliar response was recognized if QTL for each trait were either co-located or in LD. A comparison based on the physical map position of associated SNP markers indicated that QTL for glume and foliar response neither co-located nor were in LD within or between environments in 2018–2020 (**Table 7** and **Figure 1**). Furthermore, QTL detected in this study were not in LD with other QTL for foliar response detected in other WA environments (Francki et al., 2020; **Figure 1**). The lack of QTL co-located or in LD makes it reasonable to assume, therefore, that glume and foliar responses to SNB are controlled by multiple but independent genes that respond in specific environments.

Snn loci were positioned on physical chromosome maps with QTL for glume and foliar response detected in 2018–2020. *Snn4*, *Snn1*, *Snn5* were mapped on chromosomes 1A, 1B, and 4B, respectively while both *Snn3-B1* and *Tsn1* mapped to chromosome 5B (**Figure 1**). Neither QTL for glume nor foliar response detected across four environments in 2018–2020 were in LD to the *Snn* loci based on physical map position, indicating that interactions with known NE were not evident in any field environments in 2018–2020. The exception was *QSnl.MJ18.daw-5B* in LD with *Tsn1* (**Figure 1**) previously reported in Francki et al. (2020).

DISCUSSION

There is increasing evidence that disease response to glume and foliar SNB in the field is controlled by many independent and mostly environmental-specific QTL (Ruud and Lillemo, 2018; Czembor et al., 2019; Ruud et al., 2019; Francki et al., 2020; Lin et al., 2020) exacerbating the complexity of genetic resistance and susceptibility to SNB in wheat. The majority of the QTL detected for either glume or foliar response to SNB in this study were detected at one location but not another, confirming the inherent and convoluted genetic mechanisms for resistance and susceptibility in field assessment. The outcome of this study confirms an independent genetic relationship between glume and foliar response when wheat lines were evaluated at any particular location, evident by the lack of SNP markers associated with QTL that were neither co-located nor in LD. It is assumed, therefore, corresponding genes for biological mechanisms underpinning resistance and susceptibility to pathogen infection and disease progression are dissimilar in glumes and foliage whereby several host genes may be influenced by developmental stages and host-isolate-environmental interactions.

It was presumed that environment-isolate interactions could have a significant effect on host genes responding to SNB in WA (Francki et al., 2020). This study monitored climatic conditions in successive years at Manjimup in 2018–2020 and showed similar daily average air temperature, relative humidity, rainfall, solar exposure and pan evaporation. On the contrary, South Perth in 2020 had higher daily average air temperature, solar exposure and pan evaporation but lower rainfall and relative humidity than any of the Manjimup environments. Therefore, it was expected that SNB response across 232 wheat lines would be consistent across Manjimup environments but variable to South Perth. Although climate impacted disease progression between Manjimup and South Perth sites, there was insubstantial effects for disease response in 2018–2020 evident through high phenotypic correlations and low environment interactions. However, this conclusion is in contrast to moderate correlation reported for foliar response of wheat genotypes across six WA environments in 2016–2018 (Francki et al., 2020). Differences in aggressiveness due to isolate-by-environment interactions (Pariaud et al., 2009; Sharma and Verma, 2019) could partly explain variable SNB response across environments in 2016–2018 (Francki et al., 2020). Since isolates in this study were different to those reported in Francki et al. (2020) it is plausible, therefore, aggressiveness of isolates selected for this study could be less affected by environmental variables in 2018–2020. Alternatively, several but different host loci from diverse germplasm may respond independently to varying levels of aggressiveness of isolates (Krupinksy, 1997) and may account for higher phenotypic correlations between environments. There is a need, therefore, for increased knowledge on the significance of specific environment-by-isolate and genotype-by-isolate interactions and their effects on host quantitative genetic resistance to provide a holistic perception of the tripartite interaction central for glume and foliar SNB disease response in different field environments.

Finlay-Wilkinson regression can reveal trends of variety performance across environments and select lines either based on

TABLE 7 | Summary of marker trait associations for PGAD (glume) and PLAD (foliar) scores from four Western Australian environments in 2018–2020.

Environment	Trait	QTL	Chromosome	SNP id	SNP name	SNP[a]	IWGSC-bp[b]	Consensus map position-cM[c]	R^2	MAF[d]	Allele effect estimate %[e]	*p*-value	$-\log_{10}(p)$
Manjimup 2018	Glume	QSng.MJ18.daw-2A.1	2A	IWB59332	RAC875_c57998_165	[T/**C**]	202,872,663	341.14	0.08	0.42	20.25	3.56E-05	4.45
		QSng.MJ18.daw-2A.2	2A	IWB35263	IAAV6884	[**T**/C]	423,204,105	341.14	0.10	0.45	−20.93	2.18E-06	5.66
		QSng.MJ18.daw-2A.3	2A	IWB908	BobWhite_c1634_563	[A/**G**]	453,520,296	341.14	0.07	0.46	16.77	7.61E-05	4.12
			2A	IWB51426	Ra_c21219_505	[**A**/G]	461,417,569	348.36	0.08	0.45	−18.86	3.85E-05	4.41
Manjimup 2019	Glume	QSng.MJ19.daw-2A	2A	IWB35263	IAAV6884	[**T**/C]	423,204,105	341.14	0.09	0.45	−20.93	1.49E-05	4.83
Manjimup 2020	Glume	QSng.MJ20.daw-1D	1D	IWB35174	IAAV6247	[**A**/G]	10,661,637	53.03	0.08	0.41	−7.72	7.20E-05	4.14
			1D	IWB26984	Excalibur_c4876_832	[A/**G**]	10,662,717	53.03	0.10	0.43	8.31	4.50E-06	5.35
			1D	IWB18376	D_GBF1XID01C7T2Q_63	[T/**C**]	10,668,578	53.03	0.09	0.40	7.92	3.90E-05	4.41
			1D	IWA7533	wsnp_Ra_c1020_2062200	[**A**/G]	10,719,634	53.03	0.09	0.45	−7.75	2.62E-05	4.58
South Perth 2020	Glume	QSng.SP20.daw-1D	1D	IWB8605	BS00051826_51	[**A**/G]	56,751,122	108.87	0.08	0.12	−13.79	7.03E-05	4.15
		QSng.SP20.daw-3A	3A	IWB14389	CAP7_rep_c12940_130	[**T**/C]	646,272,690	346.53	0.07	0.07	−15.26	4.74E-05	4.32
		QSng.SP20.daw-7B	7B	IWB30294	Excalibur_rep_c107796_229	[**T**/C]	105,559,208	229.43	0.09	0.15	−12.80	1.94E-05	4.71
Manjimup 2018 †	Foliar	QSnl.MJ18.daw-1B	1B	IWB49491	Kukri_rep_c111213_148	[**A**/G]	300,949,280	206.69	0.08	0.13	−18.24	5.44E-05	4.26
			1B	IWB72968	Tdurum_contig63991_404	[**T**/C]	301,257,710	206.01	0.10	0.14	−19.32	5.17E-06	5.29
			1B	IWB40986	Kukri_c13156_129	[T/**C**]	301,257,922	206.01	0.08	0.14	17.51	4.57E-05	4.34
			1B	IWB55131	RAC875_c21131_3615	[T/**C**]	302,206,634	206.01	0.08	0.15	17.80	2.72E-05	4.56
			1B	IWB23446	Excalibur_c20228_135	[**T**/C]	305,270,049	206.01	0.09	0.14	−19.09	1.43E-05	4.84
			1B	IWB71062	Tdurum_contig42289_1857	[**A**/C]	306,072,514	206.69	0.08	0.14	−18.34	2.32E-05	4.63
			1B	IWB74187	tplb0024i16_800	[**A**/G]	307,427,828	206.69	0.08	0.14	−17.51	2.92E-05	4.53
			1B	IWB72756	Tdurum_contig60809_268	[T/**G**]	308,587,768	206.01	0.08	0.14	17.08	4.61E-05	4.34
			1B	IWB72755	Tdurum_contig60809_255	[**T**/C]	308,587,781	206.01	0.08	0.14	−17.95	2.97E-05	4.53
			1B	IWB37294	JD_c2834_381	[**T**/C]	309,387,695	206.69	0.09	0.13	−18.57	1.38E-05	4.86
			1B	IWB71413	Tdurum_contig43346_108	[T/**C**]	309,491,071	209.95	0.08	0.13	17.33	5.91E-05	4.23
			1B	IWB63613	RFL_Contig1354_484	[**A**/G]	315,383,705	208.49	0.08	0.17	−15.85	4.37E-05	4.36
			1B	IWB64056	RFL_Contig2784_641	[**A**/G]	317,320,498	206.69	0.08	0.18	−15.57	7.32E-05	4.14
		QSnl.MJ18.daw-5A	5A	IWB35961	IACX448	[**T**/C]	588,377,301	453.34	0.08	0.39	−12.57	6.90E-05	4.16
		QSnl.MJ18.daw-5B	5B	IWB43679	Kukri_c29267_215	[T/**C**]	539,460,125	252.96	0.09	0.07	18.24	1.52E-05	4.82
Manjimup 2019	Foliar	QSnl.MJ19.daw-1A	1A	IWB6426	BS00011521_51	[T/**C**]	579,830,542	431.50	0.07	0.49	9.83	7.65E-05	4.12
		QSnl.MJ19.daw-2B	2B	IWB9450	BS00065105_51	[**T**/C]	69,648,943	262.16	0.07	0.08	−19.36	6.06E-05	4.22
		QSnl.MJ19.daw-4B.1	4B	IWB57527	RAC875_c39524_181	[**A**/G]	126,323,033	182.55	0.10	0.06	−21.86	8.18E-06	5.09
		QSnl.MJ19.daw-4B.2	4B	IWB41569	Kukri_c16392_1468	[**T**/C]	558,051,887	209.83	0.08	0.12	−20.16	5.66E-05	4.25
			4B	IWB38540	Ku_c16392_2687	[A/**C**]	558,053,253	209.83	0.08	0.11	19.30	6.33E-05	4.20
			4B	IWB52053	Ra_c41921_1056	[**T**/G]	558,053,925	209.83	0.09	0.11	−20.63	2.40E-05	4.62
			4B	IWB35570	IAAV8975	[**T**/C]	558,057,833	209.83	0.09	0.12	−22.16	7.61E-06	5.12
			4B	IWB63337	RAC875_rep_c95493_490	[**T**/C]	558,059,510	209.83	0.08	0.10	−20.31	2.58E-05	4.59
			4B	IWB53588	RAC875_c12762_791	[T/**C**]	558,580,422	209.83	0.08	0.07	20.59	4.46E-05	4.35

(Continued)

TABLE 7 | Continued

Environment	Trait	QTL	Chromosome	SNP id	SNP name	SNP[a]	IWGSC-bp[b]	Consensus map position-cM[c]	R^2	MAF[d]	Allele effect estimate %[e]	*p*-value	$-\log_{10}(p)$
		QSnl.MJ19.daw-5A	5A	IWB7820	BS00031117_51	[**T**/C]	588,375,856	453.34	0.07	0.42	−13.46	7.21E-05	4.14
Manjimup 2020	Foliar	QSnl.MJ20.daw-1A.1	1A	IWB45604	Kukri_c46010_872	[T/**G**]	32,894,182	ND	0.08	0.12	11.12	1.30E-05	4.89
			1A	IWB26996	Excalibur_c4887_1814	[T/**C**]	35,533,570	184.34	0.07	0.16	9.45	5.64E-05	4.25
		QSnl.MJ20.daw-1A.2	1A	IWB10491	BS00070695_51	[T/**C**]	586,914,453	462.61	0.11	0.45	8.95	7.30E-07	6.14
		QSnl.MJ20.daw-5B	5B	IWA7227	wsnp_Ku_c6464_11320381	[T/**C**]	402,843,711	152.47	0.09	0.34	8.53	1.58E-05	4.80
			5B	IWB8558	BS00049793_51	[T/**G**]	402,843,834	152.47	0.08	0.37	8.39	5.01E-05	4.30
South Perth 2020	Foliar	QSnl.SP20.daw-3D	3D	IWB17658	D_F5XZDLF02HWOJZ_227	[**A**/G]	31,764,661	284.57	0.07	0.05	−24.50	6.69E-05	4.17
		QSnl.SP20.daw-6D	6D	IWB70297	Tdurum_contig31718_229	[T/**C**]	307,881,449	183.08	0.08	0.36	12.53	2.35E-05	4.63
			6D	IWB36455	Jagger_c1746_113	[**T**/C]	307,882,817	183.08	0.08	0.36	−12.00	5.53E-05	4.26
		QSnl.SP20.daw-7A	7A	IWB52779	Ra_c8937_191	[A/**G**]	81,498,302	332.69	0.08	0.27	13.66	5.47E-05	4.26
			7A	IWB64358	RFL_Contig3447_1177	[A/**G**]	81,498,578	332.69	0.07	0.27	13.46	6.22E-05	4.21

All SNP markers within QTL have moderate to high level of significance based on threshold values of $P < 7.65 \times 10^{-5}$ ($-log_{10}(p) > 4.12$).

[a]*Desirable SNP for reduced disease, based on the allele effect estimate, is in bold and underlined.*

[b]*Base pair (bp) location of the single base change in the IWGSC RefSeq v1.0.*

[c]*Consensus map position as reported in Wang et al. (2014), cM: centimorgans.*

[d]*MAF: minor allele frequency.*

[e]*The effect estimates the difference between the average phenotypic values of the homozygous A genotype relative to the homozygous B genotype.*

†*Data previously reported in Francki et al. (2020).*

ND, Not determined.

stability or on responsiveness to environment potential (Finlay and Wilkinson, 1963). Evaluation of 232 wheat lines for glume response to SNB across four environments identified 35 lines that showed PGAD scores <20% and are resistance donors for breeding glume blotch resistance. EGA Bonnie Rock and ZWW09Qno177 were of particular interest because of their high stability and predictability for glume resistance across multiple field environments, where the former also showed consistently low mean PLAD scores and stability across multiple WA environments. Included in the panel were eight lines with low foliar response when evaluated against 42 different isolates across six environments in 2016–2018 (Francki et al., 2020) which indicated sustained foliar resistance but with varying degrees of stability. The phenotypic correlation between glume and foliar response in the GWAS population was generally higher within each environment to those previously reported for bi- or multi-parental populations evaluated in Australia (Shankar et al., 2008), Europe (Wicki et al., 1999; Aguilar et al., 2005) and Nordic regions (Lin et al., 2020).

We further explored the genetic relationship between glume and foliar response in any particular environment by projecting SNP markers associated with QTL on the physical map and identifying those co-located or in LD to assess if there was common genetic control for these traits. Despite eight QTL for glume and 14 for foliar resistance detected, none were either co-located or in LD within or between four environments. Therefore, GWAS using higher resolution genetic mapping confirmed that genetic control for glume and foliar response is independent even though high phenotypic correlation was observed across environments for each trait. High correlation for glume and foliar response may be attributed to the cumulative influence of different QTL having phenotypic effects in specific environments, including any with small effects that may not have been detected in this study due to the lack of statistical power in GWAS analysis. Interestingly, the cumulative influence of environment-specific QTL of small and larger effect contributing to high phenotypic correlation across Australian environments was recently reported for durable rust resistance (Joukhadar et al., 2020). The increased number of loci detected for both traits and better precision in mapping of alleles using GWAS gives particular credence to the independent control of glume and foliar response and the potential role of cumulative but small effect of environment-specific QTL in SNB response. Independent loci with small phenotypic effects controlling glume and foliar response is in agreement with previous studies evaluating bi-parental and multi-parental mapping populations (Fried and Meister, 1987; Bostwick et al., 1993; Wicki et al., 1999; Shankar et al., 2008; Czembor et al., 2019; Lin et al., 2020).

QTL for heading date and height were not co-located or in LD with any QTL for glume response. Therefore, it is reasonable to assume that the QTL represented true resistance rather than a pleiotropic effect of heading date and plant height. The majority of QTL for glume resistance in this study were detected in one environment only. The exception was a QTL on chromosome 2A at 423.20 Mbp detected at Manjimup in 2018 and 2019 (*QSng.MJ18.daw-2A.2* and *QSng.MJ19.daw-2A*, respectively) with a large allele effect estimate of 20.63% for

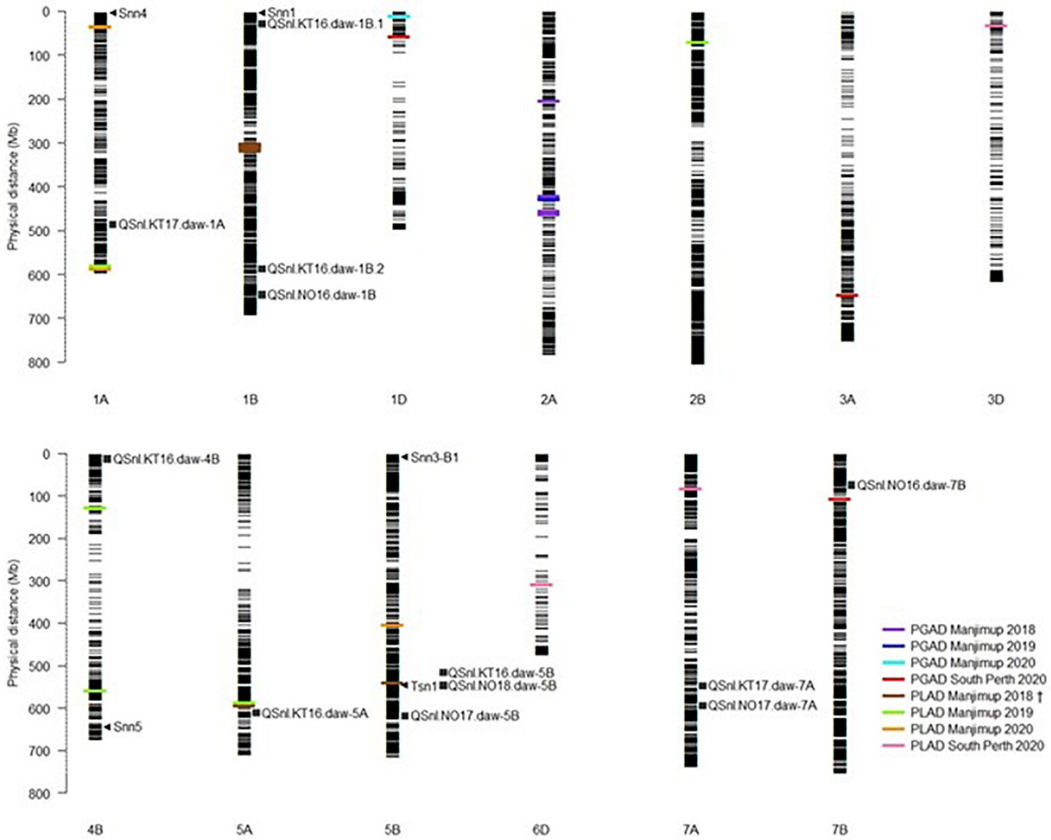

FIGURE 1 | Comparison of QTL for PGAD and PLAD resistance. Assignment of known *Tsn* and *Snn* loci and position of MTA detected in multiple environments in 2018–2020 on the Chinese Spring physical map (IGWSC RefSeq v1.0). Black horizontal lines represent the physical locations (Mb) of SNP markers used in GWAS analysis. Colored bars represent the MTA detected in different environments in 2018–2020. Arrows indicate putative location of known *Snn* and *Tsn1* loci. Squares indicate QTL for foliar SNB resistance detected in 2016–2018 and reported in Francki et al., 2020. †PLAD Manjimup 2018 also reported in Francki et al. (2020).

average phenotypic values indicating the same QTL may be effective in different but not all environments. Interestingly, the nature of QTL for glume resistance in this study was in agreement with previous reports in that some were detected in only one environment (Shankar et al., 2008; Czembor et al., 2019; Lin et al., 2020) while only a few QTL in the same genomic region were detected across multiple environments (Schnurbusch et al., 2003; Uphaus et al., 2007; Shankar et al., 2008; Lin et al., 2020). QTL for glume resistance has not been previously identified on chromosome 1D, so it appears that *QSng.MJ20.daw-1D* and *QSng.SP20.daw-1D* are novel and accentuates the importance of evaluating wider germplasm pools to identify new sources of variation suitable for breeding glume blotch resistance. A comparison of the physical position of SNP markers associated with QTL for glume response on chromosome 2A, 3A and 7B were neither co-located nor in LD with QTL for glume resistance reported by Lin et al. (2020) confirming the minor and different gene effects for SNB response in earlier studies (Fried and Meister, 1987; Wicki et al., 1999. The physical co-location of QTL for glume resistance previously reported on chromosomes 2A (Schnurbusch et al., 2003), 3A (Schnurbusch et al., 2003; Aguilar et al., 2005) and 7B (Schnurbusch et al., 2003) was not readily discernible due to ambiguous positioning of markers and, consequently, validation for the same genomic regions controlling glume response between populations was inconclusive.

Similar to glume response, QTL for morphological traits did not co-locate or were in LD with QTL for foliar response so it appears that loci detected are specific to SNB disease. We used SNP markers associated with foliar resistance to SNB in adult plants from other studies, wherever possible, to anchor and validate QTL and compare their location on the physical map. Foliar QTL detected in 2018–2020 other than *QSnl.MJ18.daw-1B* neither co-located nor were in LD with previous QTL detected when the population was evaluated in WA environments (Francki et al., 2018, 2020). However, some QTL including *QSnl.MJ18.daw-1A, QSnl.*MJ20.daw-1A.2 and *QSnl.MJ19.daw-2B* were either co-located or in LD with similar genomic regions controlling foliar resistance on chromosomes 1A, and 2B reported by Ruud et al. (2019). It is reasonable to assume, therefore, that these QTL are within common genomic regions that harbor genes controlling SNB response in different regions of the world and presumably genetically different isolates. Similar to the comparison for glume resistance, it was not

discernible to accurately validate existing or identify novel QTL for some foliar SNB resistance on the physical map from earlier studies (Schnurbusch et al., 2003; Aguilar et al., 2005; Friesen et al., 2009; Czembor et al., 2019) mainly due to low resolution genetic mapping and ambiguous anchoring of markers other than SNPs. Nevertheless, a myriad of loci responded to foliar SNB infection in an environmental-specific manner and/or as a result of variability in pathogen isolates.

High abundance of SNP markers discriminated co-located QTL from low resolution genetic mapping into separate but closely accompanying QTL may contain clusters of concomitant disease-related genes for glume and foliar SNB resistance (Francki et al., 2018) with increasing evidence from recent GWAS studies that these clusters respond to pathogen infection in a genotype-by-environment-by isolate manner (Francki et al., 2020). This study identified accompanying QTL for glume resistance separated by a physical distance of ∼30 Mbp on chromosome 2A, *QSng.MJ18.daw-2A.2* and *QSng.MJ18.daw-2A.3*, providing further evidence that some genes responding to SNB are within distinct clusters on chromosomes. Likewise, a pair of QTL for foliar response in LD were detected on chromosome 1A in regions 579.83 Mbp to 586.91 Mbp (*QSnl.MJ19.daw-1A* and *QSnl.MJ20.daw-1A.2*, respectively) and within a 1,445 bp region on 5A around 588.37 Mbp (*QSnl.MJ18.daw-5A* and *QSnl.MJ19.daw-5A*) providing further credibility that clusters of genes reside within a small physical distance and respond to different environments and/or isolates. Sequence analysis will reveal whether the region on 1D and 1A contain related disease resistance gene classes and whether the QTL on 5A has one or tandem genes.

It was expected that QTL detected using GWAS would identify those co-located or in LD with known *Snn* and *Tsn1* loci particularly in genomic regions with high-density SNP markers for loci on chromosomes 1A, 1B, 4B and 5B. Although the physical location of *Snn4*, *Snn1*, *Snn5* were located on chromosomes 1A, 1B and 4B respectively and *Snn3-B1* and *Tsn1* mapping to chromosome 5B, the QTL for glume and foliar response were not in LD with *Snn* loci. The only exception was *QSnl.MJ18.daw-5B* previously identified to be in LD with *Tsn1* on 5B (Francki et al., 2020). Therefore, it does not appear that known NE-*Snn* interactions have a prominent effect on glume or foliar disease when wheat was evaluated in any of the four WA environments in 2018–2020. This may be due to different NE genes in isolates, variations in *Snn* and *Tsn* sensitivity genes represented in the 232 wheat lines and/or different environmental effects that influence compatible NE-*Snn* interactions for disease progression in the field. Nevertheless, taken collectively with multiple field evaluation in Francki et al. (2020), this study validated that known NE-*Snn* interactions do not appear to influence quantitative glume and foliar resistance in WA environments, a supposition shared in other studies when wheat was evaluated for SNB response in the eastern region of the United States (Cowger et al., 2020) and Europe (Czembor et al., 2019). We cannot exclude the possibility that undetected NE-*Snn* interactions may serve a role in SNB response in wheat. If so, a myriad of interactions would be assumed given that multiple and environment-specific loci contribute to glume and foliar response. The importance of increasing our knowledge on the genetic diversity of isolates, the interaction of environmental effects on pathogenicity and aggressiveness and on host genes would play a critical role in deciphering the biological mechanisms underpinning glume and foliar response to SNB. In the meantime, breeding for improved SNB resistance in wheat remains a challenging task. Enrichment of resistance alleles using SNP markers identified in this study may contribute minor effects in specific environments but development of breeding lines with robust resistance would significantly benefit by recurrent phenotypic selection against different isolates and multiple environments. Developing a genomic selection breeding strategy would be a worthwhile proposition but would require multi-environment trial, biological and biophysical environmental information for modeling and deriving accurate prediction equations.

CONCLUSION

The majority of QTL for glume resistance to SNB were environmentally-specific in four environments and provided further understanding of genotype-by-environment interactions. Moreover, QTL for glume resistance did not coincide with foliar resistance confirming the added complexity of different genotype-pathogen-environment interactions and underpinning biological pathways leading to alternative SNB responses in adult plants. GWAS did not detect QTL co-located or in LD with known *Snn* or *Tsn* loci so their role in controlling either glume or foliar response to SNB is not apparent in the environments selected in this study. It is important, however, to consider further research on potentially different disease response pathways to gain a better understanding on fundamental biology underpinning resistance and susceptibility. In the meantime, strategies for breeding will rely on recurrent phenotypic evaluation to capture and retain favorable alleles for both glume and foliar resistance relevant to the particular environment.

DATA AVAILABILITY STATEMENT

Requests to access the datasets should be directed to the corresponding author.

AUTHOR CONTRIBUTIONS

MF acquired research funding, designed experiments, collated, analyzed and interpreted data, and wrote the manuscript. EW contributed to data acquisition, analysis and interpretation, and contributed to writing the manuscript. CM and WM contributed to trial designs, planting, maintenance, and data acquisition. All authors read and approved the final manuscript.

FUNDING

This work was financially supported by the Grains Research Development Corporation through project DAW00248 awarded to MF.

ACKNOWLEDGMENTS

The authors gratefully acknowledge Manisha Shankar for preparation of fungal isolates, Ian Guthridge and Graham Blincow for management of field trials at the Manjimup Research Station. The authors dedicate our research to the late Professor Herb Ohm who has been an inspiration to our work on SNB resistance in wheat.

SUPPLEMENTARY MATERIAL

The Supplementary Material for this article can be found online at: https://www.frontiersin.org/articles/10.3389/fgene.2021.681768/full#supplementary-material

REFERENCES

Abeysekara, N. S., Friesen, T. L., Keller, B., and Faris, J. D. (2009). Identification and characterization of a novel host-toxin interaction in the wheat-*Stagonospora nodorum* pathosystem. *Theor. Appl. Genet.* 120, 117–126. doi: 10.1007/s00122-009-1163-6

Aguilar, V., Stamp, P., Winzeler, M., Winzeler, H., Schachermayr, G., Keller, B., et al. (2005). Inheritance of field resistance to *Stagonospora nodorum* leaf and glume blotch and correlations with other morphological traits in hexaploid wheat (*Triticum aestivum* L.). *Theor. Appl. Genet.* 111, 325–336. doi: 10.1007/s00122-005-2025-5

Alomari, D. Z., Eggert, K., von Wirén, N., Pillen, K., and Röder, M. S. (2017). Genome-wide association study of calcium accumulation in grains of European wheat cultivars. *Front. Plant Sci.* 8:1797.

Bostwick, D. E., Ohm, H. W., and Shaner, G. (1993). Inheritance of Septoria glume blotch resistance in wheat. *Crop Sci.* 33, 439–443. doi: 10.2135/cropsci1993.0011183x003300030005x

Bradbury, P. J., Zhang, Z., Kroon, D. E. T., Casstevens, M., Ramdoss, Y., and Buckler, E. S. (2007). TASSEL: software for association mapping of complex traits in diverse samples. *Bioinformatics* 23, 2633–2635. doi: 10.1093/bioinformatics/btm308

Cowger, C., Ward, B., Brown-Guedira, G., and Brown, J. K. M. (2020). Role of effector-sensitivity gene interactions and durability of quantitative resistance to *Septoria nodorum* Blotch in eastern U.S. wheat. *Front. Plant Sci.* 11:155.

Czembor, P., Arseniuk, E., Radecka-Janusik, M., Piechota, U., and Słowacki, P. (2019). Quantitative trait loci analysis of adult plant resistance to *Parastagonospora nodorum* blotch in winter wheat cv. Liwilla (*Triticum aestivum* L.). *Eur. J. Plant Path.* 155, 1001–1016. doi: 10.1007/s10658-019-01829-5

Downie, R. C., Bouvet, L., Furuki, E., Gosman, N., Gardner, K. A., MacKay, I. J., et al. (2018). Assessing European sensitivities to *Parastagonospora nodorum* necrotrophic effectors and fine-mapping the Snn3-B1 locus conferring sensitivity to the effector SnTox3. *Front. Plant Sci.* 9:881.

Eyal, Z., Scharen, A. L., Prescott, J. M., and van Ginkel, M. (1987). *The Septoria Diseases of Wheat: Concepts and Methods of Disease Management*. Mexico: CIMMYT.

Finlay, K., and Wilkinson, G. (1963). The analysis of adaptation in a plant-breeding programme. *Crop Pasture Sci.* 14, 742–754. doi: 10.1071/ar9630742

Francki, M. G., Shankar, M., Walker, E., Golzar, H., Loughman, R., and Ohm, H. W. (2011). New quantitative trait loci for flag leaf resistance to *Stagonospora nodorum* blotch. *Phytopathology* 101, 1278–1284. doi: 10.1094/PHYTO-02-11-0054

Francki, M. G. (2013). Improving *Stagonospora nodorum* resistance in wheat: a review. *Crop Sci.* 53, 355–365. doi: 10.2135/cropsci2012.06.0347

Francki, M. G., Walker, E., Li, D., and Forrest, K. (2018). High-density SNP mapping reveals closely linked QTL for resistance to *Stagonospora nodorum* blotch (SNB) in flag leaf and glume in hexaploid wheat. *Genome* 61, 145–149. doi: 10.1139/gen-2017-0203

Francki, M. G., Walker, E., McMullan, C. J., and Morris, W. G. (2020). Multi-location evaluation of global wheat lines reveal multiple QTL for adult plant resistance to *Septoria nodorum* blotch (SNB) detected in specific environments and in response to different isolates. *Front. Plant Sci.* 11:771.

Fried, P. M., and Meister, E. (1987). Inheritance of leaf and head resistance of winter wheat to *Septoria nodorum* in a diallel cross. *Phytopathology* 77, 1371–1375. doi: 10.1094/phyto-77-1371

Friesen, T. L., Chu, C., Xu, S. S., and Faris, J. D. (2012). SnTox5-Snn5: A novel *Stagonospora nodorum* effector- wheat gene interaction and its relationship with SnToxA-Tsn1 and SnTox3-Snn3-B1 interactions. *Mol. Plant Path.* 13, 1101–1109. doi: 10.1111/j.1364-3703.2012.00819.x

Friesen, T. L., Chu, C. G., Liu, Z. H., Xue, S. S., Halley, S., and Faris, J. D. (2009). Host-selective toxin produced by *Stagonospora nodorum* confer disease susceptibility in adult wheat plants under field conditions. *Theor. Appl. Genet.* 118, 1489–1497. doi: 10.1007/s00122-009-0997-2

Gao, L., Turner, M. K., Chao, S., Kolmer, J., and Anderson, J. A. (2016). Genome wide association study of seedling and adult plant leaf rust resistance in elite spring wheat breeding lines. *PLoS One* 11:e0148671. doi: 10.1371/journal.pone.0148671

Gao, Y., Faris, J. D., Liu, Z., Kim, Y. M., Syme, R. A., Oliver, R. P., et al. (2015). Identification and characterization of the SnTox6-Snn6 interaction in the *Parastagonospora nodorum*-wheat pathosystem. *Mol. Plant Microbe Inter.* 28, 615–625. doi: 10.1094/mpmi-12-14-0396-r

James, W. C. (1971). An illustrated series of assessment keys for plant diseases, their preparation and usage. *Can. Plant Dis. Surv.* 51, 39–65.

Joukhadar, R., Hollaway, G., Shi, F., Kant, S., Forrest, K., Wong, D., et al. (2020). Genome-wide association reveals a complex architecture for rust resistance in 2300 worldwide bread wheat accessions screened under various Australian conditions. *Theor. Appl. Genet.* 133, 2695–2712. doi: 10.1007/s00122-020-03626-9

Keeble-Gagnère, G., Isdale, D., Suchecki, R., Kruger, A., Lomas, K., Carroll, D., et al. (2019). Integrating past, present and future wheat research with Pretzel. *bioRxiv*[Preprint] doi: 10.1101/517953

Krupinksy, J. M. (1997). Aggressiveness of *Stagonospora nodorum* isolates obtained from wheat in the Northern Great Plains. *Plant Dis.* 81, 1027–1031. doi: 10.1094/pdis.1997.81.9.1027

Lin, M., Corsi, B., Ficke, A., Tan, K. C., Cockram, J., and Lillemo, M. (2020). Genetic mapping using a wheat multi-founder population reveals a locus on chromosome 2A controlling resistance to both leaf and glume blotch caused by the necrotrophic fungal pathogen *Parastagonospora nodorum*. *Theor. Appl. Genet.* 133, 785–808. doi: 10.1007/s00122-019-03507-w

Maccaferri, M., Zhang, J., Bulli, P., Abate, Z., Chao, S., Canto, D., et al. (2016). A genome-wide association study of resistance to stripe rust (*Puccinia striiformis* f. sp. *tritici*) in a worldwide collection of hexaploid spring wheat. *Genes Genom. Genet.* 5, 449–465. doi: 10.1534/g3.114.014563

Marroni, S., Pinosio, G., Zaina, F., Fogolari, N., Felice, F., Cattonaro, F., et al. (2011). Nucleotide diversity and linkage disequilibrium in Populus nigra cinnamyl alcohol dehydrogenase (CAD4) gene. *Tree Genet. Genom.* 7, 1011–1023. doi: 10.1007/s11295-011-0391-5

McDonald, M. C., and Solomon, P. S. (2018). Just the surface. Advances in the discovery and characterization of necrotrophic wheat effectors. *Curr. Op. Microbiol.* 46, 14–18. doi: 10.1016/j.mib.2018.01.019

Muqaddasi, Q. H., Zhao, Y., Rodemann, B., Plieske, J., Ganal, M. W., and Röder, M. S. (2019). Genome-wide association mapping and prediction of adult stage Septoria tritici blotch infection in European winter wheat via high-density marker arrays. *Plant Genome* 12, 180029. doi: 10.3835/plantgenome2018.05.0029

Murray, G. M., and Brennan, J. P. (2009). Estimating disease losses to the Australian wheat industry. *Aust. Plant Path.* 38, 558–570. doi: 10.1071/ap09053

Pariaud, B., Ravigné, V., Halkett, F., Goyeau, H., Carlier, J., and Lannou, C. (2009). Aggressiveness and its role in the adaptation of plant pathogens. *Plant Path.* 58, 409–424. doi: 10.1111/j.1365-3059.2009.02039.x

Phan, H. T. T., Ryback, K., Furuki, E., Breen, S., Solomon, P. S., Oliver, R. P., et al. (2016). Differential effector expression underpins epistasis in a plant fungal disease. *The Plant J.* 87, 343–354. doi: 10.1111/tpj.13203

Purcell, S., Neale, B., Todd-Brown, K., Thomas, L., Ferreira, M. A. R., Bender, D., et al. (2007). PLINK: a toolset for whole-genome association and population-based linkage analysis. *Am. J. Human Genet.* 81, 559–579. doi: 10.1086/519795

R Core Team (2018). *R: A Language and Environment for Statistical Computing*. Vienna: R Foundation for Statistical Computing.

Ruud, A. K., Dieseth, J. A., Ficke, A., Furuki, E., Phan, H. T. T., Oliver, R. P., et al. (2019). Genome-wide association mapping of resistance to *Septoria nodorum* blotch in a Nordic spring wheat collection. *The Plant Genome* 12, 3.

Ruud, A. K., and Lillemo, M. (2018). *Diseases Affecting Wheat: Septoria nodorum* Blotch. In: Integrated Disease Management of Wheat and Barley. Burleigh Dodds: Burleigh Dodds series in agricultural science.

Ruud, A. K., Wingju, S., Belova, T., Friesen, T. L., and Lillemo, M. (2017). Mapping of SnTox3-Snn3 as a major determinant of field susceptibility to *Septoria nodorum* leaf blotch in the SHA3/CBRD x Naxos population. *Theor. Appl. Genet.* 130, 1361–1374. doi: 10.1007/s00122-017-2893-5

Schnurbusch, T., Paillard, S., Fossati, D., Messmer, M., Schachermayr, G., Winzeler, M., et al. (2003). Detection of QTLs for Stagonospora glume blotch resistance in Swiss winter wheat. *Theor. Appl. Genet.* 107, 1226–1234. doi: 10.1007/s00122-003-1372-3

Shankar, M., Walker, E., Golzar, H., Loughman, R., Wilson, R. E., and Francki, M. G. (2008). Quantitative trait loci for seedling and adult plant resistance to *Stagonospora nodorum* in wheat. *Phytopathology* 980, 886–893. doi: 10.1094/phyto-98-8-0886

Sharma, R., and Verma, S. (2019). Environment-pathogen interactions in plant diseases. *Agric. Rev.* 40, 192–199.

Shi, G., Friesen, T. L., Saini, J., Xu, S. S., Rasmussen, J. B., and Faris, J. D. (2015). The wheat Snn7 gene confers susceptibility on recognition of the *Parastagonospora nodorum* necrotrophic effector SnTox7. *The Plant Genome* 8, 2.

Turner, S. (2017). *Qqman: Q-Q and Manhattan Plots for GWAS Data.* R Package Version 0.1.4. Available online at: https://CRAN.R-project.org/package=qqman (accessed October, 2020).

Uphaus, J., Walker, E., Shankar, M., Golzar, H., Loughman, R., Francki, M., et al. (2007). Quantitative trait loci identified for resistance to Stagonospora glume blotch in wheat in the USA and Australia. *Crop Sci.* 47, 1813–1822. doi: 10.2135/cropsci2006.11.0732

Wang, S., Wong, D., Forrest, K., Allen, A., Chao, S., Huang, B. E., et al. (2014). Characterization of polyploid wheat genomic diversity using a high-density 90 000 single nucleotide polymorphism array. *Plant Biotech. J.* 12, 787–796. doi: 10.1111/pbi.12183

Wicki, W., Winzeler, M., Schmid, J. E., Stamp, P., and Messmer, M. (1999). Inheritance of resistance to leaf and glume blotch caused by *Septoria nodorum* Berk. in winter wheat. *Theor. Appl. Genet.* 99, 1265–1272. doi: 10.1007/s001220051332

Wray, N., and Visscher, P. (2008). Estimating trait heritability. *Nat. Educ.* 1:29.

Conflict of Interest: The authors declare that the research was conducted in the absence of any commercial or financial relationships that could be construed as a potential conflict of interest.

frontiers in Genetics

ORIGINAL RESEARCH
published: 11 August 2021
doi: 10.3389/fgene.2021.724527

High-Throughput Sequencing-Based Identification of miRNAs and Their Target mRNAs in Wheat Variety Qing Mai 6 Under Salt Stress Condition

*Xiaoyan He[1†], Zhen Han[1†], Huayan Yin[1], Fan Chen[1], Yihuan Dong[1], Lufei Zhang[1], Xiaoqing Lu[1], Jianbin Zeng[1], Wujun Ma[1,2] and Ping Mu[1]**

[1]College of Agronomy, Qingdao Agricultural University, Qingdao, China, [2]State Agricultural Biotechnology Centre, College of Science, Health, Engineering and Education, Murdoch University, Perth, WA, Australia

OPEN ACCESS

Edited by:
Cheng Liu,
Shandong Academy of Agricultural Sciences, China

Reviewed by:
Dezhi Wu,
Zhejiang University, China
Asad Prodhan,
University of Western Australia, Australia

***Correspondence:**
Ping Mu
muping@qau.edu.cn

[†]These authors have contributed equally to this work and share first authorship

Specialty section:
This article was submitted to Plant Genomics, a section of the journal Frontiers in Genetics

Received: 13 June 2021
Accepted: 20 July 2021
Published: 11 August 2021

Citation:
He X, Han Z, Yin H, Chen F, Dong Y, Zhang L, Lu X, Zeng J, Ma W and Mu P (2021) High-Throughput Sequencing-Based Identification of miRNAs and Their Target mRNAs in Wheat Variety Qing Mai 6 Under Salt Stress Condition. Front. Genet. 12:724527. doi: 10.3389/fgene.2021.724527

Soil salinization is one of the major abiotic stresses that adversely affect the yield and quality of crops such as wheat, a leading cereal crop worldwide. Excavating the salt-tolerant genes and exploring the salt tolerance mechanism can help breeding salt-tolerant wheat varieties. Thus, it is essential to identify salt-tolerant wheat germplasm resources. In this study, we carried out a salt stress experiment using Qing Mai 6 (QM6), a salt-tolerant wheat variety, and sequenced the miRNAs and mRNAs. The differentially expressed miRNAs and mRNAs in salt stress conditions were compared with the control. As results, a total of eight salt-tolerance-related miRNAs and their corresponding 11 target mRNAs were identified. Further analysis revealed that QM6 enhances salt tolerance through increasing the expression level of genes related to stress resistance, antioxidation, nutrient absorption, and lipid metabolism balance, and the expression of these genes was regulated by the identified miRNAs. The resulting data provides a theoretical basis for future research studies on miRNAs and novel genes related to salt tolerance in wheat in order to develop genetically improved salt-tolerant wheat varieties.

Keywords: wheat, salt stress, transcriptome, microRNA, target gene, expression verification

INTRODUCTION

Salt stress due to saline soil is one of the most severe abiotic stress that impedes crop growth and yield. It adversely affects more than 20% of the irrigated soil worldwide (Singh, 2020). More than 70 million hectares of the land area is affected by secondary saline-alkaline (FAO).[1] Global climate change, immoderate irrigation, unsustainable development, and other factors are causing a continuous increase of salinized land (D'Odorico et al., 2013; Prăvălie et al., 2021). Soil salinization has severely affected agricultural land globally, posing a severe threat to agricultural development. Utilizing the saline land and controlling the land salinization level

[1]http://www.fao.org/home/en/

have become a global issue in relation to food security and agriculture sustainability (Li et al., 2014). Multiple studies have proven that cultivating and planting salt-tolerant crops is the most economical and effective way to utilizing saline-alkaline land for crop production (Galvani, 2007).

Wheat is one of the three major food crops worldwide and is a staple food for more than 30% of the world population that provides nearly 20% of the global energy consumption (FAO; see footnote 1). Its plantation accounts for about 17% of the total cultivated area worldwide, globally, wheat is one of the major crops being cultivated on saline-alkaline land, which plays an important role in managing and utilizing saline-alkaline soil. A continuous worsen in global warming, industrial pollution, lack of water resources, and abnormal irrigation has alarmingly increased soil salinization in the world's leading wheat-producing areas, which has posed a serious threat to wheat production worldwide (Nadeem et al., 2020). In this study, we investigated the salt tolerance genes in a unique wheat genotype with an aim to improve wheat salt tolerance.

Recent advances in high-throughput sequencing technology have substantially increased the wheat genome data availability and promoted the investigative studies on wheat transcriptome and miRNAs (Kuang et al., 2019). The miRNAs are non-coding single-stranded small RNAs (18–24 nt) that are involved in post-transcriptional regulation by binding to their specific target mRNA (Singh et al., 2020). In plants, RNA polymerase II mediates the transcription of pri-miRNAs with cap structure and polyadenylate tail from endogenous miRNA genes. pri-miRNAs are then cleaved by Drosha/DGCR8 complex to form hairpin pre-miRNAs, which are exported to cytoplasm from the nucleus *via* Exportin-5 and Ran-GTP. In the cytoplasm, the Dicer enzyme converts this pre-miRNA to 20 bp double-stranded miRNAs. Under the RNA silencing complex (RISC), mature miRNAs regulate the target gene expression by inhibiting its translation or mediating its degradation. As shown in a previous study, miRNA plays a vital role in plant morphogenesis, growth regulation, hormone secretion, and signal transduction (Zhang and Unver, 2018). Additionally, miRNA-mediated post-transcriptional regulation is crucial to improving stress tolerance in crops (Pagano et al., 2021). However, regardless of its importance, there are few studies so far on miRNAs in salt-tolerance in wheat.

To investigate the salt-tolerance-related miRNAs and their target mRNAs in wheat and to explore their involvement in salt-tolerance, a salt-tolerant variety Qing Mai 6 (QM6) was analyzed under NaCl-induced salt stress in this study and led to identification of a set of differentially expressed miRNAs and mRNAs in the cultivar under salt stress. Target genes of differentially expressed miRNAs were predicted based on the differentially expressed mRNAs, and functional analysis of these target genes was performed. The biological processes and pathways associated with the differential miRNAs and their target mRNAs were identified. In addition, miRNA mediated salt-tolerance mechanism of QM6 was discussed. This study provides a reference for future studies on salt-tolerance-related miRNAs in wheat and unravels some candidate genes for genetic improvement of salt-tolerant wheat variety.

MATERIALS AND METHODS

Hydroponic Experiment

This study uses two wheat genotypes, a cultivar QM6 and an old wheat line Chinese Spring (CS). QM6 is one of the widely cultivated wheat varieties in Shandong Province, one of China's primary wheat-producing areas and is known as a salt-tolerant wheat variety, while CS is a salt-sensitive variety. QM6 and CS wheat seeds with full and uniform size were selected and sterilized with 75% alcohol for 5 min. Distilled water was used to rinse these wheat seeds 2–3 times. The sterilized wheat seeds were placed in petri dishes with two layers of wet test paper to germinate. After 7 days, the germinated wheat seeds were transferred to a 5 L black plastic bucket containing 1/5 Hoagland nutrient solution and placed in a controlled glasshouse, which was set to 25°C with a photoperiod of 12 h, a luminous flux of 3,000 Lx, and relative humidity of 65%. The nutrient solution was changed every 2–3 days during the seedling growth. The pH of the nutrient solution was set to 5.8–6.0 and was continuously aerated with pumps throughout the experiment. At two-leaf seedlings stage, half of the buckets were treated with 200 mM NaCl to induce salt stress. The plants without stress treatment were considered as control. Each treatment has three biological replicates. After 24 h, roots from the two treatments were quickly collected and cooled in liquid nitrogen and then stored in a refrigerator at −80°C for RNA extraction. The remaining plants underwent a further 2-week growth under stress or regular conditions, then all plants were collected and their dry weights of roots and shoots were measured after drying them for 48 h in an oven at 80°C.

miRNA Library Construction and Sequencing

The total RNA was extracted using Takara MiniBEST Plant RNA Extraction Kit as per the manufacturer's instruction. The concentration and purity of the extracted RNA were determined using NanoDrop ND1000 (NanoDrop Technologies, United States). RNA integrity was inspected using 1% agarose gel electrophoresis and Agilent 2100 (Agilent Technologies, United States). High-throughput sequencing of miRNA was performed by Annoroad Gene Technology Inc. (Beijing, China). Appropriate fragments were selected from the RNA samples that passed the quality test, and the 17–30 nt RNA fragments were enriched using gel separation technology. Connectors were added to the two ends of miRNA (a hydroxyl group at the 3' end and phosphate group at the 5' end) and reverse transcribed into cDNA. The sequencing library was constructed post-PCR amplification. The SE50 sequencing strategy was used to perform Illumina high-throughput sequencing for the constructed sequencing library (Hafner et al., 2008; Dillies et al., 2013).

Prediction and Analysis of miRNA

The Illumina high-throughput sequencing was initially presented in an original image data file. After base calling, it was converted into raw reads using CASAVA v1.8.2 (Illumina Inc., 2011). The raw reads were spliced, low-quality reads were filtered,

and fragments were selected using cutadapt v1.12[2] to obtain clean reads for subsequent analysis (Martin, 2011). The clean reads were mapped to GenBank[3] and Rfam[4] databases to obtain annotation of non-coding RNAs. The interference of non-coding RNA, such as snoRNA, snRNA, tRNA, and rRNA, was eliminated through screening and then the selected reads were analyzed and aligned in miRbase v21.0[5] according to the principle of most two mismatches (Kozomara and Griffiths-Jones, 2014). Clean reads that matched in miRBase v21.0 were termed as "known miRNAs" and the other reads were analyzed using miRDeep2 v0.01[6] for "novel miRNAs" prediction.

The number of reads was firstly standardized for miRNA expression analysis (Transcripts Per Kilobase Million, TPKM). Then, the miRNA expression was calculated based on TPKM (Wagner et al., 2012). Finally, DESeq2 v1.20.0[7] (Love et al., 2014) was used for differential expression analysis. The screening criteria for differential miRNA were false discovery rate (FDR) ≤ 0 and $|\log_2 FC| \geq 1$. FC represents fold change.

mRNA Library Construction and Sequencing

The total root RNA from the three biological replicates of the two treatments was extracted using Takara MiniBEST Plant RNA Extraction Kit for sequencing library construction; thus, a total of six RNA samples were obtained. Agarose gel electrophoresis and NanoDrop were used to evaluate the RNA quality. The RNA concentration was determined by Qubit instrument (Thermo Fisher Scientific, Germany) and the RNA integrity was checked using Agilent 2100 Bioanalyzer (Agilent Technologies, United States).

Dynabeads Oligo (dT) was applied to enrich mRNA. Then, fragmentation buffer was added to break mRNA into short fragments. The first strand of cDNA was synthesized by random hexamers using short mRNA fragments as the template. The second strand of cDNA was synthesized after adding buffer, dNTPs, RNase H, and DNA Polymerase to tubes containing first strand of cDNA.

cDNA was purified using QiaQuick PCR Kit, and the EB buffer solution was used for cDNA elution. After terminal repair, base A was added to cDNA, followed by the addition of the sequencing adapters. Furthermore, agarose gel electrophoresis was used to recover the target size cDNA fragments for PCR amplification and RNA sequencing library construction. The constructed library was used for Illumina HiSeq sequencing.

mRNA Sequencing Data Analysis

Quality evaluation was performed on the raw sequencing data. The adapters and the low-quality reads were removed to obtain clean reads. HISAT2 program[8] was used to match clean reads with wheat reference genome (IWGSC v1.0) and to obtain annotation of clean reads with statistically analyzed (Kim et al., 2015). Based on the selected reference genome, the mapped reads were spliced using StringTie v1.3.4 (Pertea et al., 2015).[9] After comparing the original genome annotation information, the uncommented transcriptional regions were identified as the novel transcripts and genes. The amino acid reads of novel genes were screened against the Pfam database[10] using HMMER v3.2.1[11] software to obtain the annotations of novel genes (Potter et al., 2018). The gene expression level was obtained through quantitative calculation of reads using FPKM (fragments per kilobase of transcript per million fragments mapped) method (Florea et al., 2013). The differentially expressed genes (DEGs) between the stressed and control samples were analyzed by Deseq2 v1.20.0 (see footnote 7) combined with statistical significance analysis to obtain values of p. Additionally, multiple tests for values of p were conducted based on FDR. Finally, genes with FDR < 0.05 and relative expression $|\log_2 FC| \geq 2$ were used to identify DEGs FC represents fold change.

Gene Ontology (GO) enrichment and KEGG analysis were performed for differentially expressed mRNAs using Blast and HMMER software. According to the differentially expressed miRNAs and mRNAs, psRobot v1.2[12] was used to predict the target mRNAs of miRNAs (Wu et al., 2012).

Verification of Expressions of miRNA and Target Genes by qRT-PCR

Qing Mai 6 salt-treated root samples were prepared with three biological replicates. RNA was extracted from these samples and its concentration and integrity were detected as mentioned above. Mir-XTM miRNA First-Strand Synthesis Kit (Takara, Japan) was used to reverse transcribe miRNA single-strand into cDNA. Single strand cDNA of mRNA was reverse transcribed using Evo M-MLV RT Kit with gDNA Clean for qPCR IIKit (AG, China). Subsequently, the fluorescent quantitative PCR of miRNAs and their target mRNAs was performed on a CFX96 PCR instrument (Bio-Rad, United States) using SYBR-Green fluorescent dye (Bio-Rad, United States). U6 and actin were used as an internal control to correct the expression value (Paolacci et al., 2009; Feng et al., 2012). The specific procedure of PCR was 40 cycles at 95°C and 30 s (95°C for 5 s and 60°C for 30 s). The dissolution curve program was 60–95°C, 5 s in each step, increasing by 0.5°C. The specificity of PCR primers was verified by the dissolution curve. Finally, the original expression value of fluorescent quantitative PCR was obtained, and the relative expression values of genes were calculated through the 2-ΔΔCq relative quantitative method. Each experiment was repeated three times. qRT-PCR primers were designed using the reads sequences

[2]https://cutadapt.readthedocs.io/en/stable/
[3]https://www.ncbi.nlm.nih.gov/
[4]https://rfam.org/
[5]http://www.mirbase.org/
[6]https://github.com/rajewsky-lab/mirdeep2/releases
[7]http://www.bioconductor.org/packages/devel/bioc/html/DESeq2.html
[8]http://www.ccb.jhu.edu/software/hisat/
[9]http://ccb.jhu.edu/software/stringtie/
[10]http://pfam.xfam.org/
[11]http://www.hmmer.org/download.html
[12]http://omicslab.genetics.ac.cn/psRobot/

(**Supplementary Table 1**). The primers used in this study are shown in **Supplementary Table 2**.

Data Analysis

SPSS software was used to analyze the significant difference between the data through the Tukey test. Origin software was used to draw the column diagram.

RESULTS

Determination of Salt Tolerance in QM6

Qing Mai 6 and CS phenotypes did not vary significantly under the control condition. However, CS root and shoot growth were inhibited more significantly than that of QM6 under 200 mM NaCl treatment for 14 days (**Figure 1A**). Compared to the control, the dry weight of CS root decreased significantly by 59.03% under salt-stress, while the QM6 root only decreased by 36.56%, which is significantly less than that of CS (**Figure 1B**). For shoot dry weights, the CS and QM6 both decreased significantly by salt-stress, decreased by 75.85% in CS and 66.71% in QM6 (**Figure 1C**). These results suggest that the salt tolerance of QM6 was significantly higher than CS.

Identification of QM6 miRNA

23,919,344 and 22,852,249 clean reads from QM6 roots under control and NaCl-induced salt stress conditions were obtained, respectively. Most reads were annotated into different categories (**Table 1**). rRNA preponderances of 13,629,988 (56.98%) and 11,586,708 (50.70%) reads were observed in the control and NaCl salt-treated root samples, respectively (**Table 1**). The known miRNA accounted for 0.62% (147,885) and novel miRNA accounted for 0.78% (185,934; **Table 1**) of the total reads from control conditions. However, under salt stress, the known miRNA accounted for 0.88% (202,005) while novel miRNA accounted for 1.62% (369,704; **Table 1**) of the total reads.

TABLE 1 | Summary of small RNA-seq data in QM6 under two treatments.

Treatment	Classification	Reads	Percentage (%)
Control	Clean reads	23,919,344	100
	Exon+	2,633,855	11.01
	Exon–	2,069,878	8.65
	Intron+	573,740	2.40
	Intron–	469,293	1.96
	Known miRNA	147,885	0.62
	Novel miRNA	185,934	0.78
	Repeat	28,766	0.12
	rRNA	13,629,988	56.98
	snRNA	354,419	1.48
	snoRNA	229,749	0.96
	tRNA	3,122,092	13.05
	Other	473,745	1.98
Salt stress	Clean reads	22,852,249	100
	Exon+	2,105,445	9.21
	Exon–	2,200,768	9.63
	Intron+	344,826	1.51
	Intron–	328,650	1.44
	Known miRNA	202,005	0.88
	Novel miRNA	369,704	1.62
	Repeat	17,575	0.08
	rRNA	11,586,708	50.70
	snRNA	302,457	1.32
	snoRNA	164,191	0.72
	tRNA	4,892,895	21.41
	Other	337,025	1.47

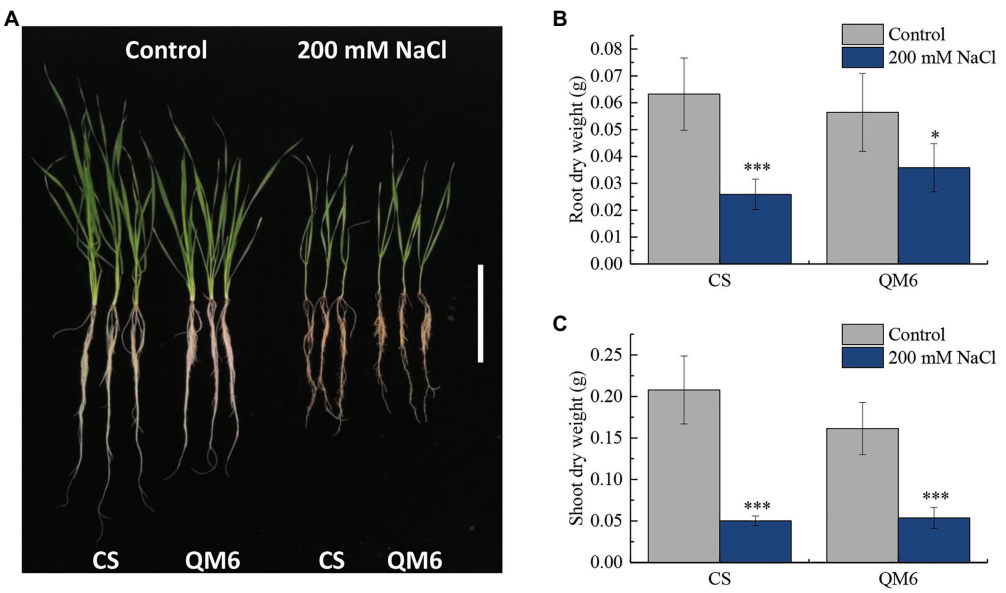

FIGURE 1 | The Chinese Spring (CS) and Qing Mai 6 (QM6) phenotype under 200 mM NaCl-induced salt stress and control conditions. **(A)** The phenotypic difference of CS and QM6 in response to salt stress; bar = 5 cm. **(B)** The CS and QM6 root dry weights under 200 mM NaCl-induced salt stress and control conditions. **(C)** The CS and QM6 shoot dry weights under 200 mM NaCl-induced salt stress and control conditions. $n = 3$; $^{*}p < 0.05$; $^{***}p < 0.001$.

These results showed the differences in miRNA expression between the control and NaCl-treated QM6 root samples.

The length distribution of miRNA showed that the number of reads from 24 to 30 nt was higher in control than that in NaCl-treated samples. However, the number of reads from 17 to 23 nt was higher in the control than that of the NaCl-treated samples. Moreover, the 24 nt nucleotide miRNA was found to be the most abundant in both control and NaCl-treated QM6 root samples (**Figure 2**). A total of 687 miRNAs were identified in both control and NaCl-treated QM6 root samples, of which 108 were known miRNAs (**Supplementary Table 3**) and 579 were novel miRNAs (**Supplementary Table 4**).

Identification of QM6 mRNA Sequencing Data

A total of 224,115,086 clean reads from QM6 root samples were obtained after removing adapter and low-quality reads and then selecting fragment from the original transcriptome sequencing data. The clean bases were more than 9.50 Gb in all samples. Q30, the base mass value, was more than 92.86% and the GC content was 40–60% (**Supplementary Table 5**). In the control group, 67,583,952, 71,982,771, and 61,141,717 mapped reads were obtained, which account for 89.67, 89.95, and 89.63% of the total reads, respectively. In NaCl-treated samples, 60,915,291, 65,287,118, and 63,225,488 mapped reads were obtained, accounting for 84.72, 84.74, and 83.55% of the total reads, respectively (**Table 2**). The utilization rate of transcriptome data in control and NaCl-treated QM6 root samples was more than 83.55%, which met the requirement of the subsequent analysis. In the control group, reads matched to the unique position of the reference genome were 86.35, 86.73, and 86.42%, while in the NaCl-treated group, the unique mapped reads were 81.71, 81.76, and 80.58%. At least 44.21 and 41.28% of reads matched to the positive strand, and at least 44.41 and 41.42% of reads matched to the negative strand of the reference genome in the control and NaCl-treated QM6 root groups, respectively (**Table 2**).

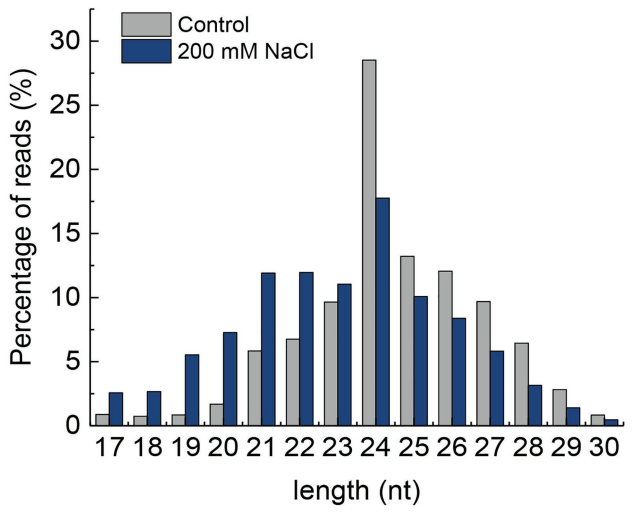

FIGURE 2 | Length distribution of small RNAs in the QM6 roots under 200 mM NaCl-induced salt stress and control conditions. *Y*-axis, the percentage of small RNA reads.

Identification of QM6 miRNA and mRNA in Response to Salt Stress

In this study, 210 differentially expressed miRNAs were identified in QM6 roots between control and salt stress conditions. Out of these, 35 were known miRNAs (**Supplementary Table 6**; **Supplementary Figure 1**) and 175 were novel miRNAs (**Supplementary Table 7**; **Supplementary Figure 2**). For the 35 known miRNAs, two were significantly up-regulated and 33 were significantly down-regulated (**Figure 3A**). Out of the 175 novel miRNAs, 57 were significantly up-regulated and 118 were significantly down-regulated in response to salt stress (**Figure 3A**). A total of 10,847 DEGs were identified in QM6 roots between control and salt stress conditions, of which 5,771 were up-regulated and 5,076 were down-regulated (**Figure 3B; Supplementary Figure 3**; **Supplementary Table 8**).

Salt-Tolerance Related miRNAs and Their Target mRNAs

In order to explore the potential biological functions of differentially expressed miRNA in QM6 root samples under salt stress conditions, the differentially expressed miRNAs and mRNAs were analyzed. Target mRNAs of the differentially expressed miRNAs were predicted based on the obtained differentially expressed mRNAs. As results, eight miRNAs (seven known miRNA and one novel miRNA) and their corresponding 11 target mRNAs were determined (**Table 3**). The target mRNAs mainly included MYB-like gene, Cytochrome P450, POT family, NB-ARC domain protein, and GDSL-like lipase (**Table 3**). miRNAs including tae-miR1122a, tae-miR1131, tae-miR9774, and tae-miR9668-5p each had two target mRNAs while tae-miR319, tae-miR9674b-5p, tae-miR9666b-3p, and Novel_72 each had only one target mRNA (**Table 3**).

TABLE 2 | Summary of high throughput transcriptome sequencing of QM6 under two treatments.

Sample	Total reads	Mapped reads	Unique mapped reads	Multiple map reads	Reads map to "+"	Reads map to "–"
QM6 CK1	75,367,810	67,583,952 (89.67%)	65,082,516 (86.35%)	2,501,436 (3.32%)	33,318,887 (44.21%)	33,474,236 (44.41%)
QM6 CK2	80,024,874	71,982,771 (89.95%)	69,402,325 (86.73%)	2,580,446 (3.22%)	35,518,921 (44.38%)	35,664,950 (44.57%)
QM6 CK3	68,212,420	61,141,717 (89.63%)	58,948,101 (86.42%)	2,193,626 (3.22%)	30,174,820 (44.24%)	30,294,445 (44.41%)
QM6 T1	71,906,110	60,915,291 (84.72%)	58,753,740 (81.71%)	2,161,551 (3.01%)	30,100,486 (41.86%)	30,203,211 (42.00%)
QM6 T2	77,046,224	65,287,118 (84.74%)	62,993,212 (81.76%)	2,293,906 (2.98%)	32,255,771 (41.87%)	32,363,004 (42.00%)
QM6 T3	75,672,734	63,225,488 (83.55%)	60,974,788 (80.58%)	2,250,700 (2.97%)	31,240,150 (41.28%)	31,342,034 (41.42%)

Expressions of Salt-Tolerance Related miRNAs and Their Target mRNAs

All eight miRNAs and their 11 corresponding target mRNA were subjected to qRT-PCR based validation. The accuracy of miRNA and mRNA sequencing and target gene identification was also validated. qRT-PCR based on three biological replicates and at least two technical replicates showed that all miRNAs were down-regulated whereas their target mRNAs were up-regulated (**Figure 4**), which were highly consistent with the sequencing results. In conclusion, a negative correlation was observed between the expression levels of the eight verified miRNAs and their target genes. It demonstrated the reliability of the miRNA sequencing results and the identification of their target mRNAs.

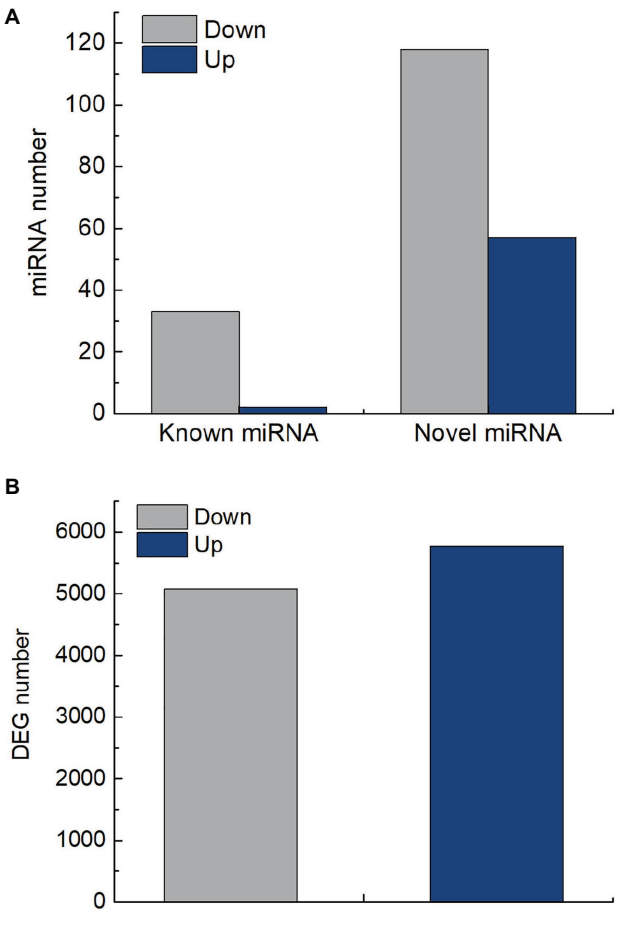

FIGURE 3 | The number of differentially expressed miRNAs and genes in QM6 roots in response to salt stress. **(A)** The number of up-regulated and down-regulated known and novel miRNAs after 24 h of salt stress. **(B)** The number of up-regulated and down-regulated genes after 24 h of salt stress.

DISCUSSION

miRNAs are a class of non-coding single-stranded small RNAs, which mediate multiple biological processes, including plant growth, development, and stress response by post-transcriptional or translational regulation of target genes (Kumar et al., 2017; Tang and Chu, 2017; Nair et al., 2019; Cui et al., 2020). As reported previously, miRNAs can improve salt tolerance in rice (Shen et al., 2017), barley (Kuang et al., 2019), *Arabidopsis thaliana* (Schommer et al., 2014), pearl chestnut (Harshraj et al., 2020), and other plants by regulating plant development and stress response. However, only few studies have been carried in wheat miRNAs related salt tolerance.

In this study, we investigated a salt-tolerant and widely cultivated wheat cultivar, QM6, using high-throughput sequencing and qRT-PCR based validation. And the rRNA reads accounted for less than 60% of total reads from plant RNA samples, indicating a good sequencing quality (Zhao et al., 2014). It led to the identification of eight differentially expressed miRNAs and their corresponding 11 target mRNAs involved in transcriptional regulation (MYB), oxidation resistance (CYP450), nutrient uptake (POT), stress tolerance (NB-ARC), lipid balance (GDSL-like lipase), and other biological processes, which can potentially be utilized to improve the salt tolerance of wheat (**Figure 5**).

tae-miR319 and tae-miR9666b-3p Affected Salt Tolerance of Wheat by Regulating MYB Transcription Factor

miR319, an essential miRNA, plays a vital role in the growth and development, immune response, and abiotic stress in *A. thaliana*, barley, wheat, and other plants by regulating TCP, MYB transcription factor, and other miRNAs. *Arabidopsis thaliana*

TABLE 3 | Salt tolerance related miRNAs and their target genes in QM6.

miRNA	miRNA log_2^{FC}	Target gene ID	Target gene log_2^{FC}	Gene annotation
tae-miR1122a	−1.64	TraesCS3D02G020600	1.24	GDSL-like lipase
		TraesCS3B02G020700	2.48	Unknown
tae-miR1131	−1.84	TraesCS7B02G312500	1.19	POT family
		TraesCS7D02G136400	2.03	Cytochrome P450
tae-miR319	−1.53	TraesCS3A02G108000	1.52	MYB-like gene
tae-miR9774	−1.34	Triticum_aestivum_newGene_26286	1.09	NB-ARC domain
		Triticum_aestivum_newGene_26283	1.96	NB-ARC domain
tae-miR9674b-5p	−1.16	Triticum_aestivum_newGene_7847	1.07	Unknown
tae-miR9666b-3p	−3.41	TraesCS1B02G449200	2.58	MYB-like gene
tae-miR9668-5p	−1.69	TraesCS1A02G025500	2.65	NB-ARC domain
		TraesCS7A02G038900	2.78	NB-ARC domain
Novel_72	−8.43	TraesCS7B02G312500	1.19	POT family

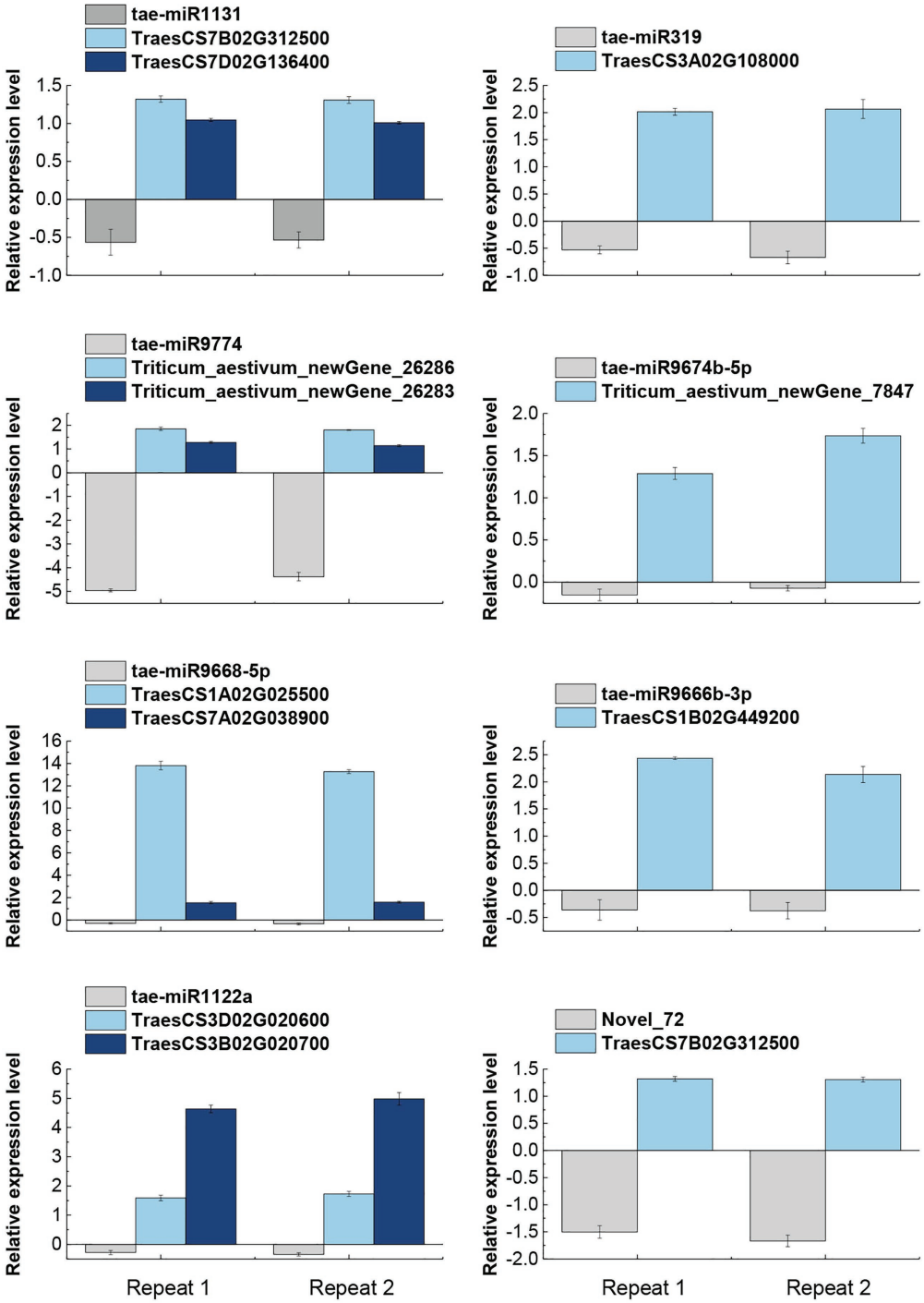

FIGURE 4 | qRT-PCR based validation of miRNAs and their target genes expression pattern in response to salt stress. The expression data are means of three biological replicates and two technical repeats. tae-miR1131, tae-miR9774, tae-miR9668-5p, and tae-miR1122a miRNAs were found to have two target genes each, while tae-miR319, tae-miR9674b-5p, tae-miR9666b-3p, and Novel_72 miRNAs had only one target gene each.

miR319a affects plant leaf development (Schommer et al., 2014) through TCP transcription factor regulation and plant root growth through MYB transcription factor regulation and *MYB33* gene transcription (Li et al., 2020). Barley miR319a regulates and participates in salt stress response by inhibiting the miR396e-mediated *GRF* gene pathway through *TCP4* expression (Kuang et al., 2019). Wheat miR319 is involved in regulating plant architecture, flowering, yield, and other important agronomic traits by targeting the *TaMYB34* gene (Jian et al., 2019). Furthermore, some members of the miR9666 family play a

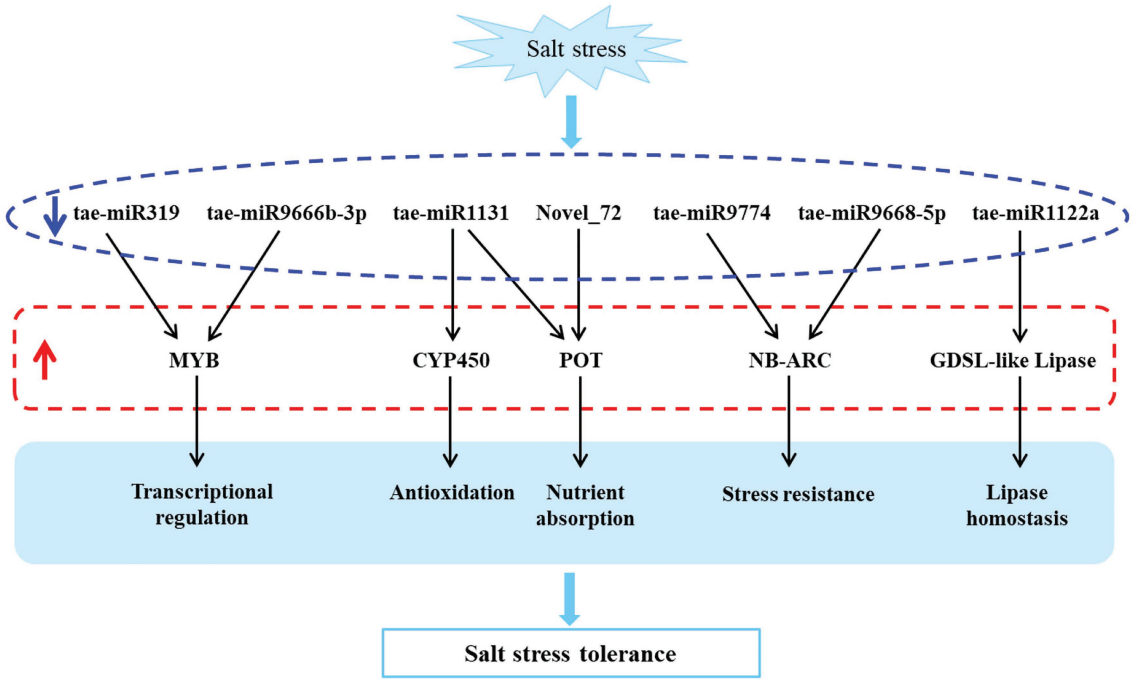

FIGURE 5 | A predicted salt tolerant model of QM6 based on the differentially expressed miRNAs and their target genes. The blue arrow represents down-regulation and the red arrow represents up-regulation.

crucial role in abiotic stress response (Li et al., 2017). A previous study showed that tae-miR9666b miRNA is only expressed at the seedling stage of wheat (Han et al., 2014). However, no study has been carried in salt tolerance aspect about tae-miR9666b.

As one of the major transcription factors in plants, MYB plays a crucial role in plant growth and plants response to abiotic stress. As shown previously, MYB gene family members in maize and cotton enhanced the tolerance to drought and salt stress by regulating the ABA signaling pathway (Wu et al., 2019; Zhao et al., 2019). R2R3-type MYB transcription factors, *OsMYB91* and *TaSIM*, in rice and wheat had positive effects on salt stress tolerance (Zhu et al., 2015; Yu et al., 2017). The tae-miR319 and tae-miR9666b-3p miRNAs identified in this study were down-regulated under salt stress conditions, whereas, their target genes, traesCS3A02G108000 and traesCS1B02G449200 (*MYB-like* gene) were up-regulated, indicating that tae-miR319 and tae-miR9666b-3p influence the salt tolerance of wheat by regulating the MYB gene.

tae-miR1131 Enhances Antioxidant Stress Capacity of Wheat by Regulating CYP450

Under normal environmental conditions, reactive oxygen species (ROS) in plants are in a dynamic equilibrium state of generation and elimination. However, under salt stress, plants produce a high concentration of ROS, which accumulates in cells, damages the membrane lipid structure, and affects normal physiological metabolism. CYP450, a multifunctional oxidase, plays a crucial role in plant biosynthesis, metabolism, detoxification, and stress resistance (Li and Wei, 2020). *TaCYP78A3* influences integumentary cell proliferation and thus regulates wheat seed size (Ma et al., 2015). Downregulated *OsCYP707A7* induced a higher ABA content and antioxidant enzyme activity in rice (Cai et al., 2015). *CYP85A1* up-regulation in spinach improved the drought resistance of transgenic tobacco (Duan et al., 2017). We speculated that tae-miR1131 identified in this study enhances the antioxidant stress capacity of wheat by negatively regulating the target genes traesCS7D02G136400 (*CYP450*) and improves the salt tolerance of wheat.

tae-miR1131 and Novel_72 Co-regulate *POT* Gene to Promote Nutrient Uptake of Wheat

Previous studies demonstrated that wheat tae-miR1131 targets N and P nutrition-related genes that have important roles in wheat N and P nutrient absorption (Kumar et al., 2018). POT is a proton-coupled oligopeptide transporter and is an important nutrient absorption transporter (Newstead, 2017). In the current study, nutrient uptake-related gene TraesCS7B02G312500 (*POT*) was found to be the target gene of tae-miR1131 and predicted Novel_72 miRNAs. It suggests that tae-miR1131 and Novel_72 under salt stress enhance wheat nutrient absorption and salt tolerance by co-regulating *POT* expression.

tae-miR9774 and tae-miR9668-5p Target Stress Resistance Gene *NB-ARC* for Wheat Salt Tolerance Enhancement

It is known that miR9774 in barley is involved in drought stress (Bakhshi et al., 2017). Besides, tae-miR9774 increases the soil cadmium stress tolerance in wheat plants (Zhou et al., 2019).

tae-miR9668-5p improves wheat's resistance to powdery mildew, leaf rust, and other fungal diseases (Nair et al., 2019). However, only a few studies have explored the salt tolerance of these two miRNAs. NB-ARC family, an important class of stress resistance proteins in plants, plays a vital role in wheat disease resistance (Chandra et al., 2017). Nevertheless, the role of these genes in the salt tolerance aspect of wheat remains unknown. In this study, tae-miR9774 and tae-miR9668-5p were found to be down-regulated under salt stress condition, while their target genes TraesCS1A02G025500, TraesCS7A02G038900, Triticum_aestivum_newGene_26283, and Triticum_aestivum_newGene_26286 (NB-ARC through function prediction) were up-regulated. These results suggest that tae-miR9774 and tae-miR9668-5p regulate the adaptability of wheat to salt stress by negatively regulating the expression of NB-ARC family genes.

tae-miR1122a Regulates GDSL-Like Lipase to Maintain Lipid Balance in Wheat

Previous studies showed that tae-miR1122a plays a crucial role in the growth and development as well as stress response of wheat. Besides, tae-miR1122a was found to be involved in the anther development of wheat male sterility (Sun et al., 2018). In alkali-tolerant SR4 wheat, tae-miR1122a was found to inhibit ROS accumulation and enhance alkaline stress tolerance by regulating its target gene *Rboh* expression (Han et al., 2018). GDSL esterase also plays a vital role in abiotic stress, pathogen defense, seed development, and lipid metabolism (Tan et al., 2014; Su et al., 2020). However, there is no report about the effect of GDSL esterase on wheat salt tolerance. tae-miR1122a, which was found to be significantly down-regulated in this study under salt stress, could target and negatively regulate the TraesCS7B02G312500 (GDSL-like lipase). Thus, we speculate that tae-miR1122a regulates the lipid balance in wheat in response to the harmful effect of salt stress by regulating GDSL-like lipase.

CONCLUSION

In our study, salt-tolerant wheat variety QM6 miRNAs and their target genes in response to salt stress were identified using miRNA and mRNA sequencing. The sequencing data were validated using qRT-PCR. The bioinformatics analysis led to the identification of eight down-regulated miRNAs (tae-miR319, tae-miR9666b-3p, tae-miR1131, tae-miR1131, Novel_72, tae-miR9774, tae-miR9668-5p, and tae-miR1122a) and 11 up-regulated target mRNAs. These mRNAs were found to be involved in transcriptional regulation (MYB), antioxidant stress (CYP450), nutrient uptake (POT), stress tolerance (NB-ARC), lipid balance (GDSL-like lipase), and other biological processes under salt stress. These results indicate that these miRNAs form a complex regulatory network by negatively regulating the expression of their target genes, which play an important role in conferring salt tolerance of the QM6 wheat cultivar. The study enhanced our understanding towards the salt tolerance related miRNAs and their target genes, which can potentially help breeding salt tolerant wheat varieties.

DATA AVAILABILITY STATEMENT

The datasets presented in this study can be found in online repositories. The names of the repository/repositories and accession number(s) can be found in the article/ **Supplementary Material**.

AUTHOR CONTRIBUTIONS

XH and PM: experimental design. ZH, FC, YD, LZ, and XL: experimental performance. XH, ZH, FC, and YD: data analysis. XH and ZH: manuscript writing. HY and JZ: manuscript revision. WM and PM: English language improvement. All authors contributed to the article and approved the submitted version.

FUNDING

This work was supported by the Foundation of Research and Application of Whole Genome Selection in Wheat (2019LZGC016), the Wheat Innovation Team of Modern Agricultural Production Systems in Shandong Province (SDAIT01-05), the High-Level Talents Project of Qingdao Agricultural University (663/1119013), and the National Natural Science Foundation of China (31601231).

SUPPLEMENTARY MATERIAL

The Supplementary Material for this article can be found online at: https://www.frontiersin.org/articles/10.3389/fgene.2021.724527/full#supplementary-material

REFERENCES

Bakhshi, B., Fard, E. M., Gharechahi, J., Safarzadeh, M., Nikpay, N., Fotovat, R., et al. (2017). The contrasting microRNA content of a drought tolerant and a drought susceptible wheat cultivar. *J. Plant Physiol.* 216, 35–43. doi: 10.1016/j.jplph.2017.05.012

Cai, S., Jiang, G., Ye, N., Chu, Z., Xu, X., Zhang, J., et al. (2015). A key ABA catabolic gene, *OsABA8ox3*, is involved in drought stress resistance in rice. *PLoS One* 10:e0116646. doi: 10.1371/journal.pone.0116646

Chandra, S., Kazmi, A. Z., Ahmed, Z., Roychowdhury, G., Kumari, V., Kumar, M., et al. (2017). Genome-wide identification and characterization of NB-ARC resistant genes in wheat (*Triticum aestivum* L.) and their expression during leaf rust infection. *Plant Cell Rep.* 36, 1097–1112. doi: 10.1007/s00299-017-2141-0

Cui, G., Zhao, M., Zhang, S., Wang, Z., and Xi, Y. (2020). MicroRNA and regulation of auxin and cytokinin signaling during post-mowing regeneration of winter wheat (*Triticum aestivum* L.). *Plant Physiol. Biochem.* 155, 769–779. doi: 10.1016/j.plaphy.2020.08.032

D'Odorico, P., Bhattachan, A., Davis, K. F., Ravi, S., and Runyan, C. W. (2013). Global desertification: drivers and feedbacks. *Adv. Water Resour.* 51, 326–344. doi: 10.1016/j.advwatres.2012.01.013

Dillies, M. A., Rau, A., Aubert, J., Hennequet-Antier, C., Jeanmougin, M., Servant, N., et al. (2013). A comprehensive evaluation of normalization

methods for Illumina high-throughput RNA sequencing data analysis. *Brief. Bioinform.* 14, 671–683. doi: 10.1093/bib/bbs046

Duan, F., Ding, J., Lee, D., Lu, X., Feng, Y., and Song, W. (2017). Overexpression of *SoCYP85A1*, a spinach cytochrome p450 gene in transgenic tobacco enhances root development and drought stress tolerance. *Front. Plant Sci.* 8:1909. doi: 10.3389/fpls.2017.01909

Feng, H., Huang, X., Zhang, Q., Wei, G., Wang, X., and Kang, Z. (2012). Selection of suitable inner reference genes for relative quantification expression of microRNA in wheat. *Plant Physiol. Biochem.* 51, 116–122. doi: 10.1016/j.plaphy.2011.10.010

Florea, L., Song, L., and Salzberg, S. L. (2013). Thousands of exon skipping events differentiate among splicing patterns in sixteen human tissues. *F1000Res.* 2:188. doi: 10.12688/f1000research.2-188.v1

Galvani, A. (2007). The challenge of the food sufficiency through salt tolerant crops. *Rev. Environ. Sci. Biol.* 6, 3–16. doi: 10.1007/s11157-006-0010-3

Hafner, M., Landgraf, P., Ludwig, J., Rice, A., Ojo, T., Lin, C., et al. (2008). Identification of miRNAs and other small regulatory RNAs using cDNA library sequencing. *Methods* 44, 3–12. doi: 10.1016/j.ymeth.2007.09.009

Han, R., Jian, C., Lv, J., Yan, Y., Chi, Q., Li, Z., et al. (2014). Identification and characterization of miRNAs in the flag leaf and developing seed of wheat (*Triticum aestivum* L.). *BMC Genomics* 15:289. doi: 10.1186/1471-2164-15-289

Han, H., Qi, W., Lin, W., Yu, L., Dai, J., Xia, G., et al. (2018). Small RNA and degradome sequencing used to elucidate the basis of tolerance to salinity and alkalinity in wheat. *BMC Plant Biol.* 18:195. doi: 10.1186/s12870-018-1415-1

Harshraj, S., Ambika, D., Lakshay, A., Daisuke, T., Shashi, K. G., Shenkui, L., et al. (2020). Small RNA sequencing reveals the role of pearl millet miRNAs and their targets in salinity stress responses. *S. Afr. J. Bot.* 132, 395–402. doi: 10.1016/j.sajb.2020.06.011

Illumina Inc. (2011). *CASAVA v1.8.2 User Guide*. San Diego, CA, USA: Illumina Inc.

Jian, C., Wang, X., Hao, C., Zhao, X., and Zhang, X. (2019). "Identification the function and molecular mechanism of Tae-miR319 regulating important agronomic traits in wheat." in *10th National Conference on Wheat Genomics and Molecular Breeding*; August 12, 2019.

Kim, D., Langmead, B., and Salzberg, S. L. (2015). HISAT: a fast spliced aligner with low memory requirements. *Nat. Methods* 12, 357–360. doi: 10.1038/nmeth.3317

Kozomara, A., and Griffiths-Jones, S. (2014). miRBase: annotating high confidence microRNAs using deep sequencing data. *Nucleic Acids Res.* 42, D68–D73. doi: 10.1093/nar/gkt1181

Kuang, L., Shen, Q., Wu, L., Yu, J., Fu, L., Wu, D., et al. (2019). Identification of microRNAs responding to salt stress in barley by high-throughput sequencing and degradome analysis. *Environ. Exp. Bot.* 160, 59–70. doi: 10.1016/j.envexpbot.2019.01.006

Kumar, M., Kumar, R. R., Goswami, S., Verma, P., Rai, R. D., Chinnusamy, V., et al. (2017). miR430: the novel heat-responsive miRNA identified from miRNome analysis in wheat (*Triticum aestivum* L.). *Indian J. Plant Physiol.* 22, 566–576. doi: 10.1007/s40502-017-0341-9

Kumar, A., Sharma, M., Kumar, S., Tyagi, P., Wani, S. H., Gajula, M. N. V. P., et al. (2018). Functional and structural insights into candidate genes associated with nitrogen and phosphorus nutrition in wheat (*Triticum aestivum* L.). *Int. J. Biol. Macromol.* 118, 76–91. doi: 10.1016/j.ijbiomac.2018.06.009

Li, T., Gonzalez, N., Inzé, D., and Dubois, M. (2020). Emerging connections between small RNAs and phytohormones. *Trends Plant Sci.* 25, 912–929. doi: 10.1016/j.tplants.2020.04.004

Li, J., Pu, L., Han, M., Zhu, M., Zhang, R., and Xiang, Y. (2014). Soil salinization research in China: advances and prospects. *J. Geogr. Sci.* 24, 943–960. doi: 10.1007/s11442-014-1130-2

Li, Y., and Wei, K. (2020). Comparative functional genomics analysis of cytochrome P450 gene superfamily in wheat and maize. *BMC Plant Biol.* 20:93. doi: 10.1186/s12870-020-2288-7

Li, J., Yue, L., Shen, Y., Sheng, Y., Zhan, X., Xu, G., et al. (2017). Phenanthrene-responsive microRNAs and their targets in wheat roots. *Chemosphere* 186, 588–598. doi: 10.1016/j.chemosphere.2017.08.022

Love, M. I., Huber, W., and Anders, S. (2014). Moderated estimation of fold change and dispersion for RNA-seq data with DESeq2. *Genome Biol.* 15:550. doi: 10.1186/s13059-014-0550-8

Ma, M., Wang, Q., Li, Z., Cheng, H., Li, Z., Liu, X., et al. (2015). Expression of *TaCYP78A3*, a gene encoding cytochrome P450 CYP78A3 protein in wheat (*Triticum aestivum* L.), affects seed size. *Plant J.* 83, 312–325. doi: 10.1111/tpj.12896

Martin, M. (2011). Cutadapt removes adapter sequences from high-throughput sequencing reads. *EMBnet J.* 17, 10–12. doi: 10.14806/ej.17.1.200

Nadeem, M., Ali, M., Kubra, G., Fareed, A., Hasan, H., Khursheed, A., et al. (2020). "Role of osmoprotectants in salinity tolerance in wheat," in *Climate Change and Food Security With Emphasis on Wheat.* Academic Press. 93–106.

Nair, M. M., Krishna, T. S., and Manickavelu, A. (2019). Bioinformatics insights into microRNA mediated gene regulation in *Triticum aestivum* during multiple fungal diseases. *Plant Gene* 21:100219. doi: 10.1016/j.plgene.2019.100219

Newstead, S. (2017). Recent advances in understanding proton coupled peptide transport via the POT family. *Curr. Opin. Struct. Biol.* 45, 17–24. doi: 10.1016/j.sbi.2016.10.018

Pagano, L., Rossi, R., Paesano, L., Marmiroli, N., and Marmiroli, M. (2021). miRNA regulation and stress adaptation in plants. *Environ. Exp. Bot.* 184:104369. doi: 10.1016/j.envexpbot.2020.104369

Paolacci, A. R., Tanzarella, O. A., Porceddu, E., and Ciaffi, M. (2009). Identification and validation of reference genes for quantitative RT-PCR normalization in wheat. *BMC Mol. Biol.* 10:11. doi: 10.1186/1471-2199-10-11

Pertea, M., Pertea, G. M., Antonescu, C. M., Chang, T. C., Mendell, J. T., and Salzberg, S. L. (2015). StringTie enables improved reconstruction of a transcriptome from RNA-seq reads. *Nat. Biotechnol.* 33, 290–295. doi: 10.1038/nbt.3122

Potter, S. C., Luciani, A., Eddy, S. R., Park, Y., Lopez, R., and Finn, R. D. (2018). HMMER web server: 2018 update. *Nucleic Acids Res.* 46, W200–W204. doi: 10.1093/nar/gky448

Prăvălie, R., Patriche, C., Borrelli, P., Panagos, P., and Bandoc, G. (2021). Arable lands under the pressure of multiple land degradation processes. A global perspective. *Environ. Res.* 194:110697. doi: 10.1016/j.envres.2020.110697

Schommer, C., Debernardi, J. M., Bresso, E. G., Rodriguez, R. E., and Palatnik, J. F. (2014). Repression of cell proliferation by miR319-regulated TCP4. *Mol. Plant* 7, 1533–1544. doi: 10.1093/mp/ssu084

Shen, C., Huang, Y. Y., He, C. T., Zhou, Q., and Yang, Z. Y. (2017). Comparative analysis of cadmium responsive microRNAs in roots of two *Ipomoea aquatica* Forsk. cultivars with different cadmium accumulation capacities. *Plant Physiol. Biochem.* 111, 329–339. doi: 10.1016/j.plaphy.2016.12.013

Singh, A. (2020). Soil salinization management for sustainable development: a review. *J. Environ. Manag.* 277:111383. doi: 10.1016/j.jenvman.2020.111383

Singh, A. K., Singh, N., Kumar, S., Kumari, J., and Kumar, R. (2020). Identification and evolutionary analysis of polycistronic miRNA clusters in domesticated and wild wheat. *Genomics* 112, 2334–2348. doi: 10.1016/j.ygeno.2020.01.005

Su, H. G., Zhang, X. H., Wang, T. T., Wei, W. L., and Min, D. H. (2020). Genome-wide identification, evolution, and expression of GDSL-type esterase/lipase gene family in soybean. *Front. Plant Sci.* 11:726. doi: 10.3389/fpls.2020.00726

Sun, L., Sun, G., Shi, C., and Sun, D. (2018). Transcriptome analysis reveals new microRNAs-mediated pathway involved in another development in male sterile wheat. *BMC Genomics* 19:333. doi: 10.1186/s12864-018-4727-5

Tan, X., Yan, S., Tan, R., Zhang, Z., Wang, Z., and Chen, J. (2014). Characterization and expression of a GDSL-like lipase gene from *Brassica napus* in *Nicotiana benthamiana*. *Protein J.* 33, 18–23. doi: 10.1007/s10930-013-9532-z

Tang, J., and Chu, C. (2017). MiRNAs in crop improvement: fine-tuners for complex traits. *Nat. Plants* 3:17077. doi: 10.1038/nplants.2017.77

Wagner, G. P., Kin, K., and Lynch, V. J. (2012). Measurement of mRNA abundance using RNA-seq data: RPKM measure is inconsistent among samples. *Theor. Biosci.* 131, 281–285. doi: 10.1007/s12064-012-0162-3

Wu, J., Jiang, Y., Liang, Y., Chen, L., Chen, W., and Cheng, B. (2019). Expression of the maize MYB transcription factor ZmMYB3R enhances drought and salt stress tolerance in transgenic plants. *Plant Physiol. Biochem.* 137, 179–188. doi: 10.1016/j.plaphy.2019.02.010

Wu, H. J., Ma, Y. K., Chen, T., Wang, M., and Wang, X. J. (2012). PsRobot: a web-based plant small RNA meta-analysis toolbox. *Nucleic Acids Res.* 40, W22–W28. doi: 10.1093/nar/gks554

Yu, Y., Ni, Z., Chen, Q., and Qu, Y. (2017). The wheat salinity-induced R2R3-MYB transcription factor TaSIM confers salt stress tolerance in *Arabidopsis thaliana*. *Biochem Biophys. Res. Commun.* 491, 642–648. doi: 10.1016/j.bbrc.2017.07.150

Zhang, B., and Unver, T. (2018). A critical and speculative review on miRNA technology in crop improvement: current challenges and future directions. *Plant Sci.* 274, 193–200. doi: 10.1016/j.plantsci.2018.05.031

Zhao, W., He, X., Hoadley, K. A., Parker, J. S., Hayes, D. N., and Perou, C. M. (2014). Comparison of RNA-Seq by poly (A) capture, ribosomal RNA depletion, and DNA microarray for expression profiling. *BMC Genomics* 15:419. doi: 10.1186/1471-2164-15-419

Zhao, Y., Yang, Z., Ding, Y., Liu, L., and Ge, X. (2019). Over-expression of an R2R3 MYB gene, *GhMYB73*, increases tolerance to salt stress in transgenic *Arabidopsis*. *Plant Sci.* 286, 28–36. doi: 10.1016/j.plantsci.2019.05.021

Zhou, M., Zheng, S., Liu, R., Lu, L., and Wu, Y. (2019). The genome-wide impact of cadmium on microRNA and mRNA expression in contrasting cd responsive wheat genotypes. *BMC Genomics* 20:615. doi: 10.1186/s12864-019-5939-z

Zhu, N., Cheng, S., Liu, X., Du, H., Dai, M., Zhou, D. X., et al. (2015). The R2R3-type MYB gene *OsMYB91* has a function in coordinating plant growth and salt stress tolerance in rice. *Plant Sci.* 236, 146–156. doi: 10.1016/j.plantsci.2015.03.023

Conflict of Interest: The authors declare that the research was conducted in the absence of any commercial or financial relationships that could be construed as a potential conflict of interest.

Publisher's Note: All claims expressed in this article are solely those of the authors and do not necessarily represent those of their affiliated organizations, or those of the publisher, the editors and the reviewers. Any product that may be evaluated in this article, or claim that may be made by its manufacturer, is not guaranteed or endorsed by the publisher.

frontiers in Genetics

ORIGINAL RESEARCH
published: 09 November 2021
doi: 10.3389/fgene.2021.771814

Genome-wide Identification and Evolutionary Analysis of NBS-LRR Genes From *Secale cereale*

Lan-Hua Qian[1†], Yue Wang[2†], Min Chen[2], Jia Liu[2], Rui-Sen Lu[2], Xin Zou[3], Xiao-Qin Sun[2] and Yan-Mei Zhang[2*]*

[1]Suzhou Polytechnic Institute of Agriculture, Suzhou, China, [2]Institute of Botany, Jiangsu Province and Chinese Academy of Sciences, Nanjing, China, [3]Seed Administrative Station of Suzhou, Suzhou, China

Secale cereale is an important crop in the Triticeae tribe of the Poaceae family, and it has unique agronomic characteristics and genome properties. It possesses resistance to many diseases and serves as an important resource for the breeding of other Triticeae crops. We performed a genome-wide study on *S. cereale* to identify the largest group of plant disease resistance genes (*R* genes), the nucleotide-binding site-leucine-rich repeat receptor (NBS-LRR) genes. In its genome, 582 NBS-LRR genes were identified, including one from the RNL subclass and 581 from the CNL subclass. The NBS-LRR gene number in the *S. cereale* genome is greater than that in barley and the diploid wheat genomes. *S. cereale* chromosome 4 contains the largest number of NBS-LRR genes among the seven chromosomes, which is different from the pattern in barley and the genomes B and D of wheat but similar to that in the genome A of wheat. Further synteny analysis suggests that more NBS-LRR genes on chromosome 4 have been inherited from a common ancestor by *S. cereale* and the wheat genome A than the wheat genomes B and D. Phylogenetic analysis revealed that at least 740 NBS-LRR lineages are present in the common ancestor of *S. cereale*, *Hordeum vulgare* and *Triticum urartu*. However, most of them have only been inherited by one or two species, with only 65 of them preserved in all three species. The *S. cereale* genome inherited 382 of these ancestral NBS-LRR lineages, but 120 of them have been lost in both *H. vulgare* and *T. urartu*. This study provides the full NBS-LRR profile of the *S. cereale* genome, which is a resource for *S. cereale* breeding and indicates that *S. cereale* can be an important material for the molecular breeding of other Triticeae crops.

Keywords: ***Secale cereale*, NBS-LRR gene, disease resistance, triticeae crops, evolutionary analysis**

OPEN ACCESS

Edited by:
Pengtao Ma,
Yantai University, China

Reviewed by:
Jun Guo,
Shandong Academy of Agricultural Sciences, China
Wang Jing,
Institute of Genetics and Developmental Biology (CAS), China

***Correspondence:**
Xiao-Qin Sun
xiaoqinsun@cnbg.net
Yan-Mei Zhang
yanmeizhang@cnbg.net

[†]These authors have contributed equally to this work

Specialty section:
This article was submitted to Plant Genomics, a section of the journal Frontiers in Genetics

Received: *07 September 2021*
Accepted: *25 October 2021*
Published: *09 November 2021*

Citation:
Qian L-H, Wang Y, Chen M, Liu J, Lu R-S, Zou X, Sun X-Q and Zhang Y-M (2021) Genome-wide Identification and Evolutionary Analysis of NBS-LRR Genes From Secale cereale. *Front. Genet. 12:771814. doi: 10.3389/fgene.2021.771814*

INTRODUCTION

Plants are affected by many biotic and abiotic stresses during their lifespan. In responding to these stressors, plants have evolved a two-layer immune system against pathogen infection (Jones and Dangl, 2006). The first layer of immunity recognizes conserved pathogen associated molecular patterns (PAMPs) through cell-surface located receptor-like proteins and receptor-like kinases and is termed PAMP-triggered immunity (PTI) (Jones and Dangl, 2006). To overcome the PTI process, some successful pathogens can release effector proteins into the intracellular part of plant cells and disturb the PTI process (Jones and Dangl, 2006). These effector proteins can be recognized directly or

indirectly by intracellular proteins encoded by plant disease resistance genes (*R* genes), which will activate the second layer of plant immunity termed effector-triggered immunity (ETI) (Jones and Dangl, 2006). Among over 300 cloned *R* genes, more than 60% of them belong to the nucleotide-binding site leucine-rich repeat (NBS-LRR) gene family (Kourelis and van der Hoorn, 2018). The proteins encoded by typical NBS-LRR genes have two common domains, which are the central NBS domain and the C-terminal LRR domain (DeYoung and Innes, 2006). The sequences of the NBS domain encoded by different NBS-LRR genes are highly conserved (DeYoung and Innes, 2006). In contrast, the LRR domain of NBS-LRR proteins, which generally takes the role of pathogen recognition, is highly variable among different NBS-LRR proteins (DeYoung and Innes, 2006).

In angiosperms, NBS-LRR genes are divided into three subclasses based on their phylogenetic relationship (Shao et al., 2016). Characteristic N-terminal domains have been found for three NBS-LRR subclasses, including the toll-like/interference receptor/Resistance (TIR) domain, the coiled-coil (CC) domain and the RPW8 domain. Accordingly, the three NBS-LRR subclasses encoding these domains are named as TIR-NBS-LRR (TNL), CC-NBS-LRR (CNL) and RPW8-NBS-LRR (RNL) genes (Shao et al., 2016), respectively. The origin of NBS-LRR genes and the divergence of the three NBS-LRR subclasses can be traced to the common ancestor of the green lineage (Shao et al., 2019). After plant colonization of the land, NBS-LRR genes expanded greatly in land plant genomes (Liu et al., 2021), suggesting that NBS-LRR genes may have served as a major receptor of the plant immune system for millions of years. Importantly, nearly all NBS-LRR genes with a known function are involved in plant immunity (Kourelis and van der Hoorn, 2018).

Due to the specialized function of the NBS-LRR gene family in plant immunity and its high abundance in plant genomes, many studies have involved genome-wide identification of NBS-LRR genes from crops and their closely related non-crop species since early studies on the genomes of rice and *Arabidopsis thaliana* (Bai et al., 2002; Meyers et al., 2003). Hundreds of NBS-LRR genes have been identified from the genomes of rice, maize, wheat, barley and soybean (Liu et al., 2021). These studies provide fundamental resources for mining and utilization of functional NBS-LRR genes in crops. For example, by comparative analysis of NBS-LRR genes among different rice varieties and species from the Poaceae family, more than 100 NBS-LRR genes against rice blast have been cloned (Yang et al., 2013; Zhang et al., 2015; Guo et al., 2016).

Secale cereale together with common wheat (*Triticum aestivum*) and barley (*Hordeum vulgare*) are important crops in the Triticeae tribe of the Poaceae family. *S. cereale* has unique characteristics in both agronomic performance and genome properties (Crespo-Herrera et al., 2017). It has resistance to many fungal diseases that cause severe economic losses in wheat and other Triticeae crops (Singh et al., 2016). The 1RS chromosome arm of *S. cereale* has been transferred to the wheat genome, which has contributed to the control of powdery mildew and stripe rust diseases in worldwide wheat production (Szakacs et al., 2020). However, the exact genes that contribute to the resistance are unknown. Recent studies have identified NBS-LRR genes from barley and several wheat genomes, taking advantage of the published genomes (Andersen et al., 2020; Li Q. et al., 2021). However, the NBS-LRR profile of *S. cereale* has not been determined. Herein, the genome-wide identification and evolutionary analysis of NBS-LRR genes were performed on a recently released *S. cereale* genome (Li G. et al., 2021). The uncovered NBS-LRR gene profile in this study may serve as a resource for further mining and application of functional *R* genes in *S. cereale* and other Triticeae species.

MATERIALS AND METHODS

Data Used in This Study

Genome sequences and annotation files of *S. cereale*, *T. aestivum* and *H. vulgare* were downloaded from https://bigd.big.ac.cn/, https://ftp.ensemblgenomes.org/pub/plants/release-51/fasta/triticum_aestivum/dna/, and http://doi.org/10.5447/ipk/2021/3, respectively. The NBS-LRR genes of *T. aestivum*, *T. urartu* and *H. vulgare* were retrieved from previous studies (Li Q. et al., 2021; Liu et al., 2021).

Identification of NBS-LRR Genes

NBS-LRR gene identification was performed on the annotated proteins of *S. cereale* as described previously (Zhang et al., 2020). Briefly, the Hidden Markov Model (HMM) profile of the NB-ARC domain (Pfam accession number: PF00931) was used as a query to perform the HMMsearch using the HMMER-3.0 package against the protein sequences of *S. cereale* with an E-value setting of 1.0. Then, the obtained amino acid sequences were used as queries to perform a round BLASTp search against the protein sequences of *S. cereale* with an E-value setting of 1.0. The obtained protein sequences of BLASTp search were scanned by HMMscan against the Pfam-A database to confirm the presence of the NB-ARC domain (E-value set to 0.0001). Genes without a conserved NBS domain were removed from the datasets. All of the non-redundant candidate sequences were compared with the NCBI Conserved Domains Database (CDD) to further verify the CC, TIR (Pfam accession number: PF01582), RPW8 (Pfam accession number: PF05659), LRR and other integrated domains.

MEME analysis (Bailey et al., 2009) was performed to discover conserved motifs in the NB-ARC domain of the identified NBS-LRR genes. The number of displayed motifs was set to 20 with all other parameters at default settings.

Distribution of NBS-LRR Genes on Different Chromosomes

The distribution of NBS-LRR genes on the chromosomes of the *S. cereale* genome was determined by extracting and parsing genomic locations of the NBS-LRR genes from the GFF3 annotation file. A sliding window analysis was performed with a window size of 250 kb to identify the number of genes that appeared in a cluster on a chromosome as described by Ameline-Torregrosa et al. (2008). If two successive annotated NBS-LRR

genes were located within 250 kb on a chromosome, they were considered as clustered.

Phylogenetic Analysis

Phylogenetic analysis of NBS-LRR genes was performed as described by Zhang et al. (2020). Briefly, amino acid sequences of the conserved NB-ARC domain of the NBS-LRR genes from *S. cereale*, *T. urartu* and *H. vulgare* were aligned using ClustalW with default options and then manually corrected in MEGA 7.0 (Kumar et al., 2016). Too short or extremely divergent sequences were excluded from the analysis to generate the finally matrix (**Supplementary Dataset 1**). Phylogenetic analysis was carried out with IQ-TREE using the maximum likelihood method after selecting the best-fit model using ModelFinder (Nguyen et al., 2015; Kalyaanamoorthy et al., 2017). Branch support values were estimated using UFBoot2 (Minh et al., 2013) and SH-aLRT tests (Anisimova and Gascuel, 2006). Reconciling the NBS-LRR phylogeny with the species tree was performed as described in a previous study (Shao et al., 2014) by using Notung software (Stolzer et al., 2012).

Synteny and Gene Duplication Analysis

For cross-species synteny analysis, pair-wise inter-species all-against-all BLAST was performed for the *S. cereale*, *T. aestivum* and *H. vulgare* protein sequences. The obtained results and the GFF annotation file were then subjected to MCScanX (Wang et al., 2012) for inter-species synteny detection. For intra-species synteny analysis of *S. cereale*, pair-wise intra-species all-against-all BLAST was performed for the *S. cereale* protein sequences. The obtained results and the GFF annotation file were then subjected to MCScanX for intra-species microsynteny detection and determination of the gene duplication type (Wang et al., 2012). Microsynteny relationships were displayed using TBtools (Chen et al., 2020).

RESULTS

Identification of NBS-LRR Genes in the *S. cereale* Genome

We identified 582 NBS-LRR genes (**Supplementary Table S1**) in the *S. cereale* genome accounting for more than 0.6% of the 86,991 annotated protein coding genes. The number of NBS-LRR genes in *S. cereale* is greater than that in the *H. vulgare* genome (467 genes) and slightly more than that in the diploid wheat *T. urartu* genome (537 genes) (Li Q. et al., 2021; Liu et al., 2021). This suggests that it is an important resource for Triticeae R gene mining. To assign these NBS-LRR genes to different subclasses, their amino acid sequences were subjected to BLASTp analysis against the well-annotated *A. thaliana* NBS-LRR proteins, as described previously (Zhang et al., 2016; Zhang et al., 2020). The results showed that 581 of the 582 *S. cereale* NBS-LRR genes belong to the CNL subclass, whereas only one gene was classified to the ADR1-lineage of the RNL subclass. This is consistent with the studies on *H. vulgare* and *T. urartu*, which also identified only one RNL gene in each of the two genomes (Li Q. et al., 2021; Liu et al., 2021), mirroring the conserved function of RNL genes. No TNL gene was detected in the *S. cereale* genome as have been observed in *H. vulgare* and *T. urartu*, supporting the theory that TNL genes were lost in the common ancestor of monocots (Liu et al., 2021).

Domain Composition and Arrangement of *S. cereale* NBS-LRR Proteins

Analysis of the domain composition of the *S. cereale* NBS-LRR proteins revealed that not all of them have the characteristic domains at the N-terminal and the LRR domain at the C-terminal. In contrast, the NBS-LRR proteins show high domain composition and structure diversity (**Figure 1** and **Supplementary Table S1**). The protein encoded by the single RNL gene contains both NBS and LRR domains but lacks a detectable RPW8 domain at the N-terminal. Among the 581 genes in the CNL subclass, 205 genes encode intact CNL proteins that simultaneously contain the typical N-terminal CC domain, the central NBS domain and the C-terminal LRR domain, accounting for 35% of all CNL genes (**Figure 1A**). There are 63 CNL genes encoding proteins without the N-terminal CC domain forming the NBS-LRR (NL) structure, and 137 CNL genes encoding proteins without the C-terminal LRR domain forming the NBS-LRR (NL) structure. We also found 145 genes encoding proteins that lack both N-terminal and C-terminal domains. The remaining 31 CNL genes have complicated domain structures (assigned to the "other" group in **Figure 1A**).

Additional integrated domains (IDs) were found at the N-terminal and/or the C-terminal of 49 of 581 CNL genes (**Supplementary Table S1**), forming the CNL-ID (23 genes), ID-CNL (25 genes) and ID-CNL-ID (one gene) structures. A total of 22 different IDs, including Jacalin, ZnF_BED and WRKY, were detected from 49 *S. cereale* NBS-LRR proteins, accounting for 8% of all NBS-LRR proteins.

Detection of Key Motifs at the NBS Domain of *S. cereale* NBS-LRR Proteins

Several key motifs have been identified in the NBS domain of many NBS-LRR genes, including the P-loop, Kinase-2, RNBS-B, GLPL and RNBS-D (DeYoung and Innes, 2006). The distribution and sequence profile of these motifs in the NBS domain of *S. cereale* NBS-LRR proteins were detected by the Multiple Em for Motif Elicitation (MEME) suite (Bailey et al., 2009). The results showed that the NBS domain of 400 NBS-LRR proteins has all five motifs, accounting for 69% of all NBS-LRR proteins (**Figure 1B**). In contrast, the 182 remaining NBS-LRR proteins lack at least one of these motifs at the NBS domain, including 77 proteins that lost one motif, 37 proteins that lost two motifs, 29 that lost three motifs and 21 that lost four motifs. The ratio of NBS-LRR genes containing all five motifs at the NBS domain in *S. cereale* is higher than that in barley, for which only 283 NBS-LRR proteins preserve all five motifs at the NBS domain, accounting for 60% of all NBS-LRR proteins (Li Q. et al., 2021). Analyzing the sequence features of the motifs of

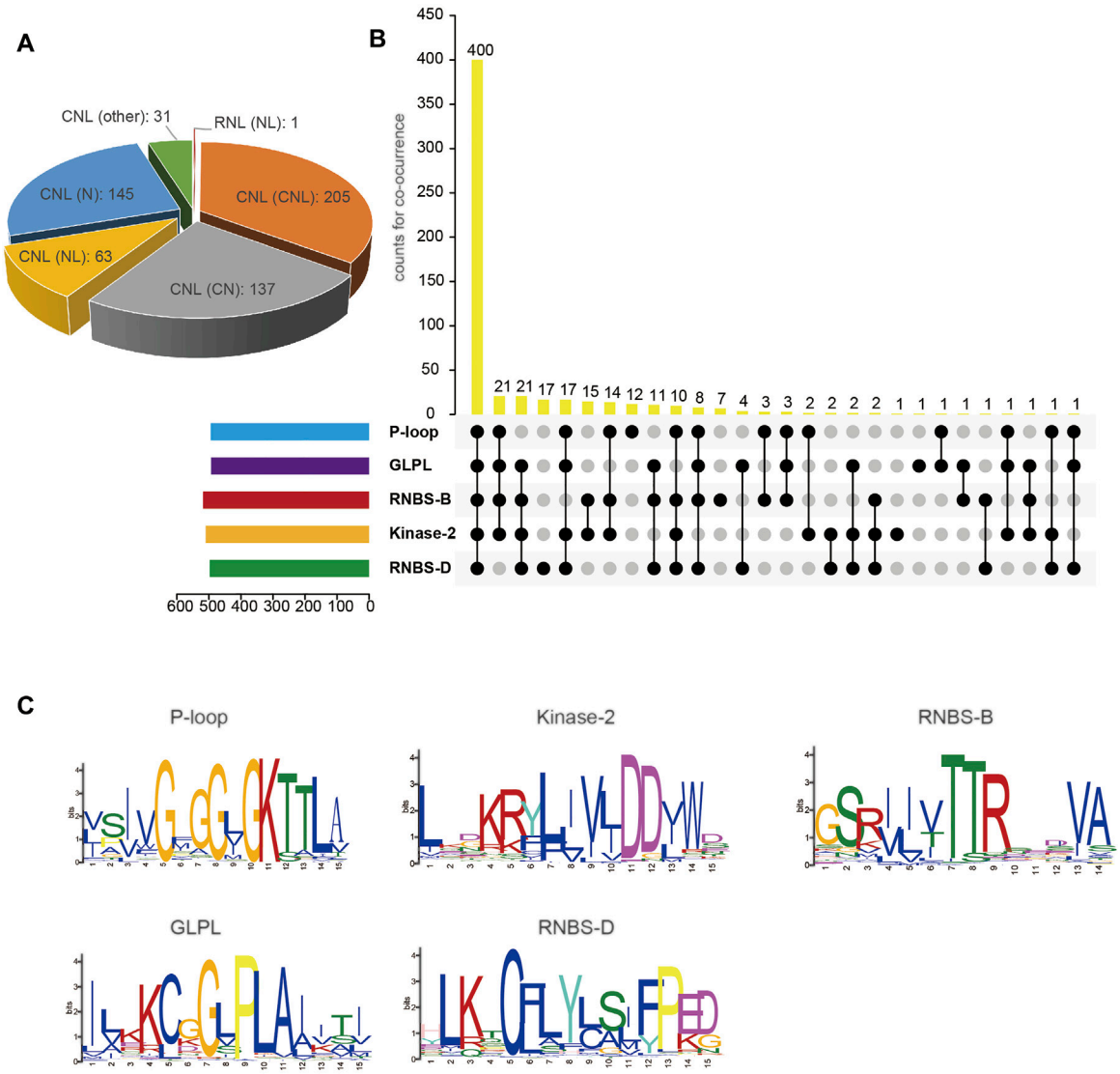

FIGURE 1 | Classification and sequence features of NBS-LRR genes in *S. cereale*. **(A)** Classification and domain compositions of *S. cereale* NBS-LRR proteins. **(B)** Presence of five key motifs in the amino acid sequence of the NBS domain of *S. cereale* NBS-LRR protein. **(C)** Amino acid features of five key motifs in the amino acid sequence of the NBS domain of *S. cereale* NBS-LRR protein.

CNL proteins (**Figure 1C**) revealed that the sequence profiles of Kinase-2 and RNBS-B show the characteristic feature of CNL genes "DDVW" and "TTR," which was reported by Shao et al. (2016).

Chromosomal Distribution of NBS-LRR Genes in the *S. cereale* Genome

To determine the distribution of the 582 NBS-LRR genes on the seven chromosomes of *S. cereale*, the physical locations of NBS-LRR genes were retrieved from the GFF3 annotation file. The result showed that *S. cereale* NBS-LRR genes are unevenly distributed on the seven chromosomes (**Figure 2**). Among the 582 NBS-LRR genes identified from the *S. cereale* genome, 558 were anchored on the seven chromosomes in the annotation file, whereas the chromosomal location of 24 NBS-LRR genes was not determined by the genomic annotation. Chromosome 4 has the most NBS-LRR genes (111), and this is nearly two times the number of NBS-LRR genes on chromosome 2 (54). Chromosomes 1, 3, 5, 6 and 7 have 77, 74, 71, 104 and 61 NBS-LRR genes, respectively. We also compared the chromosome distribution pattern of NBS-LRR genes in the *S. cereale* genome with that in the barley and wheat genomes (Li Q. et al., 2021; Liu et al., 2021), because the three species have the same number of chromosomes and have only diverged from each other for about 10 myr. Since the diploid wheat *T. urartu* with AA genome does not have a chromosomal level gff annotation file, we used the data of the hexaploid wheat *T. aestivum*, which contain

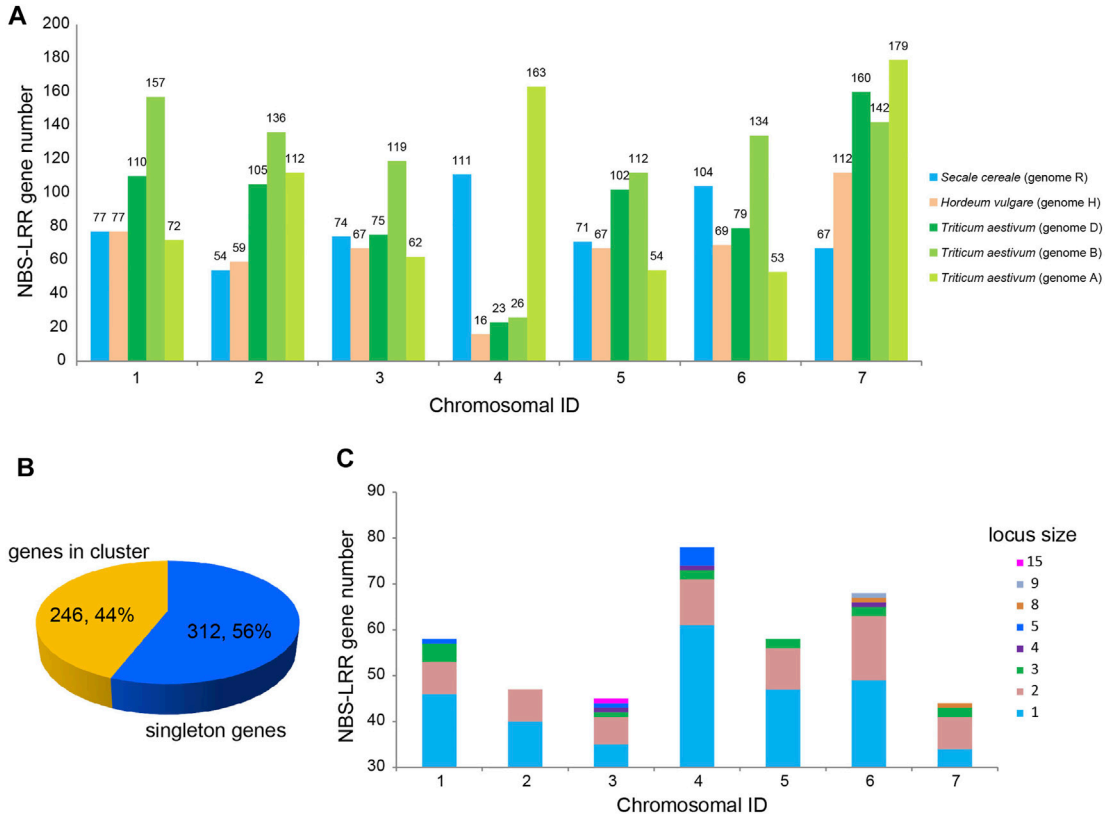

FIGURE 2 | Chromosomal distribution of NBS-LRR genes in *S. cereale*. **(A)** Comparative analysis of chromosomal distribution of NBS-LRR genes in *S. cereale*, *H. vulgare* and *T. aestivum*. **(B)** Proportion of NBS-LRR genes appearing as singletons (blue) and clusters (yellow) in the *S. cereale* genome. **(C)** Proportion of NBS-LRR genes appearing as singletons or different-size clusters on each chromosome of *S. cereale*.

information of all three sets of chromosomes (AABBDD) of wheat (Liu et al., 2021). The results showed that chromosome 4, which has the largest number of NBS-LRR genes among all chromosomes in *S. cereale*, only has 16, 23 and 26 NBS-LRR genes in barley and the B and D genomes of wheat, representing the chromosome with the fewest NBS-LRR genes in these genomes. In contrast, we found that chromosome 4 of the wheat A genome has 163 NBS-LRR genes, ranking second among the seven chromosomes in the A genome. This feature is quite similar to that found in *S. cereale*.

NBS-LRR genes on chromosomes can appear as a singleton locus or a cluster locus. The NBS-LRR cluster locus is defined as several NBS-LRR genes with an interval of less than 250 kb (Ameline-Torregrosa et al., 2008). Based on the physical locations, the 558 NBS-LRR genes on the seven *S. cereale* chromosomes were classified into 398 loci, including 312 singletons and 86 clusters (**Figure 2**). This suggested that 246 (44%) of the NBS-LRR genes are present in the 86 clusters, with an average of three genes per cluster. Among the 86 loci clusters, the smallest ones only have two NBS-LRR genes, including 7, 7, 6, 9, 9, 14 and 7 such loci on chromosome 1–7 (**Supplementary Table S1**). The largest cluster is located on chromosome 3, which contains 15 NBS-LRR genes.

Gene Duplication Type of *Secale cereale* NBS-LRR Genes

Different types of gene duplication may contribute to the NBS-LRR gene family expansion. Our analysis revealed that about 39% of NBS-LRR genes in *S. cereale* were duplicated through tandem or proximal duplications; over 60% of NBS-LRR genes resulted from dispersed duplication, and only 1% (six genes) were generated from segmental duplications (**Figure 3A**). The six segmental duplicated genes form three gene pairs (**Figure 3B**). One pair involving SCWN1R01G487400 and SCWN3R01G378300 occurred between chromosomes 1 and 3, whereas the remaining two events were intra-chromosomal duplications on chromosomes 3 (SCWN3R01G095500 and SCWN3R01G098900) and 4 (SCWN4R01G515500 and SCWN4R01G522700), respectively.

Interspecies Synteny of NBS-LRR Genes Among Three Triticeae Crops

Gene pairs within syntenic chromosome blocks are highly confidential orthologous genes among species. Synteny analysis of *S. cereale* with the barley and wheat genomes revealed that 143 NBS-LRR gene pairs between *S. cereale* and barley are located

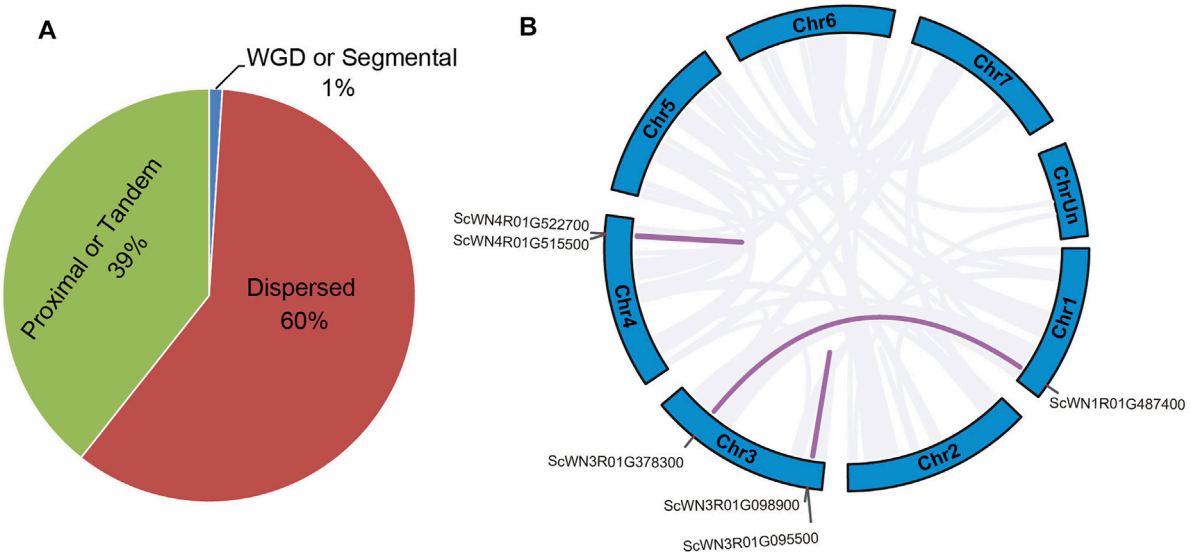

FIGURE 3 | Duplication type for NBS-LRR genes in *S. cereale*. **(A)** Proportion of NBS-LRR genes with different duplication types. **(B)** Segmental duplicated NBS-LRR gene pairs in *S. cereale*.

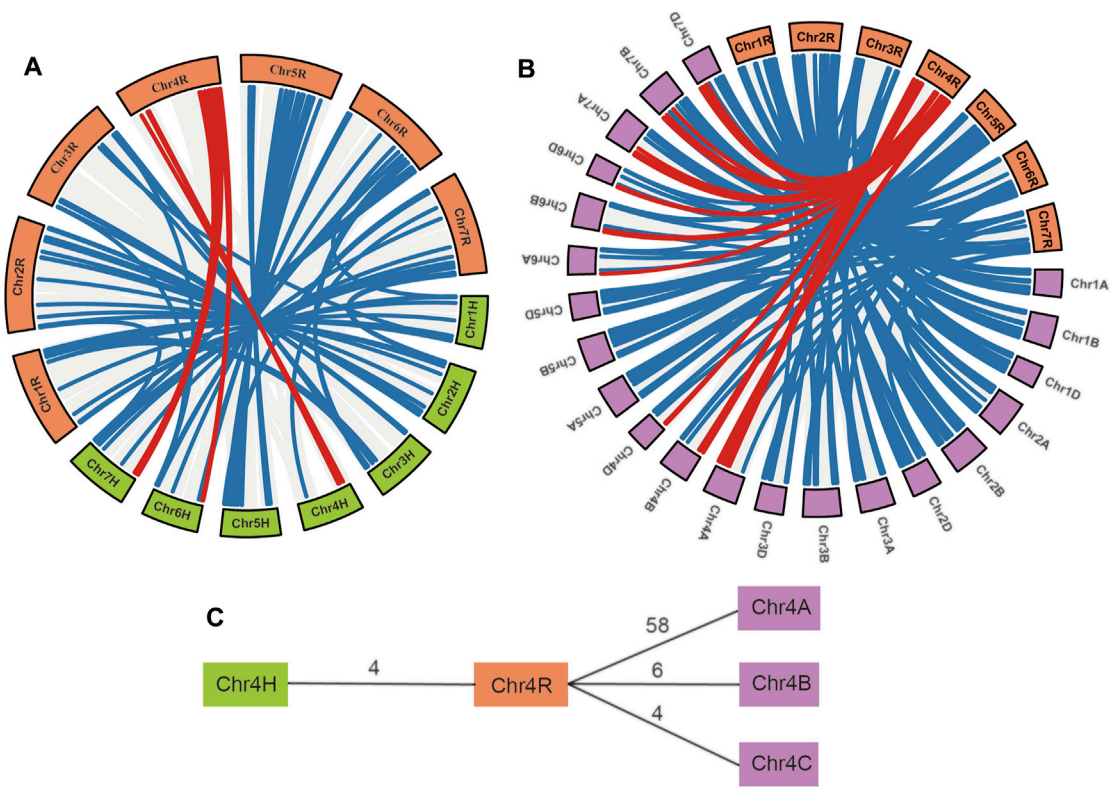

FIGURE 4 | Cross-species synteny of *S. cereale* NBS-LRR genes. **(A)** Cross-species synteny between *S. cereale* and *H. vulgare*. **(B)**. Cross-species synteny between *S. cereale* and *T. aestivum*. Gene pairs involving NBS-LRR genes on chromosome 4 of *S. cereale* were labeled with a red line. **(C)** Comparative analysis of synteny NBS-LRR pairs between *S. cereale* and *H. vulgare* with synteny NBS-LRR pairs between *S. cereale* and *T. aestivum*.

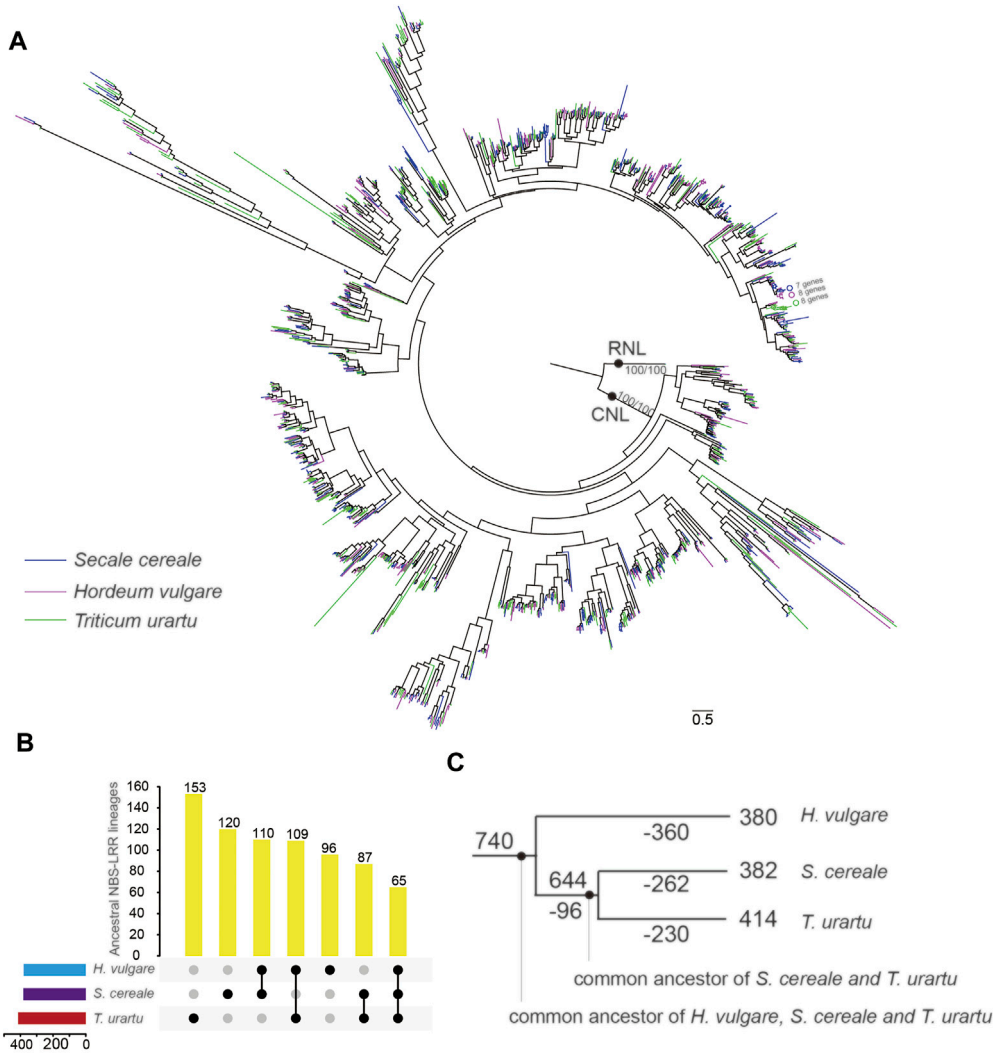

FIGURE 5 | Phylogenetic and evolutionary analysis of NBS-LRR genes in *S. cereale*. **(A)** A phylogeny for NBS-LRR genes from *S. cereale*, *H. vulgare* and *T. urartu* constructed based on the conserved NBS domain. Branch support values obtained from SH-aLRT (%) and UFBoot2 (%) are labeled on basal nodes. **(B)** Distribution of ancestral NBS-LRR lineages among the three species. **(C)** The differential inheritance of 740 predicted ancestral NBS-LRR lineages during species speciation. Ancestral NBS-LRR lineage numbers on each node/branch are indicated. Numbers of lineage loss events are indicated by numbers with '-' on each node/branch.

on syntenic chromosomal blocks of the two species (**Figure 4A** and **Supplementary Table S2**). Among the three wheat genomes, genome A has the most (245) syntenic NBS-LRR gene pairs with *S. cereale*, whereas genomes B and D have 216 and 209 syntenic NBS-LRR gene pairs, respectively (**Figure 4B** and **Supplementary Table S2**). Notably, consistent with the larger number of NBS-LRR genes on chromosome 4A than on chromosomes 4B and 4D, chromosome 4A also has 58 syntenic NBS-LRR gene pairs with chromosome 4R in *S. cereale*, which is much larger than the six gene pairs and four gene pairs between 4R with 4B and 4R with 4D, respectively (**Figure 4B and C**). This indicates that the larger number of NBS-LRR genes on chromosomes 4R and 4A is not likely a consequence of independent NBS-LRR expansion in the two genomes, but a result of convergent retention of ancestral NBS-LRR gene loci that were present in the common ancestor of the three Triticeae crops. Also, potential gene introgression may have contributed to this profile.

Phylogenetic Analysis of NBS-LRR Genes From the Three Triticeae Crops

To trace the evolutionary history of *S. cereale* NBS-LRR genes, phylogenetic analysis was performed by incorporating NBS-LRR genes from *H. vulgare* and *T. urartu* (Li Q. et al., 2021; Liu et al., 2021). The phylogenetic result (**Figure 5** and **Supplementary Figure S1**) showed that the three RNL genes from the three species form an independent clade that shares the same topology with the species tree with a high support value. This suggests a highly conserved evolutionary pattern of RNL genes. CNL genes

from the three species form another highly supported clade. The topology supports that RNL and CNL subclasses diverged anciently in NBS-LRR gene evolution (Shao et al., 2019). The phylogeny shows the species-specific expansion of some CNL lineages when genes from the three species are labeled with different colors. As shown in **Figure 5A**, branches containing seven to eight NBS-LRR genes from a single species can be detected due to species-specific gene duplication.

Frequent gene losses and gains can be further resolved by resolving the gene tree with the phylogenetic relationship of the three species. The results showed that NBS-LRR genes from the three species can be traced to 740 ancestral lineages in their common ancestor approximately 15 myr ago (Figure S1). Among them, only 60 ancestral NBS-LRR lineages were inherited by all three species. Most of them conservatively evolved in each species without large duplication (Figure S1). In contrast, more than 90% (680) of ancestral NBS-LRR lineages were only inherited by one or two species after speciation (**Figure 5B**), including 380, 382 and 414 ancestral NBS-LRR lineages inherited by *H. vulgar*, *S. cereale* and *T. urartu*, respectively. Tracing the dynamics of the NBS-LRR gene evolutionary history revealed that 96 of the ancestral NBS-LRR lineages were lost in the common ancestor of *S. cereale* and *T. urartu* after it separated from *H. vulgare*, while 654 ancestral NBS-LRR lineages were preserved (**Figure 5C**). However, after the separation of *S. cereale* and *T. urartu*, a large proportion of ancestral NBS-LRR lineages experienced further gene loss, resulting in 492 ancestral NBS-LRR lineages being lost in either of the two species (262 in *S. cereale* and 230 *T. urartu*), while only 152 ancestral NBS-LRR lineages were shared by the two species (**Figures 5B,C**). The results indicate that NBS-LRR diversity among the three species is largely different due to their differential inheritance of ancestral lineages. Similar to the consistently occurring gene losses, gene duplication also frequently occurred during speciation, which contributed to the current NBS-LRR gene profile in the three species.

DISCUSSION

Since the first *R* gene Hm1 resistant to the fungus *Cochliobolus carbonum* race 1 was cloned from maize nearly 30 years ago, over 300 functional *R* genes have been identified. Most of these are from plant species that are important crops including rice, wheat and tomato (Johal and Briggs, 1992; Kourelis and van der Hoorn, 2018). Characterization of functional *R* genes was dependent on traditional map-based cloning methods in earlier studies. With the development of DNA sequencing technology, many crops have now been sequenced. The availability of these genomic resources has greatly accelerated the mining of functional *R* genes in economically important plants (Sanchez-Martin et al., 2016; Witek et al., 2016; Liu et al., 2020; Walkowiak et al., 2020) and has initiated a new era of molecular breeding (Poland and Rutkoski, 2016).

Most known *R* genes belong to the NBS-LRR gene family (Kourelis and van der Hoorn, 2018). The typical domain composition and high sequence similarity of genes in this gene family have enabled batch identification of NBS-LRR genes at the whole genome scale (Bai et al., 2002; Meyers et al., 2003). Large-scale screens of functional *R* genes from the NBS-LRR gene family conducted in the rice genome have enabled the identification of dozens of *R* genes that are active against the fungal pathogen *Magnaporthe oryzae* (Zhang et al., 2015; Guo et al., 2016), which is much more efficient than the traditional method. Genome-wide comparative analysis of NBS-LRR genes among several grass family species also helped in the identification of additional functional genes against *M. oryzae* in close-relatives of rice, including maize, sorghum and *Brachypodium*. This indicates that phylogenetically related species are important resources for *R* gene mining of crops (Yang et al., 2013).

The Triticeae is a tribe of the Poaceae family that contains many important grain crops, including wheat, barley, *S. cereale* and triticale. These crops are cultivated worldwide and are frequently challenged by pathogens and pests during their growth. Although resistance breeding has improved the performance of Triticeae crops (Forster, 1992; Delventhal et al., 2017), only a few functional *R* genes have been cloned from these crops (Kourelis and van der Hoorn, 2018). The recently released reference genome and pan-genome of wheat and barley have accelerated the identification of functional *R* genes more efficiently in these species (Jayakodi et al., 2020; Walkowiak et al., 2020). For example, a CNL gene resistant to the orange wheat blossom midge (OWBM, *Sitodiplosis mosellana* Géhin) has recently been cloned by analysis of the wheat pan-genome (Walkowiak et al., 2020). Four stem rust resistance genes have been cloned by combining association genetics with *R* gene enrichment sequencing in wild diploid wheat (Arora et al., 2019). Two CNL genes introduced from tall wheat grass (*Thinopyrum ponticum*), Sr26 and Sr61, against stem rust have been cloned from wheat by mutational genomics and targeted exome capture methods (Zhang et al., 2021). All of the above studies have benefited from understanding the NBS-LRR profile in the genomes.

Besides the wild wheat resources, both barley and *S. cereale* have been used to transfer genetic materials to wheat to improve its quality. The disease-resistance genes carried by the 1RS chromosome arm of *S. cereale* have been transferred to the wheat genome to confer resistance against powdery mildew and stripe rust diseases (Szakacs et al., 2020). However, without the genomic information, the *R* gene profile on the transferred chromosomal segment is unclear. In this study, genome-wide analysis identified 582 NBS-LRR genes in *S. cereale*. The number of NBS-LRR genes in *S. cereale* is larger than that in barley and *T. urartu* (Li G. et al., 2021). The high NBS-LRR gene number indicated that *S. cereale* would be an important resource for mining and transfer of functional *R* genes to barley and wheat. The distribution of NBS-LRR genes on different chromosomes of *S. cereale* was determined and serves as fundamental molecular information for the introduction of chromosomal segments from *S. cereale* to other Triticeae crops. An interesting finding is that both the chromosome 4 of *S. cereale* and the A genome of wheat retained a larger number of NBS-LRR genes than barley and genomes B and D of wheat. This result highlights chromosome 4 of *S. cereale* as an important resource for disease resistance breeding and also implies that chromosome 4 of wheat genome A has experienced a different evolutionary history compared to genomes B and D, at least for the NBS-LRR genes.

Although the number of NBS-LRR genes in the three Triticeae does not differ dramatically, a large proportion of the NBS-LRR

genes from the three species are inherited from different ancestral NBS-LRR lineages that diverged in the common ancestor of the three species. The result suggested that the NBS-LRR diversity would be significantly increased if the three Triticeae species are considered as a 'Triticeae NBS-LRR gene pool' in resistance-gene mining. The high abundance of NBS-LRR genes in *S. cereale* and their distinct genetic origin with NBS-LRR genes in barley and wheat suggest that *S. cereale* could be an important resource for obtaining functional NBS-LRR genes for molecular breeding. This also provides a molecular basis for developing *S. cereale* as a donor material for Triticeae breeding.

In conclusion, we uncovered the NBS-LRR profile in *S. cereale* and compared the chromosomal distribution and evolutionary history of this gene family in three Triticeae species. This information provides a fundamental resource for mining functional *R* genes from *S. cereale*. Since cross-species transformation of genomic segments has been frequently used for the molecular breeding of Triticeae species, the NBS-LRR profile of *S. cereale* expands the gene pool for Triticeae molecular breeding.

DATA AVAILABILITY STATEMENT

The original contributions presented in the study are included in the article/**Supplementary Material**, further inquiries can be directed to the corresponding authors.

AUTHOR CONTRIBUTIONS

Y-MZ and X-QS conceived and designed the study. L-HQ and YW obtained and analyzed the data. MC, JL and R-SL participated in interpreting the results. Y-MZ wrote the manuscript. X-QS revised the manuscript. All authors read and approved the final manuscript.

FUNDING

This work was supported financially by the earmarked fund for Jiangsu Agricultural Industry Technology System (JATS (2021) 118).

ACKNOWLEDGMENTS

We thank LetPub (www.letpub.com) for its linguistic assistance during the preparation of this manuscript.

SUPPLEMENTARY MATERIAL

The Supplementary Material for this article can be found online at: https://www.frontiersin.org/articles/10.3389/fgene.2021.771814/full#supplementary-material

REFERENCES

Ameline-Torregrosa, C., Wang, B.-B., O'Bleness, M. S., Deshpande, S., Zhu, H., Roe, B., et al. (2008). Identification and Characterization of Nucleotide-Binding Site-Leucine-Rich Repeat Genes in the Model Plant Medicago Truncatula. *Plant Physiol.* 146 (1), 5–21. doi:10.1104/pp.107.104588

Andersen, E. J., Nepal, M. P., Purintun, J. M., Nelson, D., Mermigka, G., and Sarris, P. F. (2020). Wheat Disease Resistance Genes and Their Diversification through Integrated Domain Fusions. *Front. Genet.* 11, 898. doi:10.3389/fgene.2020.00898

Anisimova, M., and Gascuel, O. (2006). Approximate Likelihood-Ratio Test for Branches: A Fast, Accurate, and Powerful Alternative. *Syst. Biol.* 55 (4), 539–552. doi:10.1080/10635150600755453

Arora, S., Steuernagel, B., Gaurav, K., Chandramohan, S., Long, Y., Matny, O., et al. (2019). Resistance Gene Cloning from a Wild Crop Relative by Sequence Capture and Association Genetics. *Nat. Biotechnol.* 37 (2), 139–143. doi:10.1038/s41587-018-0007-9

Bai, J., Pennill, L. A., Ning, J., Lee, S. W., Ramalingam, J., Webb, C. A., et al. (2002). Diversity in Nucleotide Binding Site-Leucine-Rich Repeat Genes in Cereals. *Genome Res.* 12 (12), 1871–1884. doi:10.1101/gr.454902

Bailey, T. L., Boden, M., Buske, F. A., Frith, M., Grant, C. E., Clementi, L., et al. (2009). MEME SUITE: Tools for Motif Discovery and Searching. *Nucleic Acids Res.* 37 (Web Server issue), W202–W208. doi:10.1093/nar/gkp335

Chen, C., Chen, H., Zhang, Y., Thomas, H. R., Frank, M. H., He, Y., et al. (2020). TBtools: An Integrative Toolkit Developed for Interactive Analyses of Big Biological Data. *Mol. Plant* 13 (8), 1194–1202. doi:10.1016/j.molp.2020.06.009

Crespo-Herrera, L. A., Garkava-Gustavsson, L., and Åhman, I. (2017). A Systematic Review of rye (Secale Cereale L.) as a Source of Resistance to Pathogens and Pests in Wheat (*Triticum aestivum* L.). *Hereditas* 154, 14. doi:10.1186/s41065-017-0033-5

Delventhal, R., Rajaraman, J., Stefanato, F. L., Rehman, S., Aghnoum, R., McGrann, G. R. D., et al. (2017). A Comparative Analysis of Nonhost Resistance across the Two Triticeae Crop Species Wheat and Barley. *BMC Plant Biol.* 17 (1), 232. doi:10.1186/s12870-017-1178-0

DeYoung, B. J., and Innes, R. W. (2006). Plant NBS-LRR Proteins in Pathogen Sensing and Host Defense. *Nat. Immunol.* 7 (12), 1243–1249. doi:10.1038/ni1410

Forster, B. P. (1992). Genetic Engineering for Stress Tolerance in the Triticeae. *Proc. Sect. B Biol. Sci.* 99, 89–106. doi:10.1017/S0269727000005522

Guo, C., Sun, X., Chen, X., Yang, S., Li, J., Wang, L., et al. (2016). Cloning of Novel rice Blast Resistance Genes from Two Rapidly Evolving NBS-LRR Gene Families in rice. *Plant Mol. Biol.* 90 (1-2), 95–105. doi:10.1007/s11103-015-0398-7

Jayakodi, M., Padmarasu, S., Haberer, G., Bonthala, V. S., Gundlach, H., Monat, C., et al. (2020). The Barley Pan-Genome Reveals the Hidden Legacy of Mutation Breeding. *Nature* 588 (7837), 284–289. doi:10.1038/s41586-020-2947-8

Johal, G. S., and Briggs, S. P. (1992). Reductase Activity Encoded by the HM1 Disease Resistance Gene in maize. *Science* 258 (5084), 985–987. doi:10.1126/science.1359642

Jones, J. D. G., and Dangl, J. L. (2006). The Plant Immune System. *Nature* 444 (7117), 323–329. doi:10.1038/nature05286

Kalyaanamoorthy, S., Minh, B. Q., Wong, T. K. F., von Haeseler, A., and Jermiin, L. S. (2017). ModelFinder: Fast Model Selection for Accurate Phylogenetic Estimates. *Nat. Methods* 14 (6), 587–589. doi:10.1038/nmeth.4285

Kourelis, J., and van der Hoorn, R. A. L. (2018). Defended to the Nines: 25 Years of Resistance Gene Cloning Identifies Nine Mechanisms for R Protein Function. *Plant Cell* 30 (2), 285–299. doi:10.1105/tpc.17.00579

Kumar, S., Stecher, G., and Tamura, K. (2016). MEGA7: Molecular Evolutionary Genetics Analysis Version 7.0 for Bigger Datasets. *Mol. Biol. Evol.* 33 (7), 1870–1874. doi:10.1093/molbev/msw054

Li, G., Wang, L., Yang, J., He, H., Jin, H., Li, X., et al. (2021). A High-Quality Genome Assembly Highlights rye Genomic Characteristics and Agronomically Important Genes. *Nat. Genet.* 53 (4), 574–584. doi:10.1038/s41588-021-00808-z

Li, Q., Jiang, X.-M., and Shao, Z.-Q. (2021). Genome-Wide Analysis of NLR Disease Resistance Genes in an Updated Reference Genome of Barley. *Front. Genet.* 12, 694682. doi:10.3389/fgene.2021.694682

Liu, Y., Du, H., Li, P., Shen, Y., Peng, H., Liu, S., et al. (2020). Pan-Genome of Wild and Cultivated Soybeans. *Cell* 182 (1), 162–176.e113. doi:10.1016/j.cell.2020.05.023

Liu, Y., Zeng, Z., Zhang, Y.-M., Li, Q., Jiang, X.-M., Jiang, Z., et al. (2021). An Angiosperm NLR Atlas Reveals that NLR Gene Reduction Is Associated with Ecological Specialization and Signal Transduction Component Deletion. *Mol. Plant*. doi:10.1016/j.molp.2021.08.001

Meyers, B. C., Kozik, A., Griego, A., Kuang, H., and Michelmore, R. W. (2003). Genome-Wide Analysis of NBS-LRR-Encoding Genes in Arabidopsis[W]. *Plant Cell* 15 (4), 809–834. doi:10.1105/tpc.009308

Minh, B. Q., Nguyen, M. A. T., and von Haeseler, A. (2013). Ultrafast Approximation for Phylogenetic Bootstrap. *Mol. Biol. Evol.* 30 (5), 1188–1195. doi:10.1093/molbev/mst024

Nguyen, L.-T., Schmidt, H. A., von Haeseler, A., and Minh, B. Q. (2015). IQ-TREE: a Fast and Effective Stochastic Algorithm for Estimating Maximum-Likelihood Phylogenies. *Mol. Biol. Evol.* 32 (1), 268–274. doi:10.1093/molbev/msu300

Poland, J., and Rutkoski, J. (2016). Advances and Challenges in Genomic Selection for Disease Resistance. *Annu. Rev. Phytopathol.* 54, 79–98. doi:10.1146/annurev-phyto-080615-100056

Sánchez-Martín, J., Steuernagel, B., Ghosh, S., Herren, G., Hurni, S., Adamski, N., et al. (2016). Rapid Gene Isolation in Barley and Wheat by Mutant Chromosome Sequencing. *Genome Biol.* 17 (1), 221. doi:10.1186/s13059-016-1082-1

Shao, Z.-Q., Xue, J.-Y., Wang, Q., Wang, B., and Chen, J.-Q. (2019). Revisiting the Origin of Plant NBS-LRR Genes. *Trends Plant Sci.* 24 (1), 9–12. doi:10.1016/j.tplants.2018.10.015

Shao, Z.-Q., Xue, J.-Y., Wu, P., Zhang, Y.-M., Wu, Y., Hang, Y.-Y., et al. (2016). Large-Scale Analyses of Angiosperm Nucleotide-Binding Site-Leucine-Rich Repeat Genes Reveal Three Anciently Diverged Classes with Distinct Evolutionary Patterns. *Plant Physiol.* 170 (4), 2095–2109. doi:10.1104/pp.15.01487

Shao, Z.-Q., Zhang, Y.-M., Hang, Y.-Y., Xue, J.-Y., Zhou, G.-C., Wu, P., et al. (2014). Long-Term Evolution of Nucleotide-Binding Site-Leucine-Rich Repeat Genes: Understanding Gained from and beyond the Legume Family. *Plant Physiol.* 166 (1), 217–234. doi:10.1104/pp.114.243626

Singh, R. P., Singh, P. K., Rutkoski, J., Hodson, D. P., He, X., Jørgensen, L. N., et al. (2016). Disease Impact on Wheat Yield Potential and Prospects of Genetic Control. *Annu. Rev. Phytopathol.* 54, 303–322. doi:10.1146/annurev-phyto-080615-095835

Stolzer, M., Lai, H., Xu, M., Sathaye, D., Vernot, B., and Durand, D. (2012). Inferring Duplications, Losses, Transfers and Incomplete Lineage Sorting with Nonbinary Species Trees. *Bioinformatics* 28 (18), i409–i415. doi:10.1093/bioinformatics/bts386

Szakács, É., Szőke-Pázsi, K., Kalapos, B., Schneider, A., Ivanizs, L., Rakszegi, M., et al. (2020). 1RS Arm of Secale Cereanum 'Kriszta' Confers Resistance to Stripe Rust, Improved Yield Components and High Arabinoxylan Content in Wheat. *Sci. Rep.* 10 (1), 1792. doi:10.1038/s41598-020-58419-3

Walkowiak, S., Gao, L., Monat, C., Haberer, G., Kassa, M. T., Brinton, J., et al. (2020). Multiple Wheat Genomes Reveal Global Variation in Modern Breeding. *Nature* 588 (7837), 277–283. doi:10.1038/s41586-020-2961-x

Wang, Y., Tang, H., Debarry, J. D., Tan, X., Li, J., Wang, X., et al. (2012). MCScanX: a Toolkit for Detection and Evolutionary Analysis of Gene Synteny and Collinearity. *Nucleic Acids Res.* 40 (7), e49. doi:10.1093/nar/gkr1293

Witek, K., Jupe, F., Witek, A. I., Baker, D., Clark, M. D., and Jones, J. D. G. (2016). Accelerated Cloning of a Potato Late Blight-Resistance Gene Using RenSeq and SMRT Sequencing. *Nat. Biotechnol.* 34 (6), 656–660. doi:10.1038/nbt.3540

Yang, S., Li, J., Zhang, X., Zhang, Q., Huang, J., Chen, J.-Q., et al. (2013). Rapidly Evolving R Genes in Diverse Grass Species Confer Resistance to rice Blast Disease. *Proc. Natl. Acad. Sci.* 110 (46), 18572–18577. doi:10.1073/pnas.1318211110

Zhang, J., Hewitt, T. C., Boshoff, W. H. P., Dundas, I., Upadhyaya, N., Li, J., et al. (2021). A Recombined Sr26 and Sr61 Disease Resistance Gene Stack in Wheat Encodes Unrelated NLR Genes. *Nat. Commun.* 12 (1), 3378. doi:10.1038/s41467-021-23738-0

Zhang, X., Yang, S., Wang, J., Jia, Y., Huang, J., Tan, S., et al. (2015). A Genome-wide Survey Reveals Abundant rice blastR Genes in Resistant Cultivars. *Plant J.* 84 (1), 20–28. doi:10.1111/tpj.12955

Zhang, Y.-M., Chen, M., Sun, L., Wang, Y., Yin, J., Liu, J., et al. (2020). Genome-Wide Identification and Evolutionary Analysis of NBS-LRR Genes from Dioscorea Rotundata. *Front. Genet.* 11, 484. doi:10.3389/fgene.2020.00484

Zhang, Y.-M., Shao, Z.-Q., Wang, Q., Hang, Y.-Y., Xue, J.-Y., Wang, B., et al. (2016). Uncovering the Dynamic Evolution of Nucleotide-Binding Site-Leucine-Rich Repeat (NBS-LRR) Genes in Brassicaceae. *J. Integr. Plant Biol.* 58 (2), 165–177. doi:10.1111/jipb.12365

Conflict of Interest: The authors declare that the research was conducted in the absence of any commercial or financial relationships that could be construed as a potential conflict of interest.

Publisher's Note: All claims expressed in this article are solely those of the authors and do not necessarily represent those of their affiliated organizations, or those of the publisher, the editors and the reviewers. Any product that may be evaluated in this article, or claim that may be made by its manufacturer, is not guaranteed or endorsed by the publisher.

frontiers in Genetics

BRIEF RESEARCH REPORT
published: 23 November 2021
doi: 10.3389/fgene.2021.801218

Comparative Analysis of HSF Genes From *Secale cereale* and its Triticeae Relatives Reveal Ancient and Recent Gene Expansions

Xiao-Tong Li†, *Xing-Yu Feng*†, *Zhen Zeng*, *Yang Liu** and *Zhu-Qing Shao**

School of Life Sciences, Nanjing University, Nanjing, China

Plants have evolved sophisticated systems to cope with the environmental stresses, with the heat shock factor (HSF) family proteins composing an integral part of the transcriptional regulation system. Understanding the evolutionary history and functional diversity of HSFs will facilitate improving tolerance of crops to adverse environmental conditions. In this study, genome-wide analysis of *Secale cereale* identified 31 HSF genes. The total number of HSF genes in *S. cereale* is larger than that in barley and the three subgenomes of wheat, suggesting it is a valuable resource for mining functional HSFs. Chromosome analysis revealed an uneven distribution of HSF genes among the 7 *S. cereale* chromosomes, with no HSF gene was detected on chromosome 4. Further interspecies synteny analysis revealed that chromosome reorganization during species-speciation may lead to the escape of HSF genes from the *S. cereale* chromosome 4. Phylogenetic analysis revealed that *S. cereale* experienced more HSF gene duplications than barley and the three wheat subgenomes. Expression analysis demonstrated that *S. cereale* HSF genes showed diverse expression patterns across plant developmental stages and upon drought and freezing treatment, suggesting functional diversity of the gene family. Notably, we detected distinct expression patterns for a recently duplicated HSF gene pair, indicating functional divergence may have occurred between the two genes. The study presents the genome organization, evolutionary features and expression patterns of the *S. cereale* HSF genes. These results provide new insights into the evolution of HSF genes in Triticeae and may serve as a resource for Triticeae molecular breeding.

Keywords: *S. cereale*, HSF gene, stress tolerance, evolution, functional diversity

OPEN ACCESS

Edited by:
Pengtao Ma,
Yantai University, China

Reviewed by:
Jiancai Li,
Shanghai Institutes for Biological Sciences (CAS), China
Xu Hongxing,
Henan University, China

***Correspondence:**
Zhu-Qing Shao
zhuqingshao@nju.edu.cn
Yang Liu
m18845043187@163.com

†*These authors have contributed equally to this work*

Specialty section:
This article was submitted to Plant Genomics, a section of the journal Frontiers in Genetics

Received: *25 October 2021*
Accepted: *08 November 2021*
Published: *23 November 2021*

Citation:
Li X-T, Feng X-Y, Zeng Z, Liu Y and Shao Z-Q (2021) Comparative Analysis of HSF Genes From Secale cereale *and its Triticeae Relatives Reveal Ancient and Recent Gene Expansions. Front. Genet. 12:801218. doi: 10.3389/fgene.2021.801218*

INTRODUCTION

Plants are consistently affected by biotic and abiotic stresses in the environment during their whole lifespan, including drought, salt, heat, cold and pathogens' infection. In the long-term evolution, plants have evolved sophisticated systems and regulatory networks to avoid or attenuate the deleterious effects of these stresses (Peck and Mittler, 2020). Many gene families have been reported for their distinct roles in responding to external environmental stresses, such as the nucleotide-binding leucine-rich-repeat (NLR) disease resistance gene family (Saur et al., 2021); and the cold-induced C-repeat binding factor (CBF) gene family (Zhou et al., 2011). There are also some gene families that can respond to multiple external stresses by their different family members (Javed et al., 2020; Wani et al., 2021). Among them, plant heat shock

factor (HSF) family proteins compose an integral part of the transcriptional regulation system for plants against external environmental stresses, by modulating the expression of different sets of plant genes in responding to heat, cold, salt stresses and the infection of pathogens (Andrasi et al., 2021).

HSF is a conserved gene family that widely spreads in eukaryotes and prokaryotes. Proteins encoded by this family were initially identified as transcription factors that regulate the expression of HSPs, whose functions as molecular chaperones to maintain protein homeostasis in cells (Boston et al., 1996). However, increasing studies in plants have revealed that HSFs are important components of the complex signaling systems that control responses not only to high temperatures but also to a number of abiotic stresses such as cold, drought, hypoxic conditions, soil salinity, and to pathogen threats (Andrasi et al., 2021). Compared to the single copy HSF gene in yeast and four HSF genes in human genome, plant genomes have expanded the HSF genes to several dozens (Wang et al., 2018). For example, 22 and 25 HSF genes have been identified from the dicot plant *Arabidopsis thaliana* and monocot species *Oryza sativa*, respectively (Guo et al., 2008).

The plant HSF family proteins have several characteristic domains that are essential for their functions, including a N-terminal DNA-binding domain (DBD) that recognizes heat shock elements in the promoter region of target genes, a following oligomerization domain (OD or HR-A/B motif) that is responsible for protein–protein interactions and trimerization during transcriptional activation (Scharf et al., 2012). Based on the length of the linker between the DBD and OD domains and the number of amino acid residues inserted into the HR-A/B regions, plant HSFs are classified into three subgroups: HSFA, HSFB and HSFC (Scharf et al., 2012). The subgroup A HSFs have additional nuclear localization signal (NLS) and nuclear export signal (NES) sequences, and a C-terminal aromatic and hydrophobic amino acid motif (AHA), which is needed for its transcriptional activation activity (Andrasi et al., 2021). The subgroup B HSFs contain a C-terminus tetrapeptide (LFGV) that functions as a repressor domain (RD) (Scharf et al., 2012; Andrasi et al., 2021).

Due to the functional importance, genome-wide identification and functional exploration of HSF genes have been carried out in model plants and many crops (Wang et al., 2018; Andrasi et al., 2021). Some HSF members have been used to enhance plant tolerance to different stresses and molecular breeding. For example, overexpression of *AtHSFA2* in *A. thaliana* increased the motolerance, salt/osmotic stress tolerance, and enhanced callus growth of the plant (Charng et al., 2007; Ogawa et al., 2007; Nishizawa et al., 2006). Overexpression of *GmHSFA1* in soybean and *SlHSFA1* in tomato enhanced thermotolerance of the transgenic plants (Mishra et al., 2002; Zhu et al., 2006).

Triticeae crops, including wheat (*Triticum aestivum*), barley (*Hordeum vulgare*) and rye (*Secale cereale*), are important grain crops, which are frequently challenged by various biotic and abiotic stresses. Recent studies revealed that overexpression of several HSF genes could enhance plants tolerance to multiple stresses (Bi et al., 2020; Poonia et al., 2020), suggesting HSF genes have significant potential for molecular breeding of Triticeae species. Genome-wide analysis of HSF genes has been conducted in wheat and barley, which provides primary resources for mining and utilizing functional HSF genes in the two species (Duan et al., 2019; Zhou et al., 2019; Mishra et al., 2020; Ye et al., 2020). However, the HSF genes composition in rye has not been investigated yet. In this study, we performed genome-wide identification and evolutionary analysis of HSF genes in a recently published rye genome (Li et al., 2021), and performed comparative analysis of HSF genes in Triticeae species.

MATERIALS AND METHODS

Identification and Classification of HSF Family Genes

The genome sequences of *S. cereale*, *H. vulgare*, *T. aestivum* (three subgenomes), *O. sativa* and *A. thaliana* were downloaded from public databases (Table S1). HSF genes were identified as described using a method by Shao et al. (2014) with some modifications. Briefly, the annotated proteins in each genome were screened for the HSF domain (Pfam accession: PF00447) by using the hmmsearch program implemented in the hmmer3.0 software (Johnson et al., 2010). The amino acid sequences of obtained HSF genes were then used to run a genome-wide BLASTp analysis for each genome. All hits were further analyzed using the hmmscan program in hmmer3.0 against the local Pfam-A database to confirm a detectable HSF domain in each sequence, with a e-value setting as 0.0001. All obtained HSF candidates were validated by subjecting to the Heatster database (Fan et al., 2021). Only genes simultaneously encoding DBD, HR-A and HR-B were recognized as true HSF genes, which were classified into the A, B, and C classes by the Heatster database.

Gene Structural Analyses and Domain Composition Analysis

The gene structure analysis for identified HSFs was constructed using the Gene Structure Display Server (GSDS) (http://gsds.cbi.pku.edu.cn/) (Suyama et al., 2006), while domain composition was presented by using the Tbtools (Chen et al., 2020).

Sequence Alignment and Phylogenetic Analysis

Amino acid sequences of the HSF domain were aligned using ClustalW program (Edgar, 2004) that is integrated in MEGA 7.0 (Kumar et al., 2016) with default options, and then was manually corrected. ModelFinder was used to estimate the best-fit model of nucleotide substitution (Kalyaanamoorthy et al., 2017). Phylogenetic analyses were performed using the IQ-TREE with

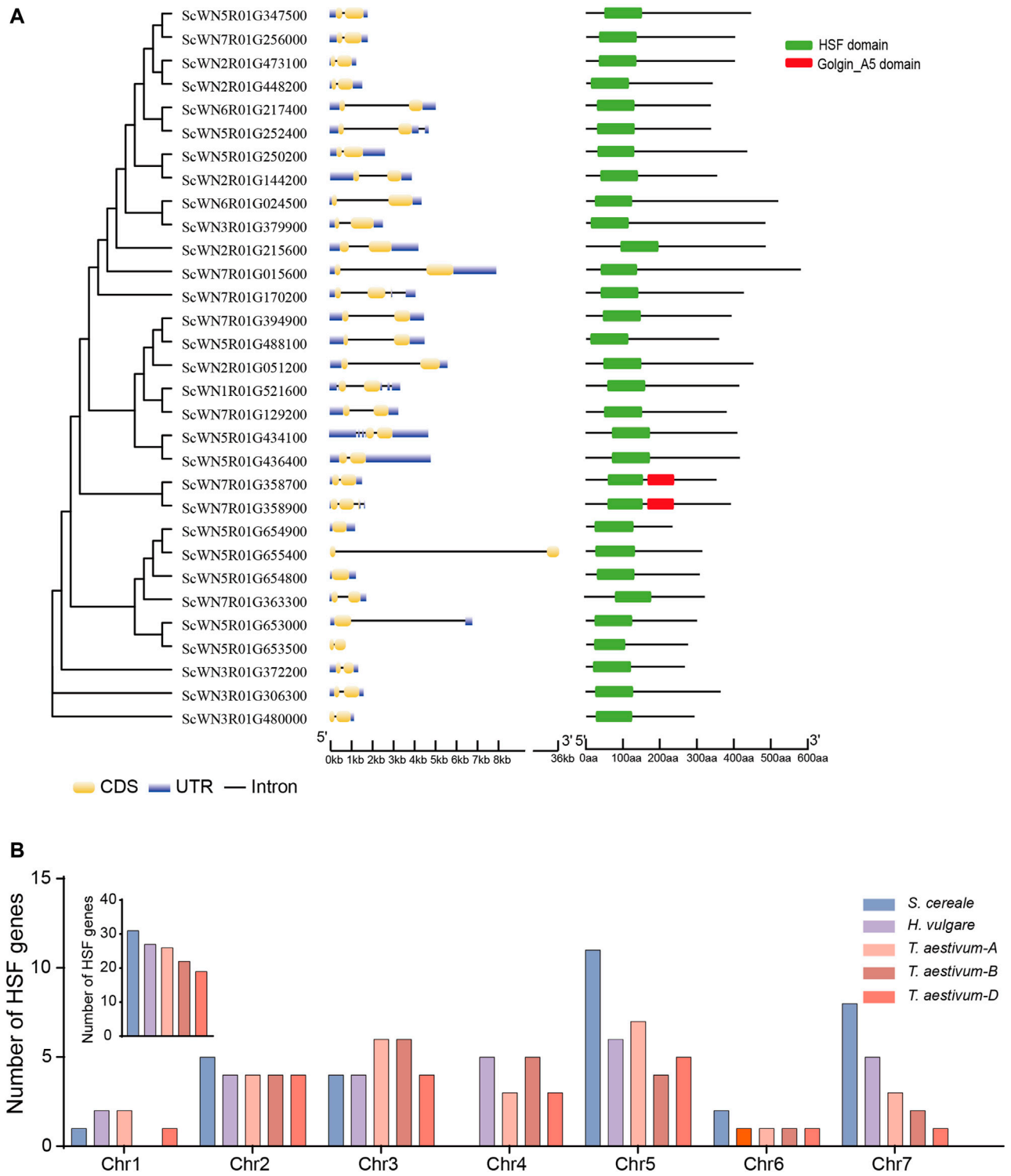

FIGURE 1 | Gene structure, domain composition and chromosome distribution of *S. cereale* HSF genes. **(A)**. HSF genes in the *S. cereale* genome were ordered by the phylogeny. Gene structure and domain composition for each gene were shown following the gene name. **(B)**. The number of HSF genes on each chromosome in *S. cereale* were shown and compared to those of *T. aestivum* and *H. vulgare*.

the maximum likelihood algorithm (Nguyen et al., 2015). Branch support values were calculated using the SH-aLRT (Anisimova et al., 2011) and the UFBoot2 (Minh et al., 2013) methods with 1,000 bootstrap replicates.

Synteny Analyses

Inter-species synteny analysis of the HSF genes from *S. cereale*, *T. aestivum* and *H. vulgare* were performed by using the MCScanX program that is integrated in the TBtools (Wang et al., 2012; Chen et al., 2020). Syntenic relationships were then drawn using Tbtools (Chen et al., 2020).

Gene Expression Analysis

RNA-seq raw reads of rye in different tissues and under different stresses were downloaded from the SRA database (Accesion: SRX9567472). The adaptors were removed using Trim_Galore (https://github.com/FelixKrueger/TrimGalore). The resulted clean reads were mapped to the rye reference genome using Hisat2 (Kim et al., 2019). Quantitation of gene expression was performed using feature Counts (Liao et al., 2014). The resulted read counts of each gene were normalized to FPKM.

RESULTS

Secale cereale Genome Contains 31 HSF Genes That Are Unevenly Distributed on the Seven Chromosomes

A total of 31 HSF family members were identified from the *S. cereale* genome by searching the annotated proteome of Weining rye (**Figure 1** and **Supplementary Table S1**). Gene structure analysis revealed that the annotated transcripts for 28 of the 31 HSF genes have both 5′ and 3′ untranslated regions (UTRs), whereas the transcript of one gene (ScWN3R01G480000) only has 3' UTR and transcripts of two genes (ScWN5R01G655400 and ScWN5R01G653500) do not have annotated UTR region, suggesting an overall high quality of the annotation. The annotated transcripts showed a high diversity of exon-intron composition among different HSF members, with 1–4 introns were found from the transcripts of the 29 genes, and 2 genes not having annotated introns. Among them, 24 HSF genes have only 1 intron, and introns for 23 of them are located at the coding sequences (CDS) of the transcripts. In contrast, 5 transcripts have 2 to 4 annotated introns. The large diversity of exon-intron composition in *S. cereale* may serve as primary resources for generating potential mRNA alternative splicing, which has been reported for several HSF genes in other plants (Ling et al., 2021). The amino acid numbers of the translated proteins from annotated CDSs of HSF genes range from 678 to 1,560 (**Supplementary Table S2**), suggesting potential fusion of additional domains by some HSF proteins. However, domain structure analysis showed that only two HSF proteins have an additional domain, namely Golgin_A5, at the C-terminal (**Figure 1A**), indicating a functional innovation of the two HSFs.

Chromosomal distribution analysis revealed that the 31 HSF genes are unevenly distributed on seven chromosomes of *S. cereale*. Chromosome 5 contains the largest number of HSF genes (11 genes), whereas no HSF genes were identified on chromosome 4 (Figure S1). The chromosome 1, 2, 3, 6, 7 have 1, 5, 4, 2, and 8 HSF genes, respectively (**Supplementary Figure S1**). Since chromosome introgression has been frequently used for Triticeae crops (Li et al., 2021), we compared the chromosomal distribution pattern of HSF genes among *S. cereale*, *H. vulgare*, and *T. aestivum*. The results showed that the overall HSF gene number in *S. cereale* (R genome) is great than that in the *H. vulgare* (H genome) and the subgenome A, B and D of wheat (**Figure 1B**). In accordance with the high HSF gene number in *S. cereale*, the numbers of HSF genes on the chromosomes 2, 5, 6, and 7 of *S. cereale* each ranks the first among the five genomes, respectively. However, in contrast to the lack of HSF genes on chromosome 4 in *S. cereale*, the *H. vulgare* genome and the subgenome A, B and D of wheat each has 5, 3, 5, and 3 HSF genes, respectively (**Figure 1B**). Considering the three species were only diverged from the common ancestor within twenty million years, it is possible that the HSF genes on the chromosome 4 of *S. cereale* have translocated to other chromosomes or underwent gene loss.

Classification of the HSF Genes in *S. cereale* and Four Other Angiosperms Reveals Species-specific HSF Composition

Plant HSFs have been classified into three classes, HSFA, B, and C, based on the linker length of the DBD and HR-A/B regions and the inserted amino acid residues number into the HR-A/B regions (Scharf et al., 2012). According to this criterion, 14 *S. cereale* HSF genes were assigned to class A, while 8 and 9 genes were assigned to class B and C, respectively (**Figure 2A**; **Supplementary Table S3**). The characteristic feature of different insertion size between HR-A/B regions could be clearly observed in the alignment, with 21, and 7 amino acid residues detected in class A and C HSFs, respectively (**Figure 2A**). No amino acid was detected between the HR-A/B regions for the sequences in class B. The boundary separating HR-A/B regions at the end of HR-A is conserved within each class but differs among the three classes. For example, a conserved motif of 'RQEQ' is readily detected at the end of HR-A region in most class A HSFs, whereas nearly all class C HSFs have a 'MWRR' motif. In comparison, the boundary of HR-B is less conserved in each class.

The proportion of HSF genes in each class only varied slightly among *S. cereale* (A: 29.0%; B: 25.8%; C: 45.2), *H. vulgare* (A: 25.9%; B: 22.2%; C: 51.9%) and the subgenome B (A: 33.3%; B: 25%; C: 41.7%) and D (A: 31.6%; B: 26.3%; C: 42.1%) of *T. aestivum*. In contrast, the wheat A subgenome showed an elevated proportion of class A (46.1%) HSFs and a decreased proportion of class C (30.8%) HSFs. The HSF genes from *O. sativa* and *A. thaliana* were also identified and their class compositions were compared with those in the three Triticeae species. The results showed that *O. sativa* has a more expanded class A (59.5%) and more contracted class C (13.5%)

A1	3.23%	3.70%	3.85%	8.33%	5.26%	4.00%	20.00%
A2	16.13%	11.11%	11.54%	8.33%	10.53%	16.00%	5.00%
A3	3.23%	3.70%	3.85%	4.17%	5.26%	4.00%	5.00%
A4	3.23%	7.41%	7.69%	4.17%	0.00%	8.00%	10.00%
A5	3.23%	3.70%	3.85%	4.17%	5.26%	4.00%	5.00%
A6	6.45%	7.41%	7.69%	4.17%	10.53%	4.00%	10.00%
A7	6.45%	11.11%	3.85%	4.17%	0.00%	8.00%	10.00%
A8	3.23%	3.70%	3.85%	4.17%	5.26%	4.00%	5.00%
B1	6.45%	3.70%	3.85%	8.33%	5.26%	4.00%	5.00%
B2	12.90%	11.11%	11.54%	8.33%	10.53%	12.00%	10.00%
B3/4	6.45%	7.41%	7.69%	8.33%	10.53%	16.00%	10.00%
C1	9.68%	11.11%	15.38%	12.50%	21.05%	8.00%	5.00%
C2	19.35%	14.81%	15.38%	20.83%	10.53%	8.00%	0.00%

FIGURE 2 | Class and subclass division of *S. cereale* HSF genes. **(A)**. Classification of HSF genes in *S. cereale* based on protein sequence characteristics. **(B)**. Proportion of different classes and subclasses of HSF genes in *S. cereale*, *H. vulgare*, *T. aestivum* (three subgenomes), *O. sativa* and *A. thaliana* respectively.

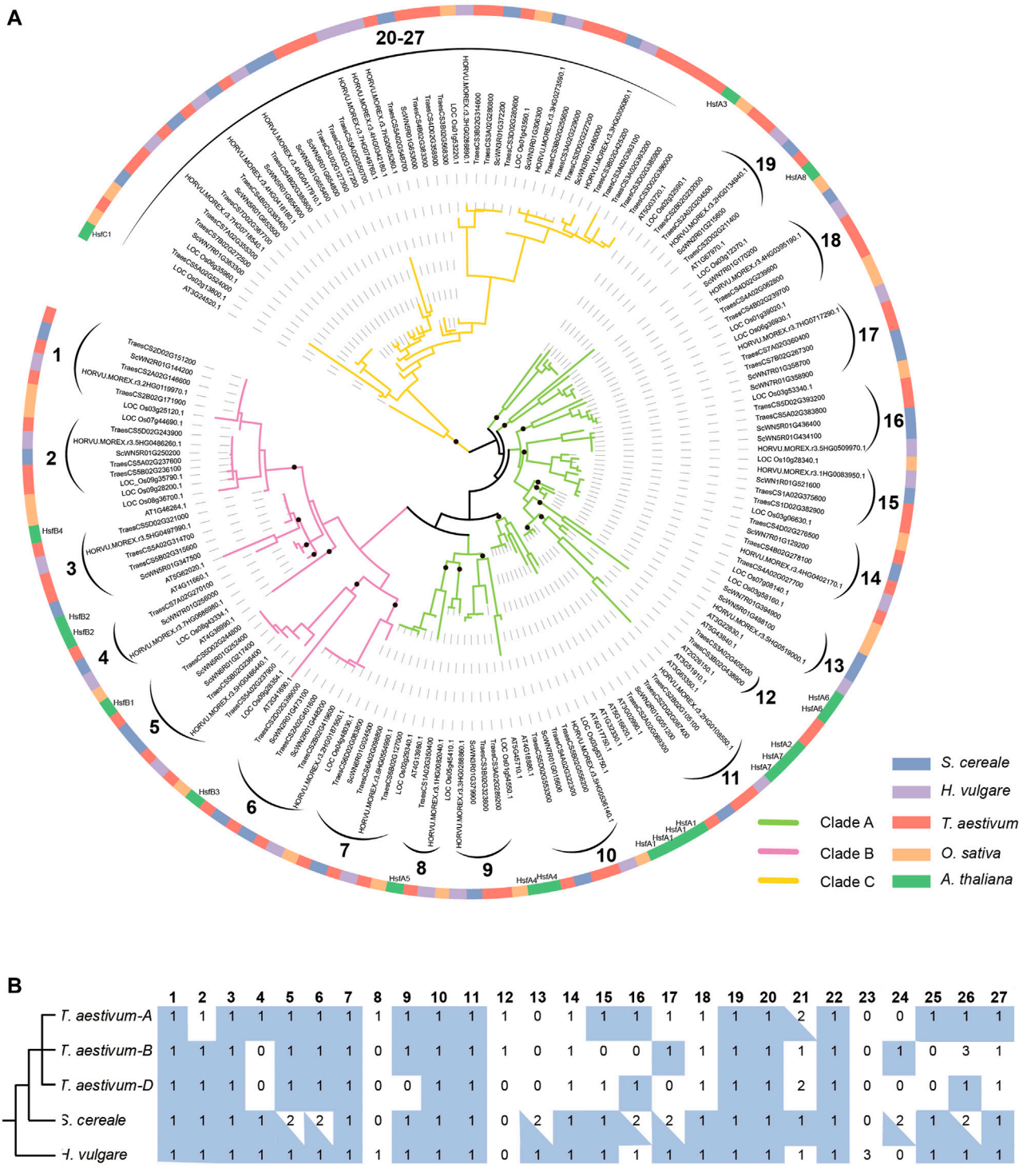

FIGURE 3 | Phylogenetic analysis of HSF genes from *S. cereale, H. vulgare, T. aestivum, O. sativa* and *A. thaliana*. **(A)**. A phylogeny of HSF genes from *S. cereale*, *H. vulgare*, *T. aestivum* (three subgenomes), *O. sativa* and *A. thaliana* based on the amino acid sequences of the HSF domain. Black brackets indicate a group of orthologous HSFs in Triticeae. The identification of class C Triticeae HSF orthologous group were based on an additional phylogeny provided in **Supplementary Figure S2**, which is constructed by using the full-length protein sequences encoded by HSFC genes. Black dots on the basal of several lineages indicate ancestral HSF lineages of monocots and dicots. **(B)**. The number of HSF genes from different species in each Triticeae HSF orthologous group. A blue rectangle background indicates the HSF gene and HSF genes from at least one other species are in collinear blocks. A blue triangle indicates one of the HSFs in this orthologous group has a collinear relationship with HSF genes from at least one other species.

than that in the wheat subgenome A. The *A. thaliana* genome has the highest ratio of HSFA members (75.0%) and the lowest ratio of HSFC members (5%) among all investigated genomes. This result is consistent with results from previous studies that the class C HSFs have undergone expansion in monocot species (Guo et al., 2016). The proportion of HSFB members is stable among all investigated genomes, ranging from 22.2 to 27.0%. The subclass composition of HSF family also varies cross-species (**Figure 2B**). For example, subclass C2 occupied the highest proportion of HSFs in *S. cereale*, *H. vulgare* and the wheat subgenome A and B, whereas subclass C1, A2 and A1 occupied the highest proportion of HSFs in the wheat subgenome D, *O. sativa* and *A. thaliana*, respectively.

Phylogenetic Analysis Reveals Dynamic Loss and Gain of HSF Genes Among Triticeae Species

To clarify the evolutionary relationship of HSF genes among *S. cereale*, *H. vulgare*, and *T. aestivum*, and trace the evolutionary trajectory during species-speciation of Triticeae, a phylogenetic analysis was performed for HSF genes from the three Triticeae species with those from *O. sativa* and *A. thaliana* (**Figure 3A**). The result showed that members of HSFB and HSFC form two separate monophyletic clades, containing 43 and 47 genes respectively, whereas members of HSFA form a paraphyletic group containing 81 genes. The topology of the HSF phylogeny is also highly consistent with a previous study which showed that HSFC may be diverged from HSFA in a rooted plant HSF phylogeny (Wang et al., 2018). This HSF phylogeny also supports the classification result based on characteristic features of the protein sequences. Tracing the evolutionary history of different HSF classes revealed that the monocot and dicot HSFA genes are inherited from at least 13 ancestral lineages, while the HSFB genes are inherited from 7 ancestral lineages that are presented in the common ancestor of monocot and dicot species (**Figure 3A**). Interestingly, there is only 1 *A. thaliana* (At3G24520) gene presented in the HSFC clade which contains 46 monocot sequences (**Figure 3A**), including 9, 9, 24 and 4 genes from *S. cereale*, *H. vulgare*, *T. aestivum* and *O. sativa*, suggesting the ancestral HSFC lineage that presented in the common ancestor of monocot and dicot has experienced drastic expansion in monocot species.

Further analysis of the phylogeny revealed that HSF genes from the *S. cereale*, *H. vulgare* and *T. aestivum* form 27 independent groups, suggesting that the 21 ancestral HSF genes in the common ancestor of monocot and dicot further diverged into at least 27 Triticeae HSF lineages before the separation of the three Triticeae species (**Figure 3A**). Interspecific synteny analysis showed that 24 genes of the 27 Triticeae HSF lineages could be detected at syntenic chromosomal blocks from at least two species, providing additional evidence to support the orthologous relationship of genes in each lineage. Interestingly, several interspecies syntenic blocks were detected among chromosome 7 of *S. cereale*, chromosome 4 or 5 of *H. vulgare* and/or the subgenome A, B of wheat (**Supplementary Figure S3**; **Supplementary Table S4**). The result suggests that chromosome rearrangement may have occurred in the *S. cereale* genome, causing HSF genes escaped from its chromosome 4.

Different extent of gene duplication and gene loss could be traced from *S. cereale*, *H. vulgare*, and the three subgenomes of *T. aestivum*. Among them, *S. cereale* has the most duplicated genes for the 27 Triticeae HSF lineages. Seven of the Triticeae HSF lineages have duplicated in the *S. cereale* genome, including 3, 2 and 2 lineages in the HSF A, B and C classes, respectively (**Figures 3A,B**; **Supplementary Figure S2**). The duplicated gene pairs are presented at adjacent, distant region of the same chromosome or at different chromosomes, suggesting tandem, dispersed, small-scale segmental duplications and ectopic duplications have been evolved in generating new HSF copies in the genome. In contrast, *H. vulgare* and the three subgenomes of *T. aestivum* each has one duplicated Triticeae HSF lineage. Loss of Triticeae HSF lineages was also detected in the three species. The *H. vulgare* genome lost 2 Triticeae HSF lineages (lineage 12 and 24), while the *S. cereale* and the subgenome A, B and D of wheat lost 3, 3, 7 and 9 Triticeae HSF lineages, respectively.

A Majority of *S. cereale* HSF Genes Show Tissue-Specific or Developmental Stage-Dependent Expression and can Response to Multiple Stresses

To explore the potential involvement of HSF members in development and resistance to environmental stresses, we analyzed their expression patterns using the public data (Li et al., 2021). An obvious tissue-specific or developmental stage-specific high expression was observed for nearly all HSF members (**Figure 4**). Furthermore, the expressions of most HSF genes are higher in root than in leaf and stem, except four genes, including 3 from the class A and 1 from the class B, which have the highest expression in stem among the three tissues (**Figure 4**). During *S. cereal* development after flowering, four genes show the highest expression in spike 1 week after flowering, whereas five genes have the highest expression in 40-days seed. The expression levels of most HSFs gradually increased during 10-days to 40-days after pollination.

We also analyzed the expressions of HSFs in leaves and roots under drought and freezing conditions. The results show that most HSF genes were induced by drought in leaf at least at one time point compared to the control, except ScWN7R01G015600, ScWN7R01G129200 and ScWN2R01G144200, which were down-expressed at the drought condition. A similar pattern was also observed for a large number of HSF genes in freezing leaves, except ScWN7R01G358900 and ScWN2R01G448200, the expressions of which were repressed by freezing treatment. In contrast to the pattern observed in leaves, only a few HSFs showed induced expression upon freezing treatment in root, whereas a considerable number of HSFs genes were down-expressed (**Figure 4**). The result suggests that leaf and root

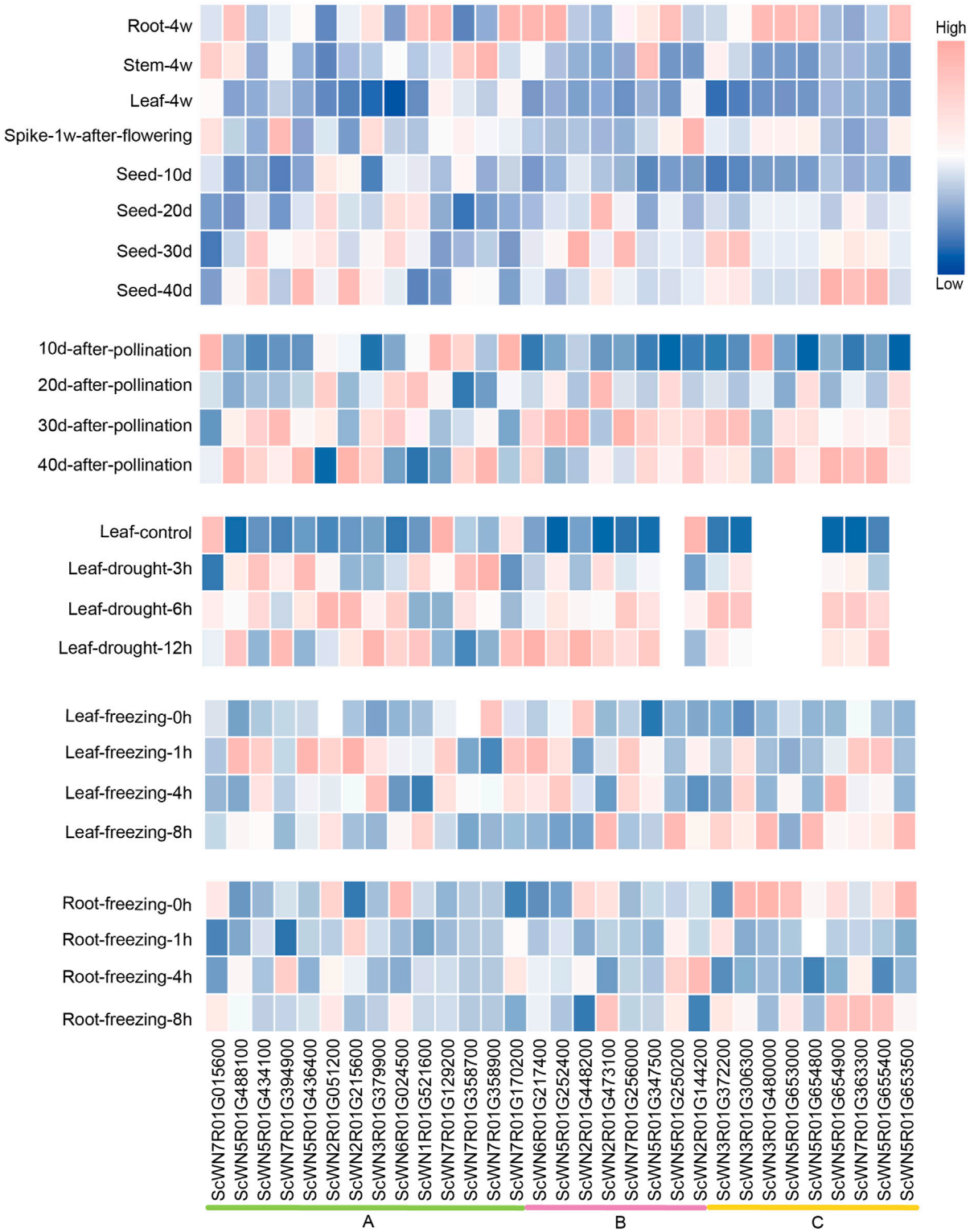

FIGURE 4 | Expression analysis of HSF genes in *S. cereale* across different tissues, development stages and different stress treatments.

may adapt different combinations of HSF genes to respond to the freezing stress. We also observed expression divergence of a newly duplicated gene with its parental gene. The ScWN7R01G394900, which is duplicated by ectopic duplication from the ScWN5R01G488100, shows the highest expression in spike, whereas ScWN5R01G488100 only highly expressed in root but not in other all detected tissues. Similar pattern of expression divergence could also be detected in stress treatment. ScWN7R01G394900 was induced in root upon freezing treatment, whereas ScWN5R01G488100 showed no obvious expression alteration. The results suggest functional divergence may have occurred in the gene pairs.

DISCUSSION

Understanding the molecular mechanisms of how plants respond to abiotic and biotic stresses is important for improving plant tolerance to stresses and crop productivity. HSF family proteins can modulate the expression of genes in responding to heat, cold, salt stresses and pathogens (Andrasi et al., 2021). The present study identified 31 HSF genes from the recently released *S. cereale* genome and traced the dynamic evolution of the HSF genes in three Triticeae species. *S. cereale* is an important cereal crop, which has high tolerance to many biotic and abiotic stresses (Li et al., 2021). The identification of HSF genes from *S. cereale* in this study provides a primary resource for mining functional genes that will facilitate the molecular breeding of *S. cereale*. Moreover, *S. cereal* plays an important role in the improvement of wheat breeding (Merker, 1984). It has great potential to expand the genetic variability of *T. aestivum*. Actually, genes with different functions have been transformed from *S. cereal* to *T. aestivum* to improve the growth or resistance to biotic and abiotic stress (Szakacs et al., 2020). The *S. cereale* HSF genes should also be served as a potential resource for wheat and other crops' breeding.

Different numbers of HSF genes have been identified from model and crop plants (Wang et al., 2018), however the evolutionary history of HSF genes in a specific plant lineage has rarely been investigated. By incorporating HSF genes from *O. sativa* and *A. thaliana* for the phylogenetic analysis, we found that the HSF gene family had undergone extensive expansion prior to the divergence of monocot and dicot, with at least 21 ancestral lineages being recovered. This number exceeded the quantity of the currently defined HSF subclass (Berz et al., 2019), suggesting an updated subclass definition by including HSF genes from more plant genomes is needed to help functional distinguish anciently diverged lineages. The ancestral HSF lineages further expanded before the radiation of Triticeae, with at least 27 ancestral Triticeae HSF lineages could be traced to the common ancestor of the three Triticeae species. These genes were differentially inherited by *S. cereale*, *H. vulgare*, and *T. aestivum*. *S. cereale* lost three of the ancestral Triticeae HSF lineages that presented in the common ancestor the three Triticeae species, while *H. vulgare* and *T. aestivum* both lost two. However, the *S. cereale* genome has more HSF genes than the *H. vulgare* genome and the three *T. aestivum* subgenomes, because of more specie-specific gene duplications and fewer gene loss events have been occurred after it separated with the other two species. A recent study of wheat revealed that both A subgenome and D subgenome have more HSF genes than their wild ancestors (*T. urartu*, 15 genes and *A. tauschii*, 16 genes) and concluded that the number of HSF increased in transition from diploidy to hexaploidy (Zhou et al., 2019). However, our data does not support this notion, because only one gene has gained by the wheat A genome after its separation from rye and barley, whereas three gene lost occurred. Similarly, only one gene has gained by the wheat D genome after its separation from rye and barley, whereas 9 gene lost occurred. Therefore, the fewer HSF genes in the genome of *T. urartu* and *A. tauschii* than those in wheat A and D subgenomes is more likely due to the increased gene loss in the two genomes.

Gene duplication provides raw resource for gene function innovation (Guo et al., 2019). As shown by the expression data, HSF genes from different ancestral lineages show diverse expression patterns across different tissues, development stages and stress treatments. This is consistent with the previous studies in wheat, suggesting multiple functions of HSF genes (Ye et al., 2020). Recent gene duplications also contribute to plant adaptive evolution (Zhang and Long, 2014). While few HSF gene duplications were detected in the barley genome, the wheat genome obviously benefitted from harboring three subgenomes to have a neatly tripled HSF number. The *S. cereale* genome adopted a different strategy to amplify its HSF content, with six gene duplications generated by different mechanisms detected. The newly birthed genes provide opportunities for functional innovation of HSF genes in *S. cereale*. To support our speculation, we found that a pair of genes from one duplication showed inconsistent expression patterns, suggesting functional innovation may have occurred in the recently duplicated *S. cereale* HSF genes.

CONCLUSION

In summary, this study presents a complete profile of HSF genes in *S. cereale*, which is composed by 31 genes from three classes. Chromosomal reorganization may have contributed to the HSF escape from chromosome 4 in *S. cereale*. Phylogenetic and syntenic analysis supported that at least 27 ancestral HSF lineages were presented in the common ancestor of *S. cereale*, *H. vulgare*, and *T. aestivum*. *S. cereale* experienced the most HSF gene duplications among the Triticeae A, B, D, R and H genomes. Expression analysis revealed the potential involvement of HSF genes in growth, development and response to abiotic stress of *S. cereale*, and indicated the functional innovation of recently duplicated HSF genes. The results provide new insights into the

evolution of HSF genes in Triticeae and may serve as a resource for Triticeae molecular breeding.

DATA AVAILABILITY STATEMENT

The original contributions presented in the study are included in the article/**Supplementary Material**, further inquiries can be directed to the corresponding authors.

AUTHOR CONTRIBUTIONS

Z-QS and YL conceived and designed the study. X-TL, X-YF, ZZ, and YL obtained and analyzed the data. X-TL and X-YF wrote the manuscript. Z-QS and YL revised the manuscript. All authors read and approved the final manuscript.

ACKNOWLEDGMENTS

We greatly appreciate the Frontiers editors and reviewers for handling our manuscript and providing critical suggestions.

SUPPLEMENTARY MATERIAL

The Supplementary Material for this article can be found online at: https://www.frontiersin.org/articles/10.3389/fgene.2021.801218/full#supplementary-material

REFERENCES

Andrási, N., Pettkó-Szandtner, A., and Szabados, L. (2021). Diversity of Plant Heat Shock Factors: Regulation, Interactions, and Functions. *J. Exp. Bot.* 72, 1558–1575. doi:10.1093/jxb/eraa576

Anisimova, M., Gil, M., Dufayard, J.-F., Dessimoz, C., and Gascuel, O. (2011). Survey of Branch Support Methods Demonstrates Accuracy, Power, and Robustness of Fast Likelihood-Based Approximation Schemes. *Syst. Biol.* 60, 685–699. doi:10.1093/sysbio/syr041

Berz, J., Simm, S., Schuster, S., Scharf, K. D., Schleiff, E., and Ebersberger, I. (2019). Heatster: A Database and Web Server for Identification and Classification of Heat Stress Transcription Factors in Plants. *Bioinform Biol. Insights* 13, 1177932218821365. doi:10.1177/1177932218821365

Bi, H., Zhao, Y., Li, H., and Liu, W. (2020). Wheat Heat Shock Factor TaHsfA6f Increases ABA Levels and Enhances Tolerance to Multiple Abiotic Stresses in Transgenic Plants. *Int. J. Mol. Sci.* 21, 3121. doi:10.3390/ijms21093121

Boston, R. S., Viitanen, P. V., and Vierling, E. (1996). Molecular Chaperones and Protein Folding in Plants. *Plant Mol. Biol.* 32, 191–222. doi:10.1007/bf00039383

Charng, Y.-Y., Liu, H.-C., Liu, N.-Y., Chi, W.-T., Wang, C.-N., Chang, S.-H., et al. (2007). A Heat-Inducible Transcription Factor, HsfA2, Is Required for Extension of Acquired Thermotolerance in Arabidopsis. *Plant Physiol.* 143, 251–262. doi:10.1104/pp.106.091322

Chen, C., Chen, H., Zhang, Y., Thomas, H. R., Frank, M. H., He, Y., et al. (2020). TBtools: An Integrative Toolkit Developed for Interactive Analyses of Big Biological Data. *Mol. Plant* 13, 1194–1202. doi:10.1016/j.molp.2020.06.009

Duan, S., Liu, B., Zhang, Y., Li, G., and Guo, X. (2019). Genome-Wide Identification and Abiotic Stress-Responsive Pattern of Heat Shock Transcription Factor Family in *Triticum A* L. *Bmc Genomics* 20, 257. doi:10.1186/s12864-019-5617-1

Edgar, R. C. (2004). MUSCLE: Multiple Sequence Alignment with High Accuracy and High Throughput. *Nucleic Acids Res.* 32, 1792–1797. doi:10.1093/nar/gkh340

Fan, K., Mao, Z., Ye, F., Pan, X., Li, Z., Lin, W., et al. (2021). Genome-Wide Identification and Molecular Evolution Analysis of the Heat Shock Transcription Factor (HSF) Gene Family in Four Diploid and Two Allopolyploid Gossypium Species. *Genomics* 113, 3112–3127. doi:10.1016/j.ygeno.2021.07.008

Guo, H., Jiao, Y., Tan, X., Wang, X., Huang, X., Jin, H., et al. (2019). Gene Duplication and Genetic Innovation in Cereal Genomes. *Genome Res.* 29, 261–269. doi:10.1101/gr.237511.118

Guo, J., Wu, J., Ji, Q., Wang, C., Luo, L., Yuan, Y., et al. (2008). Genome-Wide Analysis of Heat Shock Transcription Factor Families in rice and Arabidopsis. *J. Genet. Genomics* 35, 105–118. doi:10.1016/s1673-8527(08)60016-8

Guo, M., Liu, J.-H., Ma, X., Luo, D.-X., Gong, Z.-H., and Lu, M.-H. (2016). The Plant Heat Stress Transcription Factors (HSFs): Structure, Regulation, and Function in Response to Abiotic Stresses. *Front. Plant Sci.* 7, 114. doi:10.3389/fpls.2016.00114

Javed, T., Shabbir, R., Ali, A., Afzal, I., Zaheer, U., and Gao, S. J. (2020). Transcription Factors in Plant Stress Responses: Challenges and Potential for Sugarcane Improvement. *Plants (Basel)* 9, 491. doi:10.3390/plants9040491

Johnson, L. S., Eddy, S. R., and Portugaly, E. (2010). Hidden Markov Model Speed Heuristic and Iterative HMM Search Procedure. *BMC Bioinformatics* 11, 431. doi:10.1186/1471-2105-11-431

Kalyaanamoorthy, S., Minh, B. Q., Wong, T. K. F., Von Haeseler, A., and Jermiin, L. S. (2017). ModelFinder: Fast Model Selection for Accurate Phylogenetic Estimates. *Nat. Methods* 14, 587–589. doi:10.1038/nmeth.4285

Kim, D., Paggi, J. M., Park, C., Bennett, C., and Salzberg, S. L. (2019). Graph-Based Genome Alignment and Genotyping with HISAT2 and HISAT-Genotype. *Nat. Biotechnol.* 37, 907–915. doi:10.1038/s41587-019-0201-4

Kumar, S., Stecher, G., and Tamura, K. (2016). MEGA7: Molecular Evolutionary Genetics Analysis Version 7.0 for Bigger Datasets. *Mol. Biol. Evol.* 33, 1870–1874. doi:10.1093/molbev/msw054

Li, G., Wang, L., Yang, J., He, H., Jin, H., Li, X., et al. (2021). A High-Quality Genome Assembly Highlights rye Genomic Characteristics and Agronomically Important Genes. *Nat. Genet.* 53, 574–584. doi:10.1038/s41588-021-00808-z

Liao, Y., Smyth, G. K., and Shi, W. (2014). featureCounts: An Efficient General Purpose Program for Assigning Sequence Reads to Genomic Features. *Bioinformatics* 30, 923–930. doi:10.1093/bioinformatics/btt656

Ling, Y., Mahfouz, M. M., and Zhou, M. (2021). Pre-mRNA Alternative Splicing as a Modulator for Heat Stress Response in Plants. *Trends Plant Sci.* 28, 18. doi:10.1016/j.tplants.2021.07.008

Merker, A. (1984). The Rye Genome in Wheat Breeding. *Hereditas* 100, 183–191.

Minh, B. Q., Nguyen, M. A. T., and Von Haeseler, A. (2013). Ultrafast Approximation for Phylogenetic Bootstrap. *Mol. Biol. Evol.* 30, 1188–1195. doi:10.1093/molbev/mst024

Mishra, S. K., Poonia, A. K., Chaudhary, R., Baranwal, V. K., Arora, D., Kumar, R., et al. (2020). Genome-Wide Identification, Phylogeny and Expression Analysis of HSF Gene Family in Barley during Abiotic Stress Response and Reproductive Development. *Plant Gene* 23, 100231. doi:10.1016/j.plgene.2020.100231

Mishra, S. K., Tripp, J., Winkelhaus, S., Tschiersch, B., Theres, K., Nover, L., et al. (2002). In the Complex Family of Heat Stress Transcription Factors, HsfA1 Has a Unique Role as Master Regulator of Thermotolerance in Tomato. *Genes Dev.* 16, 1555–1567. doi:10.1101/gad.228802

Nguyen, L.-T., Schmidt, H. A., Von Haeseler, A., and Minh, B. Q. (2015). IQ-TREE: A Fast and Effective Stochastic Algorithm for Estimating Maximum-Likelihood Phylogenies. *Mol. Biol. Evol.* 32, 268–274. doi:10.1093/molbev/msu300

Nishizawa, A., Yabuta, Y., Yoshida, E., Maruta, T., Yoshimura, K., and Shigeoka, S. (2006). Arabidopsis Heat Shock Transcription Factor A2 as a Key Regulator in Response to Several Types of Environmental Stress. *Plant J.* 48, 535–547. doi:10.1111/j.1365-313x.2006.02889.x

Ogawa, D., Yamaguchi, K., and Nishiuchi, T. (2007). High-Level Overexpression of the Arabidopsis HsfA2 Gene Confers Not Only Increased Themotolerance but Also Salt/osmotic Stress Tolerance and Enhanced Callus Growth. *J. Exp. Bot.* 58, 3373–3383. doi:10.1093/jxb/erm184

Peck, S., and Mittler, R. (2020). Plant Signaling in Biotic and Abiotic Stress. *J. Exp. Bot.* 71, 1649–1651. doi:10.1093/jxb/eraa051

Poonia, A. K., Mishra, S. K., Sirohi, P., Chaudhary, R., Kanwar, M., Germain, H., et al. (2020). Overexpression of Wheat Transcription Factor (TaHsfA6b) Provides Thermotolerance in Barley. *Planta* 252, 53. doi:10.1007/s00425-020-03457-4

Saur, I. M. L., Panstruga, R., and Schulze-Lefert, P. (2021). NOD-Like Receptor-Mediated Plant Immunity: from Structure to Cell Death. *Nat. Rev. Immunol.* 21, 305–318. doi:10.1038/s41577-020-00473-z

Scharf, K.-D., Berberich, T., Ebersberger, I., and Nover, L. (2012). The Plant Heat Stress Transcription Factor (Hsf) Family: Structure, Function and Evolution. *Biochim. Biophys. Acta (Bba) - Gene Regul. Mech.* 1819, 104–119. doi:10.1016/j.bbagrm.2011.10.002

Shao, Z.-Q., Zhang, Y.-M., Hang, Y.-Y., Xue, J.-Y., Zhou, G.-C., Wu, P., et al. (2014). Long-Term Evolution of Nucleotide-Binding Site-Leucine-Rich Repeat Genes: Understanding Gained from and Beyond the Legume Family. *Plant Physiol.* 166, 217–234. doi:10.1104/pp.114.243626

Suyama, S., Abe, S., Inoue, Y., Toukairin, A., Ohtake, Y., and Ohkubo, Y. (2006). The Involvement of Transferrin in the Uptake of Iron-59 by Hepatocytes of Carbon Tetrachloride-Damaged Rats. *Biol. Pharm. Bull.* 29, 1387–1390. doi:10.1248/bpb.29.1387

Szakács, É., Szőke-Pázsi, K., Kalapos, B., Schneider, A., Ivanizs, L., Rakszegi, M., et al. (2020). 1RS Arm of Secale Cereanum 'Kriszta' Confers Resistance to Stripe Rust, Improved Yield Components and High Arabinoxylan Content in Wheat. *Sci. Rep.* 10, 1792. doi:10.1038/s41598-020-58419-3

Wang, X., Shi, X., Chen, S., Ma, C., and Xu, S. (2018). Evolutionary Origin, Gradual Accumulation and Functional Divergence of Heat Shock Factor Gene Family with Plant Evolution. *Front. Plant Sci.* 9, 71. doi:10.3389/fpls.2018.00071

Wang, Y., Tang, H., Debarry, J. D., Tan, X., Li, J., Wang, X., et al. (2012). MCScanX: A Toolkit for Detection and Evolutionary Analysis of Gene Synteny and Collinearity. *Nucleic Acids Res.* 40, e49. doi:10.1093/nar/gkr1293

Wani, S. H., Anand, S., Singh, B., Bohra, A., and Joshi, R. (2021). WRKY Transcription Factors and Plant Defense Responses: Latest Discoveries and Future Prospects. *Plant Cel Rep* 40, 1071–1085. doi:10.1007/s00299-021-02691-8

Ye, J., Yang, X., Hu, G., Liu, Q., Li, W., Zhang, L., et al. (2020). Genome-Wide Investigation of Heat Shock Transcription Factor Family in Wheat (*Triticum A* L.) and Possible Roles in Anther Development. *Int. J. Mol. Sci.* 21, 608. doi:10.3390/ijms21020608

Zhang, Y. E., and Long, M. (2014). New Genes Contribute to Genetic and Phenotypic Novelties in Human Evolution. *Curr. Opin. Genet. Develop.* 29, 90–96. doi:10.1016/j.gde.2014.08.013

Zhou, M. Q., Shen, C., Wu, L. H., Tang, K. X., and Lin, J. (2011). CBF-dependent Signaling Pathway: A Key Responder to Low Temperature Stress in Plants. *Crit. Rev. Biotechnol.* 31, 186–192. doi:10.3109/07388551.2010.505910

Zhou, M., Zheng, S., Liu, R., Lu, J., Lu, L., Zhang, C., et al. (2019). Genome-Wide Identification, Phylogenetic and Expression Analysis of the Heat Shock Transcription Factor Family in Bread Wheat (*Triticum A* L.). *BMC Genomics* 20, 505. doi:10.1186/s12864-019-5876-x

Zhu, B., Ye, C., Lü, H., Chen, X., Chai, G., Chen, J., et al. (2006). Identification and Characterization of a Novel Heat Shock Transcription Factor Gene, GmHsfA1, in Soybeans (Glycine max). *J. Plant Res.* 119, 247–256. doi:10.1007/s10265-006-0267-1

Conflict of Interest: The authors declare that the research was conducted in the absence of any commercial or financial relationships that could be construed as a potential conflict of interest.

Publisher's Note: All claims expressed in this article are solely those of the authors and do not necessarily represent those of their affiliated organizations, or those of the publisher, the editors and the reviewers. Any product that may be evaluated in this article, or claim that may be made by its manufacturer, is not guaranteed or endorsed by the publisher.

frontiers in Genetics

ORIGINAL RESEARCH
published: 13 December 2021
doi: 10.3389/fgene.2021.784545

Programmed Degradation of Pericarp Cells in Wheat Grains Depends on Autophagy

Yong-Bo Li[1], Mei Yan[2], De-Zhou Cui[1], Chen Huang[1], Xin-Xia Sui[1], Feng Zhi Guo[3], Qing-Qi Fan[1]* and Xiu-Sheng Chu[1,4]**

[1]Crop Research Institute, Shandong Academy of Agricultural Sciences, Jinan, China, [2]Shandong Luyan Seed Company, Jinan, China, [3]Heze Academy of Agricultural Sciences, Heze, China, [4]School of Life Science, Shandong Normal University, Jinan, China

Wheat is one of the most important food crops in the world, with development of the grains directly determining yield and quality. Understanding grain development and the underlying regulatory mechanisms is therefore essential in improving the yield and quality of wheat. In this study, the developmental characteristics of the pericarp was examined in developing wheat grains of the new variety Jimai 70. As a result, pericarp thickness was found to be thinnest in grains at the top of the spike, followed by those in the middle and thickest at the bottom. Moreover, this difference corresponded to the number of cell layers in the pericarp, which decreased as a result of programmed cell death (PCD). A number of autophagy-related genes (*ATGs*) are involved in the process of PCD in the pericarp, and in this study, an increase in ATG8-PE expression was observed followed by the appearance of autophagy structures. Meanwhile, following interference of the key autophagy gene *ATG8*, PCD was inhibited and the thickness of the pericarp increased, resulting in small premature grains. These findings suggest that autophagy and PCD coexist in the pericarp during early development of wheat grains, with both processes increasing from the bottom to the top of the spike. Moreover, PCD was also found to rely on *ATG8*-mediated autophagy. The results of this study therefore provide a theoretical basis for in-depth studies of the regulatory mechanisms of wheat grain development.

Keywords: wheat, pericarp, autophagy, programmed cell death, autophagy-related genes

OPEN ACCESS

Edited by:
Pengtao Ma,
Yantai University, China

Reviewed by:
Guohao Han,
Institute of Genetics and Developmental Biology (CAS), China
Qiaoling Luo,
Institute of Genetics and Developmental Biology (CAS), China

****Correspondence:***
Feng Zhi Guo
fanqingqi@163.com
Qing-Qi Fan
lklgfz2014@163.com
Xiu-Sheng Chu
xschu2007@sina.com

Specialty section:
This article was submitted to Plant Genomics, a section of the journal Frontiers in Genetics

Received: *28 September 2021*
Accepted: *19 November 2021*
Published: *13 December 2021*

Citation:
Li Y-B, Yan M, Cui D-Z, Huang C, Sui X-X, Guo FZ, Fan Q-Q and Chu X-S (2021) Programmed Degradation of Pericarp Cells in Wheat Grains Depends on Autophagy. Front. Genet. 12:784545. doi: 10.3389/fgene.2021.784545

INTRODUCTION

Wheat, one of the most important cereal crops worldwide, is characterized by its process of grain development. Although grains in the middle spikelet are first to bloom, the upper grains mature first, followed by the middle, and then the lower grains. The wheat grain is a type of caryopsis, whereby the pericarp and episperm develop from the integument and are tightly integrated (Zhou et al., 2009). Development of the pericarp is closely related to grain yield and overall wheat quality. Developing from the ovary wall, it can be divided into the exocarp, mesocarp and endocarp (Xiong et al., 2013). The pericarp covers the seed tegument, and endosperm and embryo tissues of the grain (Brinton et al., 2017) and controls the water transport into the endosperm cavity (Wang and Fisher, 1994), the synthesis of organic compounds (Fujita and Taira, 1998; Foxon et al., 1990), and the temporal storage of starch (Yu et al., 2015).

It was previously suggested that development of the pericarp is a typical process of programmed cell death (PCD) (Pennell and Lamb, 1997; Zhou et al., 2009), a genetically-regulated process of cell

suicide that results in the remobilization of cellular contents, nourishing new filial tissues, such as the embryo and endosperm, and providing space for grain filling (Radchuk et al., 2011; Dominguez and Cejudo, 2014). Meanwhile, autophagy is responsible for the delivery of cellular components to the lysosome/vacuole for subsequent degradation, especially under nutrient limitations and other stress conditions, thereby supporting cellular proteostasis and longevity (Ghosh et al., 2015). Autophagic processes mainly serve survival functions during cellular homeostasis, stress adaptation and immune responses, but have also been found to possess cell death-promoting activities (Bozhkov, 2018). Genetic suppression of autophagy in plants is correlated with an overall decrease in plant fitness, including reduced vegetative growth and fecundity, accelerated senescence and enhanced susceptibility to diverse types of stress (Bozhkov, 2018). However, the role of autophagy in regulating PCD in plants remains unknown and a subject of debate (Ustun et al., 2017).

In wheat, autophagy is involved in the regulation of various biotic and abiotic stresses. Under hypoxia, wheat roots can remove reactive oxygen species by autophagy, thus maintaining cell survival (Lin et al., 2021). Under salt stress, interfering of autophagy-related genes *ATG2* or *ATG7* causes PCD in leaves (Yue et al., 2021). Inhibition of autophagy can accelerate PCD of seedlings caused by drought (Li et al., 2019). Short-term waterlogging and cold stress promote autophagy of wheat root cells (Valitova et al., 2019; Zhou et al., 2021). Autophagy-related genes *ATG4*, *ATG6*, and *ATG8* of wheat participate in the regulation of basic resistance to powdery mildew (Pei et al., 2014). *ATG8* contributes to wheat resistance to stripe rust fungus by regulating cell death (Ma et al., 2012). However, it is unclear whether autophagy is involved in the regulation of wheat grain development.

In this study, we used the new wheat variety Jimai 70 to examine the regulation of autophagy on grain development and PCD in pericarp. Our data suggested that autophagy and PCD coexist in the development of the pericarp; and both processes increasing from the bottom to the top of the spike, which determines the thickness of the pericarp at the corresponding position.

TABLE 1 | Primers used in this study. *ATG* (*4*, *6*, *7*, *8*, *12*) QRT primers were used for quantitative real-time reverse transcription-PCR (qRT-PCR) of autophagy-related genes (*ATGs*). RNAi primers of *ATG8* were used to amplify the interference sequence of autophagy-related *ATG8*.

Primer name	Sequence (5′ - 3′)
ATG4QRTf	GAAAGCCCGCACAGAGTC
ATG4QRTr	ACCCGAGACCACATAGAGC
ATG6QRTf	TTTCCGTCTCGGTCGTCT
ATG6QRTr	CAAACTTATGGCAAACTCG
ATG7QRTf	TGCCTCACTGGTGCTTAG
ATG7QRTr	CAATCCTTGAGTTGCCTTA
ATG8QRTf	AGGCTGATAAGTCTGATGTCC
ATG8QRTr	CGTCCTCGTCCTTGTTTT
ATG12QRTf	ACAAGTTCAGGATTTCAGGACGAG
ATG12QRTr	TGCCGACAAAGCATAGTTTACCAC
ATG8RNAiF	ATGGCGAAGAGCTCGTTCAAG
ATG8RNAiR	TGGCAGACATCAGGGCAGC
DsGFPF	ATGGTGAGCAAGGGCGAGG
DsGFPR	GGACGTAGCCTTCGGGCATGG
?-TubulinF	AACTTCGCCCGTGGTCAT
?-TubulinR	CAGCGTTGAATACAAGGAATC

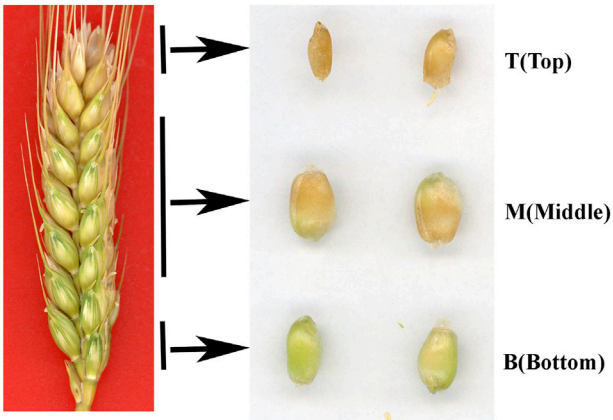

FIGURE 1 | Phenotypes of grains taken from the **top (T), middle (M)** and **bottom (B)** of the spike 25 days after flowering.

MATERIALS AND METHODS

Plant Materials

Wheat cultivar Jimai 70 was developed by the Crop Research Institute, Shandong Academy of Agricultural Sciences, China. It possesses a number of elite traits, such as high and stable yield, lodging resistance, strong wind resistance, and slow stripe rust resistance.

Quantitative Real-Time Reverse Transcription-PCR

Total RNA was extracted from the pericarp using RNAprep Pure Plant Kit (DP432, TIANGEN, Beijing, China) according to the manufacturer's instructions. After determining RNA quality by electrophoresis on 1% agarose gel, 2 μg of RNA was reverse transcribed into cDNA using EasyScript One-Step gRNA Removal and cDNA Synthesis Super Mix (L20602, Transgen, Beijing, China). The resulting cDNA was then used as a template in the PCR reactions. qRT-PCR was performed using TransStart Tip Green qPCR SuperMix (L20803, Transgen) according to the manufacturer's instructions in a real-time thermal cycler (LightCycler R 480 II, Roche, Basel, Switzerland). α-Tubulin was amplified for internal standardization. The experiments were repeated three times and the experimental data were statistically analyzed using the Student's t-test. Relative expression data from the qRT-PCR experiments were obtained using the $2^{-\Delta\Delta CT}$ method (Ustun et al., 2017). Relevant primers were listed in **Table 1**.

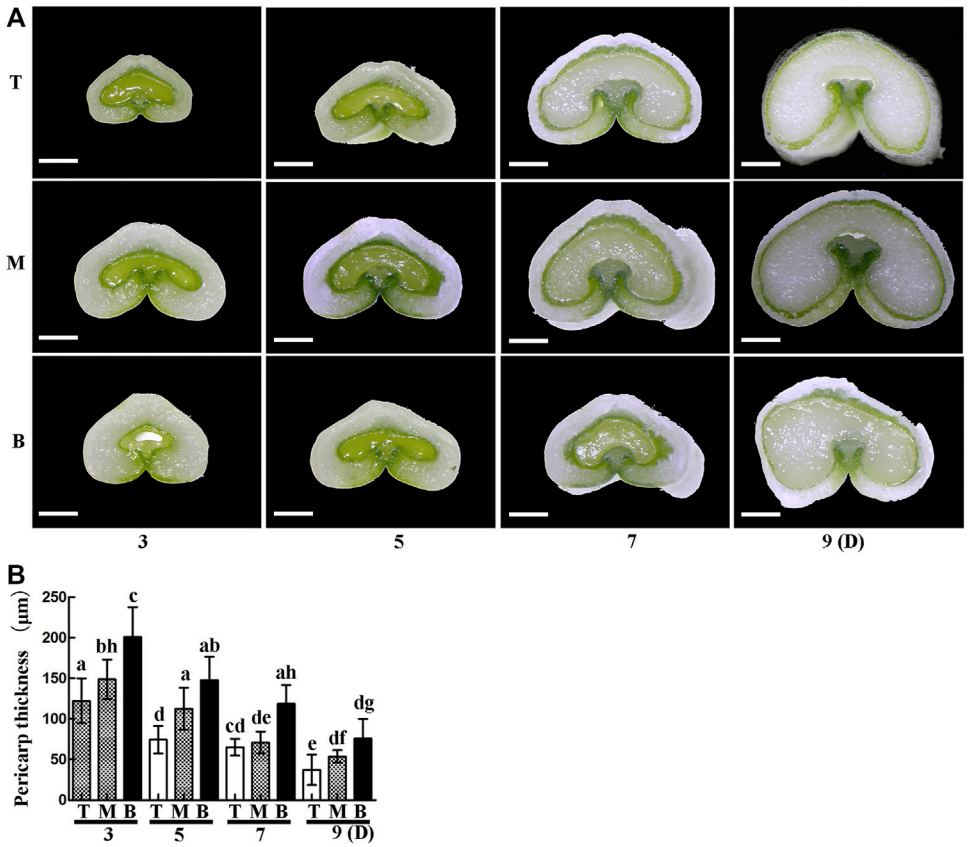

FIGURE 2 | Cross-sections of grains from the **top (T), middle (M)** and **bottom (B)** of the spike 3, 5, 7 and 9 days after flowering. **(A)**. Scale bars: 500 μm. **(B)**. Statistical analysis of pericarp thickness at each position on the spike. Bars represent the mean ± SD of three independent experiments. Asterisks indicate a significant difference as determined by ANOVA, and different letters represent a significant difference between positions on the spike.

Preparation of Polyclonal Antibodies of ATG8 and α-Tubulin

Synthetic peptide (5 mg) samples obtained from the ATG8 protein sequence were first coupled to Keyhole Limpet Hemocyanin. The coupling polypeptide was then used as an antigen to produce rabbit polyclonal antibodies (anti-ATG8 antibodies) as described previously (Liu et al., 2014). A partial cDNA sequence containing 90 - 750 bp of α-tubulin was then amplified with the selected primers α-tubulin F/R (**Table 1**), and inserted into the *pGEX4T-AB1* plasmid. The recombinant plasmid was then transformed into competent *Escherichia coli* (BL21-DE3). The expressed α-tubulin was then obtained as a supernatant and purified before using the target protein as an antigen to produce rabbit polyclonal antibodies (anti-α-tubulin antibodies) as with the ATG8 antibodies.

Western Blot (Immunoblotting)

Total proteins from the pericarp were extracted using Plant Total Protein Lysis Buffer (P1258, Applygen Technologies Inc., Beijing, China). The protein concentration was then measured according to the Bradford method (Bradford, 1976), and equal amounts (30 μg) of each sample were subjected to SDS-PAGE. Proteins were then electrophoretically transferred onto a nitrocellulose membrane and incubated with blocking buffer [2% skim milk powder dissolved in TBS (8.8 g NaCl, 5 ml of 2 M Tris-HCl, pH 7.6, and 995 ml of H_2O)] at room temperature for 1 h. Rabbit source polyclonal antibody ATG8 or α-tubulin was then diluted to 1:500 in blocking buffer in TBS and incubated with the membrane at 4°C overnight. After washing, the membrane was incubated with secondary antibody (alkaline phosphatase conjugated goat anti-rabbit IgG diluted 1:10,000 in blocking buffer) (ZB2308, Zhong Shan Jin Qiao, Beijing, China) at room temperature for 2.5 h then the protein signal was visualized using an Alkaline Phosphatase Color Development Kit (C3206, Beyotime, Shanghai, China). Protein bands on the membrane were then analyzed using Image J software.

Virus Induced Gene Silencing of *ATG8*

The barley stripe mosaic virus (BSMV)-based VIGS method was used to create gene knockdown plants (Ma et al., 2012; Dong et al., 2019). Briefly, a 283-bp fragment of wheat *ATG8* from the conserved coding sequence was amplified and purified, with a same-sized fragment of GFP used as a control. The γ strand of BSMV was then digested in XmacI and fused with the *ATG8* or *GFP* fragment to form the vectors BSMVγ-ATG8 and BSMVγ-

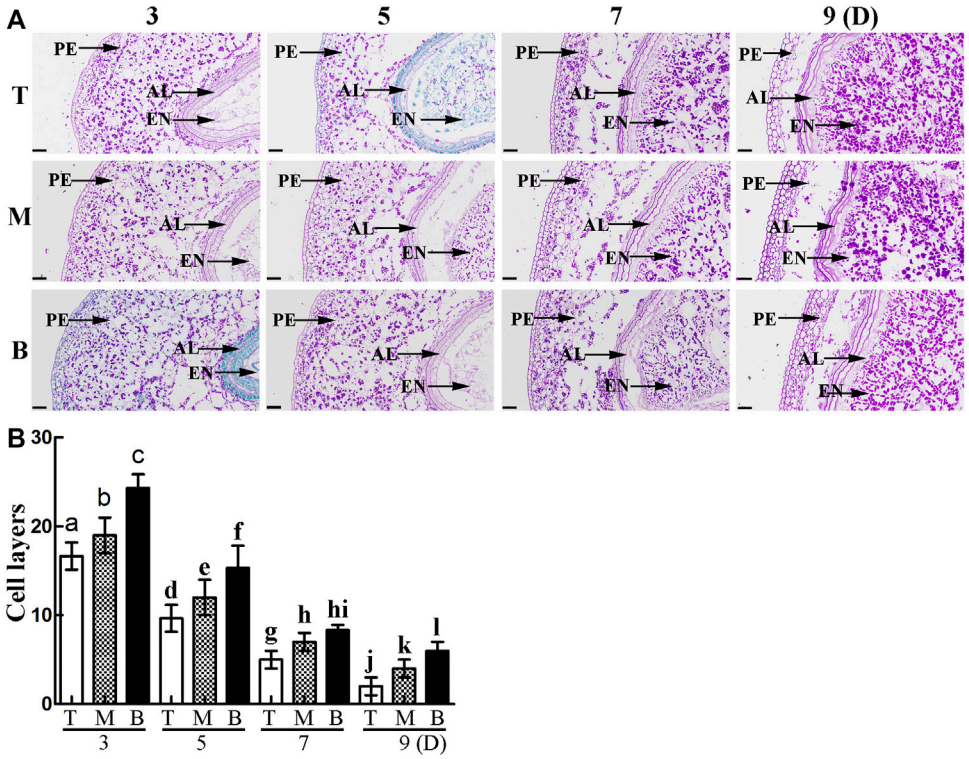

FIGURE 3 | (A). PAS staining showing grain morphology and structure. PE: pericarp, AL: aleurone layer, EN: endosperm. Scale bars: 50 μm. **(B)**. Statistical analysis of cell layers in the pericarp of grains taken from the **top (T), middle (M)** and **bottom (B)** of the spike. Bars represent the mean ± SD of three independent experiments. Asterisks indicate a significant difference as determined by ANOVA., and different letters represent a significant difference between positions on the spike.

GFP, respectively. BSMV-α was then linearized with MIuI, BSMV-β was linearized with SpeI, and BSMVγ-ATG8 and BSMVγ-GFP were linearized with BssHII then the linearized vectors were transcribed *in vitro* to produce 5′-capped infectious BSMV RNA molecules using the RiboMAX Large-Scale RNA Production-T7 Kit (Promega, Madison, WI, United States), with a cap analog added to the transcription mixture. They were then mechanically infected with a 1:1:1 mixture of RNAα, RNAβ and RNAγ-ATG6, or RNAγ- GFP in 1 × GKP buffer (50 mM Gly, 30 mM K2HPO3, 1% bentonite and 1% kieselguhr). In the field, inoculation of BSMV was performed at the heading stage by inoculating 50 spikes with 20 μL of BSMV-ATG8 or BSMV-GFP transcript mixture, respectively.

Immunohistochemistry

Wheat seeds were removed from the spike then treated with 4% paraformaldehyde at 4°C overnight and gradient-dehydrated. The prepared grain tissues were then embedded in paraffin, cut into 7-μm sections, adhered to gelatin-coated glass slides, and dried at 37°C overnight. The slides were then dewaxed, gradient-dehydrated, and digested with 20 μM proteinase K at 37°C for 10 min before blocking in 2% BSA at 37°C for 30 min. Rabbit anti-ATG8 antibody was then added before incubating the slides at 47°C overnight. They were then washed three times with PBS before adding 1 μL secondary antibody (goat anti-rabbit-Alexa Fluor 555 antibody in 10 ml blocking buffer), and incubating at 37°C for 1 h. The nuclei were then stained with 4′, 6-diamidino-2-phenylindole (DAPI) (AnaSpec Inc., San Jose, CA, United States) at room temperature for 10 min. Fluorescence was observed with a fluorescence microscope (HT7700, Hitachi, Tokyo, Japan).

TUNEL Assay

Wheat seeds were removed from the spike then treated with 4% paraformaldehyde at 4°C overnight. A TUNEL assay was then carried out as described previously (Li et al., 2019).

Periodic Acid-Schiff Staining

The paraffin-embedded seeds were transected down the middle, placed in xylene for 20 min, anhydrous ethanol for 5 min, and 75% alcohol for 5 min, and then washed with tap water three times for 30 s each time. The sections were then dyed in periodate dye solution for 10 min, rinsed with tap water then distilled water, and dyed in Schaeffer dye solution for 20 min before a final rinse in running water for 5 min. They were then stained in Hematoxylin solution for 3–5 min, rinsed with tap water, and differentiated in 1% HCl alcohol solution for 30 s. Following a final rinse in tap water, they were then placed in blue-back solution for 5 min before rinsing with running water. The prepared slices were examined under a microscope, and images were collected for analysis of cell structure.

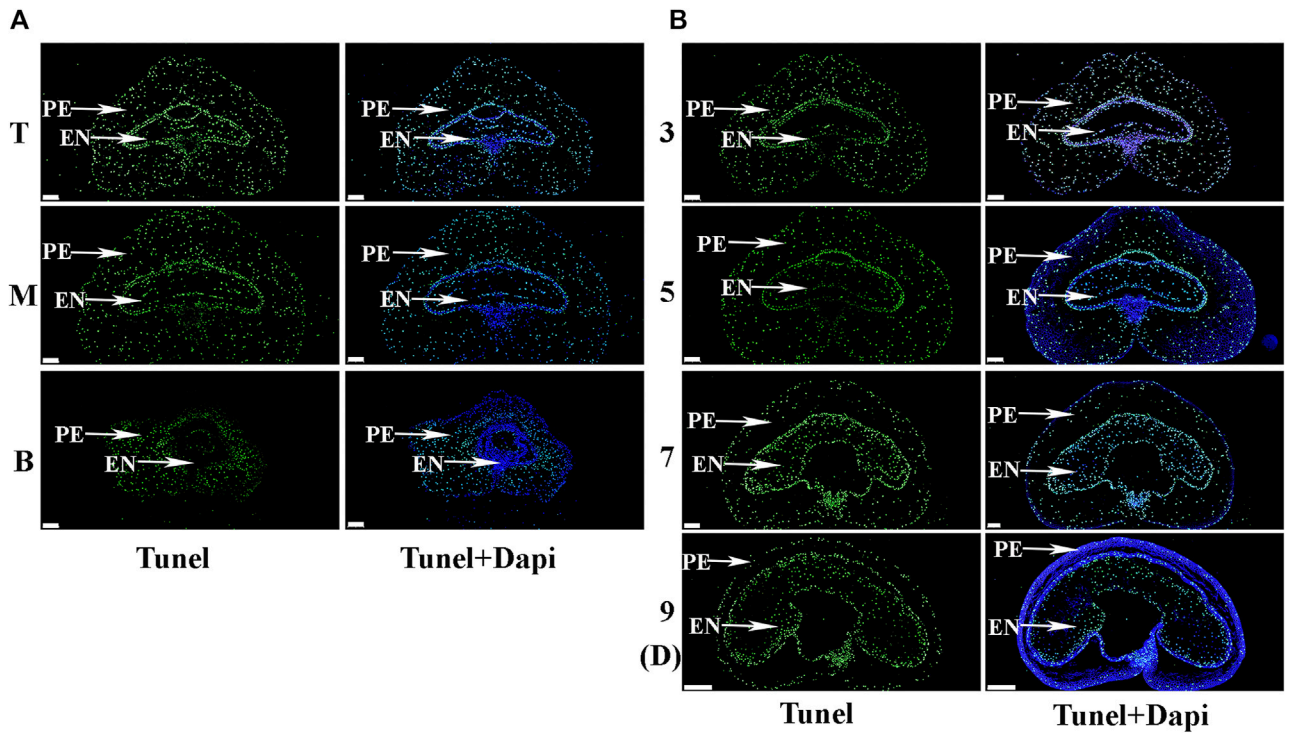

FIGURE 4 | The process of programmed cell death (PCD) in the pericarp during early grain development as detected by TUNEL staining. **(A)**. Images of grains sampled from the **top (T), middle (M)** and **bottom (B)** of the spike 3 days after flowering. PE: pericarp, AL: aleurone layer, EN: endosperm. TUNEL images indicate nuclei following PCD, while DAPI images indicate all nuclei. Scale bars: 200 μm. **(B)**. Grains taken from the middle of the spike 3, 5, 7 and 9 days after flowering. Scale bars: 200 μm.

RESULTS

The Thickness of the Pericarp in the Developing Grains Differs According to the Position on the Spike and the Developmental Stage

It is well known that differences in light, temperature and nutrient supply cause wheat grains to mature at different rates in different positions on the spike. In this study, grains at the top of the spike were premature and small, while those in the middle matured faster and were big and full, and those on the bottom matured late and were also relatively small (**Figure 1**). The thickness of the pericarp was then examined in grains obtained from the top, middle and bottom of the spike at different development stages. Cross-sections revealed that the thickness was smallest at the top of the spike, followed by the middle, then the bottom, with a gradual decrease in thickness with increasing development (**Figures 2A,B**). These results indicate that pericarp thickness significantly differs at different positions on the spike and at different developmental stages.

The Loss of Cell Layers Caused by PCD Results in a Decrease in Pericarp Thickness

To further explore the differences in pericarp thickness, PAS staining was carried out. The results showed that pericarp samples obtained from the top of the spike had the least number of cell layers, followed by those in the middle, with most numerous layers in those from the bottom (**Figure 3A**). The number of cell layers also decreased gradually with increasing development (**Figure 3B**). TUNEL staining is often used to determine PCD in the pericarp (Dominguez et al., 2001), with green fluorescence indicating TUNEL-positive signals in the nuclei indicative of PCD (Zhou et al., 2009). Here, TUNEL signals were extremely intense in pericarp samples from the top of the spike, followed by those in the middle, with weakest signals in those from the bottom, and this trend was consistent for 3 – 9 days after flowering (**Figure 4**). These data suggest that the reduction in pericarp thickness was the result of a loss in cell layers induced by PCD.

Autophagy Is Involved in PCD in the Pericarp

In order to determine the regulatory mechanism underlying PCD, we examined autophagy in the pericarp of developing grains obtained from different positions of the spike and different development stages. QRT-PCR showed that key autophagy-related genes (*ATG4*, *ATG6*, *ATG7*, *ATG8*, and *ATG12*) were highly expressed in samples from the top of the spike, followed by those in the middle, with weakest expression in those from the bottom (**Figure 5**). Moreover, highest peaks

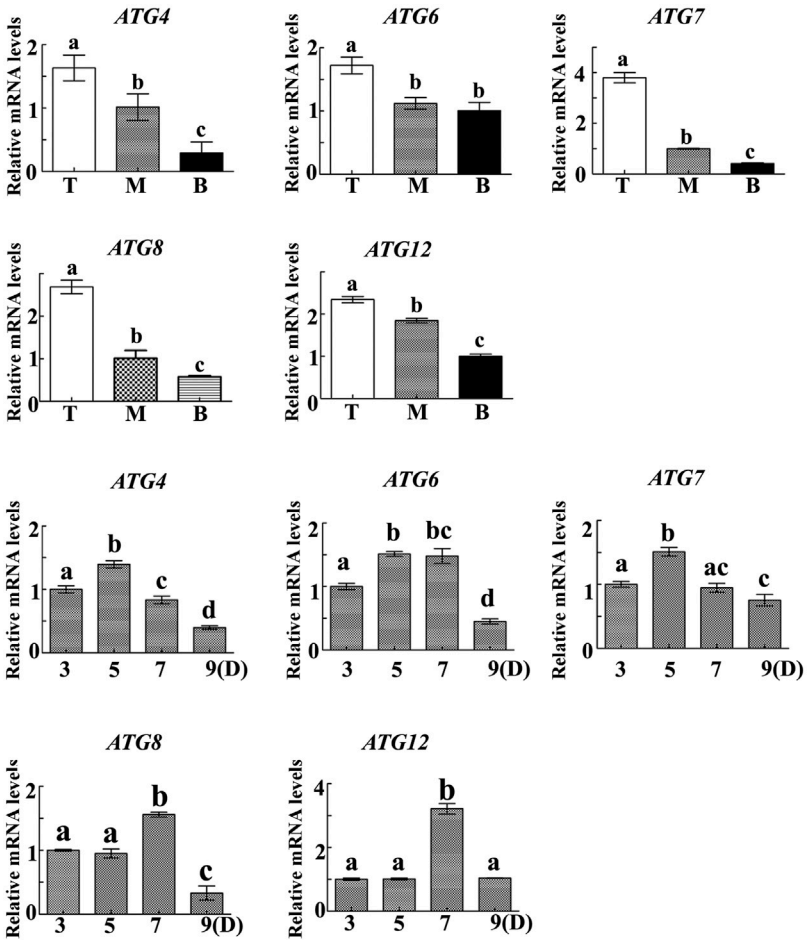

FIGURE 5 | The relative expression of autophagy-related genes in the pericarp of grains taken from the **top (T), middle (M)** and **bottom (B)** of the spike 3, 5, 7 and 9 days after flowering. α-Tubulin was used as an internal reference, and the relative expression was calculated using the $2^{-\Delta\Delta T}$ method. Asterisks indicate significant differences as determined by ANOVA, and different letters represent significant differences between columns.

appeared 5 and 7 days after flowering (**Figure 5**). Western blotting also showed that the band of ATG8-PE was greatest in the top grains followed by those in the middle, with weakest signal in the bottom grains (**Figures 6A–D**). Moreover, expression of ATG8-PE was increasing for 3 - 7 days after flowering (**Figures 6E,F**). In addition, immunohistochemistry showed that most autophagy structures were observed in samples obtained from the top of the spike, followed by those in the middle, with least structures in those from the bottom (**Figure 7**). These results indicate that autophagy increases from the bottom to the top of the spoke, and is involved in the regulation of PCD in the pericarp during early stages of grain development.

Inhibition of Autophagy Increases Pericarp Thickness

In order to determine the effect of autophagy on PCD, we carried out knockdown of the key autophagy gene (*ATG8*). The results showed that interference of *ATG8* (**Figures 8C,D**) resulted in a significant increase in the thickness of the pericarp (**Figures 8A,B**) and the number of cell layers (**Figures 8E,F**), with an obvious delay in the process of PCD (**Figure 8G**). These findings indicate that PCD in the pericarp cells of developing wheat grains is dependent on *ATG8*-mediated autophagy.

Analysis of Wheat Phenotypes After Inhibition of Autophagy

To further examine the effect of autophagy, changes in the wheat phenotype were also examined following knockdown of *ATG8*. The results showed that interference resulted in earlier maturation by 4 days (**Figures 9A,B**), with smaller, less full grains (**Figure 9C**).

DISCUSSION

PCD is central to the development, homeostasis, and integrity of multi-cellular organisms (Ameisen, 2002). In plant cells, extensive chromatin condensation and degradation of nuclear

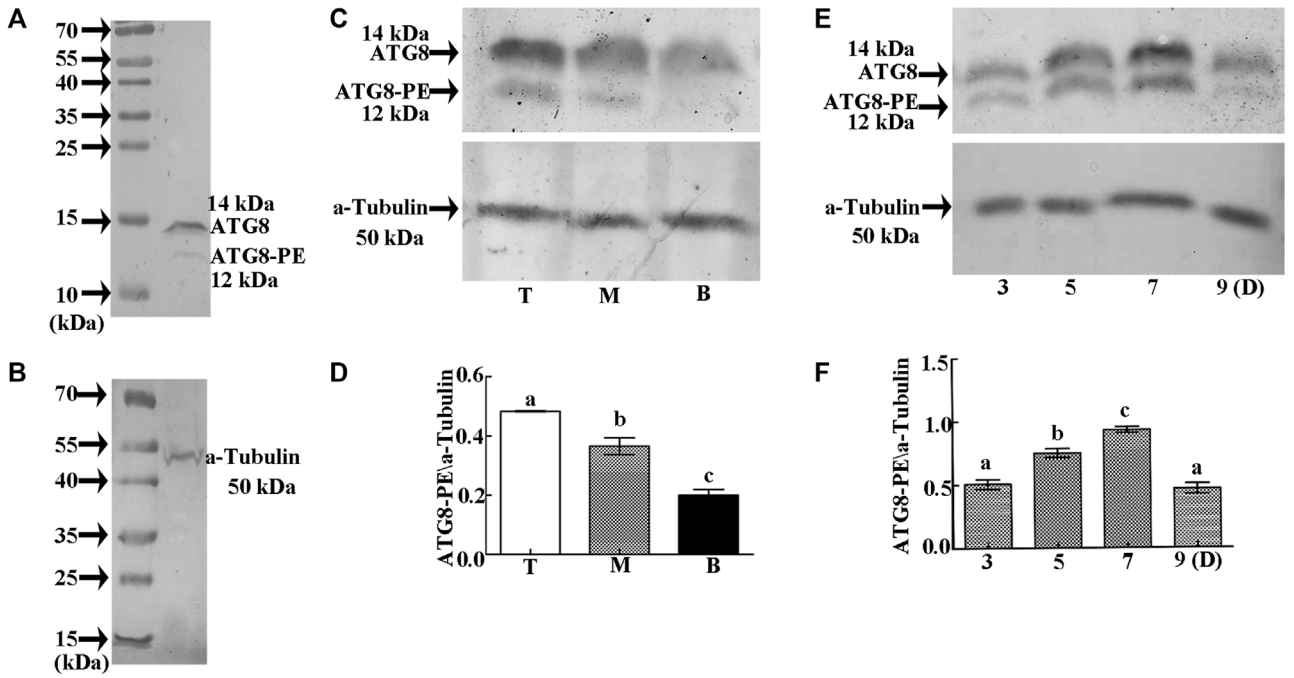

FIGURE 6 | Relative expression of ATG8-PE as detected by Western blotting. **(A)**. Specific detection of ATG8 polyclonal antibody on 15% SDS gel. **(B).** Specific detection of α-tubulin polyclonal antibody on 12.5% SDS gel. **(C).** Relative expression of ATG8-PE in grains taken from the **top (T), middle (M),** and **bottom (B)** of the spike 3 days after flowering. **(D).** Statistical analysis of ATG8-PE expression at each position on the spike. **(E).** Relative expression of ATG8-PE at 3, 5, 7 and 9 days **(D)** after flowering. **(F).** Statistical analysis of ATG8-PE expression at each development stage. β-actin was used as a standard. Data represent the mean ± SD of three independent experiments. Asterisks indicate a significant difference as determined by ANOVA. Different letters represent significant differences between columns.

DNA is one of the most conspicuous features of cells undergoing PCD (Latrasse et al., 2016). For example, during the early development of barley grains, PCD in the pericarp cells provides space and nutrients for subsequent grain filling (Radchuk et al., 2018). Meanwhile, autophagy is responsible for degrading unnecessary components and redistributing nutrients, thereby ensuring normal grain development (Li et al., 2015; Masclaux-Daubresse et al., 2017; Di Berardino et al., 2018). The process of autophagy begins with the formation of a phagophore with a double-membrane cup-shaped structure, which expands to form a double-membrane vesicle called an autophagosome. Upon completion, the autophagosome docks and fuses with the vacuole for cargo degradation (Feng et al., 2014) then the resulting breakdown products are released back into the cytosol to maintain nutrient and energy homeostasis (Yin et al., 2016). However, whether or not autophagy is involved in regulating PCD in the pericarp of developing wheat grains, and the underlying regulatory mechanism, remains unknown. Our data suggest that autophagy is indeed involved, with repression of *ATG8*-mediated autophagy seeming to delay PCD, resulting in an increased thickness and number of cell layers within the pericarp.

High temperatures after anthesis can significantly reduce the grain weight in wheat, thereby causing a reduction in yield (Zahedi et al., 2003; Djanaguiraman et al., 2020). However, grains in different positions of the spike are affected by environmental stress to a differing degree (Yu et al., 2014; Li et al., 2016). Light and temperature stress have the most serious effect on grains at the top of the spike, followed by those in the middle, and lastly, those on the bottom (Steinmeyer et al., 2013). Top grains therefore reach maturity earlier and are smaller in size, while bottom grains mature later, but are also relatively small due to the lack of light and insufficient supply of nutrients. It was previously reported that stress promotes autophagy and PCD in plants (Bassham et al., 2006; Kabbage et al., 2017; Chua et al., 2019). Pericarp and endosperm PCD are necessary for grain maturation (Dominguez and Cejudo, 2014). In this study, both processes occurred most strongly in the pericarp of grains at the top of the spike, followed by those in the middle, and lastly, to a weaker degree, those at the bottom. The top-to-bottom maturation sequence of wheat grain and its peel is actually a process of abiotic stress that causes wheat autophagy and PCD.

Plant development requires specific cells to be eliminated in a predictable and genetically regulated manner referred to as programmed cell death (PCD). However, the target cells do not merely die but they also undergo autophagy to degrade their cellular corpses (Escamez and Tuominen, 2017). In plants, controversy remains over the regulatory effect of autophagy on PCD. One viewpoint is that autophagy negatively regulates PCD; for example, mutation of autophagy was found to result in leaf senescence in Arabidopsis (Hanaoka et al., 2002), and autophagy in plants was found to eliminate reactive oxygen species induced by various abiotic stresses (Avin-Wittenberg, 2019). Meanwhile, the opposing view suggests that

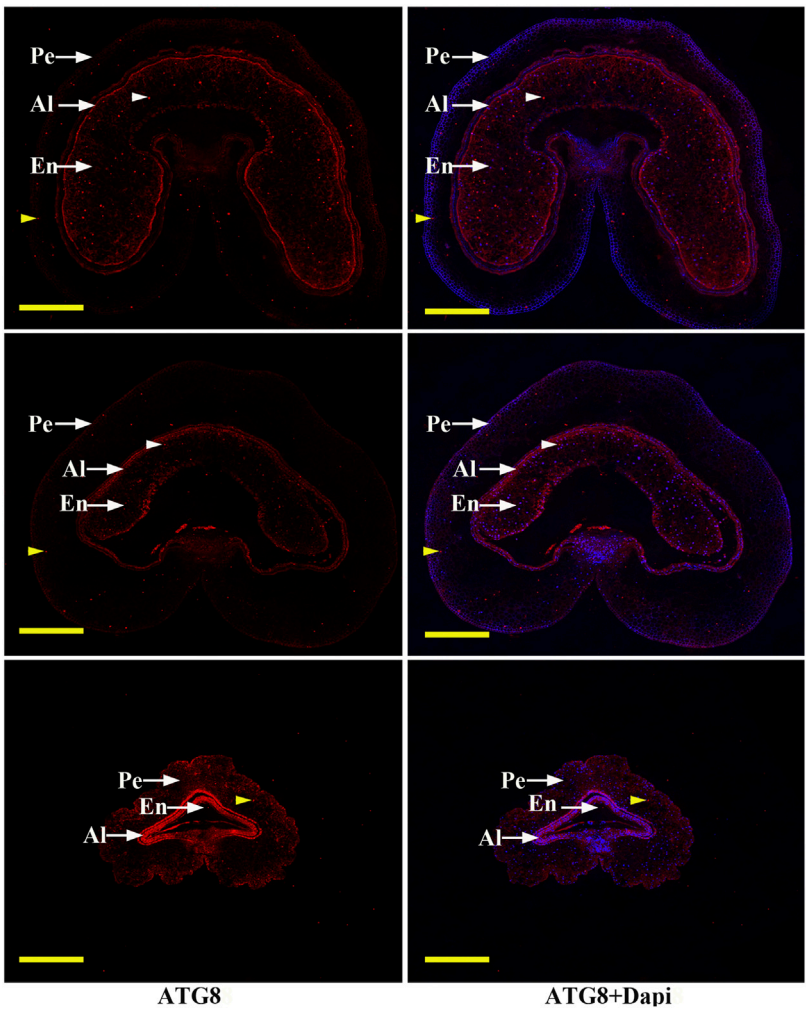

FIGURE 7 | Immunohistochemical analysis of autophagy structures in grains taken from the **top (T), middle (M)** and **bottom (B)** of the spike. Short arrows indicate autophagy structures (brown indicate pericarp autophagy structures, white indicate endosperm autophagy structures). Grains were obtained 3 days after flowering, then the pericarp was stained with DAPI and anti-ATG8 antibody followed by Alexa 555-labeled secondary antibody. PE: pericarp, AL: aleurone layer, EN: endosperm; Scale bars: 200 μm.

autophagy promotes PCD; for example, mutation of autophagy caused degradation of rice pollen tapetum (Kurusu et al., 2014), and autophagic components contributed to hypersensitive cell death in Arabidopsis (Hofius et al., 2009). In this study, however, the characteristics of autophagy and PCD coexisted in the pericarp during early development of the wheat grains, providing an ideal model for studies on the relationship between autophagy and PCD.

Autophagy occurs not only in the pericarp, but also in the embryo and endosperm of grain (Steinmeyer et al., 2013). At the whole-plant level, autophagy is an essential process for nutrient remobilization from leaves to seeds, and is fundamental for seed filling (Avin-Wittenberg, 2019). In *ATG8*-RNAi lines of rice, autophagic activity was slightly inhibited, grain yield and quality were reduced, and grains matured early (Fan et al., 2020). In our study, knockdown of wheat *ATG8* also resulted in early maturity and smaller grains. The main reason is that inhibition of *ATG8*-mediated autophagy leads to the decrease of nutrient recycling into wheat grains. So, it can be inferred that other spike positions will also show the corresponding phenomena of smaller grains and early maturity after *ATG8* interference.

The *ATG8* gene is an evolutionarily conserved gene that is expressed in various plant tissues (Boycheva Woltering and Isono, 2020). In rice, *ATG8* interference lines exhibited abnormal roots, a reduced number of grains per panicle, and other unfavorable agronomic traits (Fan et al., 2020). It is therefore difficult to rule out the negative effects of *ATG8* knockout on other agronomic traits in analysis of grain phenotypes. In this study, we therefore carried our BSMV-mediated transient interference of *ATG8* to minimize interference of other agronomic traits. As a result, PCD was weakened, and the thickness of the pericarp increased, suggesting strong dependency on ATG8-mediated autophagy, and a positive regulatory effect. Overall, the findings suggest that positive and negative regulation of PCD by autophagy

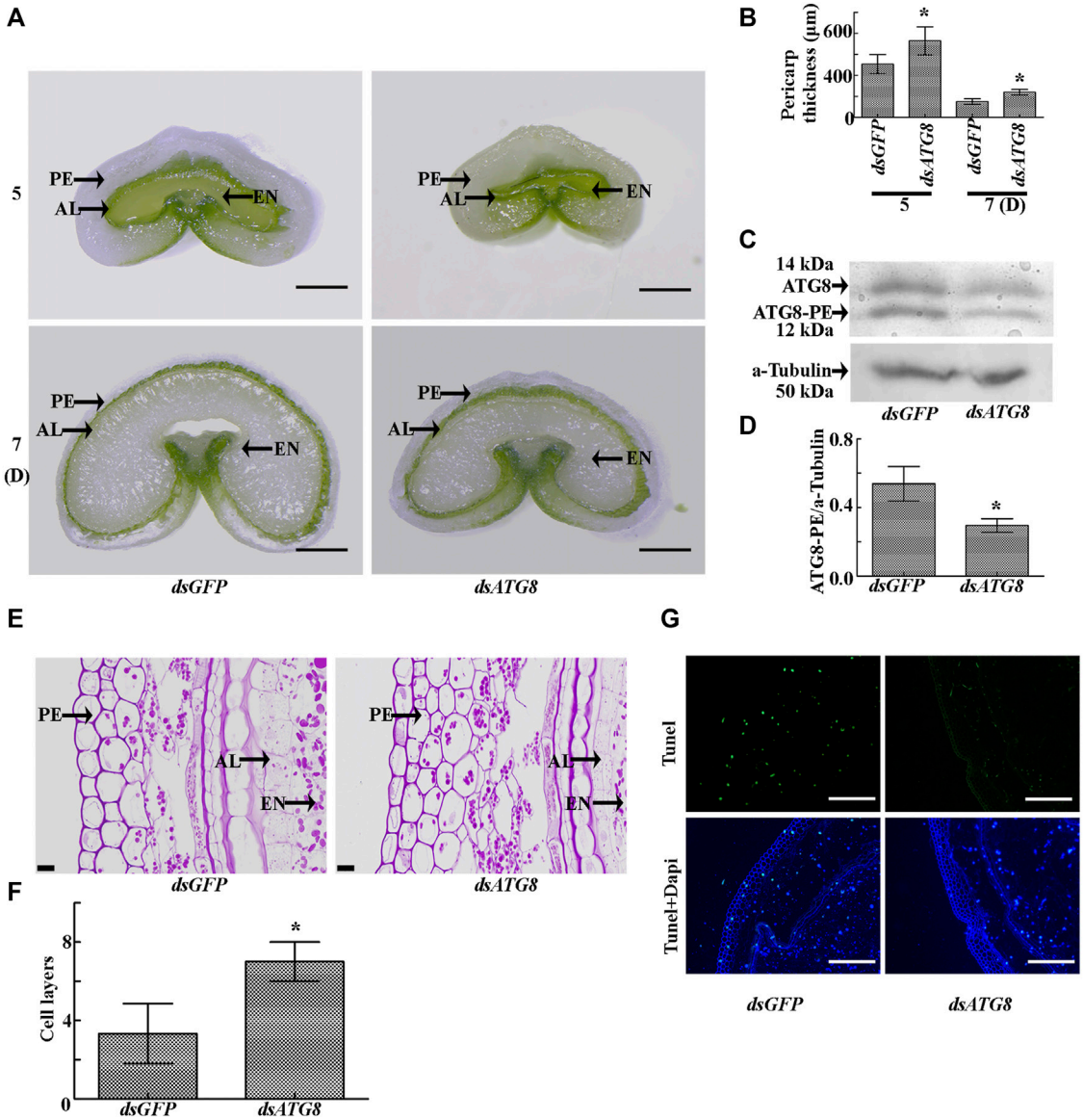

FIGURE 8 | Morphology of the grains after knockdown of *ATG8*. **(A)**. Cross sections of grains sampled five and 7 days after flowering following *ATG8* knockdown. dsGFP was used as a control. PE: pericarp, AL: aleurone layer, EN: endosperm; Scale bars: 500 μm. **(B).** Statistical analysis of pericarp thickness following *ATG8* knockdown. Asterisks indicate a significant difference based on the Student's t-test, $p < 0.05$. **(C).** Knockdown efficiency of *ATG8* as determined by Western blotting. α-tubulin was used as the internal reference. **(D).** Statistical analysis of the knockdown efficiency of *ATG8*. Asterisks indicate a significant difference based on the Student's t-test, $p < 0.05$. **(E).** PAS staining 7 days after flowering showing the morphology and structure of the grains following *ATG8* knockdown. Scale bars: 20 μm. **(F).** Statistical analysis of pericarp cell layers following *ATG8* knockdown. Bars represent the mean ± SD of three independent experiments. Asterisks indicate a significant difference according to the Student's t-test, $p < 0.05$. **(G).** TUNEL staining 7 days after flowering showing the morphology and structure of the grains following *ATG8* knockdown. Scale bars: 50 μm.

mainly depends on the types of plant tissue and stress. Autophagy is dependent on a set of autophagy-related (ATG) proteins, of which the ubiquitin-like protein ATG8 plays a central role, functioning in autophagosome formation, and mediating membrane tethering, elongation and fusion (Nakatogawa et al., 2007). Upon autophagy activation, ATG8 undergoes lipidation to generate a membrane-bound ATG8-phosphatidylethanolamine (ATG8-PE) conjugate that localizes on growing phagophores and autophagosomes. ATG8 proteins are therefore often used as reliable markers to assess the induction and progression of autophagy (Yoshimoto et al., 2004). In this study, ATG8 was required for PCD in the pericarp of developing wheat grains. ATG8 lipidation occurs in both the outer and inner membrane of the phagophore, the precursor to autophagosomes, and is involved in autophagosome formation, as well as the recognition of specific cargo specifically targeted for autophagy (Kellner et al., 2017). These cargo receptors then interact with ATG8 proteins *via* short peptide motifs known as AIMs (ATG8-family interacting motifs) (Fracchiolla et al., 2017). Vacuolar processing enzymes (VPEs), a class of conserved cysteine proteases, are also involved in plant

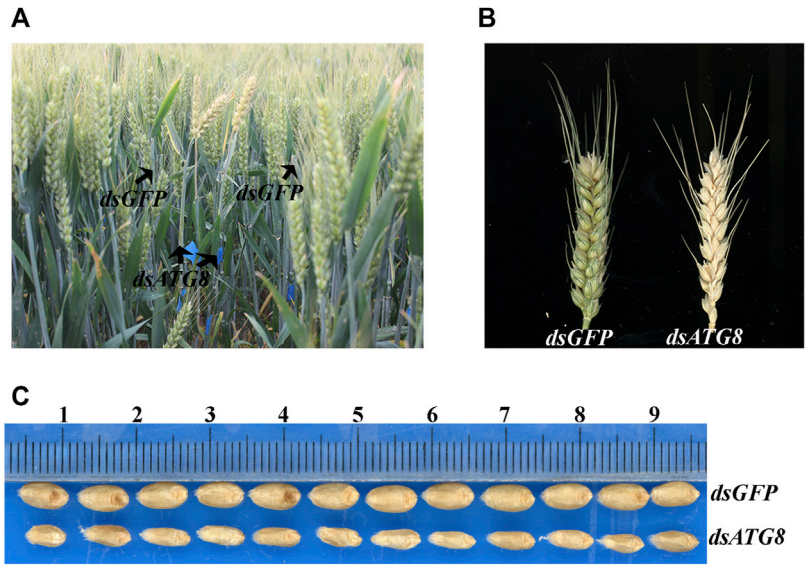

FIGURE 9 | Phenotype of wheat following *ATG8* knockdown. **(A)**. The phenotype of wheat in the field 25 days after flowering following *ATG8* knockdown. **(B)**. The phenotype of the spike 25 days after flowering. **(C)**. mature grains following *ATG8* knockdown.

PCD (Hatsugai et al., 2004; Rojo et al., 2004). For example, VPE4 in barley is required for PCD in the pericarp during grain development (Radchuk et al., 2018), while VPE1 in tomato is translocated to the vacuole through the autophagy pathway, co-localizing with ATG8 in the autophagosomes and autolysosomes to induce PCD (Teper-Bamnolker et al., 2020). However, whether VPE1 interacts with ATG8, and is transported to the vacuole to exert its function on PCD requires further clarification.

CONCLUSION

The findings of this study suggest that autophagy and PCD coexist in the pericarp during the early development of wheat grains. Moreover, autophagy and PCD increased from the bottom to the top of the spike, and PCD was dependent on *ATG8*-mediated autophagy. Meanwhile, following knockdown of *ATG8*, the thickness of the pericarp increased, resulting in small premature grains. Overall, this dependence between autophagy and PCD determines the early development of grain pericarp.

DATA AVAILABILITY STATEMENT

The datasets presented in this study can be found in online repositories. The names of the repository/repositories and accession number(s) can be found below: https://www.ncbi.nlm.nih.gov/genbank/, KF294798.1 https://www.ncbi.nlm.nih.gov/genbank/, AM075827.1 https://www.ncbi.nlm.nih.gov/genbank/, KF294804.1 https://www.ncbi.nlm.nih.gov/genbank/, FJ750848.1 https://www.ncbi.nlm.nih.gov/genbank/, KF294819.1 https://www.ncbi.nlm.nih.gov/genbank/, U76558.1.

AUTHOR CONTRIBUTIONS

Y-BL performed most of the experiments. MY, D-ZC, FZ-G, Q-QF, and CH analyzed the data. X-XS and X-SC conceived and coordinated the study and edited the paper. All authors reviewed the results and approved the final version of the manuscript. All co-authors have checked and confirmed their contribution statement.

FUNDING

This work was supported by grants from the National Natural Science Foundation of China (32001542), Shandong Natural Science Foundation (ZR2020QC114), Open Project of State Key Laboratory for Wheat and Maize Engineering (2018LYZWS06) and Innovation Project of Shandong Academy of Agricultural Sciences Key Techniques of Crop Breeding (CXGC 2021A09).

REFERENCES

Ameisen, J. C. (2002). On the Origin, Evolution, and Nature of Programmed Cell Death: a Timeline of Four Billion Years. *Cell Death Differ* 9, 367–393. doi:10.1038/sj.cdd.4400950

Avin-Wittenberg, T. (2019). Autophagy and its Role in Plant Abiotic Stress Management. *Plant Cel Environ* 42, 1045–1053. doi:10.1111/pce.13404

Bassham, D. C., Laporte, M., Marty, F., Moriyasu, Y., Ohsumi, Y., Olsen, L. J., et al. (2006). Autophagy in Development and Stress Responses of Plants. *Autophagy* 2, 2–11. doi:10.4161/auto.2092

Boycheva Woltering, S., and Isono, E. (2020). Knowing when to Self-Eat - Fine-Tuning Autophagy through ATG8 Iso-Forms in Plants. *Front. Plant Sci.* 11, 579875. doi:10.3389/fpls.2020.579875

Bozhkov, P. V. (2018). Plant Autophagy: Mechanisms and Functions. *J. Exp. Bot.* 69, 1281–1285. doi:10.1093/jxb/ery070

Bradford, M. M. (1976). A Rapid and Sensitive Method for the Quantitation of Microgram Quantities of Protein Utilizing the Principle of Protein-Dye Binding. *Anal. Biochem.* 72, 248–254. doi:10.1016/0003-2697(76)90527-3

Brinton, J., Simmonds, J., Minter, F., Leverington-Waite, M., Snape, J., and Uauy, C. (2017). Increased Pericarp Cell Length Underlies a Major Quantitative Trait Locus for Grain Weight in Hexaploid Wheat. *New Phytol.* 215, 1026–1038. doi:10.1111/nph.14624

Chua, A., Fitzhenry, L., and Daly, C. T. (2019). Sorting the Wheat from the Chaff: Programmed Cell Death as a Marker of Stress Tolerance in Agriculturally Important Cereals. *Front. Plant Sci.* 10, 1539. doi:10.3389/fpls.2019.01539

Di Berardino, J., Marmagne, A., Berger, A., Yoshimoto, K., Cueff, G., Chardon, F., et al. (2018). Autophagy Controls Resource Allocation and Protein Storage Accumulation in Arabidopsis Seeds. *J. Exp. Bot.* 69, 1403–1414. doi:10.1093/jxb/ery012

Djanaguiraman, M., Narayanan, S., Erdayani, E., and Prasad, P. V. V. (2020). Effects of High Temperature Stress during Anthesis and Grain Filling Periods on Photosynthesis, Lipids and Grain Yield in Wheat. *BMC Plant Biol.* 20, 268. doi:10.1186/s12870-020-02479-0

Domínguez, F., and Cejudo, F. J. (2014). Programmed Cell Death (PCD): an Essential Process of Cereal Seed Development and Germination. *Front. Plant Sci.* 5, 366. doi:10.3389/fpls.2014.00366

Domínguez, F., Moreno, J., and Cejudo, F. J. (2001). The Nucellus Degenerates by a Process of Programmed Cell Death during the Early Stages of Wheat Grain Development. *Planta* 213, 352–360. doi:10.1007/s004250000517

Dong, J., Zheng, Y., Fu, Y., Wang, J., Yuan, S., Wang, Y., et al. (2019). PDIL1-2 Can Indirectly and Negatively Regulate Expression of the AGPL1 Gene in Bread Wheat. *Biol. Res.* 52, 56. doi:10.1186/s40659-019-0263-2

Escamez, S., and Tuominen, H. (2017). Contribution of Cellular Autolysis to Tissular Functions during Plant Development. *Curr. Opin. Plant Biol.* 35, 124–130. doi:10.1016/j.pbi.2016.11.017

Fan, T., Yang, W., Zeng, X., Xu, X., Xu, Y., Fan, X., et al. (2020). A Rice Autophagy Gene OsATG8b Is Involved in Nitrogen Remobilization and Control of Grain Quality. *Front. Plant Sci.* 11, 588. doi:10.3389/fpls.2020.00588

Feng, Y., He, D., Yao, Z., and Klionsky, D. J. (2014). The Machinery of Macroautophagy. *Cell Res* 24, 24–41. doi:10.1038/cr.2013.168

Foxon, G. A., Catt, L., and Keeling, P. L. (1990). Starch Synthesis in Developing Wheat Grain : The Effect of Light on Endosperm Starch Synthesis *In Vitro* and *In Vivo*. *Planta* 181, 104–108. doi:10.1007/BF00202331

Fracchiolla, D., Sawa-Makarska, J., and Martens, S. (2017). Beyond Atg8 Binding: The Role of AIM/LIR Motifs in Autophagy. *Autophagy* 13, 978–979. doi:10.1080/15548627.2016.1277311

Fujita, N., and Taira, T. (1998). A 56-kDa Protein Is a Novel Granule-Bound Starch Synthase Existing in the Pericarps, Aleurone Layers, and Embryos of Immature Seed in Diploid Wheat (Triticum Monococcum L.). *Planta* 207, 125–132. doi:10.1007/s004250050464

Ghosh, A., Jana, M., Modi, K., Gonzalez, F. J., Sims, K. B., Berry-Kravis, E., et al. (2015). Activation of Peroxisome Proliferator-Activated Receptor α Induces Lysosomal Biogenesis in Brain Cells. *J. Biol. Chem.* 290, 10309–10324. doi:10.1074/jbc.m114.610659

Hanaoka, H., Noda, T., Shirano, Y., Kato, T., Hayashi, H., Shibata, D., et al. (2002). Leaf Senescence and Starvation-Induced Chlorosis Are Accelerated by the Disruption of an Arabidopsis Autophagy Gene. *Plant Physiol.* 129, 1181–1193. doi:10.1104/pp.011024

Hatsugai, N., Kuroyanagi, M., Yamada, K., Meshi, T., Tsuda, S., Kondo, M., et al. (2004). A Plant Vacuolar Protease, VPE, Mediates Virus-Induced Hypersensitive Cell Death. *Science* 305, 855–858. doi:10.1126/science.1099859

Hofius, D., Schultz-Larsen, T., Joensen, J., Tsitsigiannis, D. I., Petersen, N. H. T., Mattsson, O., et al. (2009). Autophagic Components Contribute to Hypersensitive Cell Death in Arabidopsis. *Cell* 137, 773–783. doi:10.1016/j.cell.2009.02.036

Kabbage, M., Kessens, R., Bartholomay, L. C., and Williams, B. (2017). The Life and Death of a Plant Cell. *Annu. Rev. Plant Biol.* 68, 375–404. doi:10.1146/annurev-arplant-043015-111655

Kellner, R., De La Concepcion, J. C., Maqbool, A., Kamoun, S., and Dagdas, Y. F. (2017). ATG8 Expansion: A Driver of Selective Autophagy Diversification? *Trends Plant Sci.* 22, 204–214. doi:10.1016/j.tplants.2016.11.015

Kurusu, T., Koyano, T., Hanamata, S., Kubo, T., Noguchi, Y., Yagi, C., et al. (2014). OsATG7 Is Required for Autophagy-dependent Lipid Metabolism in rice Postmeiotic Anther Development. *Autophagy* 10, 878–888. doi:10.4161/auto.28279

Latrasse, D., Benhamed, M., Bergounioux, C., Raynaud, C., and Delarue, M. (2016). Plant Programmed Cell Death from a Chromatin point of View. *Exbotj* 67, 5887–5900. doi:10.1093/jxb/erw329

Li, F., Chung, T., Pennington, J. G., Federico, M. L., Kaeppler, H. F., Kaeppler, S. M., et al. (2015). Autophagic Recycling Plays a central Role in maize Nitrogen Remobilization. *Plant Cell* 27, 1389–1408. doi:10.1105/tpc.15.00158

Li, Y. B., Cui, D. Z., Sui, X. X., Huang, C., Huang, C. Y., Fan, Q. Q., et al. (2019). Autophagic Survival Precedes Programmed Cell Death in Wheat Seedlings Exposed to Drought Stress. *Int. J. Mol. Sci.* 20, 5777. doi:10.3390/ijms20225777

Li, Y., Cui, Z., Ni, Y., Zheng, M., Yang, D., Jin, M., et al. (2016). Plant Density Effect on Grain Number and Weight of Two Winter Wheat Cultivars at Different Spikelet and Grain Positions. *PLoS One* 11, e0155351. doi:10.1371/journal.pone.0155351

Lin, Z., Wang, Y.-L., Cheng, L.-S., Zhou, L.-L., Xu, Q.-T., Liu, D.-C., et al. (2021). Mutual Regulation of ROS Accumulation and Cell Autophagy in Wheat Roots under Hypoxia Stress. *Plant Physiol. Biochem.* 158, 91–102. doi:10.1016/j.plaphy.2020.11.049

Liu, W., Cai, M.-J., Wang, J.-X., and Zhao, X.-F. (2014). In a Nongenomic Action, Steroid Hormone 20-hydroxyecdysone Induces Phosphorylation of Cyclin-dependent Kinase 10 to Promote Gene Transcription. *Endocrinology* 155, 1738–1750. doi:10.1210/en.2013-2020

Ma, M., Yan, Y., Huang, L., Chen, M., and Zhao, H. (2012). Virus-induced Gene-Silencing in Wheat Spikes and Grains and its Application in Functional Analysis of HMW-GS-Encoding Genes. *BMC Plant Biol.* 12, 141. doi:10.1186/1471-2229-12-141

Masclaux-Daubresse, C., Chen, Q., and Havé, M. (2017). Regulation of Nutrient Recycling via Autophagy. *Curr. Opin. Plant Biol.* 39, 8–17. doi:10.1016/j.pbi.2017.05.001

Nakatogawa, H., Ichimura, Y., and Ohsumi, Y. (2007). Atg8, a Ubiquitin-like Protein Required for Autophagosome Formation, Mediates Membrane Tethering and Hemifusion. *Cell* 130, 165–178. doi:10.1016/j.cell.2007.05.021

Pei, D., Zhang, W., Sun, H., Wei, X., Yue, J., and Wang, H. (2014). Identification of Autophagy-Related Genes ATG4 and ATG8 from Wheat (*Triticum aestivum* L.) and Profiling of Their Expression Patterns Responding to Biotic and Abiotic Stresses. *Plant Cel Rep* 33, 1697–1710. doi:10.1007/s00299-014-1648-x

Pennell, R. I., and Lamb, C. (1997). Programmed Cell Death in Plants. *Plant Cell* 9, 1157–1168. doi:10.1105/tpc.9.7.1157

Radchuk, V., Tran, V., Radchuk, R., Diaz-Mendoza, M., Weier, D., Fuchs, J., et al. (2018). Vacuolar Processing Enzyme 4 Contributes to Maternal Control of Grain Size in Barley by Executing Programmed Cell Death in the Pericarp. *New Phytol.* 218, 1127–1142. doi:10.1111/nph.14729

Radchuk, V., Weier, D., Radchuk, R., Weschke, W., and Weber, H. (2011). Development of Maternal Seed Tissue in Barley Is Mediated by Regulated Cell Expansion and Cell Disintegration and Coordinated with Endosperm Growth. *J. Exp. Bot.* 62, 1217–1227. doi:10.1093/jxb/erq348

Rojo, E., Martı´n, R., Carter, C., Zouhar, J., Pan, S., Plotnikova, J., et al. (2004). VPEγ Exhibits a Caspase-like Activity that Contributes to Defense against Pathogens. *Curr. Biol.* 14, 1897–1906. doi:10.1016/j.cub.2004.09.056

Steinmeyer, F. T., Lukac, M., Reynolds, M. P., and Jones, H. E. (2013). Quantifying the Relationship between Temperature Regulation in the Ear and Floret Development Stage in Wheat (*Triticum aestivum* L.) under Heat and Drought Stress. *Funct. Plant Biol.* 40, 700–707. doi:10.1071/fp12362

Teper-Bamnolker, P., Danieli, R., Peled-Zehavi, H., Belausov, E., Abu-Abied, M., Avin-Wittenberg, T., et al. (2020). Vacuolar Processing Enzyme Translocates to the Vacuole through the Autophagy Pathway to Induce Programmed Cell Death. *Autophagy* 17, 1–15. doi:10.1080/15548627.2020.1856492

Üstün, S., Hafrén, A., and Hofius, D. (2017). Autophagy as a Mediator of Life and Death in Plants. *Curr. Opin. Plant Biol.* 40, 122–130. doi:10.1016/j.pbi.2017.08.011

Valitova, J., Renkova, A., Mukhitova, F., Dmitrieva, S., Beckett, R. P., and Minibayeva, F. V. (2019). Membrane Sterols and Genes of Sterol

Biosynthesis Are Involved in the Response of *Triticum aestivum* Seedlings to Cold Stress. *Plant Physiol. Biochem.* 142, 452–459. doi:10.1016/j.plaphy.2019.07.026

Wang, N., and Fisher, D. B. (1994). The Use of Fluorescent Tracers to Characterize the Post-Phloem Transport Pathway in Maternal Tissues of Developing Wheat Grains. *Plant Physiol.* 104, 17–27. doi:10.1104/pp.104.1.17

Xiong, F., Yu, X. R., Zhou, L., Wang, F., and Xiong, A. S. (2013). Structural and Physiological Characterization during Wheat Pericarp Development. *Plant Cel Rep* 32, 1309–1320. doi:10.1007/s00299-013-1445-y

Yin, Z., Pascual, C., and Klionsky, D. (2016). Autophagy: Machinery and Regulation. *Microb. Cel* 3, 588–596. doi:10.15698/mic2016.12.546

Yoshimoto, K., Hanaoka, H., Sato, S., Kato, T., Tabata, S., Noda, T., et al. (2004). Processing of ATG8s, Ubiquitin-like Proteins, and Their Deconjugation by ATG4s Are Essential for Plant Autophagy. *Plant Cell* 16, 2967–2983. doi:10.1105/tpc.104.025395

Yu, A., Li, Y., Ni, Y., Yang, W., Yang, D., Cui, Z., et al. (2014). Differences of Starch Granule Distribution in Grains from Different Spikelet Positions in winter Wheat. *PLoS One* 9, e114342. doi:10.1371/journal.pone.0114342

Yu, X., Li, B., Wang, L., Chen, X., Wang, W., Wang, Z., et al. (2015). Systematic Analysis of Pericarp Starch Accumulation and Degradation during Wheat Caryopsis Development. *PLoS One* 10, e0138228. doi:10.1371/journal.pone.0138228

Yue, J.-y., Wang, Y.-j., Jiao, J.-l., and Wang, H.-z. (2021). Silencing of ATG2 and ATG7 Promotes Programmed Cell Death in Wheat via Inhibition of Autophagy under Salt Stress. *Ecotoxicology Environ. Saf.* 225, 112761. doi:10.1016/j.ecoenv.2021.112761

Zahedi, M., Sharma, R., and Jenner, C. F. (2003). Effects of High Temperature on Grain Growth and on the Metabolites and Enzymes in the Starch-Synthesis Pathway in the Grains of Two Wheat Cultivars Differing in Their Responses to Temperature. *Funct. Plant Biol.* 30, 291–300. doi:10.1071/fp02205

Zhou, L.-L., Gao, K.-Y., Cheng, L.-S., Wang, Y.-L., Cheng, Y.-K., Xu, Q.-T., et al. (2021). Short-term Waterlogging-Induced Autophagy in Root Cells of Wheat Can Inhibit Programmed Cell Death. *Protoplasma* 258, 891–904. doi:10.1007/s00709-021-01610-8

Zhou, Z., Wang, L., Li, J., Song, X., and Yang, C. (2009). Study on Programmed Cell Death and Dynamic Changes of Starch Accumulation in Pericarp Cells of *Triticum aestivum* L.*. *Protoplasma* 236, 49–58. doi:10.1007/s00709-009-0046-7

Conflict of Interest: The authors declare that the research was conducted in the absence of any commercial or financial relationships that could be construed as a potential conflict of interest.

Publisher's Note: All claims expressed in this article are solely those of the authors and do not necessarily represent those of their affiliated organizations, or those of the publisher, the editors and the reviewers. Any product that may be evaluated in this article, orclaim that may be made by its manufacturer, is not guaranteed or endorsed by the publisher.

frontiers in Genetics

ORIGINAL RESEARCH
published: 04 February 2022
doi: 10.3389/fgene.2022.832013

Screening of Salt-Tolerant *Thinopyrum ponticum* Under Two Coastal Region Salinity Stress Levels

Chunyan Tong[1,2], *Guotang Yang*[1,3], *AoenBolige*[2], *Terigen*[2], *Hongwei Li*[1], *Bin Li*[1], *Zhensheng Li*[1] *and Qi Zheng*[1]*

[1]State Key Laboratory of Plant Cell and Chromosome Engineering, Institute of Genetics and Developmental Biology, The Innovative Academy of Seed Design, Chinese Academy of Sciences, Beijing, China, [2]College of Life Science and Technology, Inner Mongolia Normal University, Hohhot, China, [3]University of Chinese Academy of Sciences, Beijing, China

To accelerate the exploitation and use of marginal soils and develop salt-tolerant forage germplasm suitable for the coastal regions of China, seven lines of decaploid tall wheatgrass [*Thinopyrum ponticum* (Podp.) Barkworth and D. R. Dewey, $2n = 10x = 70$] were transplanted under low (.3%) and high (.5%) salt conditions for a comprehensive analysis at the adult-plant stage. Differences were observed among these materials, especially in terms of grass yield, agronomic characteristics, and physiological and biochemical indices. Line C2 grew best with the highest shoot total fresh and dry weights under all conditions except for the milk-ripe stage in Dongying in 2019. The total membership value of C2 also reflected its excellent performance after transplanting. As superior germplasm, its relatively high antioxidant enzyme activities and chlorophyll *a/b* ratio suggested C2 may maintain normal metabolic and physiological functions under saline conditions. Furthermore, decaploid tall wheatgrass as a forage grass species has a high nutritive value beneficial for animal husbandry. Accordingly, line C2 may be used as excellent germplasm to develop salt-tolerant cultivars in the Circum-Bohai sea.

Keywords: *Thinopyrum ponticum*, salt tolerance, adult-plant stage, agronomic traits, physiological index, nutrient content

OPEN ACCESS

Edited by:
Pengtao Ma,
Yantai University, China

Reviewed by:
Xu Hongxing,
Henan University, China
Lei Chen,
Yantai University, China

***Correspondence:**
Qi Zheng
qzheng@genetics.ac.cn

Specialty section:
This article was submitted to Plant Genomics, a section of the journal Frontiers in Genetics

Received: *09 December 2021*
Accepted: *10 January 2022*
Published: *04 February 2022*

Citation:
Tong C, Yang G, AoenBolige, Terigen, Li H, Li B, Li Z and Zheng Q (2022) Screening of Salt-Tolerant Thinopyrum ponticum *Under Two Coastal Region Salinity Stress Levels. Front. Genet. 13:832013. doi: 10.3389/fgene.2022.832013*

INTRODUCTION

Soil salinization is a major environmental stress factor that inhibits normal plant growth while also leading to soil degradation and significant deterioration of the global ecosystem (Bazihizina et al., 2012; Ding et al., 2021). More than 800 million hectares (6.5%) of the land area worldwide contain saline-alkali soil (FAO, 2017; Zhang et al., 2018). In China, the related figure is 100 million, of which over 80% are undeveloped (Xie et al., 2021). Salinized soils, which are mainly distributed in the northwestern, northern, northeastern, and coastal regions of China, result from seawater impregnation, volcanic movement, salt bioaccumulation, uplift of saline groundwater, and agricultural irrigation (Wang et al., 2020). The most effective and environmentally friendly methods for controlling soil salinization involve the absorption, transformation, or transfer of salt from the soil *via* the metabolic and growth activities of plants and microorganisms. Cultivating salt-tolerant crops on salinized land may lead to increased transpiration, decreased groundwater levels, and inhibited soil salinization (Qadir and Oster, 2004). For the past decade, studies on many forage species, such as *Leymus chinensis* (Wang et al., 1994), *Achnatherum splendens* (Xu et al., 2008), and *Hordeum jubatum* L. (Chen

et al., 2021), revealed that these species have adapted to salinized soil, suggesting they are useful for controlling and improving salinized soils.

Decaploid tall wheatgrass [*Thinopyrum ponticum* (Podp.) Barkworth and D. R. Dewey, $2n = 10x = 70$, syn. *Agropyron elongatum* (Host) P. Beauv., *Elytrigia pontica* (Podp.) Holub, and *Lophopyrum ponticum* (Podp.) Á Löve] is a perennial forage grass species and an essential wild relative to improving wheat (Shannon, 1978; Sharma et al., 1989). Previous study indicated that it had stronger salt tolerance than most monocotyledonous species, such as rice, wheat, and barley, and some dicotyledonous species, such as alfalfa (Munns and Tester, 2008). Colmer et al. (2006) determined that several *Th. ponticum* accessions could survive a treatment with 750 mM NaCl and some could grow reasonably well at an electrical conductivity of 13.9 $dS{\cdot}m^{-1}$. Additionally, the enhanced salt tolerance of *Lophopyrum elongatum*, which is an ancestor of *Th. ponticum*, appears to be mediated by genes on chromosomes $2E^e$, $3E^e$, $4E^e$, and $7E^e$ (Dvořák et al., 1988). Furthermore, chromosome $3E^e$ was linked to a 50% decrease in Na^+ accumulation in the flag leaf (Omielan et al., 1991). Researchers subsequently used the *ph1b* mutant to induce the homoeologous recombination between chromosome $3E^e$ and wheat chromosomes 3A and 3D. An examination of the resulting recombinant lines revealed that the lines with the smallest alien segments exhibited the sodium exclusion trait (Mullan et al., 2009). Moreover, chromosome $5E^b$ of *Th. bessarabicum*, which is another ancestor of *Th. ponticum*, includes at least one major dominant gene for salt tolerance (Forster et al., 1988; King et al., 1997). Thus, *Th. ponticum* chromosomal segments likely carry genes that can be used to increase the salt tolerance of wheat. For example, the dominant salt tolerance gene block in the genome of the wheat-*Th. ponticum* translocation line S148 was detected by a salinity test involving the backcross progenies of S148 and Chinese Spring (Yuan and Tomita, 2015). The saline-tolerant cultivar Shanrong No. 3, which was produced from a somatic hybridization between bread wheat and tall wheatgrass, is a valuable genetic resource for characterizing the mechanisms underlying salt tolerance. Its excellent growth recovery, ionic homeostasis, and ability to excrete toxic products were demonstrated by two-dimensional gel electrophoresis and mass spectrometry analyses (Peng et al., 2009).

The nearly 200,000 ha of saline soil in the Yellow River Delta, which is a representative coastal saline zone in China, are mainly the result of the excessive accumulation of Na^+ and Cl^- ions (Jia et al., 2013). This region has not been well exploited and used, which has seriously hindered the regional economy and ecological development. The salt content of the saline soil widely distributed in the Yellow River Delta can exceed 3% but usually ranges from .6 to 1.0%. Moreover, extreme weather conditions in this area, such as drought in the spring and excessive rainfall in the summer, have been common in recent years. In 2020, Prof. Zhensheng Li proposed a new initiative involving the development of a coastal grass belt, in which salt-tolerant forage grass species are cultivated on 667,000 ha of saline and alkaline soils around the Bohai Sea (Li et al., 2022). Because *Th. ponticum* can grow in saline soil and withstand drought and waterlogging, it may be a suitable forage species for the coastal saline zone in China (Rogers and Bailey, 1963; Shannon, 1978; Weimberg and Shannon, 1988; Jenkins et al., 2010; Guo et al., 2015; Borrajo et al., 2018; Ruf and Emmerling, 2018). Furthermore, the developed root system of tall wheatgrass can accumulate soil organic matter and improve soil fertility, which will positively contribute to regional agricultural and ecological development (Pimentel et al., 1987). To achieve this goal, *Th. ponticum* lines suitable for local conditions must be identified.

In this study, we selected the sexually reproducing plants of seven *Th. ponticum* clone lines as materials for an investigation of their agronomic traits, quality-related characteristics, and physiological and biochemical indices under salt stress conditions. The objective of this study was to identify salt-tolerant *Th. ponticum* germplasm with excellent agronomic characteristics that may be useful for breeding new *Th. ponticum* varieties, ideal for the saline soil in the coastal regions of China.

MATERIALS AND METHODS

Plant Materials

In 2008, Zhensheng Li's group selected seven phenotypically distinct tall wheatgrass individuals. Their clone lines (designated as C1–C7) were vegetatively propagated by cutting tillers with living roots. The seeds of these clone lines were collected for this study. The clone lines and the seeds were preserved in the laboratory of Zhensheng Li at the Institute of Genetics and Developmental Biology, The Innovative Academy of Seed Design, Chinese Academy of Sciences.

Study Sites and Field Experiments

The seeds of each clone line were sown in seedling trays containing a mixture of field soil and nutrient soil (3:1). The resulting seedlings with fully expanded second leaves were transplanted on 21 March 2018 to fields at the Haixing Experimental Station of Chinese Academy of Sciences (117.6°E, 38.2°N; .5% soil salt content) and on 9 April 2018 to fields at the Dongying Molecular Design Breeding Experimental Station of Chinese Academy of Sciences (118.9°E, 37.7°N; .3% soil salt content), with three plants per hole. The holes in each row were separated by 30 cm, and the rows were separated by 30 cm. Three replicates of each line were set, and each replicate was grown in a 3.0 m × 1.2 m plot. The transplanted seedlings were irrigated with freshwater to optimize the survival rate. There was no additional artificial irrigation during the cropping season. Plants were cultivated using conventional field management practices. Three uniform plants were selected from each plot, and the plant height (PH, cm), tiller number (TN), spike number (SN), spikelet number per spike (SNPS), leaf fresh weight (LFW, g), stem fresh weight (SFW, g), shoot total fresh weight (STFW, g), and shoot total dry weight (STDW, g) of the *Th. ponticum*

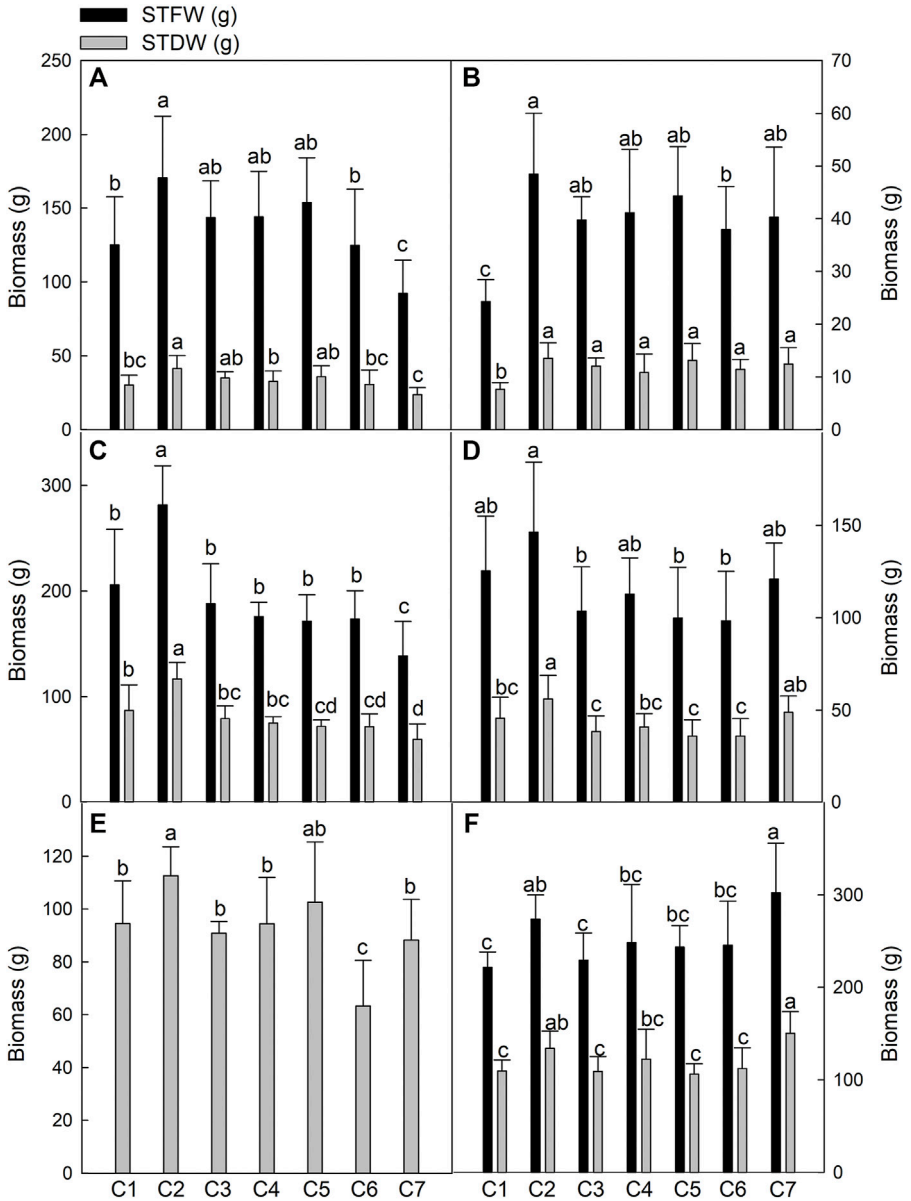

FIGURE 1 | Comparison of biomass of seven *Th. ponticum* lines at the flowering stage at Haixing station in 2018 **(A)**, at the flowering stage at Dongying station in 2018 **(B)**, at the milk-ripe stage at Haixing station in 2018 **(C)**, at the milk-ripe stage at Dongying station in 2018 **(D)**, at the flowering stage at Dongying station in 2019 **(E),** and at the milk-ripe stage at Dongying station in 2019 **(F)**. STFW, shoot total fresh weight; STDW, shoot total dry weight. Different letters indicate a significant difference between seven *Th. ponticum* lines at $p < .05$ level.

plants were analyzed at the flowering and milk-ripe stages in Haixing in 2018 (18HF and 18HM) and Dongying in 2018 (18DF and 18DM) and 2019 (19DF and 19DM). Due to the heavy rain in June 2019, the accuracy of STFW at the flowering stage might be affected. Thus, only STDW was measured in 19DF.

Analysis of Nutrient Contents

Fresh leaves of three plants were collected from each plot at the flowering stage in Haixing in 2018 and then heated at 105°C for 30 min, dried to a constant weight at 65°C, and ground to a powder and mixed in equal proportions for an analysis of the nutrient content. The dry matter (DM) content was determined after drying samples according to a published method by Zhang (2007). The crude protein (CP) content was determined using the Folin–Ciocalteu reagent (Yang, 1999). The neutral detergent fiber (NDF) content and the acid detergent fiber (ADF) content were measured on the basis of filter bag technology using the ANKOM A2000i automatic and semi-automatic fiber meters, respectively, according to Van Soest et al. (1991) with some modifications. The water-soluble carbohydrate (WSC) content was determined using an anthrone colorimetric technique (Zhang, 2007). The ether extract (EE) content and the ash content were measured as

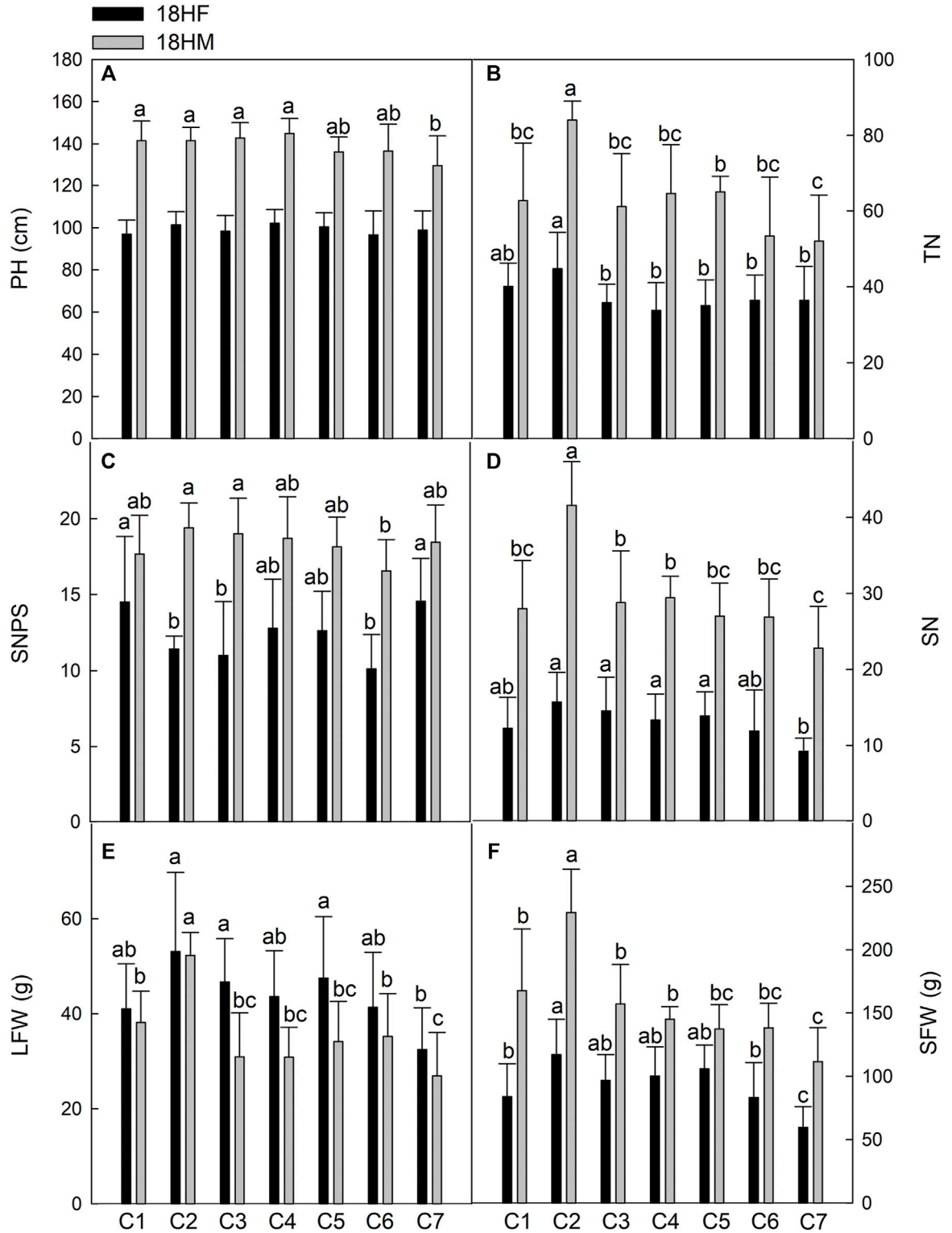

FIGURE 2 | Comparison of main agronomic traits of seven *Th. ponticum* lines at Haixing station at different growing stages. **(A)** Plant height (PH). **(B)** Tiller number (TN). **(C)** Spikelet number per spike (SNPS). **(D)** Spike number (SN). **(E)** Leaf fresh weight (LFW). **(F)** Stem fresh weight (SFW). Different letters indicate a significant difference between seven *Th. ponticum* lines at $p < .05$ level.

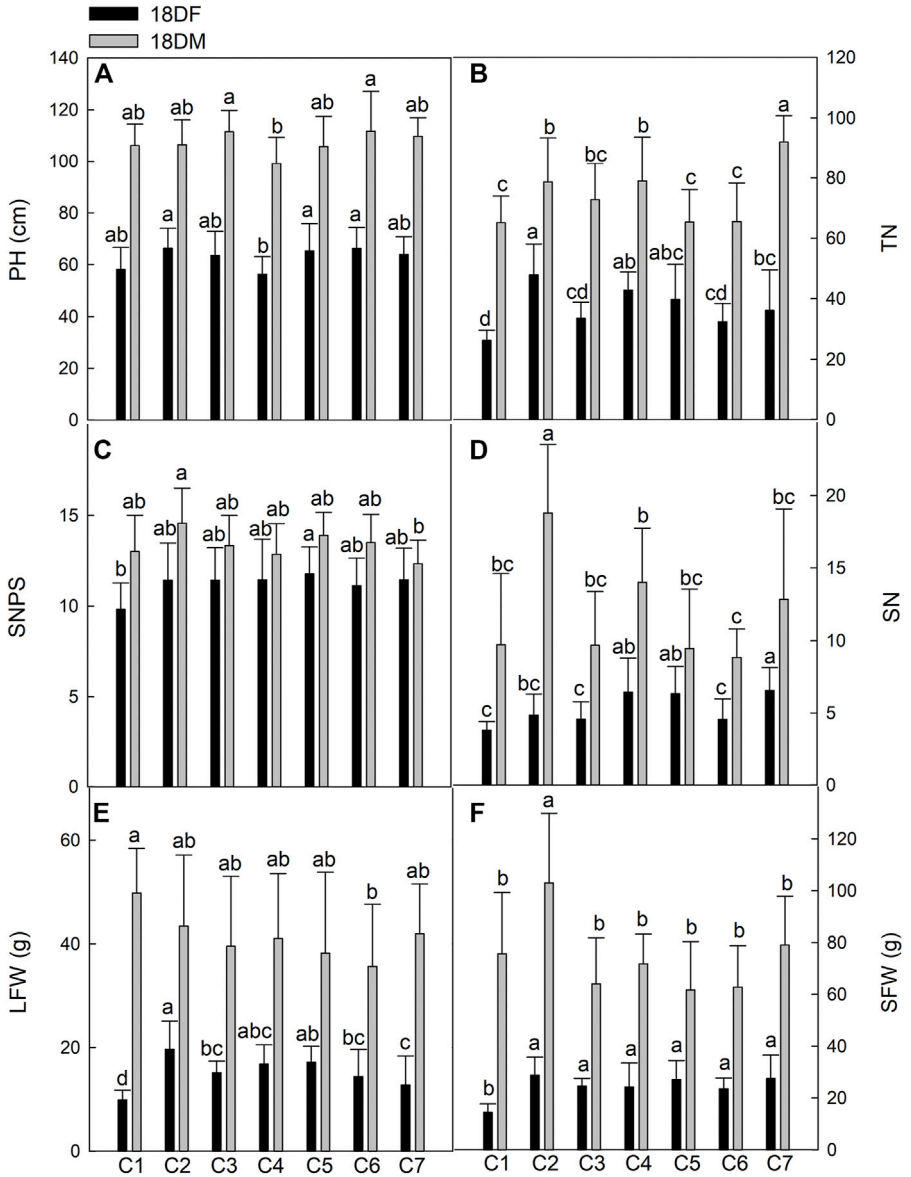

FIGURE 3 | Comparison of main agricultural traits of seven *Th. ponticum* lines at Dongying station during different growth periods. **(A)** Plant height (PH). **(B)** Tiller number (TN). **(C)** Spikelet number per spike (SNPS). **(D)** Spike number (SN). **(E)** Leaf fresh weight (LFW). **(F)** Stem fresh weight (SFW). Different letters indicate a significant difference between seven *Th. ponticum* lines at $p < .05$ level.

previously described (ISO 6492:1999, IDT and Mlejnkova et al., 2016, respectively), with some modifications. The tannin content (TC) was determined according to the vanillin hydrochloric acid method. The forage relative feeding value (RFV) and total digestible nutrient (TDN) content, as well as the relative forage quality (RFQ), were calculated on the basis of the NDF and ADF data using the following equations (Zhang et al., 2004; Schacht et al., 2010; Xiong et al., 2018):

$$\text{RFV} = \text{dry matter intake (DMI)} \times \text{digestible dry matter (DDM)}/1.29;\ \text{DMI} = 120/\text{NDF};\ \text{DDM} = 88.9 - 0.779 \times \text{ADF};\ \text{TDN} = 82.38 - 0.7515 \times \text{ADF};\ \text{RFQ} = \text{TDN} \times \text{DMI}/1.23.$$

Determination of Physiological and Biochemical Indices

For each replicate, a .05 g fresh sample of three plants was collected at the milk-ripe stage in Dongying in 2019 and used to measure the superoxide dismutase (SOD) activity (absorbance at 560 nm) as described by García-Triana et al. (2010). The catalase (CAT) activity (absorbance at 240 nm) was determined using a method developed by Sima et al. (2011). Chlorophyll *a* (Chl *a*) and chlorophyll *b* (Chl *b*) were extracted using 80% acetone, and their contents were determined by measuring the absorbances of the extracts at 645 and 663 nm

as described by Arnon (1949). All absorbances were measured using the SpectraMax190 microplate reader (Molecular Devices, America). The proline (Pro) content was determined using ninhydrin (Bates et al., 1973).

Data Analysis

The membership function value was used for the total membership value (TMV) analysis. The specific formula is as follows: $X(\mu 1) = (X - Xmin)/(Xmax - Xmin)$; $X(\mu 2) = 1 - X(\mu 1)$, where X is a certain measured value for the identified index; μ_1 is the positive correlation membership function value of each index; μ_2 is the negative correlation membership function value of each index; X_{max} is the maximum value of this index in all lines; and X_{min} is the minimum value of this index in all lines. The sum of the membership function values for the different indices of each line was calculated, and then the average value was used for ranking. Increases in TMV were associated with increasing plant salt tolerance (Liu et al., 2009; Zhang et al., 2020). Both SPSS17.0 and Excel were used to analyze data (*e.g.*, two-sample *t*-test, analysis of variance, and one-way ANOVA analysis). Average values and standard deviations were calculated for all measurements. Figures were prepared using SigmaPlot 12.5.

RESULTS

Biomass Indices

To evaluate the growth of seven *Th. ponticum* lines under coastal saline conditions, we analyzed the biomass indices, including STFW and STDW, of each line at the flowering and milk-ripe stages at the Haixing and Dongying experimental stations in 2018 and the Dongying experimental station in 2019. The results for the seven examined lines in six environments are provided in **Figure 1**. The yields of all *Th. ponticum* lines were generally higher in Haixing than in Dongying during the same growth period in 2018, possibly because the seedlings were transplanted about 20 days earlier in Haixing than in Dongying. In 2018, for most lines, the yields were greater at the milk-ripe stage than at the flowering stage at both experimental stations. A comparison of the data collected during the same developmental period in 2018 and 2019 revealed that most *Th. ponticum* lines produced more biomass in 2019.

During the milk-ripe stage in 2018, STFW was 138.62–281.64 g in Haixing and 98.43–146.40 g in Dongying, whereas STDW was 59.66–116.90 g in Haixing and 36.03–56.13 g in Dongying. In 2019, STDW was 63.26–112.63 g at the flowering stage and 106.33–150.37 g at the milk-ripe stage. Thus, there were distinct biomass differences among the samples. More specifically, STFW and STDW were highest for line C2 under all conditions, except for 19DM. Although the grass yield of line C7 was the highest in 19DM, there were no significant differences between C2 and C7 in terms of STFW and STDW. During the first growing season, the biomass of C2 was significantly higher ($p < .05$) than that of the other lines in 18HM. After one growing season, C2 could still grow vigorously, while C7 flourished similarly at the milk-ripe stage in Dongying in 2019. Compared with the corresponding growth in Dongying, C7 in Haixing had a lower STFW and STDW during both stages in 2018, implying C7 may be suitable for growth in a relatively low salinity soil with high regeneration ability. In summary, the biomass of C2 was prominent among these seven lines under salt stress.

Agronomic Traits

Traits related to growth performance, including PH, TN, SNPS, SN, LFW, and SFW, were evaluated for each *Th. ponticum* line in Haixing (**Figure 2**) and Dongying (**Figure 3**) in 2018. At the Haixing experimental station, the values of all traits, except for LFW, generally increased as plants matured. The differences among the seven lines were greater in 18HM than in 18HF. For example, there were no significant differences in PH among the seven lines in 18HF. However, in 18HM, the lines were divided into three groups according to their PH, and C7 was significantly shorter ($p < .05$) than C1, C2, C3, and C4. Additionally, PH was the highest for C4, with an average of 144.92 cm, 15.15 cm greater than the PH of C7 (**Figure 2A**). The SNPS of C2 (19.40) and C3 (19.00) were significantly higher ($p < .05$) than that of C6 (16.56) in 18HM. Line C2 had the highest TN and SN at both stages, and the differences with the corresponding values for the other lines were significant ($p < .05$) in 18HM. In contrast, C7 had the lowest TN in 18HM (**Figure 2B**) and the lowest SN in 18HF and 18HM (**Figure 2D**). In Haixing, LFW was a little lower at the milk-ripe stage than at the flowering stage for all lines. At both stages, C2 and C7 had the highest and lowest LFW, respectively. Additionally, C2 had a significantly higher LFW ($p < .05$) than the other lines in 18HM. Similarly, C2 had the highest SFW among the seven lines in both 18HF and 18HM; the differences in SFW between C2 and the other lines were significant ($p < .05$) in 18HM. Considered together, C2 exhibited excellent growth during the first growing season under high salt conditions. At 132 days after transplanting, the three individual plants in each hole of C2 were 142 cm tall, with 84 tillers, 42 spikes, and 19 spikelets, and produced 52.30 g fresh leaves and 229.34 g fresh stems. Moreover, PH, TN, SN, LFW, and SFW were lowest for C7 among the seven examined lines; the differences in these traits between C7 and C2 were significant ($p < .05$). From the flowering stage to the milk-ripe stage, line C2 decreased the minimum LFW and increased the maximum SN, which resulted in its maintaining the fastest growth rate after entering the reproductive growth stage when compared with the other lines.

In Dongying, the values for all of the measured indices increased as *Th. ponticum* plants matured. Line C2 had the highest PH (66.30 cm) at the flowering stage, whereas line C6 had the highest PH (111.68 cm) at the milk-ripe stage. The C4 plants were the shortest at the flowering and milk-ripe stages (56.27 and 99.11 cm, respectively). The TN of C2 (47.84) was significantly higher ($p < .05$) than that of C1, C3, C6, and C7 in 18DF, whereas the TN of C7 (92.00) was significantly higher ($p < .05$) than that of any other line in 18DM. With the exception of C1, all lines had an SNPS greater than 11 in 18DF, with no

TABLE 1 | Membership function analyses of salt tolerance in seven *Th. ponticum* lines.

Stages	Lines	PH	TN	SNPS	SN	LFW	SFW	STFW	STDW	TMV	Rank
18HF	C1	.05	.58	.99	.47	.42	.42	.42	.37	.46	5
	C2	.86	1.00	.30	1.00	1.00	1.00	1.00	1.00	.89	1
	C3	.30	.18	.20	.82	.69	.65	.66	.64	.52	4
	C4	1.00	.00	.60	.63	.54	.71	.66	.51	.58	3
	C5	.70	.11	.57	.72	.73	.80	.79	.69	.64	2
	C6	.00	.24	.00	.41	.43	.41	.42	.39	.29	6
	C7	.41	.24	1.00	.00	.00	.00	.00	.00	.21	7
18HM	C1	.77	.33	.39	.28	.44	.48	.47	.48	.46	2
	C2	.78	1.00	1.00	1.00	1.00	1.00	1.00	1.00	.97	1
	C3	.86	.28	.86	.32	.16	.39	.35	.34	.44	3
	C4	1.00	.39	.76	.35	.15	.28	.26	.27	.43	4
	C5	.43	.41	.55	.22	.28	.22	.23	.21	.32	5
	C6	.45	.04	.00	.22	.33	.23	.24	.21	.21	6
	C7	.00	.00	.66	.00	.00	.00	.00	.00	.08	7
18DF	C1	.18	.00	.00	.00	.00	.00	.00	.00	.02	7
	C2	1.00	1.00	.82	.38	1.00	1.00	1.00	1.00	.90	1
	C3	.73	.34	.82	.28	.54	.71	.64	.75	.60	5
	C4	.00	.77	.83	.96	.71	.69	.70	.55	.65	4
	C5	.90	.63	1.00	.92	.75	.89	.83	.93	.85	2
	C6	.99	.29	.66	.27	.46	.64	.56	.64	.56	6
	C7	.76	.46	.83	1.00	.30	.91	.66	.81	.72	3
18DM	C1	.56	.00	.30	.09	1.00	.34	.56	.48	.42	3
	C2	.58	.50	1.00	1.00	.55	1.00	1.00	1.00	.83	1
	C3	.98	.28	.45	.08	.27	.06	.11	.12	.30	5
	C4	.00	.52	.24	.52	.38	.24	.30	.25	.31	4
	C5	.53	.01	.70	.06	.18	.00	.03	.00	.19	7
	C6	1.00	.01	.53	.00	.00	.03	.00	.00	.20	6
	C7	.85	1.00	.00	.40	.45	.42	.47	.64	.53	2

Annotation: 18HF and 18HM mean investigation at the flowering and milk-ripe stages in Haixing in 2018, respectively. 18DF and 18DM indicate investigation at the flowering and milk-ripe stages in Dongying in 2018, respectively. PH, plant height; TN, tiller number; SNPS, spikelet number per spike; SN, spikelet number; LFW, leaf fresh weight; STW, stem fresh weight; STFW, shoot total fresh weight; STDW, shoot total dry weight; TMV, total membership value.

TABLE 2 | Comparison of nutrient content for seven *Th. ponticum* lines at the adult-plant stage.

Lines	Dry matter (%FW)	Curd protein (%DM)	Neutral detergent fiber (%DM)	Acid detergent fiber (%DM)	Ether extract (%DM)	Water-soluble carbohydrates (%DM)	Tannin content (mg/g FW)	Ash (%DM)
C1	40.66 ± .26	13.15 ± .63	56.30 ± 3.12	29.86 ± .86	3.57 ± .16	1.88 ± .17	$2.00 \pm .18^{cd}$	$9.69 \pm .76^{a}$
C2	39.17 ± 1.77	13.37 ± 1.05	56.21 ± .40	30.24 ± .61	3.44 ± .12	1.88 ± .03	$2.29 \pm .11^{a}$	$9.14 \pm .59^{ab}$
C3	42.59 ± 4.29	14.01 ± .41	54.80 ± 1.78	29.21 ± .78	3.67 ± .24	2.07 ± .31	$1.51 \pm .07^{f}$	$8.98 \pm .32^{ab}$
C4	41.65 ± 3.42	14.45 ± .17	55.06 ± 3.22	29.46 ± 1.24	3.42 ± .85	2.30 ± .45	$1.92 \pm .04^{d}$	$8.87 \pm .55^{ab}$
C5	41.49 ± 4.41	14.23 ± .41	54.11 ± 1.27	29.12 ± .75	3.49 ± 1.49	2.06 ± .41	$2.13 \pm .09^{b}$	$9.75 \pm .70^{a}$
C6	40.10 ± 1.13	13.86 ± .83	53.21 ± 3.01	28.18 ± 2.13	3.86 ± .85	2.04 ± .18	$1.69 \pm .04^{e}$	$8.46 \pm .19^{b}$
C7	42.85 ± 3.38	14.38 ± .87	54.55 ± 2.95	28.61 ± .99	3.45 ± 1.16	2.39 ± .46	$2.10 \pm .08^{bc}$	$8.57 \pm .55^{b}$

Annotation: different letters indicate a significant difference between seven Th. ponticum *lines at* p < *.05 level*

significant differences between lines. SNPS (11.78) of C5 was the highest in 18DF, whereas SNPS (14.56) of C2 was the highest in 18DM, significantly higher ($p < .05$) than that of C7 (12.33). However, SN was significantly higher ($p < .05$) for C7 (6.56) than for C1, C2, C3, and C6 at the flowering stage, whereas SN was significantly higher ($p < .05$) for C2 (18.78) than for any other line at the milk-ripe stage. LFW of C2 (19.63 g) was significantly higher ($p < .05$) than that of C1, C3, C6, and C7 in 18DF, whereas LFW of C1 (49.77 g) was the highest in 18DM, although there were no significant differences with the other lines, except for C6. Line C2 consistently had the highest SFW at both examined stages, with an average of 28.76 and 102.97 g at the flowering and milk-ripe stages, respectively. There were significant differences ($p < .05$) in SFW between C2 and the other lines at 18DM. In summary, PH, TN, LFW, and SFW of C2 were the highest at the flowering stage, whereas PH of C6; TN of C7; LFW of C1; and SN, SNPS, and SFW of C2 were the highest at the milk-ripe stage. Of the tested lines, C2 consistently grew the fastest. Line C1 initially grew slowly and then grew quickly, whereas C6 exhibited the opposite growth trend.

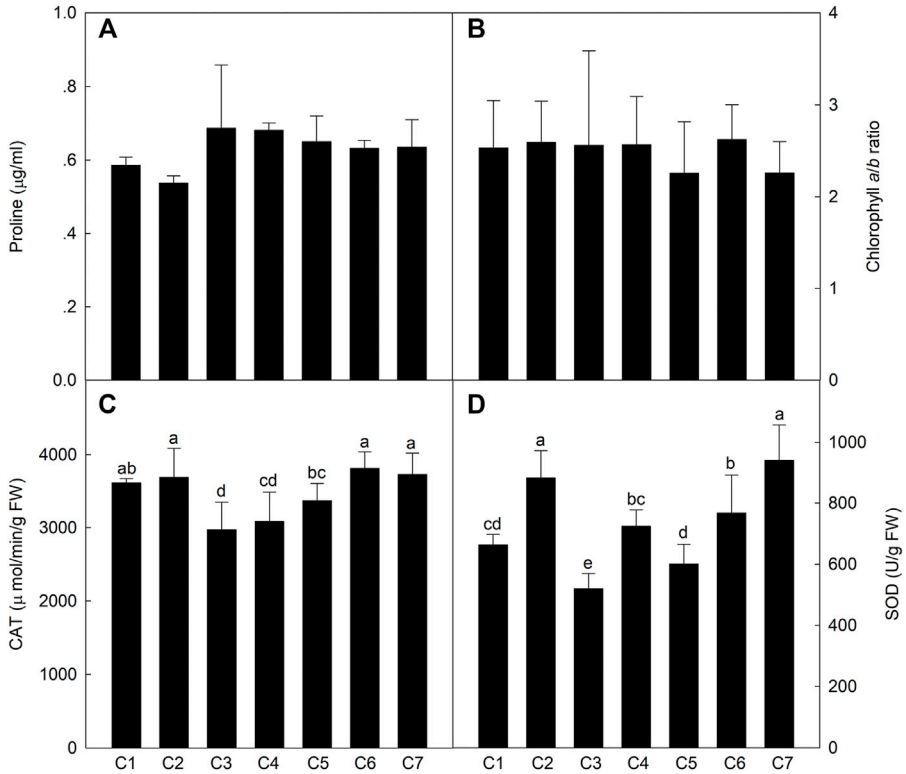

FIGURE 4 | Comparison of the content of proline **(A)**, chlorophyll *a*/*b* ratio **(B)**, activities of CAT **(C),** and SOD **(D)** in the seven *Th. ponticum* lines. Different letters indicate a significant difference between seven *Th. ponticum* lines at $p < .05$ level.

The total membership values were calculated based on the agronomic performance of the seven *Th. ponticum* lines in the four environments of 2018. There were substantial differences in the analyzed traits among the seven lines, which resulted in a wide range of TMV (**Table 1**). In Haixing, based on the size of TMV, the rank order (highest to lowest) of the membership functions was C2, C5, C4, C3, C1, C6, and C7 in 18HF, whereas it was C2, C1, C3, C4, C5, C6, and C7 in 18HM. In Dongying, the rank order (highest to lowest) of TMV was C2, C5, C7, C4, C3, C6, and C1 at the flowering stage, whereas it was C2, C7, C1, C4, C3, C6, and C5 at the milk-ripe stage. Regardless of the condition, C2 grew better than the other lines at the adult-plant stage. Its scores (.89 in 18HF and .97 in 18HM) were far higher than those of the second-best line (.64 in 18HF and .46 in 18HM) under high salt stress. Line C7 ranked third (.72 in 18DF) and second (.53 in 18DM) in Dongying but exhibited the poorest growth in Haixing, suggesting it is appropriate for soil with a salt content less than .3% (*i.e.*, it is sensitive to high salinity).

Nutrient Indices

The results of the analysis of eight nutrient indices in *Th. ponticum* lines are provided in **Table 2**. There were no significant differences among the lines for the following six indices: DM (39.17%–42.85%FW), CP (13.15%–14.45%DM), NDF (53.21%–56.30%DM), ADF (28.18%–30.24%DM), EE (3.42%–3.86%DM), and WSC (1.88%–2.39%DM). However, there were significant variations in TC and the ash content. Specifically, TC was significantly higher ($p < .05$) in C2 (2.29 mg/g FW) than in any other line. The ash content was the highest in C5 (9.75%DM) and then C1 (9.69%DM), whereas it was the lowest in C6 (8.46%DM).

The NDF and ADF data were used to calculate the RFV, TDN, and RFQ of the *Th. ponticum* lines to assess the forage quality and value. There were no significant differences in the RFV (108–118), TDN (59–62), and RFQ (103–113). In short, nutrient indices expressed no significant differences among the lines except for TC and ash.

Physiological and Biochemical Indices

To compare the physiological and biochemical indices of the different lines exposed to saline conditions, osmotic regulatory compounds and protective enzymes were analyzed in the leaves at the milk-ripe stage. The leaf Pro content was .54–.69 μg/ml (**Figure 4**), with no significant differences among the *Th. ponticum* lines. There were also no significant differences in the Chl *a*/*b* ratio. However, the Chl *a*/*b* ratio was the highest for C6 (2.62) and then C2 (2.59), whereas it was the lowest for C5 and C7 (2.26). The CAT activity of C1, C2, C6, and C7 were higher levels in these materials, and there was no significant difference between these lines. The SOD activity was the highest in C7 and C2, with no significant difference. In general, *Th. ponticum* can maintain normal physiological metabolism under

salt stress by increasing its main osmotic regulation substances, especially line C2.

DISCUSSION

A Comprehensive Analysis Is Necessary to Assess Forage Salt Tolerance

Plant salt tolerance is a comprehensive trait involving multiple signaling pathways (Strizhov et al., 1997; Gohari et al., 2021). Because of the decrease in water potential and increase in osmotic pressure associated with saline soils, plant growth and development are seriously hindered by a decrease in the absorption of water by the roots, the closing of stomata, an increase in the leaf temperature, the inhibited differentiation of tissues and organs, and delayed cells growth. Salt stress can also severely affect plant physiological processes (Munns and Tester, 2008; Roy et al., 2014). Two new salt-tolerant bread wheat cultivars ("Maycan" and "Yildiz") have significantly higher Chl *a*, Chl *b*, and total chlorophyll contents than salt-sensitive wheat varieties under saline conditions (Aycan et al., 2021). In response to salt stress, plants accumulate small organic compounds, such as Pro, to resist the adverse effects of stress while also synthesizing antioxidant enzymes to scavenge excess reactive oxygen species. As the core enzymes in the antioxidant system, SOD and CAT can minimize plant damage caused by reactive oxygen species by degrading hydrogen peroxide under saline conditions (Sekmen et al., 2007). Gohari et al. (2021) determined that, in grapevine, SOD and CAT activities increased following exposure to salinity stress. Additionally, Pro is an important component under salt treatment of plants, whose function may protect protein turnover normally and upregulate stress-protective proteins in the desert plant *Pancratium maritimum* L. (Khedr et al., 2003). Kim et al. (2016) performed Pro analyses of 46 switchgrass under salt stress, and the result revealed that salt-sensitive lines increased sharply. However, salt-resistant lines increased slightly in Pro concentration in response to salt treatment. In our study, C2 had the lowest Pro content, stable biomass advantage, and relatively high CAT and SOD activities and Chl *a*/*b* ratio, suggesting it may be better able to maintain normal metabolic and physiological activities under salt stress than the other lines.

Because plant salt tolerance varies among growth stages, it is difficult to accurately assess using a single index (An et al., 2021). To the best of our knowledge, herbage salt tolerance is currently evaluated primarily on the basis of the biomass, K^+ and Na^+ contents, and the relative water content during the germination or seedling stage (Johnson, 1991; Sagers et al., 2017). There has been relatively little research on herbage salt tolerance at the adult-plant stage, especially during the flowering and mike-ripe stages. To evaluate plant salt tolerance, a comprehensive analysis of morphological, physiological, biochemical, and other indices should be conducted. In the current study, the agronomic performance of C2 was generally the best among the *Th. ponticum* lines transplanted in coastal saline soil (.3% or .5% salinity). In Haixing, TN, SN, LFW, and SFW were the highest for C2 at two sampling stages. In Dongying, SNPS, SN, and SFW were the highest for C2 at the milk-ripe stage. A membership function analysis revealed that C2 exhibited better overall growth and produced more seeds than the other examined lines in both experimental fields. Additionally, STFW and STDW were higher for C2 than for the other six tall wheatgrass materials in six different environments, implying that C2 has a greater production potential under salt stress conditions than the other lines.

Importance of the Nutrient Content for Evaluating Forage Species

The nutrient content directly affects animal feed intake and forage palatability. The nutritional value of herbage is generally evaluated according to CP and the crude fiber (CF) content. Van Soest et al. (1991) divided CF into NDF, ADF, and acid detergent lignin, whose contents can directly affect animal feed intake and digestibility. For example, sheep feed intake decreased as NDF and ADF of perennial ryegrass (*Lolium perenne*) increased (Aitchison et al., 1986). Moreover, a high NDF in silage corn can decrease beef cattle feed intake (Tjardes et al., 2002). The CP content, which comprises protein and non-protein nitrogenous compounds, represents the essential materials for animal tissues, cells, and metabolism. An examination of the forage yield and quality traits of a collection of 50 tall wheatgrass accessions from the USDA-ARS Western Regional Plant Introduction Station demonstrated that the shoot CP ranged from 6.6 to 11% at the heading stage (Vogel and Moore, 1998). Additionally, dynamic changes were observed in forage grass CP during different growth periods. On the basis of their data for 17 *Th. ponticum* accessions from Iran, Jafari et al. (2014) revealed the average CP contents were 7.96 and 4.86% for two and one cutting managements, respectively. In the current study, the average NDF and ADF of seven tall wheatgrass lines were 54.89%DM and 29.24%DM, respectively. Furthermore, the CP of each line, which exceeded 13%DM, accounted for a higher percentage of the DM than the CP of *Poa annua* L. (9.93%) (Qu and Shi, 2017), silage corn (7.68%), and other gramineous forage species (Liu et al., 2018). Thus, *Th. ponticum* lines are useful as high-quality protein feed.

An increase in NDF and a decrease in CP will lead to an increase in TC. Some studies indicated that the bitter taste associated with a tannin DM greater than 1% would substantially decrease plant palatability. However, when TC is less than 1%, the accumulation of tannin may contribute to an increase in protein conversions and prevent ruminal tympany among herbivores (Barry and McNabb, 1999). In the present study, the TC of C2 (2.29 mg/g FW, equivalent to .45%DM) was within the relative permissible TC range and was significantly higher ($p < .05$) than the TC of the other lines, implying that C2 is a palatable line beneficial for nutrient metabolism and the prevention of bloating.

Hay quality is mainly assessed via a comprehensive analysis that divides the total digestible nutrients of forage materials on the basis of detergent fiber and DMI. As indices used for evaluating quality, TDN, RFV, and RFQ are positively correlated with forage palatability and digestibility (Rohweder

et al., 1978). Xiong et al. (2018) analyzed the nutrient content of *Avena sativa* L. in different regions in China and determined that the TDN, RFV, and RFQ of *A. sativa* were, respectively, 52, 93, and 88 in Shanxi province and 51, 86, and 81 in Gansu province. In this study, the average TDN, RFV, and RFQ values of *Th. ponticum* were 60.41, 112.31, and 107.61, respectively, which were higher than the corresponding values for *A. sativa*. The WSC and EE values of *Th. ponticum* were 2.09%DM and 3.56%DM, respectively, representing a relatively large proportion of DM. The EE of this study was greater than the EE reported for some gramineous species, including oat (2.65%), *Setaria viridis* (L.) Beauv (2.11%), and *Sorghum*–sudangrass hybrids (1.26%) (Liu et al., 2018). These findings suggest that *Th. ponticum* growing in the Circum-Bohai sea region is a forage grass species with a high nutritive value, with implications for animal husbandry.

Decaploid Tall Wheatgrass Can Accelerate the Improvement of Coastal Saline Soils

Elytrigia (now named *Thinopyrum*), which is a genus in the gramineous wheat subfamily, includes the following species: *Elytrigia repens*, *Elytrigia smithii*, *Elytrigia trichophora*, *Elytrigia elongata*, and *Elytrigia intermedia* (Geng, 1959). Many studies have confirmed the differential salt tolerance of *Elytrigia* varieties (Dewey, 1960; Shannon, 1978). *Th. ponticum*, which is usually referred to as decaploid tall wheatgrass, has been used as a wild relative for the genetic improvement of wheat stress resistance (Li et al., 2008; Wang, 2011).

There are only a few reports that describe *Th. ponticum* as a high-quality pasture crop with strong tolerance to stress conditions. Although 25 *Th. ponticum* materials were selected and compared as early as in 1960 (Dewey, 1960), relatively few *Th. ponticum* varieties are available for production (Vogel and Moore, 1998). To date, eight *Th. ponticum* varieties (Jose, Largo, Alkar, Nebraska98526, Orbit, Platte, NFTW6001, and Plainsmen) have been developed and released in the United States and Canada (Alderson and Sharp, 1994; Trammell et al., 2016; Trammell et al., 2021). Two salt-tolerant varieties (Tyrrell and Dundas) were bred in Australia (Rogers and Bailey, 1963; Smith and Kelman, 2000). In China, *Th. ponticum* was initially transported from the United States to the Tianshui Experimental Station of Soil and Water Conservation (Gansu province). Professor Zhensheng Li brought it to the Laboratory of Genetics and Plant Breeding of CAS in Beijing in 1954 and then to Northwest Institute of Botany (Yangling, Shaanxi province) in 1956 to be used for wheat distant hybridizations. There are no decaploid tall wheatgrass varieties that have been certified in China, which has seriously restricted their use. The Yellow River Delta has many undeveloped land resources that are suitable for the cultivation of salt-tolerant herbage. Because of its excellent tolerance to salt, waterlogging, and drought stresses, *Th. ponticum* is an ideal forage species for improving saline coastal soils and developing animal husbandry. Line C2, which was identified as a superior germplasm in the present study, may be used to develop improved cultivars with elite traits resulting from the cross pollination between C2 individuals or between C2 and other appropriate lines with high regeneration ability and accelerate the application of its useful genes in improving wheat genetic variability by chromosome engineering. Furthermore, these materials would achieve the target of planting 667,000 ha salt-tolerant forage grass in saline and alkaline soils in the Circum-Bohai sea region.

CONCLUSION

On the basis of its high biomass and excellent agronomic performances revealed in this study, C2 is better suited for saline environments than the other examined tall wheatgrass lines. Thus, it may be relevant for optimizing the use of marginal soils and developing improved *Th. ponticum* cultivars that can be planted in the Circum-Bohai sea region of China.

DATA AVAILABILITY STATEMENT

The raw data supporting the conclusion of this article will be made available by the authors without undue reservation.

AUTHOR CONTRIBUTIONS

ZL and QZ conceived the research. CT and QZ performed the experiments. CT, GY, and QZ drafted the manuscript. AB, Tr, HL, and BL provided substantial help in preparing materials and filed experiments. All authors read and approved the final manuscript.

FUNDING

This research was supported by the Strategic Priority Research Program of the Chinese Academy of Sciences (no. XDA26040105), the Key Programs of the Chinese Academy of Sciences (KFZD-SW-112), and the STS Project of the Chinese Academy of Sciences (KFJ-STS-ZDTP-053).

REFERENCES

Aitchison, E. M., Gill, M., Dhanoa, M. S., and Osbourn, D. F. (1986). The Effect of Digestibility and Forage Species on the Removal of Digesta from the Rumen and the Voluntary Intake of hay by Sheep. *Br. J. Nutr.* 56, 463–476. doi:10.1079/bjn19860126

Alderson, J., and Sharp, W. C. (1994). *Grass Varieties in the United States*. Washington, DC: U.S. Gov. Print. Office. USDA-SCS Agric. Handb. 170.

An, Y., Gao, Y., Tong, S., and Liu, B. (2021). Morphological and Physiological Traits Related to the Response and Adaption of *Bolboschoenus Planiculmis* Seedlings Grown under Salt-Alkaline Stress Conditions. *Front. Plant Sci.* 12, 567782. doi:10.3389/fpls.2021.567782

Arnon, D. I. (1949). Copper Enzymes in Isolated Chloroplasts. Polyphenoloxidase in Beta Vulgaris. *Plant Physiol.* 24, 1–15. doi:10.1104/pp.24.1.1

Aycan, M., Baslam, M., Asiloglu, R., Mitsui, T., and Yildiz, M. (2021). Development of New High-Salt Tolerant Bread Wheat (*Triticum aestivum* L.) Genotypes and

Insight into the Tolerance Mechanisms. *Plant Physiol. Biochem.* 166, 314–327. doi:10.1016/j.plaphy.2021.05.041

Barry, T. N., and McNabb, W. C. (1999). The Implications of Condensed Tannins on the Nutritive Value of Temperate Forages Fed to Ruminants. *Br. J. Nutr.* 81, 263–272. doi:10.1017/S0007114599000501

Bates, L. S., Waldren, R. P., and Teare, I. D. (1973). Rapid Determination of Free Proline for Water-Stress Studies. *Plant Soil* 39, 205–207. doi:10.1007/BF00018060

Bazihizina, N., Barrett-Lennard, E. G., and Colmer, T. D. (2012). Plant Growth and Physiology under Heterogeneous Salinity. *Plant Soil* 354, 1–19. doi:10.1007/s11104-012-1193-8

Borrajo, C. I., Sánchez-Moreiras, A. M., and Reigosa, M. J. (2018). Morpho-physiological Responses of Tall Wheatgrass Populations to Different Levels of Water Stress. *PLoS One* 13, e0209281. doi:10.1371/journal.pone.0209281

Chen, Z., Jin, Y., Li, X., Wei, X., Li, C., White, J. F., et al. (2021). Characterization of the Complete Chloroplast Genome of *Hordeum Jubatum* (Poaceae: Pooideae: Triticeae) and Phylogenetic Analysis. *Mitochondrial DNA B* 6, 2933–2935. doi:10.1080/23802359.2021.1972868

Colmer, T. D., Flowers, T. J., and Munns, R. (2006). Use of Wild Relatives to Improve Salt Tolerance in Wheat. *J. Exp. Bot.* 57, 1059–1078. doi:10.1093/jxb/erj124

Dewey, D. R. (1960). Salt Tolerance of Twenty-five Strains of Agropyron 1. *Agron.j.* 52, 631–635. doi:10.2134/agronj1960.00021962005200110006x

Ding, Z., Liu, Y., Lou, Y., Jiang, M., Li, H., and Lü, X. (2021). How Soil Ion Stress and Type Influence the Flooding Adaptive Strategies of *Phragmites Australis* and *Bolboschoenus Planiculmis* in Temperate saline-alkaline Wetlands? *Sci. Total Environ.* 771, 144654. doi:10.1016/j.scitotenv.2020.144654

Dvorak, J., Edge, M., and Ross, K. (1988). On the Evolution of the Adaptation of *Lophopyrum Elongatum* to Growth in saline Environments. *Proc. Natl. Acad. Sci.* 85, 3805–3809. doi:10.1073/pnas.85.11.3805

FAO (2017). FAO Soils Portal. Available at: https://www.fao.org/soils-portal/soil-management/management-of-some-problem-soils/salt-affected-soils/more-information-on-salt-affected-soils/en/, Accessed October 2021.

Forster, B. P., Miller, T. E., and Law, C. N. (1988). Salt Tolerance of Two Wheat - Agropyron Junceum Disomic Addition Lines. *Genome* 30, 559–564. doi:10.1139/g88-094

García-Triana, A., Zenteno-Savín, T., Peregrino-Uriarte, A. B., and Yepiz-Plascencia, G. (2010). Hypoxia, Reoxygenation and Cytosolic Manganese Superoxide Dismutase (cMnSOD) Silencing in *Litopenaeus Vannamei*: Effects on cMnSOD Transcripts, Superoxide Dismutase Activity and Superoxide Anion Production Capacity. *Dev. Comp. Immunol.* 34, 1230–1235. doi:10.1016/j.dci.2010.06.018

Geng, Y. L. (1959). *Flora Illustralis Plantarum Primarum Sinicarum, Gramineae*. Beijing: Science Press, 342–409.

Gohari, G., Panahirad, S., Sepehri, N., Akbari, A., Zahedi, S. M., Jafari, H., et al. (2021). Enhanced Tolerance to Salinity Stress in grapevine Plants through Application of Carbon Quantum Dots Functionalized by Proline. *Environ. Sci. Pollut. Res.* 28, 42877–42890. doi:10.1007/s11356-021-13794-w

Guo, Q., Meng, L., Mao, P.-C., and Tian, X.-X. (2015). Salt Tolerance in Two Tall Wheatgrass Species Is Associated with Selective Capacity for K^+ over Na^+. *Acta Physiol. Plant* 37, 1708. doi:10.1007/s11738-014-1708-4

Jafari, A. A., Elmi, A., and Bakhtiari, M. (2014). Evaluation of Yield and Quality Traits in 17 Populations of Tall Wheatgrass (*Agropyron Elongatum*) Grown in Rain Fed Area of Iran, under Two Cutting Management. *Rom. Agric. Res.* 31, 49–58.

Jenkins, S., Barrett-Lennard, E. G., and Rengel, Z. (2010). Impacts of Waterlogging and Salinity on Puccinellia (Puccinellia Ciliata) and Tall Wheatgrass (Thinopyrum Ponticum): Zonation on Saltland with a Shallow Water-Table, Plant Growth, and Na^+ and K^+ Concentrations in the Leaves. *Plant soil* 329, 91–104. doi:10.1007/s11104-009-0137-4

Jia, C. L., Sheng, Y. B., Zhang, H. W., Zhao, F. T., Wang, G. L., Bi, Y. B., et al. (2013). Comparisons on Forage Yield and Feeding Value of Sweet Sorghum in saline Soil of Yellow River Delta. *Pratacult. Sci.* 30, 116–119.

Johnson, R. C. (1991). Salinity Resistance, Water Relations, and Salt Content of Crested and Tall Wheatgrass Accessions. *Crop Sci.* 31, 730–734. doi:10.2135/cropsci1991.0011183X003100030039x

Khedr, A. H. A., Abbas, M. A., Wahid, A. A., Quick, W. P., and Abogadallah, G. M. (2003). Proline Induces the Expression of Salt-Stress-Responsive Proteins and May Improve the Adaptation of *Pancratium Maritimum* L. To Salt-Stress. *J. Exp. Bot.* 54, 2553–2562. doi:10.1093/jxb/erg277

Kim, J., Liu, Y., Zhang, X., Zhao, B., and Childs, K. L. (2016). Analysis of Salt-Induced Physiological and Proline Changes in 46 Switchgrass (*Panicum Virgatum*) Lines Indicates Multiple Response Modes. *Plant Physiol. Biochem.* 105, 203–212. doi:10.1016/j.plaphy.2016.04.020

King, I. P., Forster, B. P., Law, C. C., Cant, K. A., Orford, S. E., Gorham, J., et al. (1997). Introgression of Salt-Tolerance Genes from *Thinopyrum Bessarabicum* into Wheat. *New Phytol.* 137, 75–81. doi:10.1046/j.1469-8137.1997.00828.x

Li, Z., Li, B., and Tong, Y. (2008). The Contribution of Distant Hybridization with Decaploid *Agropyron Elongatum* to Wheat Improvement in China. *J. Genet. Genomics* 35, 451–456. doi:10.1016/S1673-8527(08)60062-4

Li, H. W., Zheng, Q., Li, B., Zhao, M. L., and Li, Z. S. (2022). Progress on Research of Tall Wheatgrass as a Kind of Salt Tolerant Forage Grass. *Acta Pratacult. Sin.* (in press). doi:10.11686/cyxb2021384

Liu, D. L., Qiu, W. W., and Ma, J. J. (2009). A Comparative Study on Salt Tolerance during Germinating Period of Different Alfalfa Varieties. *Pratacult. Sci.* 6, 163–169.

Liu, M., Yang, D., Zhang, J., Li, D. M., Wang, J., and Jiang, H. (2018). Determination of GI Value of Sheep Roughage in Bayannur City of Inner Mongolia. *Anim. Husb. Feed Sci.* 39, 51–54.

Mlejnkova, V., Horky, P., Kominkova, M., Skladanka, J., Hodulikova, L., Adam, V., et al. (2016). Biogenic Amines and Hygienic Quality of lucerne Silage. *Open Life Sci.* 11, 280–286. doi:10.1515/biol-2016-0037

Mullan, D. J., Mirzaghaderi, G., Walker, E., Colmer, T. D., and Francki, M. G. (2009). Development of Wheat-Lophopyrum Elongatum Recombinant Lines for Enhanced Sodium 'exclusion' during Salinity Stress. *Theor. Appl. Genet.* 119, 1313–1323. doi:10.1007/s00122-009-1136-9

Munns, R., and Tester, M. (2008). Mechanisms of Salinity Tolerance. *Annu. Rev. Plant Biol.* 59, 651–681. doi:10.1146/annurev.arplant.59.032607.092911

Omielan, J. A., Epstein, E., and Dvořák, J. (1991). Salt Tolerance and Ionic Relations of Wheat as Affected by Individual Chromosomes of Salt-Tolerant *Lophopyrum Elongatum*. *Genome* 34, 961–974. doi:10.1139/g91-149

Peng, Z., Wang, M., Li, F., Lv, H., Li, C., and Xia, G. (2009). A Proteomic Study of the Response to Salinity and Drought Stress in an Introgression Strain of Bread Wheat. *Mol. Cell Proteomics* 8, 2676–2686. doi:10.1074/mcp.M900052-MCP200

Pimentel, D., Allen, J., Beers, A., Guinand, L., Linder, R., McLaughlin, P., et al. (1987). World Agriculture and Soil Erosion. *BioScience* 37, 277–283. doi:10.2307/1310591

Qadir, M., and Oster, J. (2004). Crop and Irrigation Management Strategies for saline-sodic Soils and Waters Aimed at Environmentally Sustainable Agriculture. *Sci. Total Environ.* 323, 1–19. doi:10.1016/j.scitotenv.2003.10.012

Qu, Y. J., and Shi, S. L. (2017). Nutritional Evaluation of New Lines of *Poa Pratensis* Cv. Longmu. *Grassl. Turf.* 37, 51–60.

Rogers, A., and Bailey, E. (1963). Salt Tolerance Trials with Forage Plants in South-Western Australia. *Aust. J. Exp. Agric.* 3, 125–130. doi:10.1071/ea9630125

Rohweder, D. A., Barnes, R. F., and Jorgensen, N. (1978). Proposed hay Grading Standards Based on Laboratory Analyses for Evaluating Quality. *J. Anim. Sci.* 47, 747–759. doi:10.2527/jas1978.473747x

Roy, S. J., Negrão, S., and Tester, M. (2014). Salt Resistant Crop Plants. *Curr. Opin. Biotechnol.* 26, 115–124. doi:10.1016/j.copbio.2013.12.004

Ruf, T., and Emmerling, C. (2018). Site-adapted Production of Bioenergy Feedstocks on Poorly Drained Cropland through the Cultivation of Perennial Crops. A Feasibility Study on Biomass Yield and Biochemical Methane Potential. *Biomass Bioenergy* 119, 429–435. doi:10.1016/j.biombioe.2018.10.007

Sagers, J. K., Waldron, B. L., Creech, J. E., Mott, I. W., and Bugbee, B. (2017). Salinity Tolerance of Three Competing Rangeland Plant Species: Studies in Hydroponic Culture. *Ecol. Evol.* 7, 10916–10929. doi:10.1002/ece3.3607

Schacht, W. H., Volesky, J. D., Stephenson, M. B., Klopfenstein, T. J., and Adams, D. C. (2010). Plant and Animal Responses to Grazing Systems in the Nebraska Sandhills. *Nebr. Beef Cattle Rep.* 125, 36–37.

Sekmen, A. H., Türkan, İ., and Takio, S. (2007). Differential Responses of Antioxidative Enzymes and Lipid Peroxidation to Salt Stress in Salt-Tolerant *Plantago Maritima* and Salt-Sensitive *Plantago media*. *Physiol. Plant* 131, 399–411. doi:10.1111/j.1399-3054.2007.00970.x

Shannon, M. C. (1978). Testing Salt Tolerance Variability Among Tall Wheatgrass Lines 1. *Agron.j.* 70, 719–722. doi:10.1016/0304-3746(78)90022-710.2134/agronj1978.00021962007000050006x

Sharma, H. C., Ohm, H. W., Lister, R. M., Foster, J. E., and Shukle, R. H. (1989). Response of Wheatgrasses and Wheat × Wheatgrass Hybrids to Barley Yellow dwarf Virus. *Theoret. Appl. Genet.* 77, 369–374. doi:10.1007/BF00305830

Sima, Y.-H., Yao, J.-M., Hou, Y.-S., Wang, L., and Zhao, L.-C. (2011). Variations of Hydrogen Peroxide and Catalase Expression in Bombyx Eggs during Diapause Initiation and Termination. *Arch. Insect Biochem. Physiol.* 77, 72–80. doi:10.1002/arch.20422

Smith, K. F., and Kelman, W. M. (2000). Register of Australian Herbage Plant Cultivars Thinopyrum Ponticum (Podp.) (Tall Wheatgrass) Cv. Dundas. *Aust. J. Exp. Agric.* 40, 119–120. doi:10.1071/EA99156_CU

Strizhov, N., Ábrahám, E., Ökrész, L., Blickling, S., Zilberstein, A., Schell, J., et al. (1997). Differential Expression of Two P5CS Genes Controlling Proline Accumulation during Salt-stress Requires ABA and Is Regulated by ABA1, ABI1 and AXR2 in Arabidopsis. *Plant J.* 12, 557–569. doi:10.1111/j.0960-7412.1997.00557.x

Tjardes, K. E., Buskirk, D. D., Allen, M. S., Tempelman, R. J., Bourquin, L. D., and Rust, S. R. (2002). Neutral Detergent Fiber Concentration in Corn Silage Influences Dry Matter Intake, Diet Digestibility, and Performance of Angus and Holstein Steers2. *J. Anim. Sci.* 80, 841–846. doi:10.2527/2002.803841x

Trammell, M. A., Butler, T. J., Word, K. M., Hopkins, A. A., and Brummer, E. C. (2016). Registration of NFTW6001 Tall Wheatgrass Germplasm. *J. Plant Registrations* 10, 166–170. doi:10.3198/jpr2015.09.0053crg

Trammell, M. A., Hopkins, A. A., Butler, T. J., and Walker, D. (2021). Registration of 'Plainsmen' Tall Wheatgrass. *J. Plant Regist.* 15, 415–421. doi:10.1002/plr2.20142

Van Soest, P. J., Robertson, J. B., and Lewis, B. A. (1991). Methods for Dietary Fiber, Neutral Detergent Fiber, and Nonstarch Polysaccharides in Relation to Animal Nutrition. *J. Dairy Sci.* 74, 3583–3597. doi:10.3168/jds.S0022-0302(91)78551-2

Vogel, K. P., and Moore, K. J. (1998). Forage Yield and Quality of Tall Wheatgrass Accessions in the USDA Germplasm Collection. *Crop Sci.* 38, 509–512. doi:10.2135/cropsci1998.0011183X003800020039x

Wang, P., Yin, L. J., and Li, J. D. (1994). Studies on the Adaptability and Tolerance of *Leymus Chinensis* to Salinity in Salinized Grassland in the Songnen Plain. *Acta Ecol. Sin.* 14, 306–311.

Wang, X. J., Hou, L., Li, G. H., Zhao, C. Z., Zhao, S. Z., and Xia, H. (2020). New Models of High-Efficient Utilization of the Yellow River Delta saline-alkali Land. *Shandong Agric. Sci.* 52, 128–135.

Wang, R. R.-C. (2011). "*Agropyron* and *Psathyrostachys*," in *Wild Crop Relatives: Genomic and Breeding Resources*. Editor C. Kole (Berlin, Heidelberg: Springer), 77–108. doi:10.1007/978-3-642-14228-4_2

Weimberg, R., and Shannon, M. C. (1988). Vigor and Salt Tolerance in 3 Lines of Tall Wheatgrass. *Physiol. Plant* 73, 232–237. doi:10.1111/j.1399-3054.1988.tb00591.x

Xie, H., Li, J., Zhang, Y., Xu, X., Wang, L., and Ouyang, Z. (2021). Evaluation of Coastal Farming under Salinization and Optimized Fertilization Strategies in China. *Sci. Total Environ.* 797, 149038. doi:10.1016/j.scitotenv.2021.149038

Xiong, Y., Xu, Q. F., Yu, Z., Zhou, Q., Ye, Z. S., Ou, X., et al. (2018). Evaluation of Nutritional and Feeding Value of Oat hay from Different Regions. *Pratacult. Sci.* 35, 2457–2462.

Xu, H. X., Zhang, X., Wang, S. M., Yan, P., and Dou, J. Z. (2008). Genetic Diversity of *Achnatherum Splendens*. *Agric. Sci. Technol.* 36, 6223–6224.

Yang, S. (1999). *Feed Analysis and Quality Test Technology*. Beijing: Beijing Agricultural University Press.

Yuan, W.-Y., and Tomita, M. (2015). *Thinopyrum Ponticum* Chromatin-Integrated Wheat Genome Shows Salt-Tolerance at Germination Stage. *Ijms* 16, 4512–4517. doi:10.3390/ijms16034512

Zhang, J. K., Lu, D. X., Liu, J. X., Bao, S. N., Zou, Q. H., and Liu, Q. H. (2004). The Present Research Situation and Progress of Crude Fodder Quality Evaluation index. *Pratacul. Sci.* 21, 55–61.

Zhang, H., Xiang, Y., Irving, L. J., Li, Q., and Zhou, D. (2018). Nitrogen Addition Can Improve Seedling Establishment of N-Sensitive Species in Degraded saline Soils. *Land Degrad. Dev.* 30, 119–127. doi:10.1002/ldr.3195

Zhang, Q., Liu, J., Liu, X., Li, S., Sun, Y., Lu, W., et al. (2020). Optimizing Water and Phosphorus Management to Improve hay Yield and Water- and Phosphorus-use Efficiency in Alfalfa under Drip Irrigation. *Food Sci. Nutr.* 8, 2406–2418. doi:10.1002/fsn3.1530

Zhang, L. Y. (2007). *Feed Analysis and Quality Test Technology*. Beijing: China Agricultural University Press.

Conflict of Interest: The authors declare that the research was conducted in the absence of any commercial or financial relationships that could be construed as a potential conflict of interest.

Publisher's Note: All claims expressed in this article are solely those of the authors and do not necessarily represent those of their affiliated organizations, or those of the publisher, the editors, and the reviewers. Any product that may be evaluated in this article, or claim that may be made by its manufacturer, is not guaranteed or endorsed by the publisher.

GLOSSARY

ADF acid detergent fiber
CAT catalase
CF crude fiber
Chl *a* chlorophyll *a*
Chl *b* chlorophyll *b*
CP crude protein
DDM digestible dry matter
DM dry matter
DMI dry matter intake
EE ether extract
LFW leaf fresh weight
NDF neutral detergent fiber
PH plant height
Pro proline
RFQ relative forage quality
RFV relative feeding value
SFW stem fresh weight
SN spike number
SNPS spikelet number per spike
SOD superoxide dismutase
STDW shoot total dry weight
STFW shoot total fresh weight
TC tannin content
TDN total digestible nutrient
TMV total membership value
TN tiller number
WSC water-soluble carbohydrate
18DF 2018 Dongying, flowering stage
18DM 2018 Dongying, milk-ripe stage
18HF 2018 Haixing, flowering stage
18HM 2018 Haixing, milk-ripe stage
19DF 2019 Dongying, flowering stage
19DM 2019 Dongying, milk-ripe stage

frontiers in Genetics

ORIGINAL RESEARCH
published: 17 February 2022
doi: 10.3389/fgene.2022.819844

Identification of the Powdery Mildew Resistance in Chinese Wheat Cultivar Heng 4568 and its Evaluation in Marker-Assisted Selection

Huiming Gao[1], *Xiaozhe Xu*[2,3], *Pengfei Ai*[1], *Fuyi Luo*[4], *Peng Guo*[1] *and Pengtao Ma*[2]*

[1]College of Food Science and Biology, Hebei University of Science and Technology, Shijiazhuang, China, [2]College of Life Sciences, Yantai University, Yantai, China, [3]School of Computer and Control Engineering, Yantai University, Yantai, China, [4]Dezhou Agricultural Technology Extension and Seed Industry Center, Dezhou, China

Powdery mildew induced by *Blumeria graminis* f. sp. *Tritici* (*Bgt*) has a devastating impact on global wheat yield and quality. Host resistance is the most effective and economical means to control this disease. In this study, Heng 4568, an elite wheat cultivar, shows high resistance to 12 *Bgt* isolates from different regions in China at the seedling stage. Genetic analysis demonstrates that the powdery mildew resistance in Heng 4568 is conferred by a single dominant locus, temporarily designated *PmH4568*. Furthermore, *PmH4568* is mapped to the reported *Pm2* interval on chromosome 5DS with five *Pm2* linked markers and flanked by the markers *Bwm20* and *Bwm21* with a genetic distance of 0.3 and 0.6 cM, respectively. To further investigate the relationship between *PmH4568* and *Pm2*, the diagnostic marker *Pm2b-map-3* of *Pm2* is used to genotype the $F_{2:3}$ population derived from the cross Heng 4568 × Daimai 2173. Notably, there is no recombination found, indicating that *PmH4568* is also probably a *Pm2* allele. In addition, five closely linked markers as well as one diagnostic marker are successfully developed and tested in 16 wheat cultivars from different agro-ecological areas in China, which have potential applications in molecular breeding by marker-assisted selection.

Keywords: wheat powdery mildew, Heng 4568, molecular markers, MAS, *Pm2*

OPEN ACCESS

Edited by:
Ahmed Sallam,
Assiut University, Egypt

Reviewed by:
Amira M. I. Mourad,
Assiut University, Egypt
Zixian Zeng,
Sichuan Normal University, China

***Correspondence:**
Pengtao Ma
ptma@ytu.edu.cn

Specialty section:
This article was submitted to Plant Genomics, a section of the journal Frontiers in Genetics

Received: *22 November 2021*
Accepted: *17 January 2022*
Published: *17 February 2022*

Citation:
Gao H, Xu X, Ai P, Luo F, Guo P and Ma P (2022) Identification of the Powdery Mildew Resistance in Chinese Wheat Cultivar Heng 4568 and its Evaluation in Marker-Assisted Selection. Front. Genet. 13:819844. doi: 10.3389/fgene.2022.819844

INTRODUCTION

Wheat powdery mildew incited by the biotrophic fungus *Blumeria graminis* f. sp. tritici (*Bgt*) is a foliar disease worldwide (Wu et al., 2019). The rapid spread of powdery mildew will cause severe wheat yield losses in a short time, especially in the winter wheat-growing regions with high inputs of irrigation and fertilizers (Luo et al., 2009; Hao et al., 2014). In China alone, the area of winter wheat affected annually by powdery mildew has exceeded 6 mha during recent decades, causing 300,000 tons of crop loss each year (http://cb.natesc.gov.cn/sites/cb/). With the climate getting warmer, the epidemics of wheat powdery mildew in China are growing more severe, which will always be a serious threat to national food security.

Given the significant yield-limiting effects of powdery mildew, the research and exploration of effective prevention and control technology has become urgent in wheat production. Currently, chemical control, biological control, and cultivation of disease-resistant varieties are common means. Chemical control is mainly by spraying fungicides to kill the *Bgt* isolates; however, it always pollutes the environment and accelerates variation of the *Bgt* isolates (Ma et al., 2018, 2019). Biological

control mainly relies on some natural beneficial microorganisms and/or some existing substances in nature, to act as a natural antagonist of pathogen to resist other plant pathogen (Curtis et al., 2012). In comparison, host resistance is relatively the most effective, economical, and environmental way to control wheat powdery mildew, including broadening wheat resistance sources, polymerizing disease-resistant genes, and spreading disease-resistant cultivars (Felsenstein et al., 2010; Ma et al., 2018, Ma et al., 2019).

To date, more than 100 powdery mildew resistance (*Pm*) genes/alleles have been identified at 63 loci in wheat and its relatives (Li et al., 2019; McIntoshet al., 2019; He et al., 2021a; He et al., 2021b). Although several *Pm* genes have been widely used in production and provided high protection at both seedling and adult plant stages, more and more *Pm* genes are no longer effective against powdery mildew due to virulent mutants of the *Bgt* isolates (Xiao et al., 2013). Therefore, it is necessary to increase the genetic diversity of the resistant genes and characterize more effective alleles in wheat germplasms.

When a *Pm* gene was identified, its utilization efficiency in wheat production was mainly decided by its effectiveness and the agronomic performance of its donor (Zhao et al., 2013; Ma et al., 2018). There are some reports that several genes cannot be easily used for genetic improvement of powdery mildew resistance because of the linkage drag, competition drag, and adverse pleiotropism (Jia et al., 2020). One example is the gene *Pm16,* which is able to provide high resistance to different *Bgt* isolates, but will cause severe reduction of 15% in yield (Summers and Brown, 2013). Usually, commercial wheat cultivars have excellent agronomic performance without significantly bad traits and could be used as donors of valuable genes. In fact, several *Pm* genes have been identified from the cultivars with broad-spectrum resistance, such as *PmJM23* from Jimai 23 (Jia et al., 2020), *Pm52* from Liangxing 99 (Zhao et al., 2013), *PmW14* from Wennong 14 (Song et al., 2014), and *PmTm4* from Tangmai 4 (Xie et al., 2017). Therefore, characterization of powdery mildew resistance in the elite cultivars is important for isolating the underlying genes, which could be rationally used in breeding.

Marker-assisted selection (MAS) has enormous potential to improve the efficiency and precision in wheat breeding. Compared to the conventional breeding, MAS can combine several functional alleles from several individuals into one single genotype more precisely, with less unintentional losses and in fewer selection cycles (Xu and Crouch. 2008; Jiang et al., 2017). To perform MAS, closely linked molecular markers play a key role in tracing the targeted genes in the breeding population. Up to now, many molecular markers closely linked to *Pm* genes have been developed for MAS and efficiently used in different genetic backgrounds, thereby generating a large number of wheat breeding lines or resistant cultivars (Ma et al., 2018; Shah et al., 2018; Yu et al., 2018; Ye et al., 2019; Jia et al., 2020; Zhang et al., 2021). For instance, using tightly linked markers to *Pm2* and *Pm21* or co-segregate with *Pm4a*, three two-gene combinations, namely, *Pm2* + *Pm4a*, *Pm2* + *Pm21*, and *Pm4a* + *Pm21*, were successfully transferred into the commercial wheat cultivar "Yangmai 158" and double homozygotes were selected from the F_2 population (Liu et al., 2000). In addition, MAS was also applied for other disease resistant in wheat, such as *Fusarium* head blight and stripe rust (Steiner et al., 2017; Nsabiyera et al., 2018; Su et al., 2018; Randhawa et al., 2019; Maré et al., 2020).

Heng 4568, an elite wheat cultivar, shows high resistance to powdery mildew. A previous study indicated that Heng 4568 most likely carries the known *Pm52* inherited from Liangxing 99 (Zou et al., 2017). Notably, Heng 4568 showed a broader resistant spectrum to different *Bgt* isolates than Liangxing 99 in our evaluation of disease resistance. Therefore, the objectives of this study include (1) analyzing its powdery mildew resistance using different *Bgt* isolates, (2) clarifying the presence of other *Pm* genes in Heng 4568 besides *Pm52*, and (3) developing molecular markers of the new identified *Pm* gene for MAS.

MATERIALS AND METHODS

Plant Materials

The winter wheat cultivar Heng 4568 crossed by Hengyou 18 and Liangxing 99 was provided by the Institute of Dry Farming Agriculture, Hebei Academy of Agriculture and Forestry Sciences, and used as the donor of resistant gene(s) against powdery mildew. Wheat cultivar Daimai 2173 served as a susceptible parent that was crossed with Heng 4568 to produce F_1 hybrids, F_2 population, and $F_{2:3}$ families for genetic analysis and molecular mapping of the *Pm* gene(s) in Heng 4568. Five wheat cultivars/lines with known *Pm* genes, namely, Liangxing99 (*Pm52*), Wennong14 (*PmW14*), Zhongmai155 (*PmZ155*), Jimai22 (*Pm52* + *PmJM23*), and Ulka/8*Cc (*Pm2a*), were used to compare their reaction patterns to different *Bgt* isolates with that of Heng 4568. Susceptible wheat cultivar Huixianhong was used as the susceptible control for phenotypic assessment. Sixteen susceptible wheat cultivars from different ecological regions in China (Hebei, Shandong, Henan, Shaanxi, Beijing, Anhui, and Jiangsu provinces in China) were used to evaluate the availability of closely linked markers for MAS.

Assessment of Disease Resistance at the Seedling Stage

From 2019 to 2021, the assessment of disease resistance at the seedling stage was carried out in the greenhouse at Hebei University of Science and Technology (Shijiazhuang, China). Twelve *Bgt* isolates were collected from different wheat production regions in China. They were used to determine the reaction patterns of Heng 4568 and wheat genotypes with known *Pm* genes. For each *Bgt* isolate, at least 20 seeds for each genotype were sown in 128-cell rectangular trays in a growth chamber. The susceptible control Huixianhong was randomly planted in the tray. When the first leaves were unfolded, the seedlings were inoculated by *Bgt* conidiospores that were previously increased on Huixianhong seedlings. Then, the inoculated seedlings were incubated in an airtight dark environment for 24 h and then allowed disease symptom development in a greenhouse with a daily cycle of 14 h of light at 22°C and 10 h of darkness at 18°C (Qu et al., 2020). To perform genetic analysis, *Bgt* isolate KD07

TABLE 1 | Infection types of Heng 4568 and other genotypes with *Pm2* alleles to 12 *Blumeria graminis* f. *sp. tritici* (*Bgt*) isolates at the seedling stage.

Cultivar/lines	Pm genes	*Blumeria graminis tritici* isolates (*Bgt*)											
		KD01	KD02	KD03	KD04	KD05	KD06	KD07	KD08	KD09	KD10	KD11	KD12
Heng 4568	*PmH4568 + Pm52*	0	0	1	0	0	0	1	1	0	0	2	0
Ulka/8*Cc	*Pm2a*	0	0	3	0	0	1	4	3	0	0	4	0
Liangxing 99	*Pm52*	0	0	4	0	0	0	4	4	0	0	4	0
Wennong 14	*PmW14*	0	0	2	0	0	0	3	3	0	0	3	0
Zhongmai 155	*PmZ155*	0	0	2	0	0	0	2	3	0	0	3	0
Jimai 22	*PmJM23+Pm52*	0	0	1	0	0	0	0	0	0	0	2	0
Daimai 2173	-	4	4	4	4	4	4	4	4	3	4	4	3
Mingxian 169	-	4	4	3	4	4	4	4	4	3	4	4	4

Note: A 0–4 scale was used to scored infection types (IT), of which 0, 0; 1 and 2 are considered to be resistant, while those with an IT score of 3 or 4 are considered to be susceptible. Wheat genotypes Huixianhong and Daimai 2173 were used as susceptible controls.

was selected to inoculate seeding of Heng 4568, the susceptible cultivar Daimai 2173, and their F_1, F_2, and $F_{2:3}$ progenies. For F_1 hybrids, 10 plants were sown; for F_2 population, 177 plants were sown; for $F_{2:3}$ families, 172 families and 20–30 plants per family were sown. Two weeks after inoculation when the spores were fully developed on the susceptible controls, infection types (ITs) on the primary leaves of plants were rated with a scale of 0, 0;, 1, 2, 3, and 4. The leaves that displayed ITs 0–2 and 3–4 were regarded as resistant and susceptible, respectively (Liu et al., 1999). Three repeated experiments were carried out using the same procedure.

Molecular Marker Analysis

Genomic DNA was extracted from the young leaf tissues following the cetyltriethylammonium bromide method (Saghai-Maroof et al., 1984). Resistant and susceptible DNA bulks were created by separately mixing equal amount of DNA from 10 homozygously resistant and 10 homozygously susceptible plants, respectively. Forty-eight molecular markers closely linked to 37 known *Pm* genes were firstly screened for their polymorphisms between Heng 4568, Daimai 2173, and their derived resistant and susceptible bulks (**Supplementary Table S1**). When the *Pm* gene in Heng 4568 was preliminarily to *Pm2* locus, other *Pm2* linked markers *Cfd81*, *Bwm20*, *Bwm21*, *Bwm25*, and *Swgi067* (Lu et al., 2015; Ma et al., 2018) and the diagnostic marker *Pm2b-map-3* (Jin et al., 2021) were also used to add the marker density for conducting the linkage map (**Supplementary Table S2**). PCR was performed in a 10-μl reaction volume containing 1 μl of 40–50 ng/μl template genomic DNA, 4.5 μl of 2×Taq Master Mix (Vazyme, China), and 0.5 μl of 10 μM/μl primer mix. The PCR program used was 95°C for 5 min; 36 cycles of 95°C for 30 s, 50–60°C (depending on specific primers) for 40 s, final extension at 72°C for 5 min; and storage at 4°C. PCR products were separated in 8.0% nondenaturing polyacrylamide gels with 29:1 ratio of acrylamide and bis-acrylamide with 1 × TBE buffer and then silver-stained and visualized as previously described (Santos et al., 1993).

Statistical Analysis and Linkage Map Construction

After confirming genotypes of $F_{2:3}$ families of Heng 4568 and Daimai 2173, the deviations of the observed phenotypic data from theoretically expected segregation ratios for goodness of fit were assessed using χ^2 test. MAPMAKER 3.0 and the Kosambi function were performed to construct the linkage map of the powdery mildew resistance gene in Heng 4568.

RESULTS

Evaluation of Powdery Mildew Resistance in Heng 4568

Heng 4568 was highly resistant to 12 *Bgt* isolates with the ITs 0–2, whereas Daimai 2173 and susceptible control Huixianhong were all highly susceptible to all the tested *Bgt* isolates (**Table 1**). Compared with the *Pm52* donor Liangxing 99, Heng 4568 was resistant to the *Bgt* isolates KD03, KD07, KD08, and KD11, while *Pm52* was susceptible to these four Bgt isolates, indicating that Heng 4568 contains other *Pm* gene(s).

Genetic Analysis of *Pm* Genes in Heng 4568

To explore other *Pm* gene(s) besides *Pm52* in Heng 4568, the isolate KD07 virulent to Liangxing 99 (with *Pm52*) and avirulent to Heng 4568 was selected to inoculate Heng 4568, Daimai 2173, and their derived F_1 seeds, F_2 population, and $F_{2:3}$ families, respectively. All the tested F_1 seedlings were resistant to KD07 similar to their parent Heng 4568. The F_2 population fitted the segregation ratio of a single dominant gene (**Table 2**). The harvested $F_{2:3}$ families from the F_2 population confirmed the expected ratio of 1:2:1 (**Table 2**). Therefore, it was concluded that another dominant *Pm* gene is also involved in Heng 4568, which was temporarily designated *PmH4568*.

Molecular Mapping of *PmH4568*

To determine the genetic location of *PmH4568*, 48 molecular markers closely linked to the known *Pm* genes were firstly used to test their polymorphisms between the parents and the two contrasting bulks. The *Pm2*-linked marker *Cfd81* showed consistent polymorphism between Heng 4568, Daimai 2173, and their derived contrasting bulks. Then, *Cfd81* was used to genotype the $F_{2:3}$ families of Heng 4568 and Daimai 2173 and confirmed its linkage relationship with *PmH4568* (**Figures 1**, **2**; **Supplementary Table S2**). This suggested that *PmH4568* was most likely located in the *Pm2* interval. To confirm this interval,

TABLE 2 | Segregation ratios of F_2 and $F_{2:3}$ generations of Heng 4568 × Daimai 2173 following inoculation with *Blumeria graminis* f. s. *tritici* (*Bgt*) isolate KD07 at the seedling stage.

Cross	Plants observed			Expected ratio	χ^2	*p*
	HR	Seg	HS			
Heng4568 × Daimai2173 F_2	130		47	3:1	0.23	0.63
Heng4568 × Daimai2173 $F_{2:3}$	43	83	46	1:2:1	0.31	0.85

Note: Values of χ^2 for statistical significance at p = *0.05 are 3.84 (1df) and 5.99 (2df); HR, homozygous resistant, Seg: segregating, HS, homozygous susceptible. Discrepancies on the line numbers between F2 and F3 generation are because several F2 plants were died during the growth process.*

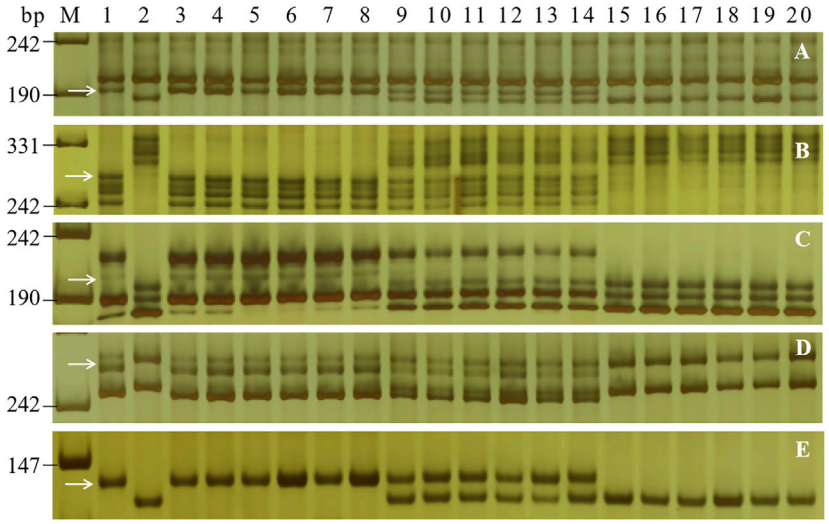

FIGURE 1 | PCR amplification patterns of the selected markers *Bwm20* **(A)**, *Bwm21***(B)**, *Bwm25***(C)**, *Cfd81* **(D)**, and the diagnostic *Pm2b-map-3* **(E)** in genotyping Heng 4568, Daimai 2173, and random selected $F_{2:3}$ families of Heng 4568 × Daimai 2173. Lane M: pUC19 *Msp* I; lanes 1–2: Heng4568 and Daimai 2173; lanes 3–8: homozygous-resistant $F_{2:3}$ families; lanes 9–14: heterozygous $F_{2:3}$ families; lanes 15–20, homozygous susceptible $F_{2:3}$ families. The white arrows indicate the polymorphic bands in Heng4568.

four additional *Pm2*-linked markers, *Bwm20*, *Bwm21*, *Bwm25*, and *Swgi067*, were also proved to be closely linked to *PmH4568* (**Figure 1**; **Supplementary Table S2**). A genetic linkage map was then conducted to locate *PmH4568* to the *Pm2* interval (**Figure 2**). To further confirm the relationship between *PmH4568* and *Pm2*, *Pm2b-map-3*, the diagnostic marker of *Pm2*, was used to genotype the $F_{2:3}$ families of Heng4568 and Daimai 2173 (**Figure 1**; **Supplementary Table S2**). No recombinants were found, suggesting that *PmH4568* was located in the *Pm2* locus and most likely a *Pm2* allele.

Evaluation of Closely Linked Markers for Marker-Assisted Selection

To transfer *PmH4568* to susceptible cultivars using MAS, five *PmH4568*-linked markers, *Bwm20*, *Bwm21*, *Bwm25*, *Swgi067*, and *Cfd81*, and the diagnostic marker *Pm2b-map-3*, were used to test Heng 4568 and 16 susceptible cultivars. The results showed that all the tested markers could amplify polymorphic bands between Heng 4568 and these susceptible cultivars, indicating that once *PmH4568* is transferred into the susceptible cultivars through conventional hybridization, these markers can be used to detect *PmH4568*, especially the diagnostic marker *Pm2b-map-3* (**Figure 3**; **Table 3**).

DISCUSSION

Heng 4568 is an elite winter wheat cultivar in Northern China. Due to its superior agronomic performance and powdery mildew resistance, Heng 4568 is considered as an attractive cultivar and serves as a favorable breeding parent for resistance improvement. A previous study indicated that the known *Pm52* located on the chromosome 2BL was involved in Heng 4568, which may confer the powdery mildew resistance (Zou et al., 2017). *Pm52* is a widely used *Pm* gene in Chinese cultivars, such as Hanong 2312, Zhongxinmai 99, Shimai 26, and DH51302. Heng 4568 was derived from the cross of Liangxing 99 with Hengyou 18, indicating that *Pm52* in Heng 4568 may be derived from its parent Liangxing 99. However, our study demonstrated that Heng 4568 showed significantly broader resistant spectrum than the *Pm52* donor Liangxing 99, suggesting that other *Pm*

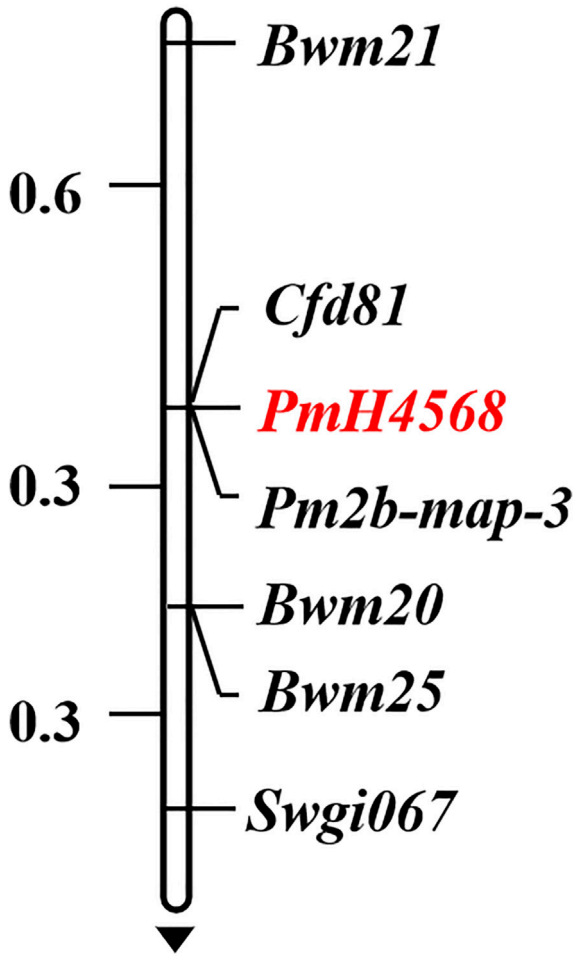

FIGURE 2 | Linkage map of *PmH4568* using the $F_{2:3}$ families of Heng 4568 × Daimai 2173. Genetic distances in cM are showed to the left. The black arrow points to the centromere.

genes may also be involved in Heng 4568. To clarify the composition of the *Pm* genes in Heng 4568, a *Bgt* isolate virulent KD07 was used to identify other *Pm* gene(s) in Heng 4568. The result showed that another dominant *Pm* gene *PmH4568* also contributed to the powdery mildew resistance in Heng 4568. This result, together with a previous study, provided an explicit genetic constitution for the powdery mildew resistance in Heng 4568, which contributes to scientific parental selection collocation.

Using *Pm2*-linked markers, *PmH4568* was mapped to the known *Pm2* interval on chromosome arm 5DS. According to previous studies, a series of *Pm2* alleles have been reported in the *Pm2* interval, such as *Pm2a* (Qiu et al., 2006), *Pm2b* (Ma et al., 2015a), *Pm2c* (Xu et al., 2015), *PmLX66* (Huang et al., 2012), *PmX3986-2* (Ma et al., 2014), *PmWFJ* (Ma et al., 2015b), *PmYB* (Ma et al., 2015c), *PmZ155* (Sun H. et al., 2015), *PmW14* (Sun Y. et al., 2015), *PmWFJ* (Ma et al., 2015a), *PmSub* (Jin et al., 2018), *Pm10V-2* (Ma et al., 2018), *PmJM23* (Jia et al., 2020), and *PmFG* (Ma et al., 2016). Using MutChromSeq (Mutant chromosome sequencing) (Sáchez-Martín et al., 2016) and analysis of the fine mapping interval (Chen et al., 2019), *Pm2* was cloned and confirmed to encode a CC-NBS-LRR protein. Haplotype analysis of 48 hexaploid common wheat carrying *Pm2* alleles showed that all these *Pm2* donors have the perfectly consistent as the cloned sequence above. However, different *Pm2* alleles derived from hexaploid common wheat have significantly different resistant spectra (Ma et al., 2018; Jia et al., 2020). This may be due to their different genetic backgrounds, and also complex genetic constitution or resistance mechanism may be involved in this interval. Anyway, *Pm2* is an elite gene locus that is very valuable for resistance breeding, even though the complex *Pm2* locus has not been fully characterized.

In wheat resistance breeding using MAS, the breeding potential of a certain gene depends not only on its resistance but also on the comprehensively agronomic traits, such as yield,

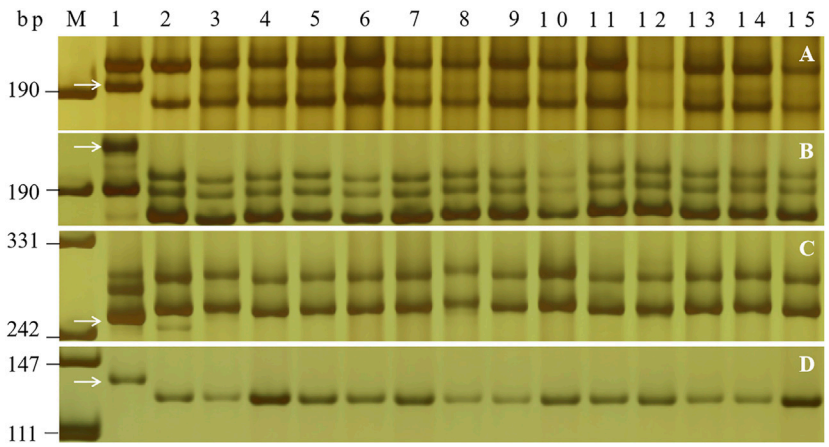

FIGURE 3 | PCR amplification patterns of the markers *Bwm20* **(A)**, *Bwm25* **(B)**, *Cfd81***(C)**, and *Pm2b-map-3* **(D)** in genotyping Heng 4568, Daimai 2173, and 13 selected wheat cultivars. Lanes M: pUC19 *Msp* I; lanes 1–2: Heng 4568 and Daimai 2173; lanes 3–15: Shannong 1538, Hanmai 13, Zhoumai 27, Xinong 979, Jimai 229, Jimai 21, Jimai 20, Zhongyu 9398, Womai 8, Shimai 15, Xinluo 4, Zhengmai 0856, and Wunong 6. The white arrows indicate the polymorphic bands in Heng 4568.

TABLE 3 | Validation of PmH4568-linked and diagnostic markers on 16 Chinese wheat cultivars in marker-assisted selection (MAS) breeding.

Cultivars	Region	*Bwm20*	*Bwm21*	*Bwm25*	*SWGI067*	*Cfd81*	*Pm2b-map-3*
Heng 4568	Hebei	+	+	+	+	+	+
Daimai 2173	Shandong	-	-	-	-	-	-
Shannong 1538	Shandong	-	-	-	-	-	-
Hanmai 13	Hebei	-	-	-	-	-	-
Zhoumai 27	Henan	-	-	-	-	-	-
Xinong 979	Shaanxi	-	-	-	-	-	-
Jimai 229	Shandong	-	-	-	-	-	-
Jimai 21	Shandong	-	-	-	-	-	-
Jimai 20	Shandong	-	-	-	-	-	-
Zhongyu 9398	Henan	-	-	-	-	-	-
Womai 8	Anhui	-	-	-	-	-	-
Shimai 15	Hebei	-	-	-	-	-	-
Xinluo 4	Henan	-	-	-	-	-	-
Zhengmai 0856	Henan	-	-	-	-	-	-
Wunong 6	Shaanxi	-	-	-	-	-	-
Huaimai 0226	Jiangsu	-	-	-	-	-	-
Luchen 185	Shandong	-	-	-	-	-	-
Zhongyu 1311	Beijing	-	-	-	-	-	-

Note: "+" represents that the markers cannot amplify the polymorphic products linked to PmH4568 *in the tested genetic backgrounds, and "-" shows the opposite result.*

quality, and high combining ability. Thus, although many *Pm* genes/alleles have been identified, only several have been widely used in breeding programs (Li et al., 2011). The main obstacle that limits the application of these genes is linkage drag in most resistance donors. After transferring these *Pm* genes into susceptible commercial cultivars, unfavorable traits linked to them will lead to poor agricultural yield or quality performances (Ma et al., 2015b). Therefore, the resistance donors with excellent agricultural performance are very popular for breeders. Fortunately, Heng 4568 is a cultivar with desirable comprehensively agronomic traits. For powdery mildew resistance, Heng 4568 also carries *Pm52* besides the *Pm2* allele *PmH4568*. In China, *Pm2* and *Pm52* are two major *Pm* genes in many resistance cultivars, such as Liangxing 66, Wennong 14, YingBo 700, Zhongmai 155, Jimai 23 (Jia et al., 2020), and Nongda 399, which all have the *Pm2* allele, and Liangxing 99, Hannong 2312, Zhongxinmai 99, DH51302, and Zhimai 26, which all have *Pm52* (Qu et al., 2020). Compared with these resistance cultivars, Heng 4568 has two resistance genes, which may show more durable resistance than a single resistance gene; such a situation also involved Jimai 22, a famous cultivar with the largest promotion area in the last 10 years (Jia et al., 2020). For the yield and quality, there was no significant defect in the recent years in our field. Particularly worth mentioning is its high combining ability in breeding; two famous wheat cultivars, Hengmai 28 and Jiamai 361, have been released in production using Heng 4568 as parent (https://www.Chinaseed114.com/seed/16/seed_77094.html; https://www.chinaseed114.com/seed/14/seed_69187.html), and in our lab, Heng 4568 is also a popular breeding parent for both resistance and yield improvement. Therefore, Heng 4568 can be not only directly popularized in region with high incidence of powdery mildew, but also used as a valuable breeding parent to improve powdery mildew resistance.

To transfer the *Pm* genes in Heng 4568, MAS is a rapid and effective way (William et al., 2007; Ashra and Foolad, 2013; Collard and Mackill, 2018). Since fine mapping of *Pm52* has been carried out, many closely linked markers of *Pm52* have been developed for MAS (Wu et al., 2019). In this study, the applicability of five closely linked markers and one diagnostic marker has been investigated in MAS with 16 susceptible wheat cultivars. In particular, the diagnostic marker *Pm2b-map-3* is a functional marker designed by SNPs within the *Pm2* sequence, suggesting that there is no recombinant in MAS. Therefore, resistance breeding using Heng 4568 as a parent is promising, and more *trans*-breeding studies using Heng 4568 are under way in our lab.

CONCLUSION

In this study, *PmH4568*, an effective *Pm* gene in the elite cultivar Heng 4568, has been identified and proved to be a *Pm2* allele. We further clarify the genetic components of the powdery mildew resistance in Heng 4568. The applicability of closely linked markers, including the diagnostic marker, was validated in MAS. Overall, this work will accelerate the utilization of the powdery mildew resistance in Heng 4568.

DATA AVAILABILITY STATEMENT

The original contributions presented in the study are included in the article/**Supplementary Material**, further inquiries can be directed to the corresponding author.

AUTHOR CONTRIBUTIONS

PM conceived the study. HG, XX, FL, PA, and PG performed the statistical analysis of the experiment. HG wrote the manuscript. All authors critically read, commented, and approved the final manuscript.

FUNDING

This research was financially supported by the Doctoral Research Start-up Fund Project of Hebei University of Science and Technology (1181438), the National Natural Science Foundation of China (32072053), the Key Research and Development Program of Shandong Province (2020CXGC010805), and Open Project Funding of the State Key Laboratory of Crop Stress Adaptation and Improvement (CX1130A0920014).

ACKNOWLEDGMENTS

We appreciate the editor and reviewers for handling our manuscript and providing critical suggestions.

SUPPLEMENTARY MATERIAL

The Supplementary Material for this article can be found online at: https://www.frontiersin.org/articles/10.3389/fgene.2022.819844/full#supplementary-material

REFERENCES

Ashraf, M., and Foolad, M. R. (2013). Crop Breeding for Salt Tolerance in the Era of Molecular Markers and Marker-Assisted Selection. *Plant Breed* 132, 10–20. doi:10.1111/pbr.12000

Chen, F., Jia, H., Zhang, X., Qiao, L., Li, X., Zheng, J., et al. (2019). Positional Cloning of *PmCH1357* Reveals the Origin and Allelic Variation of the *Pm2* Gene for Powdery Mildew Resistance in Wheat. *Crop J.* 7, 771–783. doi:10.1016/j.cj.2019.08.004

Collard, B. C. Y., and Mackill, D. J. (2008). Marker-assisted Selection: an Approach for Precision Plant Breeding in the Twenty-First century. *Phil. Trans. R. Soc. B* 363, 557–572. doi:10.1098/rstb.2007.2170

De Curtis, F., De Cicco, V., and Lima, G. (2012). Efficacy of Biocontrol Yeasts Combined with Calcium Silicate or sulphur for Controlling Durum Wheat Powdery Mildew and Increasing Grain Yield Components. *Field Crops Res.* 134, 36–46. doi:10.1016/j.fcr.2012.04.014

Felsenstein, F., Semar, M., and Stammler, G. (2010). Sensitivity of Wheat Powdery Mildew (Blumeria Graminis f.Sp. Tritici) towards Metrafenone. *Gesunde Pflanzen* 62, 29–33. doi:10.1007/s10343-010-0214-x

Hao, Y., Parks, R., Cowger, C., Chen, Z., Wang, Y., Bland, D., et al. (2014). Molecular Characterization of a New Powdery Mildew Resistance Gene *Pm54* in Soft Red winter Wheat. *Theor. Appl. Genet.* 128, 465–476. doi:10.1007/s00122-014-2445-1

He, H., Du, H., Liu, R., Liu, T., Yang, L., Gong, S., et al. (2021a). Characterization of a New Gene for Resistance to Wheat Powdery Mildew on Chromosome 1RL of Wild rye Secale Sylvestre. *Theor. Appl. Genet.* 134, 887–896. doi:10.1007/s00122-020-03739-1

He, H., Liu, R., Ma, P., Du, H., Zhang, H., Wu, Q., et al. (2021b). Characterization of *Pm68*, a New Powdery Mildew Resistance Gene on Chromosome 2BS of Greek Durum Wheat TRI 1796. *Theor. Appl. Genet.* 134, 53–62. doi:10.1007/s00122-020-03681-2

Huang, J., Zhao, Z., Song, F., Wang, X., Xu, H., Huang, Y., et al. (2012). Molecular Detection of a Gene Effective against Powdery Mildew in the Wheat Cultivar Liangxing 66. *Mol. Breed.* 30, 1737–1745. doi:10.1007/s11032-012-9757-0

Jia, M., Xu, H., Liu, C., Mao, R., Li, H., Liu, J., et al. (2020). Characterization of the Powdery Mildew Resistance Gene in the Elite Wheat Cultivar Jimai 23 and its Application in Marker-Assisted Selection. *Front. Genet.* 11, 241. doi:10.3389/fgene.2020.00241

Jiang, Y., Schulthess, A. W., Rodemann, B., Ling, J., Plieske, J., Kollers, S., et al. (2017). Validating the Prediction Accuracies of Marker-Assisted and Genomic Selection of Fusarium Head Blight Resistance in Wheat Using an Independent Sample. *Theor. Appl. Genet.* 130, 471–482. doi:10.1007/s00122-016-2827-7

Jin, Y., Shi, F., Liu, W., Fu, X., Gu, T., Han, G., et al. (2021). Identification of Resistant Germplasm and Detection of Genes for Resistance to Powdery Mildew and Leaf Rust from 2,978 Wheat Accessions. *Plant Dis.* doi:10.1094/PDIS-03-21-0532-RE

Jin, Y., Xu, H., Ma, P., Fu, X., Song, L., Xu, Y., et al. (2018). Characterization of a New *Pm2* Allele Associated with Broad-Spectrum Powdery Mildew Resistance in Wheat Line Subtil. *Sci. Rep.* 8, 475. doi:10.1038/s41598-017-18827-4

Li, G., Cowger, C., Wang, X., Carver, B. F., and Xu, X. (2019). Characterization of *Pm65*, a New Powdery Mildew Resistance Gene on Chromosome 2AL of a Facultative Wheat Cultivar. *Theor. Appl. Genet.* 132, 2625–2632. doi:10.1007/s00122-019-03377-2

Li, H.-J., Wang, X.-M., Song, F.-J., Wu, C.-P., Wu, X.-F., Zhang, N., et al. (2011). Response to Powdery Mildew and Detection of Resistance Genes in Wheat Cultivars from China. *A S* 37, 943–954. doi:10.3724/sp.j.1006.2011.00943

Liu, J., Liu, D., Tao, W., Li, W., Wang, S., Chen, P., et al. (2000). Molecular Marker-Facilitated Pyramiding of Different Genes for Powdery Mildew Resistance in Wheat. *Plant Breed.* 119, 21–24. doi:10.1046/j.1439-0523.2000.00431.x

Liu, Z., Sun, Q., Ni, Z., Yang, T., and Mcintosh, R. A. (1999). Development of SCAR Markers Linked to the *Pm21* Gene Conferring Resistance to Powdery Mildew in Common Wheat. *Plant Breed.* 118, 215–219. doi:10.1046/j.1439-0523.1999.118003215.x

Lu, Y., Wu, X., Yao, M., Zhang, J., Liu, W., Yang, X., et al. (2015). Genetic Mapping of a Putative Agropyron Cristatum-Derived Powdery Mildew Resistance Gene by a Combination of Bulked Segregant Analysis and Single Nucleotide Polymorphism Array. *Mol. Breed.* 35, 96. doi:10.1007/s11032-015-0292-7

Luo, P. G., Luo, H. Y., Chang, Z. J., Zhang, H. Y., Zhang, M., and Ren, Z. L. (2009). Characterization and Chromosomal Location of *Pm40* in Common Wheat: a New Gene for Resistance to Powdery Mildew Derived from *Elytrigia Intermedium*. *Theor. Appl. Genet.* 118, 1059–1064. doi:10.1007/s00122-009-0962-0

Ma, P., Han, G., Zheng, Q., Liu, S., Han, F., Wang, J., et al. (2020). Development of Novel Wheat-rye Chromosome 4R Translocations and Assignment of Their Powdery Mildew Resistance. *Plant Dis.* 104, 260–268. doi:10.1094/PDIS-01-19-0160-RE

Ma, P., Xu, H., Li, L., Zhang, H., Han, G., Xu, Y., et al. (2016). Characterization of a New *Pm2* Allele Conferring Powdery Mildew Resistance in the Wheat Germplasm Line FG-1. *Front. Plant Sci.* 7, 88. doi:10.3389/fpls.2016.00546

Ma, P., Xu, H., Luo, Q., Qie, Y., Zhou, Y., Xu, Y., et al. (2014). Inheritance and Genetic Mapping of a Gene for Seedling Resistance to Powdery Mildew in Wheat Line X3986-2. *Euphytica* 200, 149–157. doi:10.1007/s10681-014-1178-1

Ma, P., Xu, H., Xu, Y., Li, L., Qie, Y., Luo, Q., et al. (2015a). Molecular Mapping of a New Powdery Mildew Resistance Gene *Pm2b* in Chinese Breeding Line KM2939. *Theor. Appl. Genet.* 128, 613–622. doi:10.1007/s00122-015-2457-5

Ma, P., Xu, H., Xu, Y., Song, L., Liang, S., Sheng, Y., et al. (2018). Characterization of a Powdery Mildew Resistance Gene in Wheat Breeding Line 10V-2 and its Application in Marker-Assisted Selection. *Plant Dis.* 102, 925–931. doi:10.1094/PDIS-02-17-0199-RE

Ma, P., Xu, H., Zhang, H., Li, L., Xu, Y., Zhang, X., et al. (2015b). The Gene *PmWFJ* Is a New Member of the Complex *Pm2* Locus Conferring Unique Powdery Mildew Resistance in Wheat Breeding Line Wanfengjian 34. *Mol. Breed.* 35, 210. doi:10.1007/s11032-015-0403-5

Ma, P., Zhang, H., Xu, H., Xu, Y., Cao, Y., Zhang, X., et al. (2015c). The Gene *PmYB* Confers Broad-Spectrum Powdery Mildew Resistance in the Multi-Allelic *Pm2* Chromosome Region of the Chinese Wheat Cultivar YingBo 700. *Mol. Breed.* 35, 124. doi:10.1007/s11032-015-0320-7

Maré, A., Boshoff, W. H. P., and Herselman, L. (2020). Molecular Breeding of Wheat Lines for Multiple Rust and Fusarium Head Blight Resistance. *Euphytica* 216, 1–12. doi:10.1007/s10681-020-02697-5

McIntosh, R. A., Dubcovsky, J., Rogers, W. J., Xia, X. C., and Raupp, W. J. (2019). "Catalogue of Gene Symbols for Wheat: 2019 Supplement," in *Annual Wheat Newsletter*. Editor W. J. Raupp (Manhattan, USA, p98–113.

Nsabiyera, V., Bariana, H. S., Qureshi, N., Wong, D., Hayden, M. J., and Bansal, U. K. (2018). Characterisation and Mapping of Adult Plant Stripe Rust Resistance in Wheat Accession Aus27284. *Theor. Appl. Genet.* 131, 1459–1467. doi:10.1007/s00122-018-3090-x

Qiu, Y., Sun, X., Zhou, R., Kong, X., Zhang, S., and Jia, J. (2006). Identification of Microsatellite Markers Linked to Powdery Mildew Resistance genePm2in Wheat. *Cereal Res. Commun.* 34, 1267–1273. doi:10.1556/crc.34.2006.4.268

Qu, Y.-f., Wu, P.-p., Hu, J.-h., Chen, Y.-x., Shi, Z.-l., Qiu, D., et al. (2020). Molecular Detection of the Powdery Mildew Resistance Genes in winter Wheats DH51302 and Shimai 26. *J. Integr. Agric.* 19, 931–940. doi:10.1016/S2095-3119(19)62644-4

Randhawa, M. S., Bains, N. S., Sohu, V. S., Chhuneja, P., Trethowan, R. M., Bariana, H. S., et al. (2019). Marker Assisted Transfer of Stripe Rust and Stem Rust Resistance Genes into Four Wheat Cultivars. *Agronomy* 9, 4972073–4974395. doi:10.3390/agronomy9090497

Saghai-Maroof, M. A., Soliman, K. M., Jorgensen, R. A., and Allard, R. W. (1984). Ribosomal DNA Spacer-Length Polymorphisms in Barley: Mendelian Inheritance, Chromosomal Location, and Population Dynamics. *Proc. Natl. Acad. Sci.* 81, 8014–8018. doi:10.1073/pnas.81.24.8014

Sánchez-Martín, J., Steuernagel, B., Ghosh, S., Herren, G., Hurni, S., Adamski, N., et al. (2016). Rapid Gene Isolation in Barley and Wheat by Mutant Chromosome Sequencing. *Genome Biol.* 17, 221. doi:10.1186/s13059-016-1082-1

Santos, F. c., Pena, S. J., and Epplen, J. r. (1993). Genetic and Population Study of a Y-Linked Tetranucleotide Repeat DNA Polymorphism with a Simple Non-isotopic Technique. *Hum. Genet.* 90, 655–656. doi:10.1007/BF00202486

Shah, L., Rehman, S., Ali, A., Yahya, M., Riaz, M. W., Si, H., et al. (2018). Genes Responsible for Powdery Mildew Resistance and Improvement in Wheat Using Molecular Marker-Assisted Selection. *J. Plant Dis. Prot.* 125, 145–158. doi:10.1007/s41348-017-0132-6

Song, W., Sun, H.-G., Sun, Y.-L., Zhao, Z.-H., Wang, X.-M., Wu, X.-F., et al. (2014). Chromosomal Localization of the Gene for Resistance to Powdery Mildew in the Wheat Cultivar Wennong 14. *Acta Agronomica Sinica* 40, 798–804. doi:10.3724/SP.J.1006.2014.00798

Steiner, B., Buerstmayr, M., Michel, S., Schweiger, W., Lemmens, M., and Buerstmayr, H. (2017). Breeding Strategies and Advances in Line Selection for Fusarium Head Blight Resistance in Wheat. *Trop. Plant Pathol.* 42, 165–174. doi:10.1007/s40858-017-0127-7

Su, Z., Jin, S., Zhang, D., and Bai, G. (2018). Development and Validation of Diagnostic Markers for *Fhb1* Region, a Major QTL for Fusarium Head Blight Resistance in Wheat. *Theor. Appl. Genet.* 131, 2371–2380. doi:10.1007/s00122-018-3159-6

Summers, R. W., and Brown, J. K. M. (2013). Constraints on Breeding for Disease Resistance in Commercially Competitive Wheat Cultivars. *Plant Pathol.* 62, 115–121. doi:10.1111/ppa.12165

Sun, H., Song, W., Sun, Y., Chen, X., Liu, J., Zou, J., et al. (2015a). Resistance of 'Zhongmai 155' Wheat to Powdery Mildew: Effectiveness and Detection of the Resistance Gene. *Crop Sci.* 55, 1017–1025. doi:10.2135/cropsci2014.05.0355

Sun, Y., Zou, J., Sun, H., Song, W., Wang, X., and Li, H. (2015b). PmLX66 and PmW14: New Alleles of Pm2 for Resistance to Powdery Mildew in the Chinese Winter Wheat Cultivars Liangxing 66 and Wennong 14. *Plant Dis.* 99, 1118–1124. doi:10.1094/PDIS-10-14-1079-RE

William, H. M., Trethowan, R., and Crosby-Galvan, E. M. (2007). Wheat Breeding Assisted by Markers: CIMMYT's Experience. *Euphytica* 157, 307–319. doi:10.1007/s10681-007-9405-7

Wu, P., Hu, J., Zou, J., Qiu, D., Qu, Y., Li, Y., et al. (2019). Fine Mapping of the Wheat Powdery Mildew Resistance Gene *Pm52* Using Comparative Genomics Analysis and the Chinese spring Reference Genomic Sequence. *Theor. Appl. Genet.* 132, 1451–1461. doi:10.1007/s00122-019-03291-7

Xiao, M., Song, F., Jiao, J., Wang, X., Xu, H., and Li, H. (2013). Identification of the Gene *Pm47* on Chromosome 7BS Conferring Resistance to Powdery Mildew in the Chinese Wheat Landrace Hongyanglazi. *Theor. Appl. Genet.* 126, 1397–1403. doi:10.1007/s00122-013-2060-6

Xie, J.-z., Wang, L.-l., Wang, Y., Zhang, H.-z., Zhou, S.-h., Wu, Q.-h., et al. (2017). Fine Mapping of Powdery Mildew Resistance Gene *PmTm4* in Wheat Using Comparative Genomics. *J. Integr. Agric.* 16, 540–550. doi:10.1016/S2095-3119(16)61377-1

Xu, H., Yi, Y., Ma, P., Qie, Y., Fu, X., Xu, Y., et al. (2015). Molecular Tagging of a New Broad-Spectrum Powdery Mildew Resistance Allele *Pm2c* in Chinese Wheat Landrace Niaomai. *Theor. Appl. Genet.* 128, 2077–2084. doi:10.1007/s00122-015-2568-z

Xu, Y., and Crouch, J. H. (2008). Marker-Assisted Selection in Plant Breeding: From Publications to Practice. *Crop Sci.* 48, 391–407. doi:10.2135/cropsci2007.04.0191

Ye, X., Zhang, S., Li, S., Wang, J., Chen, H., Wang, K., et al. (2019). Improvement of Three Commercial spring Wheat Varieties for Powdery Mildew Resistance by Marker-Assisted Selection. *Crop Prot.* 125, 104889. doi:10.1016/j.cropro.2019.104889

Yu, X., Ren, S., Zhao, L., Guo, J., Bao, Y., Ma, Y., et al. (2018). Molecular Mapping of a Novel Wheat Powdery Mildew Resistance Gene Ml92145E8-9 and its Application in Wheat Breeding by Marker-Assisted Selection. *Crop J.* 6, 621–627. doi:10.1016/j.cj.2018.04.004

Zhang, X., Wang, W., Liu, C., Zhu, S., Gao, H., Xu, H., et al. (2021). Diagnostic Kompetitive Allele-specific PCR Markers of Wheat Broad-Spectrum Powdery Mildew Resistance Genes Pm21, PmV, and Pm12 Developed for High-Throughput Marker-Assisted Selection. *Plant Dis.* 105, 2844–2850. doi:10.1094/PDIS-02-21-0308-RE

Zhao, Z., Sun, H., Song, W., Lu, M., Huang, J., Wu, L., et al. (2013). Genetic Analysis and Detection of the Gene *Mllx99* on Chromosome 2bl Conferring Resistance to Powdery Mildew in the Wheat Cultivar Liangxing 99. *Theor. Appl. Genet.* 126, 3081–3089. doi:10.1007/s00122-013-2194-6

Zou, J.-W., Qiu, D., Sun, Y.-L., Zheng, C.-X., Li, J.-T., Wu, P.-P., et al. (2017). Pm52: Effectiveness of the Gene Conferring Resistance to Powdery Mildew in Wheat Cultivar Liangxing 99. *Acta Agronomica Sinica* 43, 332–342. doi:10.3724/SP.J.1006.2017.00332

Conflict of Interest: The authors declare that the research was conducted in the absence of any commercial or financial relationships that could be construed as a potential conflict of interest.

Publisher's Note: All claims expressed in this article are solely those of the authors and do not necessarily represent those of their affiliated organizations, or those of the publisher, the editors, and the reviewers. Any product that may be evaluated in this article, or claim that may be made by its manufacturer, is not guaranteed or endorsed by the publisher.

frontiers in Genetics

ORIGINAL RESEARCH
published: 15 March 2022
doi: 10.3389/fgene.2022.832898

Identification of Genetic Loci Affecting Flag Leaf Chlorophyll in Wheat Grown under Different Water Regimes

Bin Yang[1,2†], Xiaojie Wen[3†], Hongwei Wen[1], Yanru Feng[4,5], Jiajia Zhao[1], Bangbang Wu[1], Xingwei Zheng[1], Chenkang Yang[1], Sanwei Yang[2], Ling Qiao[1]* and Jun Zheng[1]**

[1]Institute of Wheat Research, Shanxi Agricultural University/ State Key Laboratory of Sustainable Dryland Agriculture, Linfen, China, [2]College of Agricultural Economics and Management, Shanxi Agricultural University, Taiyuan, China, [3]Biotechnology Research Institute, Chinese Academy of Agricultural Sciences, Beijing, China, [4]Institute of Crop Science and Resource Conservation (INRES), Crop Science, University of Bonn, Bonn, Germany, [5]Department of Agronomy and Crop Physiology, Institute for Agronomy and Plant Breeding, Justus Liebig University Giessen, Giessen, Germany

OPEN ACCESS

Edited by:
Pengtao Ma,
Yantai University, China

Reviewed by:
Zhengrui Qin,
Zhejiang University, China
Shang-Qian Xie,
Hainan University, China

***Correspondence:**
Sanwei Yang
ysvysv@163.com
Ling Qiao
qiaolingsmile@163.com
Jun Zheng
sxnkyzj@126.com

[†]These authors have contributed equally to this work and share first authorship

Specialty section:
This article was submitted to Plant Genomics, a section of the journal Frontiers in Genetics

Received: 10 December 2021
Accepted: 25 January 2022
Published: 15 March 2022

Citation:
Yang B, Wen X, Wen H, Feng Y, Zhao J, Wu B, Zheng X, Yang C, Yang S, Qiao L and Zheng J (2022) Identification of Genetic Loci Affecting Flag Leaf Chlorophyll in Wheat Grown under Different Water Regimes. Front. Genet. 13:832898. doi: 10.3389/fgene.2022.832898

Chlorophyll content of the flag leaf is an important trait for drought resistance in wheat under drought stress. Understanding the regulatory mechanism of flag leaf chlorophyll content could accelerate breeding for drought resistance. In this study, we constructed a recombinant inbred line (RIL) population from a cross of drought-sensitive variety DH118 and drought-resistant variety Jinmai 919, and analyzed the chlorophyll contents of flag leaves in six experimental locations/years using the Wheat90K single-nucleotide polymorphism array. A total of 29 quantitative trait loci (QTLs) controlling flag leaf chlorophyll were detected with contributions to phenotypic variation ranging from 4.67 to 23.25%. Twelve QTLs were detected under irrigated conditions and 18 were detected under dryland (drought) conditions. Most of the QTLs detected under the different water regimes were different. Four major QTLs (*Qchl.saw-3B.2*, *Qchl.saw-5A.2*, *Qchl.saw-5A.3*, and *Qchl.saw-5B.2*) were detected in the RIL population. *Qchl.saw-3B.2*, possibly more suitable for marker-assisted selection of genotypes adapted to irrigated conditions, was validated by a tightly linked kompetitive allele specific PCR (KASP) marker in a doubled haploid population derived from a different cross. *Qchl.saw-5A.3*, a novel stably expressed QTL, was detected in the dryland environments and explained up to 23.25% of the phenotypic variation, and has potential for marker-assisted breeding of genotypes adapted to dryland conditions. The stable and major QTLs identified here add valuable information for understanding the genetic mechanism underlying chlorophyll content and provide a basis for molecular marker–assisted breeding.

Keywords: wheat, drought, chlorophyll, flag leaf, quantitative trait locus

INTRODUCTION

Chlorophyll is the key element for photosynthesis, which captures light energy to drive electron transfer to its reaction center. Chlorophyll content is positively correlated with photosynthetic efficiency (Avenson et al., 2005), directly affecting the accumulation of photosynthates (Guo et al., 2008; Zhang et al., 2009a). Under abiotic stress situations such as drought, high temperature, salinization, and heavy metal presence, genotypes with higher chlorophyll content maintain higher photosynthetic capacity that helps to maintain higher yield achievement (Vijayalakshmi et al., 2010;

Kumar et al., 2012; Ilyas et al., 2014; Talukder et al., 2014; Awlachew et al., 2016; Gupta et al., 2020; Bhoite et al., 2021; Borjigin et al., 2021). Photosynthetic activity in the flag leaves of wheat contributes about 50% to the grain yield (Verma et al., 2004; Zhu et al., 2016). Drought stress at the grain-filling stage is a common occurrence in wheat crops. This leads to accelerated degradation of chlorophyll in photosynthetic organs such as leaves, reduced photosynthetic rate, and decreased photosynthetic efficiency (Yang B. et al., 2016), hence lower fixation and assimilation of CO_2 (Yang D. et al., 2016) leading to restricted dry matter accumulation and grain development (Farooq et al., 2014). Therefore, the chlorophyll content in flag leaves is regarded as an indicator of drought resistance in wheat under drought stress (Farooq et al., 2014; Barakat et al., 2015). Molecular studies on the genetic regulation of flag leaf chlorophyll content are therefore of considerable significance for maintaining and improving yield potential under drought stress conditions.

Synthesis and degradation of chlorophyll is a complex biological process, which not only involves many genes and cellular metabolic pathways, but is also readily affected by internal and external environments. Quantitative trait locus (QTL) analysis and gene cloning following construction of high-density genetic linkage maps is an effective way to study the genetics of chlorophyll (Verma et al., 2004; Thomas and Ougham, 2014; Rasheed et al., 2020). In rice, more than 900 QTLs affecting chlorophyll content have been identified by QTL mapping (Ye, 2016). More than 120 leaf color–related genes have been cloned (Yang et al., 2020), among which 14 were involved in chlorophyll synthesis. These included *OsCAO1* encoding a chlorophyll oxygenase (Yang Y. et al., 2016); *OsCHLH*, *OsCHLD*, and *OsCHLI* encoding subunits of a magnesium-chelating enzyme (Jung et al., 2003; Zhou et al., 2012; Zhang et al., 2015); and *YGL1* encoding a chlorophyll synthase (Liu et al., 2016). In addition, eight genes related to stay green were cloned in rice, including a *DYE1*-encoded light capture complex I subunit (Yamatani et al., 2018), *EF8* encoding a HAP3 subunit of the HAP complex (Feng et al., 2014), and *SGR* that is involved in decomposition of chlorophyll (Morita et al., 2009). Some of these cloned genes have been successfully applied to rice breeding. Chen et al. (2020) found that overexpression of chloroplast gene *D1* increased rice biomass by 20.6–22.9% and yield of transgenic rice by 8.1–21.0% under field conditions. Thus, identification of major QTLs/genes related to chlorophyll synthesis and degradation in grain crops could have application in wheat breeding.

The wheat genome is about 17 Gb, 80–90% of which are highly repetitive sequences. Studies on the genetic mechanisms regulating chlorophyll lag behind those in model crops such as rice (Sultana et al., 2021). Moreover, the studies that have been reported involved different wheat populations and growth stages (Zhang et al., 2009a; Ilyas et al., 2014; Yu et al., 2014; Yang B. et al., 2016). The 82 reported QTLs controlling chlorophyll content were distributed across all 21 chromosomes (Quarrie et al., 2006; Zhang et al., 2009a; Zhang et al., 2009b; Kumar et al., 2010; Vijayalakshmi et al., 2010; Ilyas et al., 2014; Saleh et al., 2014; Barakat et al., 2015; Li et al., 2015; Yang D. et al., 2016; Gupta et al., 2017; Shi et al., 2017; Yan et al., 2020).

As chlorophyll content is affected by water availability and environmental conditions, there are few stably expressed major QTLs (Yang D. et al., 2016). Most studies involved widely dispersed SSR markers and there are no reports on the application of QTL for chlorophyll content in wheat breeding. A few major stay green QTLs have been fine-mapped (Li et al., 2018; Wang et al., 2020a; Gupta et al., 2020). For example, the F_2 population involving early senescence mutant M114 with significantly reduced chlorophyll content in flag leaves was analyzed by BSR-Seq, and the *els1* gene was located in the *WGGB303–WGGB305* marker interval of 2BS, with 1.5 cM genetic distance (Li et al., 2018). Wang et al. (2020b) analyzed the inheritance of F_2 population constructed with premature senescence mutant LF2099 and Chinese Spring, and mapped the *els2* gene to the marker interval of *2BIP09–2BIP14* on 2BL, and its genetic distance was 0.95 cM. There is no report on map-based cloning of genes regulating wheat chlorophyll content.

Genes *Tackx4*, *Tabas1-B1*, and *TaPPH-7A* contributing to chlorophyll content in wheat were identified by homologous cloning in wheat. Chang et al. (2015) cloned the *Tackx4* allele encoding a cytokinin oxidase on chromosome 3A and validated it using a Jing411 × Hongmangchun 21 RIL population. A major QTL co-segregating with *Tackx4* contributed 8.9–20.1% to chlorophyll content in four environments. Zhu et al. (2016) cloned *Tabas1-B1* encoding 2-cys peroxiredoxin BAS1 on chromosome 2B and identified a major co-segregating QTL that contributed 9.0–19.2% of the variation in chlorophyll content in three environments. Wang et al. (2019) cloned *TaPPH-7A* encoding a pheophorbide hydrolase on chromosome 7A and found that it was closely related to the chlorophyll content of flag leaves in plants grown under drought stress. However, none of these genes was validated by transgenesis. Clearly, synthesis and degradation of chlorophyll is a complex biological process involving many genes, but currently only a few major QTLs and genes related to chlorophyll content have been reported in wheat. Thus, different research approaches and populations to map QTL are of value for a better understanding of the genetics of chlorophyll content.

In this study, the chlorophyll content of flag leaves was analyzed by QTL analysis of a DH118 × Jinmai 919 RIL population grown in six environments with different moisture conditions and validated in a Jinchun 7 × Jinmai 919 DH population to 1) identify stable QTLs that regulate chlorophyll content in flag leaves and 2) study the effects of contrasting moisture availability on the QTLs with the objective of obtaining markers for wheat breeding.

MATERIALS AND METHODS

Plant Materials and Plot Design

The populations with Jinmai 919 as a same parent included 165 F_{10} RILs from cross DH118 × Jinmai 919 (DJ) and 168

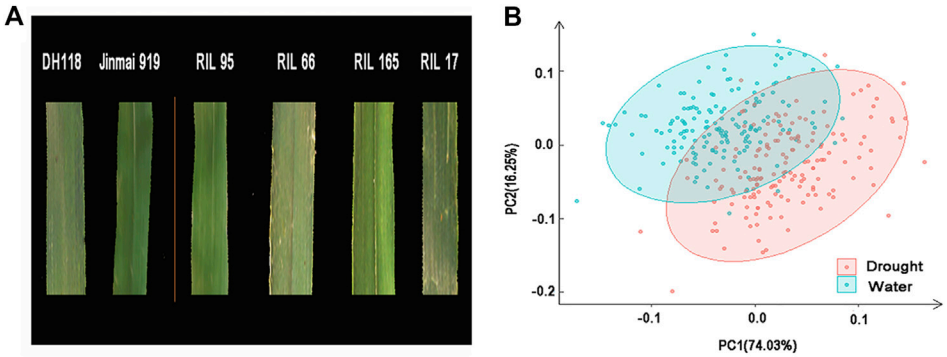

FIGURE 1 | Phenotypic characteristic of the DJ population. **(A)** Phenotypes of the parents and selected RILs. **(B)** Principal components analysis (PCA) of chlorophyll content of flag leaves estimated for RILs grown under irrigated (water) and dryland (drought) conditions. Percentage variance accounted for by PC1 and PC2 is indicated in parentheses.

doubled haploid (DH) lines from Jinchun 7 × Jinmai 919 (JJ). DH118, a high-yielding variety selected for irrigated conditions by the Institute of Wheat Research, Shanxi Agricultural University, has dark green leaves and high chlorophyll content (**Figure 1A**). Jinmai 919 developed by the Institute of Wheat Research, Shanxi Agricultural University, has strong drought resistance, light green leaves, and good stay green characteristics (**Figure 1A**). Bred by the Institute of Maize Research, Shanxi Academy of Agricultural Sciences, Jinchun 7 is also a high-yielding variety for irrigated conditions. The DJ population was used for QTL mapping, and the JJ population was used for validating QTLs identified in the mapping population.

The DJ population was planted at Yaodu Experimental Station (36°08′N, 111°52′E, YD) and Hancun Experimental Station (36°25′N, 111°67′E, HC) at Linfen in Shanxi province in 2018–2019, 2019–2020, and 2020–2021. Plants were grown under irrigated and dryland (drought stressed) conditions in each year providing six environments designated as E1 (well-watered, 2019 YD), E2 (well-watered, 2020 YD), E3 (well-watered, 2021 YD), E4 (drought stressed, 2019 HC), E5 (drought stressed, 2020 HC), and E6 (drought stressed, 2021 HC). The JJ population was planted under the environmental conditions of E1, E2, E3, E4, and E5. The field design for both populations consisted of randomized complete blocks with three replications. Each plot consisted of two 1.5 m rows spaced 0.3 m apart at 21 seeds per row. After sowing, the Hancun site relied on natural precipitation during the whole growth period, 132 mm, 154 mm, and 147 mm in 2018–2019, 2019–2020, and 2020–2021, respectively; the Yaodu site was irrigated.

Phenotypic Evaluation and Data Analysis

Ten plants flowering on the same day were randomly selected from each line at 10 days after flowering. The chlorophyll contents of flag leaves were measured using a SPAD-502 (Konica-Minolta, Japan) chlorophyll meter at 7:00 to 10:00 h. Each leaf was measured three times—at the base, mid-region, and tip—and the average value was used for analysis (Yang B. et al., 2016). Average values were also determined for each environment.

SPSS 21.0 software (SPSS, Chicago, IL, USA; http://www.spss.com) was used to perform Student's *t*-tests, correlation analysis, and ANOVA comparing phenotypic data from the two environments. SAS (SAS Institute, Cary, NC, USA; https://www.sas.com) was applied for calculating best linear unbiased predictions (BLUPs) and broad sense heritabilities (H^2).

High-Density Genetic Linkage Map Construction and QTL Mapping

DNA was extracted from all RILs and DH lines and respective parents using the CTAB method (Vijayalakshmi et al., 2010). The RIL population was genotyped with the Infinium wheat SNP 90K iSelect assay (Illumina Inc., San Diego, CA, USA) developed by the International Wheat SNP Consortium (Wang et al., 2014). IciMapping v4.0 (https://www.isbreeding.net) was used to construct a high-density genetic linkage map (Li et al., 2021). SNP markers with no recombination were placed into a single bin using the "BIN" function in IciMapping V4.0. The final markers were chosen with a minimum percentage of missing data and sorted into different groups with LOD thresholds ≤8 by the "Grouping" function in JoinMap 4.0 (Li et al., 2021).

The QTLs were detected using WinQTLCart version 2.5 (https://brcwebportal.cos.ncsu.edu/qtlcart/WQTLCart.htm) based on the composite interval mapping method. QTLs were proclaimed significant at logarithm of odds (LOD) scores >2.5. The QTL contributing more than 10% to phenotypic variation in a certain environment (including BLUP) and detected in three environments (including BLUP) was considered as a stable and major QTL. QTLs less than 1 cM apart or sharing common flanking markers were treated as a single locus. The QTLs were named according to McCouch et al. (1997). The closest marker sequences flanking QTL were compared with the Chinese Spring reference genome sequence in the wheat multiomics website database (http://wheatomics.sdau.edu.cn/jbrowse-1.12.3-release/?data=Chinese_Spring1.0) to determine the physical locations of the QTL.

TABLE 1 | Chlorophyll contents in flag leaves in parents and RILs derived from cross DH118 × Jinmai 919 in six environments

Trait	Environment	DH118	Jinmai 919	Min	Max	Mean	SD	H^2
CHL	E1	52.16*	48.80	48.02	60.04	54.04	2.37	0.90
—	E2	55.40**	50.35	47.00	57.80	54.06	2.20	—
—	E3	54.33NS	53.20	47.50	59.12	54.27	2.37	—
—	BLUP—W	53.99*	51.41	48.95	57.99	54.12	1.59	—
—	E4	60.22NS	58.42	52.84	63.50	58.50	2.31	—
—	E5	57.00**	51.63	45.40	59.42	54.21	2.25	—
—	E6	57.45*	55.13	48.32	59.74	56.44	2.60	—
—	BLUP—D	57.88*	55.30	51.35	59.26	56.36	1.66	—
—	BLUP	56.01NS	53.14	49.86	58.97	55.24	1.65	—

*H^2, broad-sense heritability; BLUP—W, best linear unbiased prediction under irrigated conditions; BLUP—D, best linear unbiased prediction under dryland conditions; BLUP, best linear unbiased prediction; *, p <0.05; **, p <0.01; NS, not significant.*

Marker Development and Validation of Major QTLs

To develop kompetitive allele specific PCR (KASP) tags from the peak marker SNP sequence of the major QTLs, two specific primers (F1/F2) and a universal primer (R) were designed for each SNP. An F1 tail that could bind to induce FAM fluorescence and an F2 tail that could bind to induce HEX fluorescence were added to the specific sequences. KASP primers were designed by Polymarker (http://www.polymarker.info/) and synthesized by Beijing Jiacheng Biotechnology Co., Ltd. (**Supplementary Table S1**). The developed KASP markers were used in PCR to detect previously identified QTLs in the JJ population as a means of validation. Following genotyping, the validation population was divided into two groups and differences in chlorophyll content of flag leaves between the groups were assessed by *t*-tests in SAS V8.0.

Gene Prediction Within QTL

Genes within the target region of major QTL were obtained using the genome browser (JBrowse) on the Triticeae Multi-omics website (http://wheatomics.sdau.edu.cn/). The GO (gene ontology) database and R package cluster profiler were applied for functional annotation and enrichment analysis of genes in the QTL regions. Identification of orthologs in wheat and rice was conducted using the Triticeae-Gene Tribe website (http://wheat.cau.edu.cn/TGT/). The expVIP public database (http://www.wheat-expression.com/) was used to search for expression data of genes in eight tissues and organs, perform log2 conversion processing, and analyze the expression patterns of candidate genes.

RESULTS

Analysis of Phenotypic Data

The chlorophyll contents of flag leaves of DH118 and Jinmai 919 ranged from 52.16 to 60.22 and 48.80 to 58.42, respectively, across the six environments. The chlorophyll content of DH118 was consistently higher than that of Jinmai 919, and the difference was significant in E1 and E6 (p <0.05), and highly significant in E2 and E5 (p <0.01) (**Table 1**). The correlation of chlorophyll contents among different environments for the RIL population was highly significant (p <0.01), and correlation coefficients ranged from 0.303 to 0.711 (**Supplementary Table S2**). The H^2 of chlorophyll content was 0.90, indicating that chlorophyll content was largely determined by genetic factors. Principal component analysis showed that environmental factors had considerable influence on phenotypic values, and drought stress increases the phenotypic variation (**Figure 1B**). Chlorophyll content of the RIL population was mostly between the two parents under E2, E3, E4, E5, and E6 environments, showing a continuous distribution. Bidirectional transgressive segregation was also observed in chlorophyll content among the RIL population under E1 condition (**Table 1**).

Linkage Map Construction

A high-density genetic linkage map for the RIL population was constructed by using Wheat90k SNP chip. The total length of the map was 5,858.63 cM with an average genetic distance of 1.65 cM, including 3,553 SNP markers and covering all 21 chromosomes (**Table 2**). The numbers of SNP markers in the A, B, and D genomes were 1,395, 1,880, and 278, respectively, and the linkage lengths were 2,394.29, 2,953.31, and 511.03 cM, with average distances between markers of 1.72, 1.57, and 1.84 cM, respectively (**Table 2**). The D genome had the lowest marker coverage; the longest linkage group was 673.66 cM for chromosome 5B, and the shortest was 23.30 cM for chromosome 4D.

QTL Mapping for Chlorophyll Content under Different Environments

A total of 29 QTLs for chlorophyll content were detected on chromosomes 1B, 2A, 2B, 2D, 3A, 3B, 4B, 5A, 5B, 6B, 7A, and 7B. The LOD scores ranged from 2.58 to 10.70 and individual QTL explained 4.67–23.25% of the phenotypic variation in different environments (**Table 3**). Favorable alleles of 20 QTLs were derived from DH118 and favorable alleles of 9 QTLs were derived from Jinmai 919.

Four major QTLs (*Qchl.saw-3B.2*, *Qchl.saw-5A.2*, *Qchl.saw-5A.3*, and *Qchl.saw-5B.2*) for chlorophyll content were detected on chromosomes 3B, 5A, and 5B, respectively. *Qchl.saw-5A.3* was detected in E2, E4, E5, E6, BLUP—D, and BLUP. The LOD values

TABLE 2 | Summary of linkage group and marker statistics obtained from a 90K SNP chip analysis of the DH118×Jinmai 919 RIL population

Chromosome	DH118 × Jinmai 919		
	No. of SNP markers	Length (cM)	Marker density (cM/marker)
1A	210	300.02	1.43
2A	166	315.04	1.90
3A	176	357.51	2.03
4A	144	272.00	1.89
5A	260	411.34	1.58
6A	245	352.09	1.44
7A	194	386.30	1.99
1B	363	557.69	1.54
2B	320	501.92	1.57
3B	279	445.65	1.60
4B	140	282.05	2.01
5B	391	673.66	1.72
6B	231	226.06	0.98
7B	156	266.29	1.71
1D	28	64.03	2.29
2D	87	138.15	1.59
3D	52	76.83	1.48
4D	9	23.30	2.59
5D	18	33.33	1.85
6D	61	100.43	1.65
7D	23	74.97	3.26
A genome	1,395	2,394.29	1.72
B genome	1,880	2,953.31	1.57
D genome	278	511.03	1.84
Total	3,553	5,858.63	1.65

ranged from 2.89 to 10.70 and the QTL explained 6.04–23.25% of the phenotypic variation. The positive allele for *Qchl.saw-5A.3* was contributed by Jinmai 919 (**Table 3**). *Qchl.saw-3B.2* was detected in E1, E3, and BLUP—W, explaining 8.19–11.43% of the phenotypic variation. *Qchl.saw-5A.2* was detected in E5, BLUP—D, and BLUP, explaining 5.28–10.76% of the phenotypic variation (**Table 3**). *Qchl.saw-5B.2* was detected in E5, BLUP—D, and BLUP, and explained 7.45–12.15% of the phenotypic variation. The positive alleles for *Qchl.saw-3B.2*, *Qchl.saw-5A.2*, and *Qchl.saw-5B.2* were contributed by DH118 (**Table 3**).

Additive Effects of the Major QTLs *Qchl.saw-3B.2*, *Qchl.saw-5A.2*, *Qchl.saw-5A.3*, and *Qchl.saw-5B.2* on Chlorophyll Content

Analysis of the additive effects of the four major QTLs showed that the number of favorable alleles increased chlorophyll content (**Figure 2A**, **Supplementary Table S3**). No RIL with all four favorable alleles was detected. The average chlorophyll content of RILs with three favorable alleles increased by 3.11–3.81 (5.91–7.24%) compared with RILs with no favorable allele. Among combinations, the average chlorophyll content of RILs with favorable alleles of *Qchl.saw-3B.2*, *Qchl.saw-5A.2*, and *Qchl.saw-5A.3* was the highest at 7.24% above that of lines with no favorable allele (**Supplementary Table S3**). In addition, the average chlorophyll content of lines with only *Qchl.saw-5A.3* allele in RIL population was higher than that of other lines with only one favorable allele (**Figure 2B**), indicating that the allele of *Qchl.saw-5A.3* had the highest genetic effect on chlorophyll content.

Validation of the Major QTL *Qchl.saw-3B.2* in the JJ Population

To validate the four major QTLs, KASP markers for each QTL were used to evaluate their effects on chlorophyll content in the JJ population. The KASP markers for *Qchl.saw-5A.2* and *Qchl.saw-5A.3* were not polymorphic between Jinchun 7 and Jinmai 919. The effect of *Qchl.saw-5B.2* did not differ significantly between two contrasting phenotypic groups in JJ population. The effect of *Qchl.saw-3B.2* was significant (p <0.05) in E1 and E3, and highly significant (p <0.01) in E2 (**Figure 2C**). The chlorophyll content of lines with the favorable *Qchl.saw-3B.2* allele was higher than that without this allele, and the difference varied from 0.95 to 2.26% across environments.

Candidate Genes in the Intervals of the Four Major QTLs

A total of 1,207 genes were identified in the four major QTLs; 73 genes in *Qchl.saw-3B.2* (52.83–54.76 Mb), 368 in *Qchl.saw-5A.2* (569.55–582.39 Mb), 735 in *Qchl.saw-5A.3* (586.59–615.30 Mb), and 31 in *Qchl.saw-5B.2* (536.05–536.68 Mb) (**Table 3**; **Supplementary Table S4**). According to gene functional annotations in the Gene Ontology (GO) public database, 174 of these genes are involved in chlorophyll metabolism and drought stress (**Supplementary Table S5**; **Supplementary Figure S1**). Analysis of gene expression in various tissues

TABLE 3 | Quantitative trait loci (QTL) for chlorophyll content detected in the DH118 × Jinmai 919 RIL population grown under different water regimes

QTL name	Environment	Chr	LOD	R^2 (%)	Add	Left marker	Right marker	Genetic interval (cM)	Physical interval (Mb)
Qchl.saw-1B	E1	1B	2.58	6.34	0.61	*wsnp_Ex_c27176_36393952*	*Kukri_c25512_53*	417.616–434.069	640.848/648.454
Qchl.saw-2A.1	E5	2A	3.42	5.90	−0.56	*CAP11_s9154_121*	*BS00100472_51*	186.071–187.965	369.833/343.887
Qchl.saw-2A.2	E3	2A	5.13	10.51	−0.81	*Excalibur_c27023_134*	*RFL_Contig3071_626*	197.103–202.211	504.275/199.7962
Qchl.saw-2B.1	E5	2B	2.65	4.67	−0.50	*Ex_c19038_1581*	*Tdurum_contig20262_440*	43.902–47.744	19.394/18.932
—	BLUP	2B	2.74	5.24	−0.39	*Ex_c19038_1581*	*Tdurum_contig20262_440*	43.902–47.744	19.394/18.932
Qchl.saw-2B.2	E1	2B	3.60	7.79	−0.67	*Kukri_c34553_110*	*RAC875_c98387_145*	409.899–410.530	766.234/766.234
Qchl.saw-2B.3	E6	2B	4.84	9.83	−0.82	*RAC875_c19685_944*	*Ku_c2936_1987*	439.101–446.163	781.584/782.154
Qchl.saw-2D.1	E2	2D	3.41	6.90	0.59	*wsnp_Ex_rep_c68555_67394261*	*BS00018028_51*	6.997–12.707	344.298/145.396
Qchl.saw-2D.2	BLUP—W	2D	4.35	9.60	0.50	*BS00018028_51*	*Kukri_c22553_60*	12.707–18.956	145.396/108.922
Qchl.saw-2D.3	E1	2D	2.65	6.35	0.61	*Kukri_c22553_60*	*RAC875_c11911_431*	18.956–23.578	108.922/110.666
Qchl.saw-3A.1	E6	3A	3.08	5.63	−0.64	*RAC875_c20134_535*	*BobWhite_c37325_92*	48.634–61.187	14.851/20.328
Qchl.saw-3A.2	E3	3A	2.82	5.58	0.57	*BobWhite_s65081_93*	*Ra_c5515_2469*	171.493–173.675	510.690/514.112
Qchl.saw-3B.1	E2	3B	3.00	6.68	−0.58	*wsnp_Ex_c16569_25082817*	*Tdurum_contig31097_254*	21.883–28.083	817.822/811.448
Qchl.saw-3B.2	E1	3B	3.68	8.19	0.70	*BS00010818_51*	*Excalibur_c8284_580*	164.650–170.772	52.832/54.756
—	E3	3B	5.17	10.59	0.80	*BS00010818_51*	*Excalibur_c8284_580*	164.650–170.772	52.832/54.756
—	BLUP—W	3B	5.38	11.43	0.56	*BS00010818_51*	*Excalibur_c8284_580*	164.650–170.772	52.832/54.756
Qchl.saw-4B.1	E4	4B	3.08	5.76	0.57	*Excalibur_c17607_542*	*RAC875_c15872_141*	180.255–199.003	311.352/140.898
Qchl.saw-4B.2	E5	4B	4.13	7.94	0.63	*wsnp_Ex_c3119_5763762*	*wsnp_JD_c1549_2185341*	171.195–180.754	443.454/363.305
Qchl.saw-4B.3	BLUP—D	4B	5.26	11.33	0.56	*RAC875_c48283_1574*	*wsnp_Ex_c30695_39579408*	195.003–216.053	140.898/20.589
Qchl.saw-5A.1	E4	5A	3.23	6.24	0.84	*RAC875_rep_c109716_67*	*IACX448*	20.398–21.319	586.597/588.377
Qchl.saw-5A.2	E5	5A	2.79	5.33	0.71	*wsnp_Ra_c3414_6378271*	*Kukri_c61046_510*	23.831–26.668	582.387/569.547
—	BLUP—D	5A	3.11	5.28	0.53	*wsnp_Ra_c3414_6378271*	*Kukri_c61046_510*	23.831–26.668	582.387/569.547
—	BLUP	5A	5.44	10.76	0.77	*wsnp_Ra_c3414_6378271*	*Kukri_c61046_510*	23.831–26.668	582.387/569.547
Qchl.saw-5A.3	E2	5A	2.89	6.04	−0.55	*GENE-2735_151*	*RAC875_c79540_228*	52.132–57.368	586.598/615.305
—	E4	5A	7.58	15.62	−1.33	*GENE-2735_151*	*RAC875_c79540_228*	52.132–57.368	586.598/615.305
—	E5	5A	6.06	12.62	−1.05	*GENE-2735_151*	*RAC875_c79540_228*	52.132–57.368	586.598/615.305
—	E6	5A	7.26	14.10	−1.01	*GENE-2735_151*	*RAC875_c79540_228*	52.132–57.368	586.598/615.305
—	BLUP—D	5A	9.73	18.36	−0.95	*GENE-2735_151*	*RAC875_c79540_228*	52.132–57.368	586.598/615.305
—	BLUP	5A	10.70	23.25	−1.09	*GENE-2735_151*	*RAC875_c79540_228*	52.132–57.368	586.598/615.305
Qchl.saw-5A.4	E5	5A	2.84	4.94	−0.54	*wsnp_Ku_c7890_13514597*	*wsnp_Ex_c9842_16228523*	264.126–268.370	19.231/15.850
Qchl.saw-5B.1	E4	5B	4.22	8.28	0.67	*Excalibur_c5594_1051*	*BS00013829_51*	292.392–294.925	520.8872/526.397
Qchl.saw-5B.2	E5	5B	4.33	8.32	0.65	*RAC875_c32611_347*	*BS00093591_51*	320.986–322.563	536.681/536.052
—	BLUP	5B	3.77	7.45	0.46	*RAC875_c32611_347*	*BS00093591_51*	320.986–322.563	536.6813/536.052
—	BLUP—D	5B	6.86	12.15	0.59	*RAC875_c32611_347*	*BS00093591_51*	320.986–322.563	536.681/536.052
Qchl.saw-6B.1	E2	6B	3.36	7.62	0.62	*BS00064027_51*	*RFL_Contig2206_1694*	129.185–138.393	680.937/690.730
Qchl.saw-6B.2	E3	6B	4.76	9.70	0.76	*Tdurum_contig61383_627*	*Tdurum_contig42301_1583*	0.000–1.900	39.198/35.367
Qchl.saw-7A.1	E4	7A	3.21	6.21	0.60	*wsnp_Ex_c40247_47349166*	*BS00047691_51*	13.785–15.675	116.113/118.327
Qchl.saw-7A.2	BLUP—D	7A	5.07	8.74	0.51	*RAC875_c62204_772*	*BS00059928_51*	32.704–36.455	615.341/603.092
—	BLUP	7A	4.02	7.68	0.47	*RAC875_c62204_772*	*BS00059928_51*	32.704–36.455	615.341/603.092
Qchl.saw-7A.3	E5	7A	3.28	6.17	0.56	*CAP7_c4608_228*	*BS00105558_51*	65.630–71.807	540.857/587.912
Qchl.saw-7A.4	E6	7A	6.39	11.79	0.93	*BobWhite_c30461_131*	*Excalibur_c22219_254*	74.905–80.888	647.934/659.374
Qchl.saw-7B.1	E4	7B	2.99	5.77	0.60	*RAC875_rep_c81362_198*	*Excalibur_c29607_442*	81.331–82.605	231.32/244.279

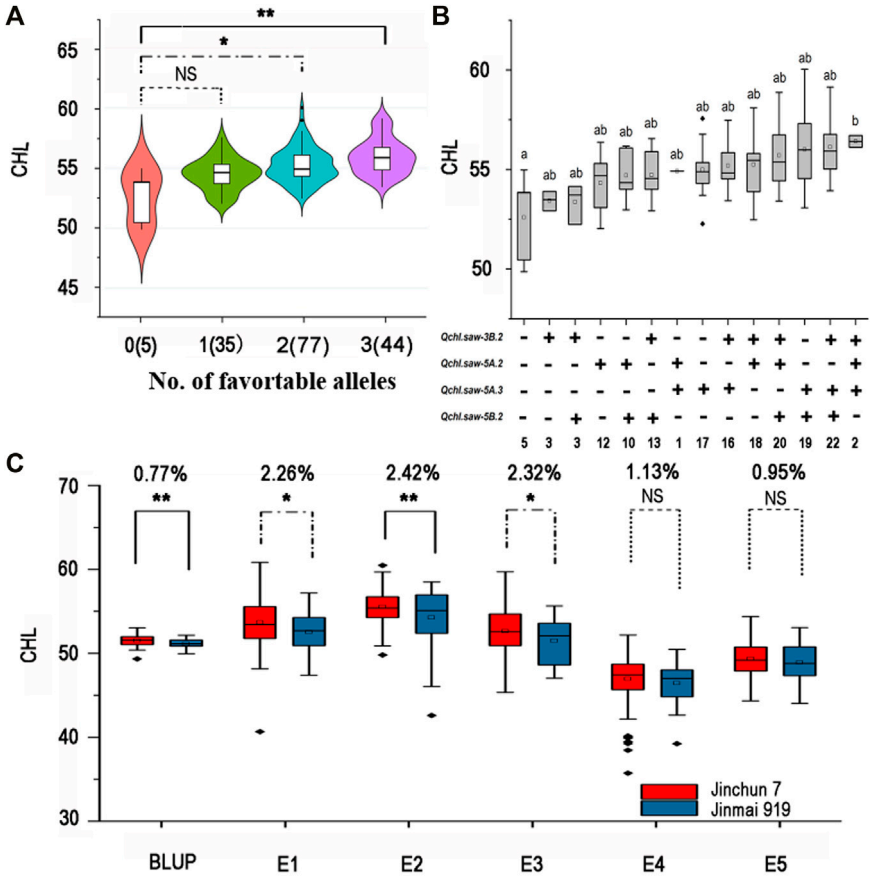

FIGURE 2 | Additive effects and validation of major QTL. **(A)** Relationship of numbers of favorable alleles and chlorophyll content in the DJ population. **(B)** Linear regressions between the additive effects of QTL and chlorophyll content in the DJ population. Numbers of lines carrying the corresponding number of favorable alleles are shown in brackets. The letter above the bars indicates comparison results at the significant level 0.05 and respectively. "+" and "–" represent lines with and without the favorable alleles. **(C)** Validation of *Qchl.saw-3B.2* in JJ population. * and ** represent significance at $p < 0.05$ and $p < 0.01$, respectively. NS represents not significant.

TABLE 4 | Functional annotation and enrichment of chlorophyll content QTLs on chromosomes 5A and 5B

Gene ID in wheat	Gene ID in rice	Gene symbol	Chr	Start (bp)	Stop (bp)	Ori	Function
TraesCS5A02G377000	—	—	chr5A	574,489,917	574,493,061	–	Integral component of membrane
TraesCS5A02G382600	*Os03g0742900*	*OsIAA13; OsIAA1*	chr5A	580,464,946	580,467,685	–	Auxin-activated signaling pathway
TraesCS5A02G376700	*Os03g0638800*	—	chr5A	574,343,360	574,348,079	+	ATP binding
TraesCS5A02G378700	*Os03g0738600*	*OsLOX2*	chr5A	575,705,508	575,709,396	–	Metal ion binding
TraesCS5A02G374500	*Os03g0645100*	—	chr5A	572,837,631	572,841,016	+	Catalytic activity
TraesCS5A02G369500	—	—	chr5A	569,546,082	569,550,560	–	ATP binding
TraesCS5A02G373600	—	—	chr5A	571,679,887	571,683,736	+	GTP binding
TraesCS5A02G414400	*Os03g0778100*	—	chr5A	602,355,957	602,357,166	–	Photosystem I
TraesCS5A02G392300	*Os03g0754800*	—	chr5A	588,548,724	588,552,987	+	Transmembrane transport
TraesCS5A02G401700	*Os03g0764800*	*OsSAPK8*	chr5A	594,570,843	594,577,495	+	ATP binding
TraesCS5A02G423000	*Os03g0784700*	*pRRFNR14*	chr5A	608,962,974	608,964,772	+	Chloroplast
TraesCS5A02G420700	—	—	chr5A	607,199,244	607,199,355	–	Chloroplast thylakoid membrane
TraesCS5A02G426100	*Os03g0787300*	—	chr5A	611,339,186	611,342,238	+	ATP binding
TraesCS5A02G429000	*Os03g0791800*	*OsUBC9*	chr5A	613,539,450	613,543,349	+	ATP binding
TraesCS5A02G424100	*Os03g0785900*	—	chr5A	609,812,809	609,814,019	+	Glutathione metabolic process
TraesCS5A02G411200	—	—	chr5A	599,809,089	599,814,381	–	Electron transport chain
TraesCS5A02G424400	*Os03g0786100*	*GLO1*	chr5A	609,862,738	609,865,710	+	Oxidation-reduction process
TraesCS5B02G356300	*Os09g0553200*	*OsUgp1*	chr5B	536,045,678	536,052,111	+	Transferase activity

identified 18 candidate genes related to chlorophyll metabolism (**Table 4**).

These 18 genes were divided into three categories according to their function. The first category was related to the composition of chloroplasts. *TraesCS5A02G420700* related to chloroplast thylakoid membrane, and *TraesCS5A02G377000* related to chloroplast membrane formation and the homologous gene *TraesCS5A02G423000* of *pRRFNR14* (*Os03g0784700*) in rice involved in the process of chloroplast composition (Aoki and Ida, 1994). The second category was related to eight new genes of chlorophyll photosynthesis, including *TraesCS5A02G414400*, *TraesCS5A02G378700* (*OsLOX*$_2$), *TraesCS5A02G373600*, *TraesCS5A02G424100*, *TraesCS5A02G376700*, *TraesCS5A02G369500*, *TraesCS5A02G392300*, and *TraesCS5B02G356300* (*OsUgp1*) (Huang et al., 2014; E et al., 2015). These genes participated in photosystem I reaction center subunit III, ATP binding, metal ion binding, and transferase activity. The third kind of genes responded to drought stress by regulating photorespiration, mediating auxin response, and participating in the regulation of ABA signal transduction pathway, such as rice homologous gene *GLO1*, *OsIAA13*/*OsIAA1*, *OsSAPK8*, and *OsUBC9* (Thakur et al., 2001; Zhang et al., 2012; Xu et al., 2013; E et al., 2015). We also identified three novel genes *TraesCS5A02G411200*, *TraesCS5A02G374500*, and *TraesCS5A02G426100* that responded to drought stress by redox reaction, activation of enzyme activity, and ATP binding (**Table 4**).

DISCUSSION

Comparison with Previous Research Results

According to reviews by Gupta et al. (2017, 2020), a total of 82 QTLs controlling chlorophyll content were identified in previous studies. These QTLs were distributed across all 21 chromosomes and explained 2.7–59.1% of the phenotypic variation, but most of these QTLs were different. The reasons could be due to 1) different methods of chlorophyll measurement that cause differences in phenotypic values, e.g., some studies used a spectrophotometer (Zhang et al., 2009b) and others used a chlorophyll meter, leading to differences in QTL analysis results (Bhusal et al., 2018); 2) chlorophyll content is a complex quantitative trait and genes controlling leaf chlorophyll are expressed differently at different developmental stages (Yang D. et al., 2016), and different measurement periods will inevitably lead to different identified genes; 3) due to different types of populations and molecular markers, it is not easy to compare results across different genetic backgrounds.

In this study, 29 QTLs controlling chlorophyll content in flag leaves were located on 12 chromosomes, most of which were A and B genome chromosomes with only three detected in the D genome. Similar results were reported in previous studies (Zhang et al., 2009b; Yang D. et al., 2016). We detected four stably expressed major QTLs on chromosomes 3B (*Qchl.saw-3B.2*), 5A (*Qchl.saw-5A.2* and *Qchl.saw-5A.3*), and 5B (*Qchl.saw-5B.2*), with contribution rates of 5.28–23.25% to the variation in chlorophyll content. These QTLs still need further validation before application in marker-assisted selection (Ahmed et al., 2021).

Fourteen, seven, and nine QTLs for chlorophyll content were located on chromosomes 3B, 5A, and 5B, respectively, in previous studies (**Table 5**). The three major QTLs controlling chlorophyll content of flag leaves identified in our study were consistent with results of previous studies. The major QTL *Qchl.saw-3B.2* on chromosome 3B was in the interval 52.83–54.75 Mb. Kumar et al. (2010) reported a major QTL *QSg.bhu-3B* for flag leaf senescence in the same region, explaining 17.9% of the variation in stay green phenotypic, and Puttamadanayaka et al. (2020) reported *QChl.iari_3B* that controlled chlorophyll content. The QTLs in our study spanned shorter physical distances and are therefore more conducive for gene cloning. *Qchl.saw-5A.2* was in the range 569.54–582.38 Mb. Puttamadanayaka et al. (2020) reported *QChl.iari_5A* for chlorophyll content spanned by *AX-94531685* (567.52 Mb) and *AX-94726381* (582.96 Mb). In the same region, Wang et al. (2017) detected three major QTLs controlling 1,000-grain weight, and their adjacent markers were *BS00073670_51*, *wsnp_Ex_c1138_2185522*, and *Tdurum_contig71499_211*, respectively. Yang et al. (2019) cloned a *TaGL3-5A* allele that conferred larger grain size based on homology with rice. Many studies have confirmed the high correlation between chlorophyll content and yield-related traits (Zhang et al., 2009b; Vijayalakshmi et al., 2010). Although there was no investigation of yield-related traits in this study, we have co-located QTL/genes for chlorophyll content, 1,000-grain weight, and grain size in the same interval with previous studies and confirmed the correlation between chlorophyll content and yield-related traits. The major QTL *Qchl.saw-5B.2* on chromosome 5B was located in the interval 536.05–536.68 Mb, which coincided with chlorophyll content QTL *Qspad.acs-5B.4* spanned by *Xwmc415* and *Xwmc508* reported by Yang et al. (2016). *Qchl.saw-5A.3* with the strongest genetic effect in our study was in the chromosome 5A interval 586.59–615.30 Mb (**Figures 3A–C**). Given no previous report of gene for chlorophyll content in this interval, *Qchl.saw-5A.3* is a novel QTL.

Effect of Environment on Expression of QTL for Chlorophyll Content

Synthesis and degradation of chlorophyll are complex biological processes and regulation likely differs under different water regimes (Yang D. et al., 2016). Under irrigated conditions, higher chlorophyll content could ensure fixation of more photosynthetic assimilates (Zhang et al., 2009b). Under drought stress conditions, stay green is closely related to higher yield (Verma et al., 2004; Thomas and Ougham, 2014). Drought-tolerant genotypes usually have higher chlorophyll content, and chlorophyll degrades more slowly under drought stress (Kumar et al., 2012; Lopes and Reynolds, 2012).

In this study, QTL analysis of chlorophyll content in flag leaves under irrigated and dryland (drought stressed) conditions was made using a RIL population derived from a cross between a

TABLE 5 | Chlorophyll QTLs on chromosomes 3B, 5A, and 5B from previous studies

Chromosome	Left marker	Right marker	Physical interval (Mb)	References
3B	*Xgwm533*	*Xgwm1037*	35.32–77.72	Kumar et al. (2010)
3B	*Xgwm566*	*Xgwm72*	77.72–216.62	Li et al. (2010)
3B	*Xbarc68*	*Xbarc101*	76.13–621.47	Kumar et al. (2012)
3B	*Xwmc326*	—	778.70	Barakat et al. (2015)
3B	*Xgwm264*	*Xgwm566*	68.91–77.72	Awlachew et al. (2016)
3B	*wsnp_Ra_c41135_48426638*	*wsnp_BE497169B_Ta_2_1*	3.41–16.04	Shirdelmoghanloo et al. (2016)
3B	*Xgwm566*	*Xgwm285*	77.72–415.92	Yang B. et al. (2016)
3B	*Xwmc808*	*Xbarc102*	17.57–42.71	Yang D. et al. (2016)
3B	*Xmag3356*	*Xwmc291*	700.81–808.66	Yang D. et al. (2016)
3B	*Xgwm566*	*Xwmc540*	77.72–132.94	Yang D. et al. (2016)
3B	*Xbarc087*	*Xaag/ctc-1*	14.39	Tahmasebi et al. (2017)
3B	*IWB10755*	—	238.82	Maulana et al. (2020)
3B	*Xwmc689*	*Xwmc78*	43.68–201.87	Puttamadanayaka et al. (2020)
3B	*Xgwm340*	*wPt8352*	826.23	Ballesteros et al. (2015)
5A	*Xgwm443*	*P2470-280*	22.71–105.43	Li et al. (2010)
5A	*Xgwm415*	*wPt9452*	692.78	Ballesteros et al. (2015)
5A	*Xbarc122*	—	766.16	Barakat et al. (2015)
5A	*Xgwm154*	*Xgwm156*	21.00–450.16	Yang B. et al. (2016)
5A	*Xwmc410*	*Xgwm595*	678.29–680.07	Yang B. et al. (2016)
5A	*AX-94414339*	*AX-94730618*	556.01–561.11	Puttamadanayaka et al. (2020)
5A	*AX-94531685*	*AX-94726381*	567.52–582.96	Puttamadanayaka et al. (2020)
5B	*Xgwm335*	*Xgwm371*	418.81–447.21	Li et al. (2010)
5B	*Xgwm371*	*Xgwm499*	477.21–477.51	Li et al. (2014)
5B	*Xbcd9*	*Xwg583*	536.05–544.57	Yu et al. (2014)
5B	*Xmag532*	*Xgwm499*	418.81–477.51	Yang D. et al. (2016)
5B	*Xwmc734*	*Xwmc235*	612.87–634.17	Yang D. et al. (2016)
5B	*Xwmc47*	*Xbarc4*	65.95	Bhusal et al. (2018)
5B	*AX-95091073*	*AX-94525,037*	13.73–21.75	Puttamadanayaka et al. (2020)
5B	*Xwmc415*	*Xwmc508*	507.92–654.92	Yang D. et al. (2016)
5B	*Xbarc140*	*Xgdm116*	598.03–618.15	Yang D. et al. (2016)

Spanning markers were used to locate positions in the physical map if the certain markers failed to be located on the physical map. The physical locations of some markers were not available leaving the physical location as a single marker.

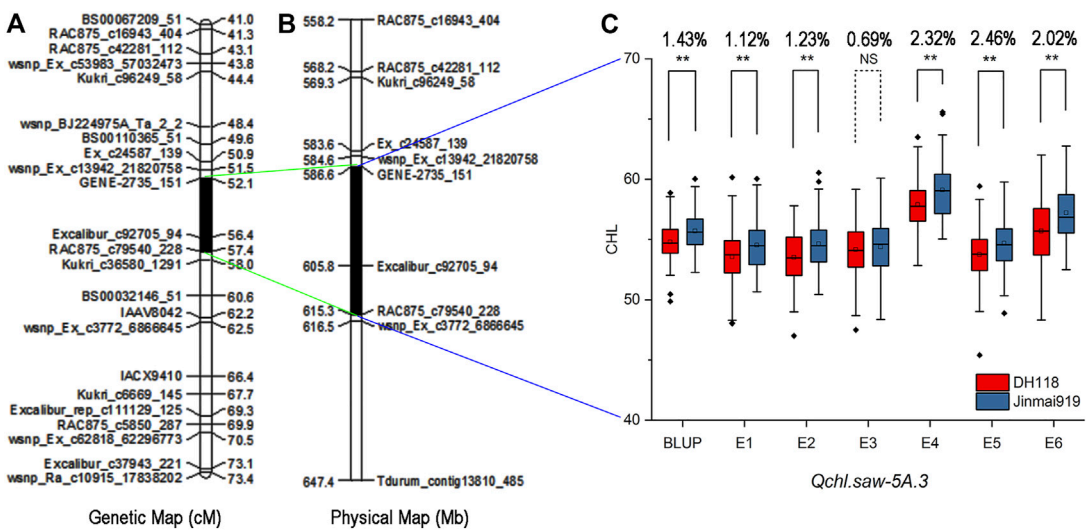

FIGURE 3 | Genetic map of the major QTL *Qchl.saw-5A.3* and its effect. **(A)** Genetic map of *Qchl.saw-5A.3* for chlorophyll content. **(B)** Physical map of flanking markers of *Qchl.saw-5A.3*. **(C)** Effect of the QTL shown as box plots calculated after dividing the DJ population into two classes based on the flanking markers. * and **, p <0.05 and p <0.01, respectively; NS, not significant.

variety DH118 recommended for irrigated conditions and drought-resistant variety Jinmai 919. Twelve QTLs were detected under irrigated conditions (E1, E2, E3 and BULP—W), and 18 QTLs were identified under drought stress (E4, E5, E6 and BULP—D) (**Table 3**). The number of QTLs under drought stress was much more than that under well-watered conditions, showing that environmental stress could induce to express genes originally keeping silent under irrigated conditions to reduce plant damages from environmental stress (Yang et al., 2007; Guo et al., 2008; Vijayalakshmi et al., 2010; Christopher et al., 2018). In addition, it was not difficult to find that there were some differences in QTL mapping data between the well-watered and drought stress, which implied that there were different QTL expression patterns under different water regimes (Yang et al., 2007; Yang B. et al., 2016; Xu et al., 2017; Hassan et al., 2018; Christopher et al., 2021). It also implies that different QTLs should be used for marker-assisted breeding of wheat varieties under irrigated conditions and dryland. For example, the *Qchl.saw-3B.2* detected in this study was not only confirmed to be stably expressed without the influence of genetic background, but also detected under several well-watered conditions, which may be more suitable for molecular marker–assisted selection of varieties under irrigated conditions. In addition, Kumar et al. (2012) and Hassan et al. (2018) considered that the major QTL detected under drought stress may contain genes that contribute to drought resistance and have the application potential to increase yield under drought stress. In our study, three major QTLs (*Qchl.saw-5A.2*, *Qchl.saw-5A.3*, and *Qchl.saw-5B.2*) were detected in drought stress environments. *Qchl.saw-5A.3* could be detected in all drought stress environments (E4, E5, and E6), and the contribution rate to phenotype was 6.04–23.25% (**Table 3**), which may be more suitable for marker-assisted selection breeding of drought-resistant varieties. In short, this study used high-density chips for QTL mapping, and the SNP and KASP markers of four major QTLs could be applied to the next development of molecular markers under different water conditions.

DATA AVAILABILITY STATEMENT

The datasets presented in this study can be found in online repositories. The names of the repository/repositories and accession number(s) can be found in the article/**Supplementary Material**.

AUTHOR CONTRIBUTIONS

SY, LQ, and JuZ designed the experiment and wrote the article. BY and XW carried out the experiments. HW and YF analyzed the data. JiZ, BW, XZ, and CY did the field experiments. All authors contributed to the article and approved the final article to publish.

FUNDING

This study was supported by the Research Program Sponsored by State Key Laboratory of Sustainable Dryland Agriculture (No. 202001-3), the Science Research of Shanxi Academy of Agricultural Sciences (No. YGJPY 2008), the Basic Research Plan of Shanxi Province (No. 20210302124505), the Project funded by Shanxi Key Laboratory of Crop Genetics and Molecular Improvement (No. KFJJ 2019-02), and the Agricultural Science Research of Shanxi Academy of Agricultural Sciences (YCX2020YQ34).

ACKNOWLEDGMENTS

We thank Jianli Chen of the University of Idaho for critical advice on the design of these experiments.

SUPPLEMENTARY MATERIAL

The Supplementary Material for this article can be found online at: https://www.frontiersin.org/articles/10.3389/fgene.2022.832898/full#supplementary-material

REFERENCES

Ahmed, A. A. M., Mohamed, E. A., Hussein, M. Y., and Sallam, A. (2021). Genomic Regions Associated with Leaf Wilting Traits under Drought Stress in Spring Wheat at the Seedling Stage Revealed by GWAS. *Environ. Exp. Bot.* 184, 104393. doi:10.1016/j.envexpbot.2021.104393

Aoki, H., and Ida, S. (1994). Nucleotide Sequence of a Rice Root Ferredoxin-Nadp+ Reductase cDNA and its Induction by Nitrate. *Biochim. Biophys. Acta (Bba) - Bioenerg.* 1183, 553–556. doi:10.1016/0005-2728(94)90085-x

Avenson, T. J., Cruz, J. A., Kanazawa, A., and Kramer, D. M. (2005). Regulating the Proton Budget of Higher Plant Photosynthesis. *Proc. Natl. Acad. Sci.* 102, 9709–9713. doi:10.1073/pnas.0503952102

Awlachew, Z. T., Singh, R., Kaur, S., Bains, N. S., and Chhuneja, P. (2016). Transfer and Mapping of the Heat Tolerance Component Traits of *Aegilops speltoides* in Tetraploid Wheat *Triticum durum*. *Mol. Breed.* 36, 78. doi:10.1007/s11032-016-0499-2

Ballesteros, D. C., Mason, R. E., Addison, C. K., Andrea Acuña, M., Nelly Arguello, M., Subramanian, N., et al. (2015). Tolerance of Wheat to Vegetative Stage Soil Waterlogging Is Conditioned by Both Constitutive and Adaptive QTL. *Euphytica* 201, 329–343. doi:10.1007/s10681-014-1184-3

Barakat, M., Saleh, M., Al-Doss, A., Moustafa, K., Elshafei, A., and Al-Qurainy, F. (2015). Identification of New SSR Markers Linked to Leaf Chlorophyll Content, Flag Leaf Senescence and Cell Membrane Stability Traits in Wheat under Water Stressed Condition. *Acta Biologica Hungarica* 66, 93–102. doi:10.1556/ABiol.66.2015.1.8

Bhoite, R., Si, P., Siddique, K. H. M., and Yan, G. (2021). Comparative Transcriptome Analyses for Metribuzin Tolerance Provide Insights into Key Genes and Mechanisms Restoring Photosynthetic Efficiency in Bread Wheat (*Triticum aestivum L.*). *Genomics* 113, 910–918. doi:10.1016/j.ygeno.2021.02.004

Bhusal, N., Sharma, P., Sareen, S., and Sarial, A. K. (2018). Mapping QTLs for Chlorophyll Content and Chlorophyll Fluorescence in Wheat under Heat Stress. *Biol. Plant* 62, 721–731. doi:10.1007/s10535-018-0811-6

Borjigin, C., Schilling, R. K., Jewell, N., Brien, C., Sanchez-Ferrero, J. C., Eckermann, P. J., et al. (2021). Identifying the Genetic Control of Salinity Tolerance in the Bread Wheat Landrace Mocho de Espiga Branca. *Funct. Plant Biol.* 48, 1148–1160. doi:10.1071/fp21140

Chang, C., Lu, J., Zhang, H.-P., Ma, C.-X., and Sun, G. (2015). Copy Number Variation of Cytokinin Oxidase Gene *Tackx4* Associated with Grain Weight and Chlorophyll Content of Flag Leaf in Common Wheat. *Plos One* 10, e0145970. doi:10.1371/journal.pone.0145970

Chen, J.-H., Chen, S.-T., He, N.-Y., Wang, Q.-L., Zhao, Y., Gao, W., et al. (2020). Nuclear-Encoded Synthesis of the D1 Subunit of Photosystem II Increases Photosynthetic Efficiency and Crop Yield. *Nat. Plants* 6, 570–580. doi:10.1038/s41477-020-0629-z

Christopher, M., Chenu, K., Jennings, R., Fletcher, S., Butler, D., Borrell, A., et al. (2018). QTL for Stay-Green Traits in Wheat in Well-Watered and Water-Limited Environments. *Field Crops Res.* 217, 32–44. doi:10.1016/j.fcr.2017.11.003

Christopher, M., Paccapelo, V., Kelly, A., Macdonald, B., Hickey, L., Richard, C., et al. (2021). QTL Identified for Stay-Green in a Multi-Reference Nested Association Mapping Population of Wheat Exhibit Context Dependent Expression and Parent-Specific Alleles. *Field Crops Res.* 270, 108181. doi:10.1016/j.fcr.2021.108181

E, Z., Zhang, Y., Li, T., Wang, L., and Zhao, H. (2015). Characterization of the Ubiquitin-Conjugating Enzyme Gene Family in Rice and Evaluation of Expression Profiles under Abiotic Stresses and Hormone Treatments. *Plos One* 10, e0122621. doi:10.1371/journal.pone.0122621

Farooq, M., Hussain, M., and Siddique, K. H. M. (2014). Drought Stress in Wheat during Flowering and Grain-Filling Periods. *Crit. Rev. Plant Sci.* 33, 331–349. doi:10.1080/07352689.2014.875291

Feng, Z., Zhang, L., Yang, C., Wu, T., Lv, J., Chen, Y., et al. (2014). *EF8* Is Involved in Photoperiodic Flowering Pathway and Chlorophyll Biogenesis in Rice. *Plant Cell Rep* 33, 2003–2014. doi:10.1007/s00299-014-1674-8

Guo, P., Baum, M., Varshney, R. K., Graner, A., Grando, S., and Ceccarelli, S. (2008). QTLs for Chlorophyll and Chlorophyll Fluorescence Parameters in Barley under Post-Flowering Drought. *Euphytica* 163, 203–214. doi:10.1007/s10681-007-9629-6

Gupta, P. K., Balyan, H. S., and Gahlaut, V. (2017). QTL Analysis for Drought Tolerance in Wheat: Present Status and Future Possibilities. *Agronomy* 7, 5. doi:10.3390/agronomy7010005

Gupta, P. K., Balyan, H. S., Sharma, S., and Kumar, R. (2020). Genetics of Yield, Abiotic Stress Tolerance and Biofortification in Wheat (*Triticum aestivum* L.). *Theor. Appl. Genet.* 133, 1569–1602. doi:10.1007/s00122-020-03583-3

Hassan, F. S. C., Solouki, M., Fakheri, B. A., Nezhad, N. M., and Masoudi, B. (2018). Mapping QTLs for Physiological and Biochemical Traits Related to Grain Yield under Control and Terminal Heat Stress Conditions in Bread Wheat (*Triticum aestivum* L.). *Physiol. Mol. Biol. Plants* 24, 1231–1243. doi:10.1007/s12298-018-0590-8

Huang, J., Cai, M., Long, Q., Liu, L., Lin, Q., Jiang, L., et al. (2014). *OsLOX2*, a Rice Type I Lipoxygenase, Confers Opposite Effects on Seed Germination and Longevity. *Transgenic Res.* 23, 643–655. doi:10.1007/s11248-014-9803-2

Ilyas, M., Ilyas, N., Arshad, M., Kazi, A. G., Kazi, A. M., and Waheed, A. (2014). QTL Mapping of Wheat Doubled Haploids for Chlorophyll Content and Chlorophyll Fluorescence Kinetics under Drought Stress Imposed at Anthesis Stage. *Pak. J. Bot.* 46, 1889–1897.

Jung, K.-H., Hur, J., Ryu, C.-H., Choi, Y., Chung, Y.-Y., Miyao, A., et al. (2003). Characterization of a Rice Chlorophyll-Deficient Mutant Using the T-DNA Gene-Trap System. *Plant Cell Physiol* 44, 463–472. doi:10.1093/pcp/pcg064

Kumar, S., Sehgal, S. K., Kumar, U., Prasad, P. V. V., Joshi, A. K., and Gill, B. S. (2012). Genomic Characterization of Drought Tolerance-Related Traits in Spring Wheat. *Euphytica* 186, 265–276. doi:10.1007/s10681-012-0675-3

Kumar, U., Joshi, A. K., Kumari, M., Paliwal, R., Kumar, S., and Röder, M. S. (2010). Identification of QTLs for Stay Green Trait in Wheat (*Triticum aestivum* L.) in the 'Chirya 3' × 'Sonalika' Population. *Euphytica* 174, 437–445. doi:10.1007/s10681-010-0155-6

Li, F., Wen, W., Liu, J., Zhai, S., Cao, X., Liu, C., et al. (2021). Genome-Wide Linkage Mapping for Canopy Activity Related Traits Using Three RIL Populations in Bread Wheat. *Euphytica* 217, 67. doi:10.1007/s10681-021-02797-w

Li, H., Tong, Y., Li, B., Jing, R., Lu, C., and Li, Z. (2010). Genetic Analysis of Tolerance to Photo-Oxidative Stress Induced by High Light in Winter Wheat (*Triticum aestivum* L.). *J. Genet. Genomics* 37, 399–412. doi:10.1016/s1673-8527(09)60058-8

Li, H., Wang, G., Zheng, Q., Li, B., Jing, R., and Li, Z. (2014). Genetic Analysis of Biomass and Photosynthetic Parameters in Wheat Grown in Different Light Intensities. *J. Integr. Plant Biol.* 56, 594–604. doi:10.1111/jipb.12174

Li, H., Ye, G., and Wang, J. (2007). A Modified Algorithm for the Improvement of Composite Interval Mapping. *Genetics* 175, 361–374. doi:10.1534/genetics.106.066811

Li, M., Li, B., Guo, G., Chen, Y., Xie, J., Lu, P., et al. (2018). Mapping a Leaf Senescence Gene *Els1* by BSR-Seq in Common Wheat. *Crop J.* 6, 236–243. doi:10.1016/j.cj.2018.01.004

Li, X.-M., He, Z.-H., Xiao, Y.-G., Xia, X.-C., Trethowan, R., Wang, H.-J., et al. (2015). QTL Mapping for Leaf Senescence-Related Traits in Common Wheat under Limited and Full Irrigation. *Euphytica* 203, 569–582. doi:10.1007/s10681-014-1272-4

Liu, H., Li, Q., Yang, F., Zhu, F., Sun, Y., Tao, Y., et al. (2016). Differential Regulation of Protochlorophyllide Oxidoreductase Abundances by VIRESCENT 5A (OsV5A) and VIRESCENT 5B (OsV5B) in Rice Seedlings. *Plant Cell Physiol* 57, 2392–2402. doi:10.1093/pcp/pcw151

Lopes, M. S., and Reynolds, M. P. (2012). Stay-Green in Spring Wheat Can Be Determined by Spectral Reflectance Measurements (Normalized Difference Vegetation Index) Independently from Phenology. *J. Exp. Bot.* 63, 3789–3798. doi:10.1093/jxb/ers071

Maulana, F., Huang, W., Anderson, J. D., and Ma, X.-F. (2020). Genome-Wide Association Mapping of Seedling Drought Tolerance in Winter Wheat. *Front. Plant Sci.* 11, 573786. doi:10.3389/fpls.2020.573786

Mccouch, S. R., Chen, X., Panaud, O., Temnykh, S., Xu, Y., Cho, Y. G., et al. (1997). Microsatellite Marker Development, Mapping and Applications in Rice Genetics and Breeding. *Plant Mol. Biol.* 35, 89–99. doi:10.1023/a:1005711431474 10.1007/978-94-011-5794-0_9

Morita, R., Sato, Y., Masuda, Y., Nishimura, M., and Kusaba, M. (2009). Defect in Non-Yellow Coloring 3, an α/β Hydrolase-Fold Family Protein, Causes a Stay-Green Phenotype during Leaf Senescence in Rice. *Plant J.* 60, 1110. doi:10.1111/j.1365-313X.2009.04019.x

Puttamadanayaka, S., Harikrishna., Balaramaiah, M., Biradar, S., Parmeshwarappa, S. V., Sinha, N., et al. (2020). Mapping Genomic Regions of Moisture Deficit Stress Tolerance Using Backcross Inbred Lines in Wheat (*Triticum aestivum* L.). *Sci. Rep.* 10, 21646. doi:10.1038/s41598-020-78671-x

Quarrie, S., Pekic Quarrie, S., Radosevic, R., Rancic, D., Kaminska, A., Barnes, J. D., et al. (2006). Dissecting a Wheat QTL for Yield Present in a Range of Environments: from the QTL to Candidate Genes. *J. Exp. Bot.* 57, 2627–2637. doi:10.1093/jxb/erl026

Rasheed, A., Takumi, S., Hassan, M. A., Imtiaz, M., Ali, M., Morgunov, A. I., et al. (2020). Appraisal of Wheat Genomics for Gene Discovery and Breeding Applications: a Special Emphasis on Advances in Asia. *Theor. Appl. Genet.* 133, 1503–1520. doi:10.1007/s00122-019-03523-w

Saleh, M. S., Al-Doss, A. A., Elshafei, A. A., Moustafa, K. A., Al-Qurainy, F. H., and Barakat, M. N. (2014). Identification of New TRAP Markers Linked to Chlorophyll Content, Leaf Senescence, and Cell Membrane Stability in Water-Stressed Wheat. *Biol. Plant* 58, 64–70. doi:10.1007/s10535-013-0351-z

Shi, S., Azam, F. I., Li, H., Chang, X., Li, B., and Jing, R. (2017). Mapping QTL for Stay-Green and Agronomic Traits in Wheat under Diverse Water Regimes. *Euphytica* 213, 246. doi:10.1007/s10681-017-2002-5

Shirdelmoghanloo, H., Taylor, J. D., Lohraseb, I., Rabie, H., Brien, C., Timmins, A., et al. (2016). A QTL on the Short Arm of Wheat (*Triticum aestivum* L.) Chromosome 3B Affects the Stability of Grain Weight in Plants Exposed to a Brief Heat Shock Early in Grain Filling. *Bmc Plant Biol.* 16, 100. doi:10.1186/s12870-016-0784-6

Sultana, N., Islam, S., Juhasz, A., and Ma, W. (2021). Wheat Leaf Senescence and its Regulatory Gene Network. *Crop J.* 9, 703–717. doi:10.1016/j.cj.2021.01.004

Tahmasebi, S., Heidari, B., Pakniyat, H., and Mcintyre, C. L. (2017). Mapping QTLs Associated with Agronomic and Physiological Traits under Terminal Drought and Heat Stress Conditions in Wheat (*Triticum aestivum* L.). *Genome* 60, 26–45. doi:10.1139/gen-2016-0017

Talukder, S. K., Babar, M. A., Vijayalakshmi, K., Poland, J., Prasad, P. V. V., Bowden, R., et al. (2014). Mapping QTL for the Traits Associated with Heat Tolerance in Wheat (*Triticum aestivum* L.). *Bmc Genet.* 15, 97. doi:10.1186/s12863-014-0097-4

Thakur, J. K., Tyagi, A. K., and Khurana, J. P. (2001). *OsIAA1*, an *Aux/IAA* cDNA from Rice, and Changes in its Expression as Influenced by Auxin and Light. *DNA Res.* 8, 193–203. doi:10.1093/dnares/8.5.193

Thomas, H., and Ougham, H. (2014). The Stay-Green Trait. *J. Exp. Bot.* 65, 3889–3900. doi:10.1093/jxb/eru037

Verma, V., Foulkes, M. J., Worland, A. J., Sylvester-Bradley, R., Caligari, P. D. S., and Snape, J. W. (2004). Mapping Quantitative Trait Loci for Flag Leaf Senescence as a Yield Determinant in Winter Wheat under Optimal and Drought-Stressed Environments. *Euphytica* 135, 255–263. doi:10.1023/b:Euph.0000013255.31618.14

Vijayalakshmi, K., Fritz, A. K., Paulsen, G. M., Bai, G., Pandravada, S., and Gill, B. S. (2010). Modeling and Mapping QTL for Senescence-Related Traits in Winter Wheat under High Temperature. *Mol. Breed.* 26, 163–175. doi:10.1007/s11032-009-9366-8

Wang, H., Wang, S., Chang, X., Hao, C., Sun, D., and Jing, R. (2019). Identification of *TaPPH-7A* Haplotypes and Development of a Molecular Marker Associated with Important Agronomic Traits in Common Wheat. *Bmc Plant Biol.* 19, 296. doi:10.1186/s12870-019-1901-0

Wang, N., Xie, Y., Li, Y., Wu, S., Li, S., Guo, Y., et al. (2020a). High-Resolution Mapping of the Novel Early Leaf Senescence Gene *Els2* in Common Wheat. *Plants* 9, 698. doi:10.3390/plants9060698

Wang, N., Xie, Y. Z., Li, Y. Z., Wu, S. N., Wei, H. S., and Wang, C. S. (2020b). Molecular Mapping of a Novel Early Leaf-Senescence Gene *Els2* in Common Wheat by SNP Genotyping Arrays. *Crop Pasture Sci.* 71, 356–367. doi:10.1071/cp19435

Wang, S.-X., Zhu, Y.-L., Zhang, D.-X., Shao, H., Liu, P., Hu, J.-B., et al. (2017). Genome-Wide Association Study for Grain Yield and Related Traits in Elite Wheat Varieties and Advanced Lines Using SNP Markers. *Plos One* 12, e0188662. doi:10.1371/journal.pone.0188662

Wang, S., Wong, D., Forrest, K., Allen, A., Chao, S., Huang, B. E., et al. (2014). Characterization of Polyploid Wheat Genomic Diversity Using a High-Density 90 000 Single Nucleotide Polymorphism Array. *Plant Biotechnol. J.* 12, 787–796. doi:10.1111/pbi.12183

Xu, M.-R., Huang, L.-Y., Zhang, F., Zhu, L.-H., Zhou, Y.-L., and Li, Z.-K. (2013). Genome-Wide Phylogenetic Analysis of Stress-Activated Protein Kinase Genes in Rice (*OsSAPKs*) and Expression Profiling in Response to *Xanthomonas oryzae* Pv. *Oryzicola* Infection. *Plant Mol. Biol. Rep.* 31, 877–885. doi:10.1007/s11105-013-0559-2

Xu, Y.-F., Li, S.-S., Li, L.-H., Ma, F.-F., Fu, X.-Y., Shi, Z.-L., et al. (2017). QTL Mapping for Yield and Photosynthetic Related Traits under Different Water Regimes in Wheat. *Mol. Breed.* 37. doi:10.1007/s11032-016-0583-7

Yamatani, H., Kohzuma, K., Nakano, M., Takami, T., Kato, Y., Hayashi, Y., et al. (2018). Impairment of Lhca4, a Subunit of LHCI, Causes High Accumulation of Chlorophyll and the Stay-Green Phenotype in Rice. *J. Exp. Bot.* 69, 1027–1035. doi:10.1093/jxb/erx468

Yan, X., Wang, S., Yang, B., Zhang, W., Cao, Y., Shi, Y., et al. (2020). QTL Mapping for Flag Leaf-Related Traits and Genetic Effect of *QFLW-6A* on Flag Leaf Width Using Two Related Introgression Line Populations in Wheat. *Plos One* 15, e0229912. doi:10.1371/journal.pone.0229912

Yang, B., Yan, X., Wang, H., Li, X., Ma, H., Wang, S., et al. (2016a). Dynamic QTL Analysis of Chlorophyll Content during Grain Filling Stage in Winter Wheat (*Triticum aestivum* L.). *Rom. Agric. Res.* 33, 77–85.

Yang, D.-L., Jing, R.-L., Chang, X.-P., and Li, W. (2007). Quantitative Trait Loci Mapping for Chlorophyll Fluorescence and Associated Traits in Wheat (*Triticum aestivum*). *J. Integr. Plant Biol.* 49, 646–654. doi:10.1111/j.1744-7909.2007.00443.x

Yang, D., Li, M., Liu, Y., Chang, L., Cheng, H., Chen, J., et al. (2016b). Identification of Quantitative Trait Loci and Water Environmental Interactions for Developmental Behaviors of Leaf Greenness in Wheat. *Front. Plant Sci.* 7, 273. doi:10.3389/fpls.2016.00273

Yang, J., Zhou, Y., Wu, Q., Chen, Y., Zhang, P., Zhang, Y., et al. (2019). Molecular Characterization of a Novel *TaGL3-5A* Allele and its Association with Grain Length in Wheat (*Triticum aestivum* L.). *Theor. Appl. Genet.* 132, 1799–1814. doi:10.1007/s00122-019-03316-1

Yang, Y. R., Huang, Q. Q., Zhao, Y. A., Tang, J. Y., and Liu, X. (2020). Advances on Gene Isolation and Molecular Mechanism of Rice Leaf Color Genes. *J. Plant Genet. Resour.* 21, 794–803.

Yang, Y., Xu, J., Huang, L., Leng, Y., Dai, L., Rao, Y., et al. (2016c). *PGL*, Encoding Chlorophyllide a Oxygenase 1, Impacts Leaf Senescence and Indirectly Affects Grain Yield and Quality in Rice. *Exbotj* 67, 1297–1310. doi:10.1093/jxb/erv529

Ye, W. (2016). Fine Mapping Leaf Chlorophyll Content QTL *$qFCC_{7L}$*& Cloning and Function Analysis of Leaf Color Gene *WSL12*. dissertation/doctor's thesis (Zhejiang: Zhejiang University).

Yu, M., Mao, S.-l., Chen, G.-y., Liu, Y.-x., Li, W., Wei, Y.-m., et al. (2014). QTLs for Waterlogging Tolerance at Germination and Seedling Stages in Population of Recombinant Inbred Lines Derived from a Cross between Synthetic and Cultivated Wheat Genotypes. *J. Integr. Agric.* 13, 31–39. doi:10.1016/s2095-3119(13)60354-8

Zhang, H., Liu, L., Cai, M., Zhu, S., Zhao, J., Zheng, T., et al. (2015). A Point Mutation of Magnesium Chelatase *OsCHLI* Gene Dampens the Interaction between CHLI and CHLD Subunits in Rice. *Plant Mol. Biol. Rep.* 33, 1975–1987. doi:10.1007/s11105-015-0889-3

Zhang, K., Fang, Z., Liang, Y., and Tian, J. (2009a). Genetic Dissection of Chlorophyll Content at Different Growth Stages in Common Wheat. *J. Genet.* 88, 183–189. doi:10.1007/s12041-009-0026-x

Zhang, K., Zhang, Y., Chen, G., and Tian, J. (2009b). Genetic Analysis of Grain Yield and Leaf Chlorophyll Content in Common Wheat. *Cereal Res. Commun.* 37, 499–511. doi:10.1556/crc.37.2009.4.3

Zhang, Z., Lu, Y., Zhai, L., Deng, R., Jiang, J., Li, Y., et al. (2012). Glycolate Oxidase Isozymes Are Coordinately Controlled by *GLO1* and *GLO4* in Rice. *Plos One* 7, e39658. doi:10.1371/journal.pone.0039658

Zhou, S., Sawicki, A., Willows, R. D., and Luo, M. (2012). C-Terminal Residues of *Oryza sativa* GUN4 Are Required for the Activation of the ChlH Subunit of Magnesium Chelatase in Chlorophyll Synthesis. *Febs Lett.* 586, 205–210. doi:10.1016/j.febslet.2011.12.026

Zhu, X.-F., Zhang, H.-P., Hu, M.-J., Wu, Z.-Y., Jiang, H., Cao, J.-J., et al. (2016). Cloning and Characterization of *Tabas1-B1* Gene Associated with Flag Leaf Chlorophyll Content and Thousand-Grain Weight and Development of a Gene-Specific Marker in Wheat. *Mol. Breed.* 36, 142. doi:10.1007/s11032-016-0563-y

Conflict of Interest: The authors declare that the research was conducted in the absence of any commercial or financial relationships that could be construed as a potential conflict of interest.

Publisher's Note: All claims expressed in this article are solely those of the authors and do not necessarily represent those of their affiliated organizations, or those of the publisher, the editors, and the reviewers. Any product that may be evaluated in this article, or claim that may be made by its manufacturer, is not guaranteed or endorsed by the publisher.

Advantages of publishing in Frontiers

OPEN ACCESS
Articles are free to read for greatest visibility and readership

FAST PUBLICATION
Around 90 days from submission to decision

HIGH QUALITY PEER-REVIEW
Rigorous, collaborative, and constructive peer-review

TRANSPARENT PEER-REVIEW
Editors and reviewers acknowledged by name on published articles

Frontiers
Avenue du Tribunal-Fédéral 34
1005 Lausanne | Switzerland

Visit us: www.frontiersin.org
Contact us: frontiersin.org/about/contact

REPRODUCIBILITY OF RESEARCH
Support open data and methods to enhance research reproducibility

DIGITAL PUBLISHING
Articles designed for optimal readership across devices

FOLLOW US
@frontiersin

IMPACT METRICS
Advanced article metrics track visibility across digital media

EXTENSIVE PROMOTION
Marketing and promotion of impactful research

LOOP RESEARCH NETWORK
Our network increases your article's readership